



Alexander, Cherry (2020) *Mechanism of ventricular arrhythmias in the Long QT Syndrome*. PhD thesis.

<https://theses.gla.ac.uk/81469/>

Copyright and moral rights for this work are retained by the author

A copy can be downloaded for personal non-commercial research or study, without prior permission or charge

This work cannot be reproduced or quoted extensively from without first obtaining permission from the author

The content must not be changed in any way or sold commercially in any format or medium without the formal permission of the author

When referring to this work, full bibliographic details including the author, title, awarding institution and date of the thesis must be given

Enlighten: Theses

<https://theses.gla.ac.uk/>  
[research-enlighten@glasgow.ac.uk](mailto:research-enlighten@glasgow.ac.uk)

**Mechanism of Ventricular Arrhythmias in the Long QT  
Syndrome**

**by**

**Cherry Alexander BSc (Hons) MBChB MRCP (UK)**

**Submitted for the degree of Doctor of Philosophy**

**To**

**The College of Medical, Veterinary and Life Sciences**

**The University of Glasgow**

**From**

**The Institute of Cardiovascular & Medical Sciences**

**University of Glasgow**

## Abstract

The Long QT Syndrome (LQTS) is associated with life-threatening ventricular arrhythmias, as there is a risk of developing a specific form of ventricular tachycardia, called Torsade des points (TdP), which can degenerate into ventricular fibrillation (VF). TdP is typically induced by a premature ventricular complex (PVC) which interacts with a vulnerable substrate to produce re-entry. LQTS can be congenital or acquired and in many cases the first presentation is sudden cardiac death (SCD). Treatment options for congenital LQTS include beta-blockers and the implantable-cardioverter defibrillator (ICD). While an ICD prevents SCD they do not reduce arrhythmia burden.

The cellular basis for QT prolongation is prolongation of the cardiac action potential (AP). Under these conditions isolated cells may develop early afterdepolarisations (EADs), which can induce a triggered AP, a possible mechanism of PVC induction. In intact hearts, where electrotonic coupling exists, synchronisation of cellular EADs would be required to produce a triggered AP. On the basis of this understanding, therapeutic approaches have been targeted at abolition of EADs and shortening the AP, which so far have been ineffective. The aim of this study was to investigate the mechanism of PVC induction in LQTS in an intact rabbit heart. A pharmacological model of LQT was established and characterised using dual optical mapping of voltage ( $V_m$ ) and calcium ( $Ca^{2+}$ ). As expected,  $Ca^{2+}$ -driven EADs and associated PVCs, bursts and TdP were produced under LQT states. However, our data suggests induction of PVCs was not mediated by synchronisation of cellular EADs but rather through electrotonic triggering as a result of steep voltage gradients found at the border of long AP islands. EADs were seen to occur within the long AP islands and were responsible for causing a dynamic increase in local voltage gradients and so indirectly contributed to PVC initiation. Given the  $V_m$ - $Ca^{2+}$  dynamics and  $V_m$  range of the observed PVCs, we hypothesised that the initial upstroke was supported by reactivation of  $I_{CaL}$ . In keeping with this, low doses of L-type  $Ca^{2+}$  channel (LTCC) block caused abolition of PVCs, crucially without loss of the LQTS substrate, with EADs and long AP islands still present at the time PVCs were abolished. This suggests a novel therapeutic approach that, instead of targeting EADs, uses low dose LTCC blockade to abolish PVCs and thereby to prevent TdP induction in the presence of QT prolongation. In addition, our data suggest that PVC induction and the pro-arrhythmic potential in LQTS is a tissue-level phenomenon that cannot be elucidated from cellular behaviour alone.

## Table of Contents

Author's Declaration.....	14
List of Abbreviations.....	15
Chapter 1: Introduction.....	19
Long QT Syndrome.....	20
What is LQTS?.....	20
Electrocardiographic QT Interval.....	21
Acquired Long QT.....	22
Electrolyte Disturbances.....	23
Congenital LQTS.....	24
Diagnosis of Long QT Syndrome.....	26
Management of LQTS.....	28
Lifestyle Changes.....	28
Additional Lifestyle Changes Genotype Specific.....	28
Pharmacological Therapy and Additional Pharmacological Genotype Specific Therapy.....	28
Interventional Therapy.....	29
Left Cardiac Sympathetic Denervation.....	29
Implantable Cardioverter-Defibrillator (ICD).....	29
Risk Stratification.....	30
Mechanistic Link.....	31
Cardiac Action Potential.....	33
Cardiac Arrhythmic Mechanisms.....	35
Automaticity.....	36
Altered Normal Automaticity.....	36
Abnormal Automaticity.....	36
Triggered Activity.....	37
Delayed Afterdepolarisation.....	37
Early Afterdepolarisation.....	38
Re-Entry.....	39
Anatomical Re-Entry.....	39
Functional Re-Entry.....	41
Clinical Examples.....	43
Re-Entry.....	44
Sustained Monomorphic Ventricular Tachycardia.....	45

Polymorphic Ventricular Tachycardia.....	46
Ventricular Fibrillation.....	47
Mechanism of Re-Entry in TdP.....	48
Early Afterdepolarisations.....	48
Repolarisation Reserve.....	48
Source-Sink Mismatch.....	49
Cellular Mechanisms of EADs.....	50
EADs in Multi-Cellular Preparations / The Intact Heart.....	51
Calcium-Dependent Mechanisms of EADs in Multi-Cellular / Intact Heart.....	52
Models Used to Investigate LQT-Associated Arrhythmias.....	53
Pharmacological LQT Models.....	53
Transgenic LQT Models.....	54
Dispersion of Ventricular Repolarisation.....	58
The Role of $I_{CaL}$ in Arrhythmogenesis in LQTS.....	59
Hypothesis and Aims.....	60
Chapter 2: Methods.....	61
The Experimental Preparation.....	62
Intact Rabbit Heart.....	62
Langendorff-Perfusion.....	63
Methods.....	63
Perfusion System and Physiological Solution.....	64
Recording ECG Signals.....	65
Atrioventricular Node Ablation.....	66
Pacing Protocols.....	69
Viability of the Preparation.....	69
Optical Mapping.....	70
Introduction.....	70
Motion Artefact.....	70
Blebbistatin.....	71
Voltage/Calcium Sensitive Dyes.....	72
Dye Preparation.....	73
Optical System and Data Acquisition.....	74
Limitations of Optical Mapping.....	75
Experimental Protocols.....	75
Dynamic Restitution.....	77

Extra-Stimulus Restitution Protocol.....	77
LQT Pacing Protocol.....	77
Data Analysis.....	78
pECG Data.....	78
Optical Data.....	78
Analysis Measurements.....	80
Statistical Analysis.....	82
Chapter 3: Set Up of a Pharmacological LQT Model in the Intact Langendorff	
Perfused Rabbit Heart.....	83
Introduction.....	84
Pharmacological LQT Models.....	84
Effect of Cycle Length on APD.....	87
Additional Conditions to Elicit EADs.....	87
The Involvement of SR $\text{Ca}^{2+}$ or $I_{\text{CaL}}$ .....	88
Aims.....	89
Methods.....	90
Experimental Protocols.....	90
Results.....	92
Summary of Experimental Numbers.....	92
Optimising the AVN Ablation.....	93
Preparation Stability.....	94
Signal-to-Noise Ratio.....	96
Preparation Viability.....	99
Restitution Analysis.....	103
Electrophysiological Characteristics Under LQT States.....	105
Apex – Base Changes in APD.....	108
Epicardial Heterogeneity of APD.....	111
Discussion.....	113
Optimisation of AVN Ablation Technique.....	113
Preparation Viability.....	113
Restitution Analysis Overview.....	114
Electrophysiological Characteristics Under LQT States Overview.....	115
Apico-Basal APD Gradients.....	116
Comparison to Other LQT Models.....	117

Limitations.....	118
Conclusions.....	119
Chapter 4: Describing the Mechanism of Triggered Activity.....	120
Introduction.....	121
Cellular Mechanisms of EADs.....	122
Intracellular Ca <sup>2+</sup> Modulates EAD Generation During APD Prolongation.....	122
Generation of EADs in the Intact Heart.....	123
Aims.....	124
Methods.....	125
Experimental Protocols.....	125
Quantification of PVC Events.....	127
Approaching the Analysis of the Mechanism of Triggered Activity.....	129
Analysis of the Triggered Activity Mechanism.....	130
Superimposing V <sub>m</sub> Traces to Elucidate the Role of AP Gradients.....	130
Investigation of the Effects of Thapsigargin on Triggered Activity.....	131
Results.....	132
Summary of Experiments.....	132
Occurrence of PVCs and Arrhythmias.....	133
Mechanism of PVC Induction.....	140
Early Afterdepolarisations.....	141
Plateau Analysis.....	142
Amplitude Analysis.....	143
Analysis of dF/dt.....	144
Superimposed V <sub>m</sub> Traces Highlighting the Role of APD Gradients.....	145
Intracellular Calcium During PVC Initiation.....	149
The Role of Sarcoplasmic Reticulum Calcium During PVC Induction.....	152
Thapsigargin and Intracellular Calcium.....	152
Thapsigargin and APD <sub>90</sub> .....	157
Effect of Thapsigargin on Arrhythmias.....	158
Discussion.....	159
Mechanism of PVC Induction is Not Driven by Cellular EADs.....	160
PVC Initiation is Associated with Repolarisation Gradients.....	161
EADs are Driven by Intracellular Calcium.....	161

Sarcoplasmic Reticulum Calcium Inhibition Does Not Suppress EADs or PVCs.....	162
Limitations.....	163
Conclusion.....	163
Chapter 5: Role of L-Type Calcium Current.....	164
Introduction.....	165
L-Type Calcium Current .....	165
Aims.....	168
Methods.....	169
Experimental Protocols.....	169
Nifedipine Protocol.....	172
Analysis of Calcium Transient Amplitudes.....	173
Results.....	174
Effect of Nifedipine on Triggered Activity.....	174
Effect of Nifedipine on the LQT Substrate.....	178
Confirmatory Protocols.....	182
Effect of Nifedipine on Calcium Transients.....	184
Discussion.....	186
Limitations.....	187
Conclusion.....	188
Chapter 6: Discussion and Conclusions.....	189
Rationale for the Current Study.....	190
Cellular Mechanisms of AP Prolongation and EADs.....	191
Extrapolating Cellular Mechanisms to the Whole Heart.....	191
Mechanisms of TdP in the Whole Heart.....	191
Hypotheses.....	192
Designing and Characterising a LQT2 Model.....	193
PVC Initiation is Directly Associated with Steep Gradients of Repolarisation.....	194
PVCs and TdP are not Abolished by TG.....	197
PVCs and TdP are Abolished by Low-Dose Nifedipine While QT Prolongation and EADs Persist.....	197
L-Type Ca Channel Blockers in LQTS.....	198
Future Directions.....	201
Conclusions.....	202



Appendix.....	203
Introduction.....	204
Aims.....	204
Methods.....	205
Modelling Results.....	206
EADs are Not Required for PVC Capture.....	206
$I_{CaL}$ is Required for Mediating PVC Capture.....	209
PVC Capture is Abolished by Low Levels of $I_{CaL}$ Block.....	211
Discussion.....	212
References.....	213

## List of Tables

Table 1.1	Schwartz Score with 1993 – 2012 LQTS diagnostic criteria.....	26
Table 1.2	Experimental conditions associated with pharmacological rabbit LQT models used to elicit EADs.....	56- 57
Table 2.1	List of important parameters and their definitions calculated during analysis.....	81
Table 3.1	Pharmacological LQT models using Langendorff-perfused rabbit hearts and their corresponding APD values.....	85-86
Table 3.2	Summary of experimental numbers and protocols.....	92
Table 3.3	Changes in APD <sub>90</sub> at different cycle lengths and conditions.....	106
Table 4.1	Summary of experiments to induce LQT conditions and corresponding APD <sub>90</sub> values.....	132
Table 4.2	pECG analysis of arrhythmic events seen under different conditions.....	137
Table 4.3	Arrhythmic events captured on pECG and optical mapping under LQT conditions.....	138
Table 4.4	Effect of TG on 10-30% decay time.....	155
Table 4.5	Change in APD <sub>90</sub> with TG.....	158
Table 5.1	Summary of experiments used for nifedipine protocol, including change in different conditions and confirmatory subsets.....	171
Table 5.2	Effect of nifedipine on arrhythmias under LQT conditions.....	175
Table 5.3	APD <sub>90</sub> after abolition of arrhythmia by nifedipine 200nM (n=5) and 500nM (n = 6).....	181
Table 5.4	APD <sub>90</sub> dispersion after abolition of arrhythmia by nifedipine 200nM (n=5) and 500nM (n = 6).....	181

## List of Figures

Figure 1.1	pECG recording demonstrating QT prolongation.....	21
Figure 1.2	Membrane currents that generate a normal cardiac AP.....	34
Figure 1.3	Summary of arrhythmia mechanisms.....	35
Figure 1.4	Cardiac AP demonstrating a phase 2 EAD.....	38
Figure 1.5	Examples of re-entry mechanisms.....	40
Figure 1.6	Clinical example of a 12-lead ECG showing an orthodromic AVRT...	44
Figure 1.7	Clinical example of a 12-lead ECG showing sustained monomorphic VT.....	45
Figure 1.8	Clinical example of a 12-lead ECG showing polymorphic VT.....	46
Figure 1.9	Clinical example of a 12-lead ECG showing PVC-dependent induction of PVT and subsequent degeneration to VF.....	47
Figure 2.1	Diagram of the Langendorff-perfusion system.....	64
Figure 2.2	Example of custom-built ECG cradle with embedded disc electrodes...	65
Figure 2.3	Diagram of the triangle of Koch .....	67
Figure 2.4	pECG recording pre and post-AV node ablation.....	68
Figure 2.5	Spectral properties of RH237 and Rhod2 with optics used in this study.....	72
Figure 2.6	Diagram of the optical mapping system.....	74
Figure 2.7	Examples of camera alignment checks prior to each experiment.....	75
Figure 2.8	The effect of spatial averaging on optical AP rise time.....	76
Figure 2.9	Snapshots of Optiq analysis of $V_m$ and CaTs.....	79
Figure 2.10	Gaussian analysis of optical APs.....	81
Figure 3.1	Summary of experimental protocols.....	91
Figure 3.2	Number of successful AVN ablations over time.....	93
Figure 3.3	Baseline APD <sub>90</sub> , pH and temperature over time.....	95
Figure 3.4	Epicardial optical APs and corresponding CaTs .....	96
Figure 3.5	Change in signal-to-noise over the duration of a single experiment.....	97
Figure 3.6	Change in signal-to- noise over the duration of combined experiments	98
Figure 3.7	Normal vs. ischaemic optical APs and CaTs.....	100
Figure 3.8	Normal vs. ischaemic APD changes.....	100
Figure 3.9	Viability assessment taken from a single experiment.....	101
Figure 3.10	Viability parameters over time following explant.....	102
Figure 3.11	Effect of $I_{Kr}$ block on APD restitution.....	104

Figure 3.12	Examples of APs and corresponding pECGs under LQT conditions...	105
Figure 3.13	Change in APD <sub>90</sub> at during dynamic restitution protocol.....	106
Figure 3.14	Change in APD <sub>90</sub> over baseline, 50% K <sup>+</sup> /Mg <sup>2+</sup> and LQT conditions...	107
Figure 3.15	Comparison of APD <sub>90</sub> between apex and base.....	109
Figure 3.16	Comparison of APD <sub>90</sub> between apex and base under LQT conditions..	110
Figure 3.17	Variability in APD <sub>90</sub> interquartile range (IQR) under LQT conditions.	112
Figure 4.1	Diagram of experimental protocol including PCL used throughout and conditions changes over time.....	126
Figure 4.2	Identification of epicardial PVCs.....	128
Figure 4.3	Quantification of APD gradients using Lammer's inhomogeneity index (LHI).....	129
Figure 4.4	Example of superimposed V <sub>m</sub> trace analysis.....	130
Figure 4.5	Changes in QT <sub>c</sub> on pECG under LQT conditions.....	134
Figure 4.6	Example of TdP induction under LQT conditions.....	136
Figure 4.7	Quantification of ventricular arrhythmias under LQT conditions.....	138
Figure 4.8	Characteristics of mapped PVCs.....	139
Figure 4.9	Summary of earliest epicardial activation in mapped PVC episodes relative to QRS.....	139
Figure 4.10	Analysis of V <sub>m</sub> activation time and APD <sub>90</sub> for paced beat and PVC under LQT conditions.....	140
Figure 4.11	V <sub>m</sub> traces during R-on-T PVCs.....	141
Figure 4.12	Plateau analysis of PVC initiation.....	142
Figure 4.13	Amplitude analysis of PVC initiation.....	143
Figure 4.14	Analysis of dF/dt <sub>max</sub> of PVC initiation.....	144
Figure 4.15	V <sub>m</sub> -Ca <sup>2+</sup> dynamics during PVC initiation.....	146
Figure 4.16	V <sub>m</sub> trace analysis to determine the role of APD gradients in PVC initiation.....	147
Figure 4.17	Relationship between PVC upstroke, EAD and peak voltage gradient..	148
Figure 4.18	V <sub>m</sub> -Ca <sup>2+</sup> dynamics during PVC initiation.....	150
Figure 4.19	V <sub>m</sub> -Ca <sup>2+</sup> dynamics PVC initiation (2).....	151
Figure 4.20	Effects of TG on intracellular Ca <sup>2+</sup> transients.....	153
Figure 4.21	Effect of TG on CaT decay.....	154
Figure 4.22	Effect of TG on Ca <sup>2+</sup> decay time.....	155
Figure 4.23	Mean change in Ca <sup>2+</sup> F/F <sub>0</sub> over time pre- and post-TG.....	156

Figure 4.24	Effect of TG on APD under LQT conditions.....	157
Figure 5.1	Summary of experimental nifedipine and confirmatory protocols.....	172
Figure 5.2	Effect of nifedipine on the occurrence of PVCs under LQT conditions.	176
Figure 5.3	The effect of nifedipine on the proportion of paced beats with PVCs....	177
Figure 5.4	Effects of nifedipine on EADs and APD gradients.....	179
Figure 5.5	Progressive changes in APD with nifedipine.....	179
Figure 5.6	Effect of nifedipine on APD and APD dispersion under LQT conditions.....	180
Figure 5.7	Effect of high-dose E-4031 on APD <sub>90</sub> and APD <sub>90</sub> dispersion in the presence of nifedipine.....	183
Figure 5.8	Effect of nifedipine on CaTs under LQT conditions.....	185
Figure 6.1	Dose-response curves for $I_{CaL}$ block with nifedipine.....	200

## Acknowledgements

This study was funded by the British Heart Foundation and I am grateful for their generosity and to all the charity donations that made this possible. Animal work comes with its challenges and it was imperative for me that not one animal suffered during this project. None of this would be possible without their sacrifice. I hope those affected by LQT share my gratitude as we make steps towards better understanding of this tragic condition.

Rachel, I still have no idea why you agreed to take me on as your student but I'm so grateful that you did. Being the protégé of the world's greatest perfectionist is no mean feat and I stand proud as the first successful PhD student of RCM. The time you spent giving guidance, support, advice, quality control, encouragement and attention to detail is undoubtedly unmatched among your peers and I benefitted greatly. Thank you so much.

Godfrey my secondary supervisor, the EP oracle, backbone of my project and pastoral support service. Thank you. I feel privileged to join the Smith Lab. I also cannot wait for this dofetilide talk you promised.

Allen Kelly and the technicians, Mike and Aileen. Thank you for all the time you spent helping me with the experimental set up, equipment disasters, troubleshooting the rig and hardship we suffered throughout. Without you guys there's no way I'd have achieved all this beautiful data. I also don't think I'll share so many enlightening experiences in a dark room with anyone else.

Annabel, Karen, Aline, Allen (again), this PhD was full of great memories and wonderful experiences and they're all associated with you. Aline Gurgel, our friendship has enriched my life and is one of the biggest gifts this PhD has given me. You are an incredible woman, I'm so glad we met and you make me strive to be a better person. Helen and I love you all like family.

Mikela, thanks for becoming a lawyer and enabling me to print my thesis in your office (free of charge) at midnight the day before submission then walking me in to Uni to submit. You're my rock, my No. 1, my best friend. May this join a long list of achievements and memories in our lifelong friendship.

Helen, all credit from this PhD goes to you as I know it hasn't been easy. Thank you for everything from encouraging me to pursue cardiology, contacting Rachel to consider me as a student, to the rollercoaster of blood, sweat and tears we endured these past few years. Throughout this PhD we moved in together, got engaged in Bermuda, married in Norton House and as I type we're expecting our first child, you are and will always be, my greatest achievement.

## Declaration

I declare that, except where explicit reference is made to the contributions of others, that this thesis is the result of my own work and has not been submitted for any other degree at the University of Glasgow or any other institution. Cardiac explant procedures were carried out by Mr Michael Dunne and Dr Rachel Myles, both also assisted in all the optical imaging experiments. Dr Francis Burton wrote the analysis software, Optiq, used to conduct all analysis. The computer simulation data presented in the appendix was performed and analysed by Dr Martin Bishop, King's College, London, who also provided all text for the methods in this Chapter.

Cherry Alexander

### ***Publications arising from this work:***

Manuscript in preparation.

### ***Presentations of this work:***

Correlation of intracellular calcium and voltage in the intact rabbit heart under long QT conditions. **C Alexander**, FL Burton, A Kelly, GL Smith, RC Myles. Poster presentation at the European Working Group in Cardiac Cellular Electrophysiology as part of European Society of Cardiology, June 2017.

Insights into the mechanisms of triggered activity during Long QT conditions in the intact heart using optical mapping. **C Alexander**, FL Burton, GL Smith, RC Myles. Young Investigator Competition. Heart Rhythm Congress, October 2017.

## List of Abbreviations

°C	Degrees centigrade
μL	Microlitre
μM	Micromolar
1D	One dimensions
2D	Two dimensions
3D	Three dimensions
2PLSM	2-photon laser scanning microscopy
ANOVA	Analysis of variance
AP	Action potential
APD	Action potential duration
APD <sub>50:90</sub>	Ratio of APD at 50% repolarisation to 90% repolarisation
APD <sub>90</sub>	Action potential duration at 90% repolarisation
ARP	Absolute refractory period
AVN	Atrioventricular node
AVNRT	Atrioventricular nodal re-entrant tachycardia
AVRT	Atrioventricular re-entrant tachycardia
BDM	2, 3, butanedione monoxime
bpm	Beats per minute
C <sub>2</sub> H <sub>3</sub> NaO <sub>2</sub>	Sodium acetate
Ca <sup>2+</sup>	Calcium
Ca <sup>2+</sup> <sub>i</sub>	Intracellular calcium
CaCl	Calcium chloride
CaT	Calcium transient
CICR	Calcium-induced calcium release
CL	Cycle length
Cl <sup>-</sup>	Chloride
CO <sub>2</sub>	Carbon dioxide



CPVT	Catecholaminergic polymorphic ventricular tachycardia
Cs	Caesium
CT	Crista terminalis
dF/dt	Change in fluorescence over time
DM	Dichroic mirror
DMSO	Dimethylsulfoxide
ECG	Electrocardiogram
ER	Eustachian ridge
ERP	Effective refractory period
EV	Eustachian valve
F/F <sub>0</sub>	Fluorescence divided by baseline fluorescence
FO	Foramen ovale
gCaL	Maximum calcium conductance
hERG	Human ether-a-go-go gene
$I_{ACh}$	Acetylcholine induced potassium current
$I_{CaL}$	L-Type calcium current
ICD	Implantable cardioverter-defibrillator
IC <sub>50</sub>	Half-maximal inhibitory concentration
$I_{K1}$	Inwardly rectifying potassium current
$I_{Kr}$	Rapid delayed rectifying potassium current
$I_{Ks}$	Slow delayed rectifying potassium current
$I_{Na}$	Sodium current
$I_{NCx}$	Sodium – calcium exchange current
IP <sub>95</sub>	95% interpercentile range
IQR	Interquartile range
IR	Intrinsic rhythm
$I_{to}$	Transient outward potassium current
K <sup>+</sup>	Potassium

KCl	Potassium chloride
kHz	Kilohertz
kg	Kilogram
LCSD	Left cardiac sympathetic denervation
LED	Light emitting diode
LHI	Lammers inhomogeneity index
LQTS1	Long QT syndrome – type 1
LQTS2	Long QT syndrome – type 2
LQTS3	Long QT syndrome – type 3
LV	Left ventricle
MAP	Monophasic action potential
mg	Milligram
Mg <sup>2+</sup>	Magnesium
MgSO <sub>4</sub>	Magnesium sulphate
ml	Millilitre
mm	Millimetre
mmHg	Millimetres of mercury
ms	Millisecond
mV	Millivolt
Na <sup>+</sup>	Sodium
NaCl	Sodium chloride
NaH <sub>2</sub> PO <sub>4</sub>	Monosodium phosphate
NaHCO <sub>3</sub>	Sodium bicarbonate
nm	Nanometre
nM	Nanomolar
O <sub>2</sub>	Oxygen
PCL	Pacing cycle length
pEAD	Pseudo-early afterdepolarisation

pECG	Pseudo-ECG
PVC	Premature ventricular complex
QT <sub>c</sub>	Corrected QT interval
RRP	Relative refractory period
RV	Right ventricle
RVOT	Right ventricular outflow tract
SAN	Sinoatrial node
SCD	Sudden cardiac death
SD	Standard deviation
SEM	Standard error of the mean
SERCA	Sarcoplasmic reticulum calcium ATPase
SNR	Signal-to-noise ratio
SR	Sarcoplasmic reticulum
TA	Triggered activity
TAP	Transmembrane action potential
TdP	Torsades des pointes
TG	Thapsigargin
TRise	Rise time
TVA	Tricuspid valve annulus
VF	Ventricular fibrillation
V <sub>m</sub>	Membrane potential
VT	Ventricular tachycardia
WF	Wide-field

# Chapter 1: Introduction

# Long QT Syndrome

## ***What is LQTS?***

The Long QT Syndrome (LQTS) is a disorder characterised by a repolarisation abnormality in cardiac myocytes that predisposes individuals to sudden cardiac death (SCD) (Priori SG *et al*, 2001a). The condition can be inherited (*i.e.* a channelopathy) or acquired. Channelopathies are diseases caused by a disruption in ion channel subunits or the proteins that regulate them. Clinically this causes prolongation of the QT<sub>c</sub> interval on an electrocardiogram (ECG) and predisposes individuals to SCD. It does so by causing a specific form of polymorphic ventricular tachycardia (VT), called Torsades de Pointes (TdP). This form of VT has multiple ventricular foci with resultant QRS complexes varying in axis, amplitude and duration, on the ECG the complexes appear to “*twist*” around the isoelectric line, hence the name translates to “*twisting of points*”. The initiation of TdP occurs when a premature ventricular complex (PVC) occurs during the preceding T-wave, known as the R-on-T phenomenon. This arrhythmia can be non-sustained, typically causing palpitations and pre-syncope. Sustained TdP however, causes syncope, seizures or SCD. The index presentation of individuals born with this condition may indeed be cardiac arrest which is why LQT is a common cause of SCD in the young. LQT affects 1:2000 healthy live births (Schwartz PJ *et al*, 2009), however this level of prevalence only reflects individuals born with abnormally long QT intervals and does not include the number of concealed positive patients. The prevalence of LQTS is likely to rise as the guideline diagnostic criteria now includes gene positive and phenotype negative patients. The repolarisation abnormality in LQTS occurs due to an imbalance in the ionic currents which generate the cardiac action potential (AP).

## Electrocardiographic QT Interval

The QT interval is the time between the start of the QRS complex and the end of the T-wave on an ECG (typically taken from lead II, as it relates closely to the mean QT across all 12 leads – Davey PP, 2000) and represents the total duration of ventricular depolarisation and repolarisation – Figure 1.1. The QT interval is calculated by measuring the time interval between the start of the Q wave (or identification of the first pacing spike) and the end of the T wave which was defined, as per Postema PG *et al*, as the intersection of the steepest slope of the last limb of the T wave and the baseline (Postema PG *et al*, 2008).

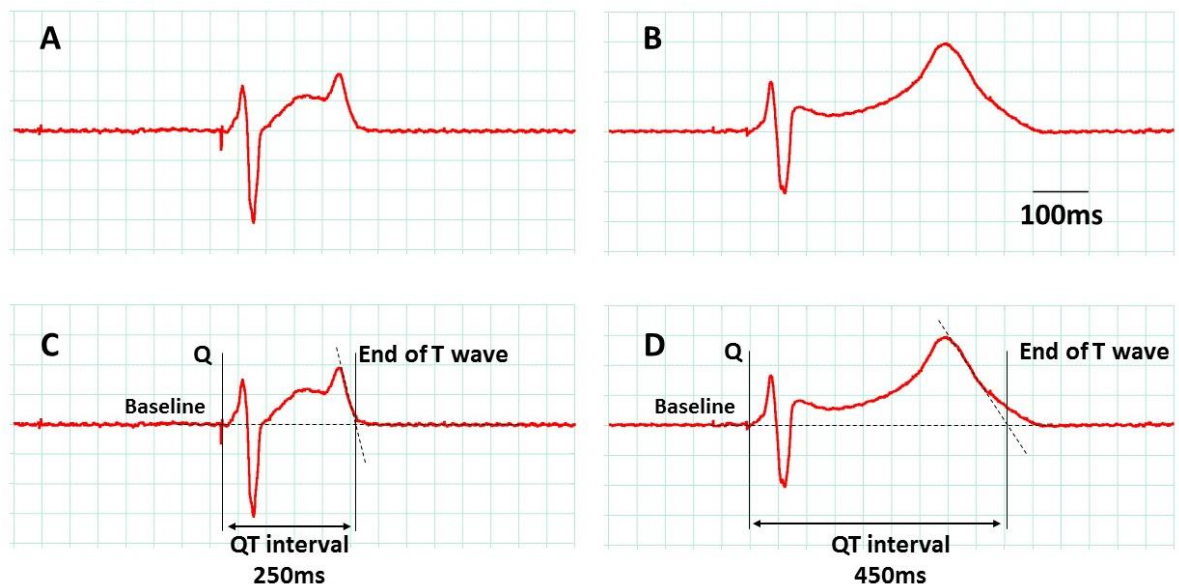


**Figure 1.1** – pECG recording demonstrating QT prolongation.

Pseudo-ECG (pECG) recordings from an intact rabbit heart, taken after atrioventricular node (AVN) ablation and paced from the left ventricular apex at 2000ms under (A) baseline and (B) LQT conditions. Accurate electrocardiographic assessment of the QT interval (Postema PG *et al*, 2008) denotes markings for QT intervals taken at (C) baseline and then prolonged under (D) LQT conditions.

The interval is dependent on heart rate (*i.e.* the faster the heart rate, the shorter the QT<sub>c</sub> interval) and should be corrected (QT<sub>c</sub>) accordingly to allow comparison of QT<sub>c</sub> values at different heart rates. This improves the detection of patients at increased risk of arrhythmias. There are various formulae in use but Bazett's formula (Bazett HC, 1920) is most common and provides adequate correction for heart rates ranging from 60-100bpm. However, it is a non-linear formula that over-corrects at faster heart rates and under-corrects for lower. A more accurate formula during the extremes of heart rate, is Fridericia's (Fridericia LS, 1920).

Bazett's formula:

$$QTc_B = \frac{QT}{\sqrt{\frac{RR}{(1s)}}}$$

Fridericia's formula:

$$QTc_F = \frac{QT}{\sqrt[3]{\frac{RR}{(1s)}}}$$

Where  $QT_c$  = corrected QT interval;  $QT$  = ECG derived QT interval;  $RR$  = ECG-derived interval between successive R waves. The QT<sub>c</sub> is measured in milliseconds (ms). Normal values are between 350 – 440ms, prolonged QT<sub>c</sub> in males is  $\geq 450$ ms and females  $\geq 480$ ms.

There are a variety of clinical circumstances that can prolong the QT<sub>c</sub> that can be either congenital or acquired. The congenital LQTS is where affected individuals inherit a cardiac channelopathy that predisposes them to LQT states. Other causes include: pharmacological agents, bradycardia, adrenergic stimulation and electrolyte abnormalities.

### **Acquired Long QT**

The  $I_{K_r}$  channel, or human ether-a-go-go gene (hERG), is inhibited by a variety of drugs which may cause acquired LQTS. For this reason, the  $I_{K_r}$  channel has become a focal point for the pharmaceutical industry when investigating new agents, to ensure there is no  $I_{K_r}$  effect that could induce acquired LQT (Thomas D *et al*, 2006; Wallis RM, 2010). The potential for compounds to inhibit this channel forms the basis of pre-clinical drug screening for QT<sub>c</sub> prolongation and TdP (Wallis R, 2010). Medications known to inhibit  $I_{K_r}$  include anti-psychotics (Suessbrich H *et al*, 1997; Thomas D *et al*, 2003a), anti-depressants

(Teschemacher AG *et al*, 1999; Thomas D *et al*, 2002), anti-histamines (Suessbrich H *et al*, 1996), anti-microbials (Kang J *et al*, 2001; Milberg P *et al*, 2002), chemotherapeutics (Thomas D *et al*, 2003b; Thomas D *et al*, 2004) and many more ([www.qtdrugs.org](http://www.qtdrugs.org)).

### *The Link Between QT<sub>c</sub> and TdP Risk*

There are multiple drugs that can prolong the QT<sub>c</sub> ([www.qtdrugs.org](http://www.qtdrugs.org)), yet not all of them cause TdP. Amiodarone is a commonly prescribed antiarrhythmic drug, that causes QT<sub>c</sub> prolongation but typically does not cause TdP. A literature review of amiodarone use made a clinical observation that amiodarone is less proarrhythmic than other QT<sub>c</sub> prolonging drugs, despite the induction of TdP associated with lesser degrees of QT<sub>c</sub> prolongation (Lazzara R, 1989). A more recent review looked at various case series to assess the cardiac safety of amiodarone, and found a low incidence of TdP with large follow-up studies reporting no cases of amiodarone-induced TdP (Connolly SJ, 1999). These suggest that for some drugs, the link between QT<sub>c</sub> and TdP is non-linear. The mechanism of action of amiodarone is complex and not fully understood, but its effects are not limited to I<sub>Kr</sub> blockade. Acutely it causes sodium (Na<sup>+</sup>), calcium (Ca<sup>2+</sup>) and I<sub>Kr</sub> channel blockade, as well as reduced conduction at the AVN (Kodama I *et al*, 1997). This multi-channel blockade prolongs both the QT<sub>c</sub> interval and refractory period (Singh BN *et al*, 1970; Mason JW *et al*, 1983).

### **Electrolyte Disturbances**

Electrolyte disturbances are recognised as having proarrhythmic potential, particularly in LQTS, either congenital or acquired. Deficiencies in either serum potassium (K<sup>+</sup>) (Helfant RH, 1986), magnesium (Mg<sup>2+</sup>) (Surawicz B *et al*, 1961; Surawicz B, 1989) and Ca<sup>2+</sup> (Sano T *et al*, 1972) are known to cause QT<sub>c</sub> prolongation and ventricular arrhythmias. A report detailing the electrophysiological effects of electrolyte disorders in normal human tissue, showed that deficiencies in either K<sup>+</sup>, Mg<sup>2+</sup> and Ca<sup>2+</sup> caused prolongation of AP duration, QT<sub>c</sub> interval on ECG and TdP (El-Sherif N *et al*, 2011). Isolated extreme electrolyte derangement may cause QT<sub>c</sub> prolongation but more often these effects are synergistic in patients with either single nucleotide polymorphisms (Schwartz PJ *et al*, 2001; Priori SG *et al*, 2013), I<sub>Kr</sub> – blocking drugs (Priori *et al*, 2015), structurally abnormal hearts or indeed heart failure (Hollifield JW, 1986; Hollifield JW, 1987; Goyal A *et al*, 2012).



## **Congenital LQTS**

Congenital LQTS affects 1:2000 births (Schwartz PJ *et al*, 2009). There are 16 distinct genes identified for LQTS, where each gene encodes a specific  $\alpha$  or axillary subunit on key ionic channels responsible for a normal cardiac AP (Schwartz *et al*, 2013). There are 3 major LQTS susceptibility genes, known as such because they are the most prevalent and account for 75% of LQT syndromes. These are KCNQ1 (LQTS1), KCNH2 (LQTS2) and SCN5A (LQTS3). A further 13 have been described and are known as the minor LQTS susceptibility genes (Splawski I *et al*, 2000; Tester DJ *et al*, 2005). These account for <5% of the clinically definite LQTS and an estimated 20% of the remaining genes are as yet unidentified.

**LQTS1** involves a loss of function mutation in the KCNQ1 gene, which is responsible for  $I_{Ks}$  and affects the pore-forming  $\alpha$ -subunit of the channel (Sanguinetti MC *et al*, 1996). The transmembrane location and degree of  $I_{Ks}$  loss are determinants of risk (Moss AJ *et al*, 2007). During increased sympathetic tone this channel is essential for maintaining AP duration and physiological  $QT_c$  shortening, *i.e.* the channel efflux increases allowing for faster repolarisation and a shorter  $QT_c$ . In patients with LQTS1 risk of arrhythmia is increased during physical and emotional stress as the  $QT_c$  interval fails to shorten (Schwartz PJ *et al*, 2001). Mutations in KCNQ1 also abolish  $I_{Ks}$  function in cochlear cells responsible for homeostasis and sound transduction, resulting in many forms of hearing loss (Wangemann P, 2006). Homozygous (or compound heterozygous) KCNQ1 mutations causes the eponymous, and extremely rare, Jervell and Lange-Nielsen syndrome (1:1,000,000 – 4,000,000 births) (Jervell A *et al*, 1957; Fraser GR *et al*, 1964; Splawski I *et al*, 1997). It is autosomal recessive and associated with extreme  $QT_c$  prolongation, high risk of SCD and bilateral sensorineural hearing loss. Heterozygous mutations cause the autosomal dominant and most common LQTS genotype, Romano-Ward syndrome (Ward OC, 1964).

**LQTS2** is caused by a heterozygous loss-of-function mutation in the KCNH2 gene, responsible for  $I_{Kr}$  and also known as hERG (Curran ME *et al*, 1995; Moss AJ *et al*, 2002; Anderson CL *et al*, 2006). Specifically, there is improper folding of the  $\alpha$ -subunits resulting in impaired trafficking of the channel to the cell surface, in turn reducing  $I_{Kr}$  channels. Loss-of-function mutations in KCHN2 result in reduction in the rapid subtype of the delayed rectifier, impairing phase 3 repolarisation and prolonging the APD. In LQTS2 patients, the

risk of arrhythmia is increased when exposed to sudden emotional or auditory stimuli, especially if suddenly woken from sleep (Schwartz PJ *et al*, 2001).

**LQTS3** is the third most common form of LQTS and unlike its counterparts, is caused by a gain-of-function genetic mutation of the SCN5A gene encoding the  $\alpha$ -subunit of  $I_{Na}$  (Wang Q *et al*, 1995; Splawski I *et al*, 2000). These mutations cause an increase in  $Na^+$  channel opening time, the net effect of this is prolongation of the APD (Bennett PB *et al*, 1995; Ruan Y *et al*, 2009). In these patients, the risk of arrhythmia is increased during periods of rest or sleep, as the  $QT_c$  typically prolongs during bradycardic states (Schwartz PJ *et al*, 2001).

## Diagnosis of Long QT Syndrome

### Diagnosis

The Schwartz Score pays particular attention to ECG findings, clinical symptoms and family history (Schwartz PJ *et al*, 1993). The score itself uses a diagnostic criteria to identify patients with a high probability of LQTS.

Findings		Points	
ECG	QT <sub>c</sub>	≥ 480ms	3
		460-479	2
		450 – 459 (males)	1
		≥ 480ms during 4 <sup>th</sup> minute of recovery from exercise	1
	TdP	2	
	T-wave alternans	1	
	Notched T-wave in 3 leads	1	
	Low heart rate for age	0.5	
<b>Clinical History</b>			
Syncope	With stress	2	
	Without stress	1	
Congenital deafness		0.5	
<b>Family History</b>			
Family members with definite LQTS		1	
Unexplained SCD at <30 years among immediate family members		0.5	

**Table 1.1.** Schwartz Score with 1993 – 2012 LQTS diagnostic criteria. Probability of LQTS based on score ≤1: low, 1.5 - 3: intermediate, ≥3.5: high. Adapted from Schwartz PJ *et al*, 2013.

The current diagnostic criteria for LQTS are (Priori SG *et al*, 2013):

1. QT prolongation  $\geq 500$ ms on ECG in the absence of a secondary cause for QT prolongation
2. Presence of a pathogenic mutation in one of the LQTS genes
3. And / or high-risk Schwartz score in the absence of secondary cause for QT prolongation
4. Unexplained syncope in patients with a QT<sub>c</sub> between 480-499ms, without a secondary cause for QT prolongation or pathogenic LQT genetic mutation

Patients with LQTS may present with symptoms of TdP, such as palpitations, pre-syncope or syncope. They may also present for routine screening after the SCD of a family member or an incidental finding after having an ECG for a different, unrelated, reason. However, the large spectrum of LQTS geno-phenotypical variability makes it a diagnostic challenge, as incomplete penetrance is common and leads to marked variation in phenotype across mutation carriers (Vincent GM *et al*, 1992). This manifests in atypical presentations, such as the asymptomatic patient with a normal/borderline QT<sub>c</sub> and no family history but still potentially at risk of TdP under specific circumstances (*e.g.* electrolyte disturbance or *I<sub>Kr</sub>* blocking drugs). Similarly, evidence suggests that the pro-arrhythmic potential of LQT-causing mutations can also be modified by the presence of common polymorphisms that affect cardiac repolarisation (Duchatelet S *et al*, 2013).

## **Management of LQTS**

### *Lifestyle Changes*

In all LQTS patients, secondary causes should be corrected such as replacing depleted electrolytes. All patients with LQTS are given recommended lifestyle changes, these include (Priori SG *et al*, 2013; Priori SG *et al*, 2015):

1. Avoidance of any QT<sub>c</sub> prolonging medications ([www.qtdrugs.org](http://www.qtdrugs.org)).
2. Maintain good hydration to prevent electrolyte abnormalities that may occur during vomiting/diarrhoea, dehydration or metabolic conditions.

### *Additional Lifestyle Changes Genotype Specific*

Geno/phenotypical targeted approaches are also adopted as a form of trigger avoidance (Guidicessi JR *et al*, 2013; Priori SG *et al*, 2013):

1. LQTS1 patients are advised to avoid extreme physical exercise and emotional stress.
2. LQTS2 should avoid sudden noises during sleep/rest such as alarm clocks (Wilde AA *et al*, 1999).
3. Females with LQTS2 have a higher arrhythmic risk (Priori SG *et al*, 2003), especially in the postpartum period (Seth R *et al*, 2007).

### *Pharmacological Therapy and Additional Pharmacological Genotype Specific Therapy*

Beta-blockade is a recognised treatment for patients with LQTS, which includes patients with a genetic diagnosis and a normal QT<sub>c</sub> (Priori SG, 2004). Beta-blockers reduce sympathetic tone, which shortens the QT<sub>c</sub> interval and are proven to reduce the incidence of arrhythmias (Priori SG *et al*, 2004). Therefore, these agents are recommended at full dose for age and weight, as tolerated. In LQTS3, a small study of 5 symptomatic patients (*i.e.* syncope or ventricular arrhythmias), were trialled with oral mexiletine in addition to beta-blocker therapy, which caused QT<sub>c</sub> shortening and abolished cardiac events (Ruan Y *et al*, 2007). A randomised, double blind, placebo-controlled trial was performed on 6 males with LQTS3, and found low-dose flecainide also reduced QT<sub>c</sub> and reduced cardiac events (Moss AJ *et al*, 2005).

### *Interventional Therapy*

Interventional options are two-fold; surgical reduction of sympathetic tone by left cardiac sympathetic denervation (LCSD) and/or prevention of SCD with an implantable cardioverter-defibrillator (ICD).

#### *Left Cardiac Sympathetic Denervation*

The surgical option of LCSD involves removal of a small portion of the intra-thoracic stellate ganglion. The LCSD technique has been shown to reduce SCD in high-risk LQTS patients (Schwartz PJ *et al*, 2004) but due to its invasive nature, it is reserved for those who cannot tolerate beta-blockers; experience ventricular arrhythmias despite optimal beta-blockade or are subject to recurrent shocks from an ICD.

#### *Implantable Cardioverter-Defibrillator (ICD)*

An ICD is recommended for (Priori SG *et al*, 2013; Priori SG *et al*, 2015):

1. Primary prevention for patients with:
  - a. recurrent syncope despite optimal medical and surgical therapy (defined as optimal beta-blockade and LCSD; or optimal beta-blockade when LCSD is not a viable option).
  - b. rare circumstances such as asymptomatic patients with extreme QT<sub>c</sub> prolongation (>550ms) with T-wave alternans on ECG who remain high risk despite optimal medical/surgical therapeutic treatment.
2. Secondary prevention for patients with a diagnosis of LQTS and survivors of a cardiac arrest.

Without question, those who have survived a cardiac arrest warrant secondary prevention ICD implantation, but for asymptomatic or low risk patients - particularly if they are young - ICD insertion requires serious consideration given their complication rates and psychological burden. Like any medical procedure, ICDs do not come without risk or unwanted effects. They have high complication rates, for example: lead displacement, pneumothorax, haematomas, infections and inappropriate shocks, ultimately leading to anxiety and a severe impact on quality of life (Ezzat VA *et al*, 2015). Studies post-ICD

found 28% of LQTS patients with an ICD experienced an inappropriate shock and 25% experienced an adverse event (Schwartz PJ *et al*, 2010).

The high rate of lead-related complications has prompted the development of new generation subcutaneous ICDs (S-ICD). These devices consist of a generator implanted in the axilla and a subcutaneous electrode tunnelled from the generator to the xiphisternum and then up the sternal edge. These devices sense an extracardiac electrogram and can deliver high-output shocks to terminate tachycardia, but are not able to provide bradycardia pacing or anti-tachycardia pacing. They are entirely out-with the vascular system and are therefore not associated with vascular damage during implantation and are less prone to infection or lead fracture (Gold MR *et al*, 2017). The major limitation of S-ICDs is the fact they are prone to T-wave oversensing and the associated risk of inappropriate shocks, which advancing technology is exploring the possibility of high pass filters to prevent this (Boersma L *et al*, 2017).

The variability in symptoms, presenting features and clinical findings of LQTS, makes the diagnosis and management challenging. Patients referred after positive genetic testing from family screening, can have LQT on ECG, or normal QT<sub>c</sub> intervals. Despite having a normal QT<sub>c</sub> interval, these patients are still diagnosed with LQTS. The QT<sub>c</sub> interval is a dynamic phenomenon, any person with a genetic mutation cannot be determined from a single normal QT<sub>c</sub> interval nor does this provide any indication of long-term risk (Zareba W, 2006). To address this, risk stratification and scoring systems have been designed to identify those at high or low risk of ventricular arrhythmia, as a means to guide management.

### ***Risk Stratification***

Individuals at the extremes of LQT, either very high or very low risk, are easier to identify and manage. Patients out-with these extremes and intermediate risk, are faced with the dilemma of prognostic uncertainty. Clinically this means patients may demonstrate QT<sub>c</sub> prolongation yet have a lifelong asymptomatic course or initial manifestations of LQT may not occur until later in life (Schwartz PJ *et al*, 1993). Untreated symptomatic patients have 20% mortality in the first year after the initial syncopal episode and approximately 50% mortality in 10 years (Schwartz PJ *et al*, 2010).

Priori *et al* developed a risk stratification scheme to identify those at risk of cardiac events (*i.e.* syncope, cardiac arrest or SCD) before the age of 40 (Priori SG *et al*, 2003). Risk groups were based on QT<sub>c</sub>, genetic locus and gender:

- **High risk (>50%):**  
QT<sub>c</sub> ≥ 500ms in LQTS1 and LQTS2 either sex; LQTS3 male sex
- **Intermediate risk (30-49%):**  
QT<sub>c</sub> ≤ 500ms LQTS2 female sex; LQTS3 either sex
- **Low risk (<30%):**  
QT<sub>c</sub> ≤ 500ms, LQTS2 male sex, LQTS1 either sex

The authors of this study concluded that prophylactic treatment with beta-blockade should be offered to all patients with a QT<sub>c</sub> ≥ 500ms with either LQTS1 or LQTS2, females with LQTS2 of any QT<sub>c</sub> duration and all patients with LQTS3. Patients who fall into a low risk category, should receive individualised treatment. Current consensus for management of LQTS state beta-blockers are recommended in all patients with a clinical diagnosis of LQTS and should be considered in carriers with a normal QT<sub>c</sub> interval (Priori SG *et al*, 2015). The Priori scheme provides clinicians with better understanding of the risk-benefit decisions and enable them to make better informed decisions on long-term management for asymptomatic patients.

Priori's identification of women with LQTS2 having higher risk regardless of QT<sub>c</sub> is congruent with experimental evidence, and indeed these patients have proven to be more at risk in the post-partum period (Seth R *et al*, 2007). Females have longer QT<sub>c</sub> intervals, greater QT prolonging effects of either drugs or bradycardia and a higher incidence of cardiac arrhythmias (Drici MD *et al*, 2001). There is a body of experimental evidence showing that oestrogens effect repolarisation and are believed to reduce repolarisation reserve (Liu T *et al*, 2005; Odening, KE *et al*, 2012). It is important to keep this in mind when conducting experimental studies as results may differ depending on the age and sex of the animals used.



## ***Mechanistic Link***

Despite these scoring systems, risk stratification is challenging and no risk stratification algorithm is perfect. The relationship between QT<sub>c</sub> and arrhythmic risk is not linear, as there are multiple factors involved. These include biological variability, such as temporal QT<sub>c</sub> variation, specific modifiers of QT<sub>c</sub> including gender, electrolytes and sympathetic status. Genetic variability is also a huge factor, which involves different ionic mechanisms for each LQTS predisposing to different levels of arrhythmic risk, depending on their interaction with biological variables, gender, as well as incomplete genetic penetrance. The mainstay of treatment for LQTS is lifestyle changes, beta-blockade and ICD implantation, neither of these treatments are curative. Even if ICDs were offered to everyone with LQTS and relieved of their complications, as well as psychological burden, they only prevent SCD and do not completely abolish arrhythmia burden.

The lack of understanding of the arrhythmia mechanisms is what underpins this problem and how QT prolongation causes TdP is not clearly understood. Further investigation into the pathophysiology of this disease would help uncover how this pro-arrhythmic substrate develops into a fatal tachyarrhythmia. Doing so would potentially lead to development of better risk stratification and novel, less invasive, therapeutic approaches with better safety profiles that could ultimately refine LQTS management. In order to develop better risk stratification and more specific therapies, there needs to be a better understanding of the arrhythmias mechanisms that cause TdP induction.

## Cardiac Action Potential

The cardiac AP is a change in voltage across the membrane of cardiomyocytes responsible for the synchronised triggering of cardiac muscle contraction. Cardiomyocytes, like skeletal muscle cells, are electrically excitable. The membrane potential ( $V_m$ ) describes the difference in the electrical potential gradient across the membrane as a consequence of transmembrane differences in ion concentrations. The predominant ions found extracellularly are  $\text{Na}^+$ , chloride ( $\text{Cl}^-$ ) and  $\text{Ca}^{2+}$ , whereas intracellularly the major cation is  $\text{K}^+$ . The normal conduction system involves propagation of depolarisation from the sinoatrial node (SAN), through the atria, to the atrio-ventricular node (AVN), down the Purkinje fibres and then ventricles. A ventricular cell responds to a propagated signal with opening of voltage-gated  $\text{Na}^+$  and then  $\text{Ca}^{2+}$  channels, leading to a rapid depolarisation.

There are 5 phases of a ventricular cardiac AP – see Figure 1.2.

- Phase 4

This starts when the cells are at rest (diastole). In this state there is balance between minimal permeabilities to  $\text{Na}^+$  and  $\text{Ca}^{2+}$  and the predominant permeability to  $\text{K}^+$  ions creating a resting  $V_m$  of approximately  $-90\text{mV}$ . This is maintained by  $\text{Na}^+\text{-K}^+$  ion exchanger pump current, forward mode  $\text{Na}^+\text{-Ca}^{2+}$  exchanger current ( $I_{\text{NCX}}$ ) to maintain the transmembrane ion concentration differences.

- Phase 0

Depolarisation propagates from adjacent cells resulting in a rapid positive change in the cell membrane. If this reaches a certain value, known as the threshold potential at  $\sim -70\text{mV}$ , it activates voltage-gated  $\text{Na}^+$  channels ( $I_{\text{Na}}$ ) resulting in a rapid depolarisation.

- Phase 1

At  $\sim 30\text{-}50\text{mV}$ , inward  $I_{\text{Na}}$  begins to inactivate and transient outward  $I_{\text{to}}$  potassium channels briefly open. This forces the  $V_m$  slightly negative, giving the ventricular AP a characteristic notched appearance.

- Phase 2

Depolarisation activates the L-type  $\text{Ca}^{2+}$  channel (LTCC) producing  $I_{\text{CaL}}$  allowing an influx of  $\text{Ca}^{2+}$  and maintains depolarisation during the plateau phase. This triggers ryanodine receptors on the sarcoplasmic reticulum (SR) membrane to release their

$\text{Ca}^{2+}$  stores, creating a positive feedback response known as  $\text{Ca}^{2+}$  induced  $\text{Ca}^{2+}$  release (CICR). This cascade of events is responsible for excitation-contraction coupling, that facilitates cardiomyocyte muscle contraction. This phase concludes with removal of cytosolic  $\text{Ca}^{2+}$ . This is coordinated by the SR  $\text{Ca}^{2+}$  ATPase (SERCA) pump moving cytosolic  $\text{Ca}^{2+}$  back into the SR; a net inward current of forward flowing  $I_{\text{NCX}}$  removing  $\text{Ca}^{2+}$  by exchanging three  $\text{Na}^+$  (in) for one  $\text{Ca}^{2+}$  (out); and late activation of  $\text{K}^+$  channels generating a rapid repolarisation.

- Phase 3

Repolarisation occurs through the delayed  $\text{K}^+$  rectifier current, comprised of a combination of  $I_{\text{Ks}}$  and  $I_{\text{Kr}}$ . These allow the efflux of  $\text{K}^+$ , causing a net outward current, restoring the resting  $V_m$  to  $-90\text{mV}$ . During repolarisation, before the resting  $V_m$  is achieved, there is a period where it is impossible to evoke an AP. This is known as the absolute refractory period (ARP). After this time, as  $V_m$  gradually returns to baseline, cells hyperpolarise from the continued extracellular flow of  $\text{K}^+$ . Initiation of a second AP can be elicited by a larger stimulus. This is known as the relative refractory period (RRP).

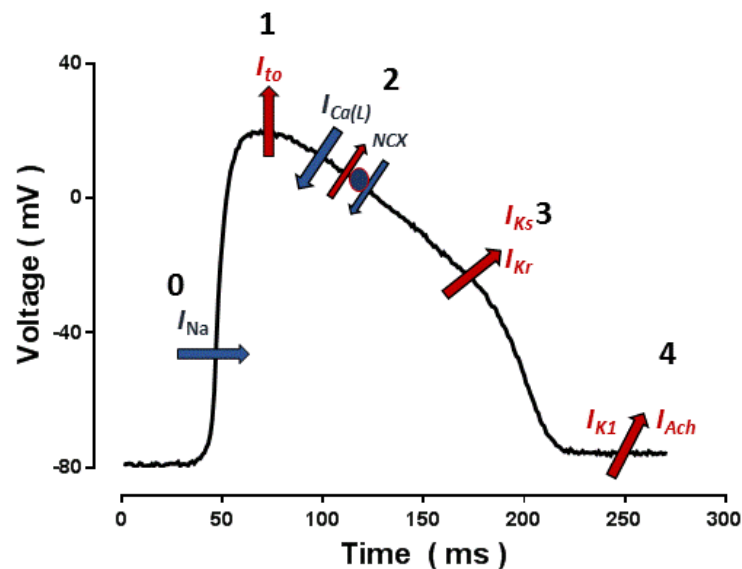


**Figure 1.2.** Membrane currents that generate a normal cardiac AP.

Inward currents denoted by blue arrows and outward currents are in red. The AP duration (APD) is approximately 150ms. The AP used in this example was taken from widefield optical recording from the surface of an isolated rabbit heart and therefore lacks the typical notched AP appearance.

## Cardiac Arrhythmia Mechanisms

A cardiac arrhythmia is defined as an abnormality in the heart rhythm. In normal sinus rhythm, the depolarising wavefront originates from the SAN, depolarises the atria and then conducts between the atrium and the ventricles via the AVN. Heart rate is therefore controlled by the SAN and regulated by the autonomic nervous systems and circulating catecholamines via effects on beta-adrenergic stimulation. There are three recognised mechanisms for arrhythmia (summarised in Figure 1.3):

1. Automaticity
2. Triggered activity
3. Re-entry

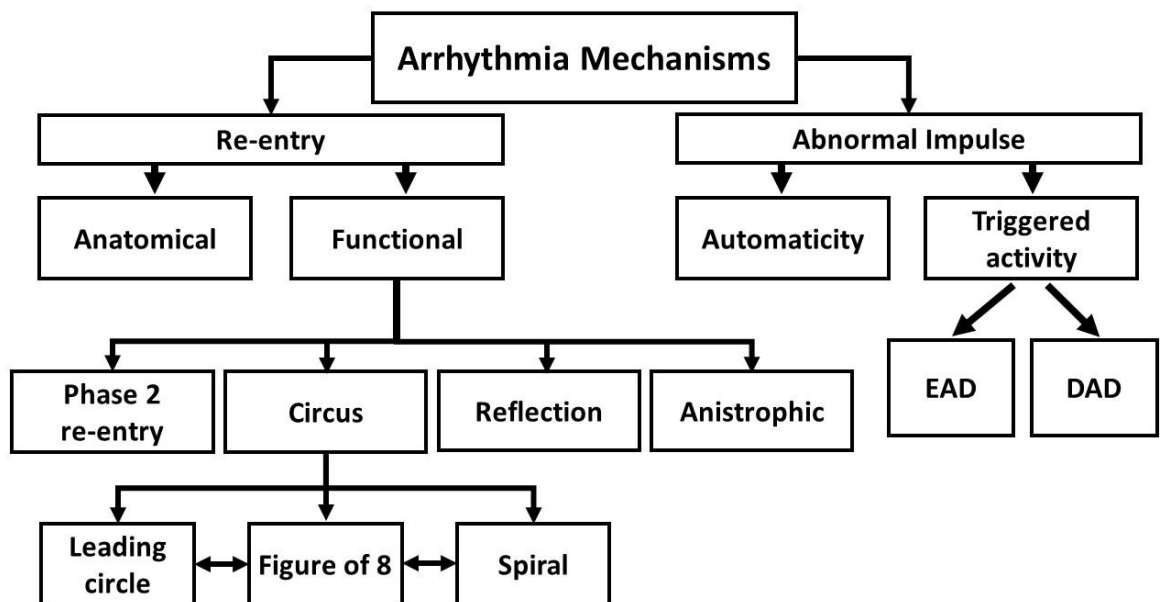


**Figure 1.3.** Summary of arrhythmia mechanisms.

## ***Automaticity***

The SAN is the dominant pacemaker of the heart and normally has the fastest intrinsic rate. If this fails or its impulses are unable to propagate, the subsidiary pacemakers take over. These are known as the AVN and Purkinje cells, both capable of generating automatic activity. If the normal conduction system is either suppressed or enhanced, this can lead to clinical arrhythmias.

### *Altered Normal Automaticity*

Altered normal automaticity can be a normal physiological process, such as sinus tachycardia associated from increased sympathetic tone during exercise, or a normal response to fever or thyrotoxicosis. It can also be pathophysiological during electrolyte disturbance, ischaemia or hypoxia (Jalife J *et al*, 2011). During states of acute myocardial infarction, digitalis toxicity, recent cardiac surgery and isoprenaline infusion, the AVN rate can discharge faster than the SAN. This causes an accelerated junctional rhythm (de Azevodo IM *et al*, 1973). Overall clinical arrhythmias arising by this mechanism are sinus tachycardia or accelerated AV junctional rhythm. Neither are malignant or life-threatening.

### *Abnormal Automaticity*

Ventricular myocytes typically do not spontaneously depolarise or demonstrate automaticity, this is due to the hierarchy of intrinsic automaticity and overdrive suppression from the SAN, however each part of the conduction system has the potential to spontaneously depolarise. In the event a collection of either atrial or ventricular cells depolarise faster than the SAN, their depolarising wavefront will conduct through the heart. This occurs under conditions that drive the diastolic potential towards the  $V_m$  threshold potential, typically under states of elevated extracellular  $K^+$ , low intracellular pH and catecholamine excess. Clinical arrhythmias arising by this mechanism are premature beats, atrial tachycardia and accelerated idioventricular rhythms.

## ***Triggered Activity***

Triggered activity (TA) is the generation of an abnormal depolarisation that is dependent on, and arises from, an imbalance that occurs during the previous AP. These can either be before, or after the AP has completely repolarised. There are two forms of TA: early afterdepolarisations (EADs) which occur during phase 2 or 3 of the cardiac AP and interrupt repolarisation; and delayed afterdepolarisations (DADs) which occur during phase 4 of the cardiac AP, once repolarisation is complete. Repetitive TA is the mechanism for right ventricular outflow tract (RVOT) VT, causing monomorphic VT that can be mapped to a single point and abolished with focal ablation. Catecholaminergic polymorphic ventricular tachycardia (CPVT) is also caused by repetitive TA.

### *Delayed Afterdepolarisations*

It is widely accepted that DADs are caused by spontaneous SR  $\text{Ca}^{2+}$  release under conditions that favour intracellular  $\text{Ca}^{2+}$  loading. This has been elicited experimentally by using high  $\text{Ca}^{2+}$  and low  $\text{K}^{+}$  in the perfusate (Miura M *et al*, 1995), pharmacological methods with fast pacing with cardiac glycosides (Zu J *et al*, 1996) or catecholamines (Marchi S *et al*, 1991; Janiak R *et al*, 1996), as well as the complex syndrome in heart failure with myocardial remodelling or alteration in  $\text{Ca}^{2+}$  homeostasis (Priori SG *et al*, 1990; Bers DM, 2006). All of these increase intracellular  $\text{Ca}^{2+}$  levels and SR load, leading to spontaneous release during diastole. This can cause either a localised release of  $\text{Ca}^{2+}$  with limited or no propagation, or if large enough, a propagation of a new depolarisation wave throughout the whole cell. Examples of DAD-induced arrhythmia include catecholamine-induced VT/VF (Nam GB *et al*, 2005) and CPVT caused by a mutation in the ryanodine receptor rendering it leaky, that is exacerbated during catecholamine stimulation (Priori SG *et al*, 2001). Also, reduction in the activity of the  $\text{Na}^{+}/\text{K}^{+}$  pump with digoxin prevents  $\text{Ca}^{2+}$  release and has been shown to cause DADs (Rosen MR, 1985), at toxic levels these can cause bidirectional fascicular tachycardia (Wieland JM *et al*, 1986).

### *Early Afterdepolarisations*

EADs are cellular events during which the normal balance of ionic currents is disrupted to produce an abnormal depolarisation before the AP has completely repolarised (Weiss JN *et al*, 2010) – see Figure 1.4. EADs can occur during phase 2 or 3 of the cardiac AP, are facilitated by prolongation of the APD (Daminao BP *et al*, 1984) and can produce triggered APs in single cells. These triggered APs are thought to be responsible for the induction of life-threatening TdP/VT in states of LQT (Cranefield PF, 1977; Roden DM, 1993; Kannankeril PJ *et al*, 2007). There is a strong correlation between the conditions required to induce EADs and the occurrence of TdP/VT, which implies there is a mechanistic link. To date, the exact mechanism for how EADs can cause a sustained ventricular arrhythmia is unclear.

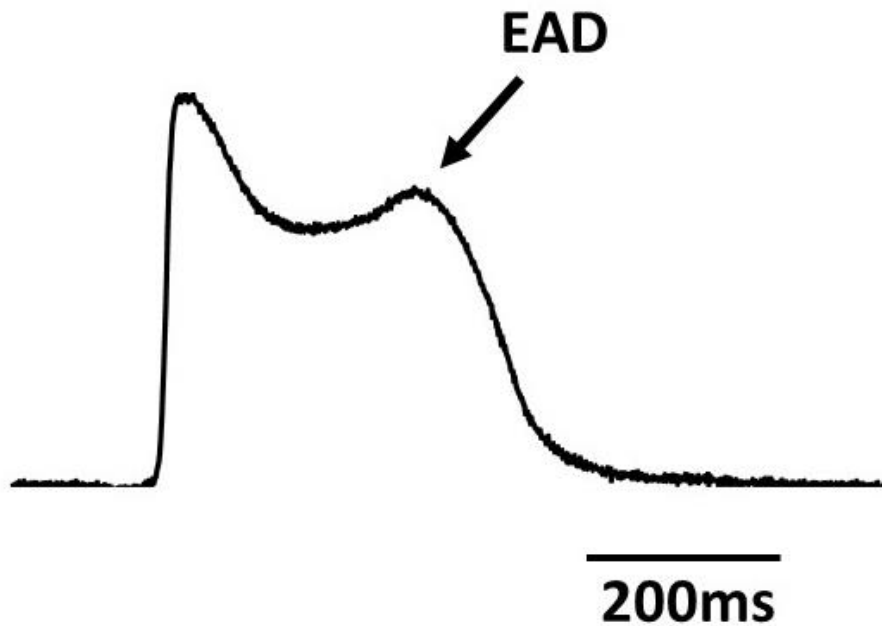


**Figure 1.4.** Cardiac AP demonstrating a phase 2 EAD.

Prolonged cardiac AP, the APD is approximately 400ms, with a depolarisation before the AP has completely repolarised and demonstrating a phase 2 EAD. The AP used in this example was taken from wide-field optical recording from the surface of an isolated rabbit heart.

## ***Re-Entry***

Normal electrical activity during cardiac conduction initiates in the SAN and propagates through the entire heart until all the fibres are refractory and the impulse dies out. Re-entry is when a region of cells either: fail to activate from the initial wavefront and retain their excitability, or fail to completely repolarise by the time neighbouring cells have. This cluster can re-activate a neighbouring region that has recovered from refractoriness and trigger a new AP. Re-entry describes continual re-activation of the ventricular tissue and is the most common mechanism in clinical arrhythmias. It involves propagation of an impulse around either an anatomical or functional obstacle that causes circuitous re-excitation of the heart. Conditions which may induce re-entry include an area of unexcitable tissue, unidirectional conduction block, a delay in the circulating wavefront from sufficiently slowed condition to allow the tissue proximal to the site of unidirectional block to recover, an area of excitable myocardium between the tail of the preceding wavefront and the head of the re-entrant wave, a critical mass of tissue able to sustain re-entrant wavefront and a trigger. Re-entry mechanisms are divided into two separate groups:

1. Anatomical
2. Functional

### *Anatomical Re-Entry*

Anatomical re-entry is also known as classical re-entry. The typical description is of a circular pathway surrounding an area of in-excitable tissue, see Figure 1.5A. When the impulse arrives at this obstacle, it splits in two. If the impulse in one limb of the circuit (a) encounters an area of unidirectional block (b), then excitation propagated from the other limb can excite that area from the other direction (c). If the area proximal to the unidirectional block has had sufficient time to recover from the initial activation, then the impulse will “re-enter” the circuit (d) thus allowing continual excitation within the circuit. Clinical examples of this include AV re-entrant tachycardia (AVRT), AV nodal re-entrant tachycardia (AVNRT) and atrial flutter. In patients with structurally normal hearts, these arrhythmias are typically benign and do not cause haemodynamic compromise. A more malignant arrhythmia caused by anatomical re-entry is post-infarction VT.



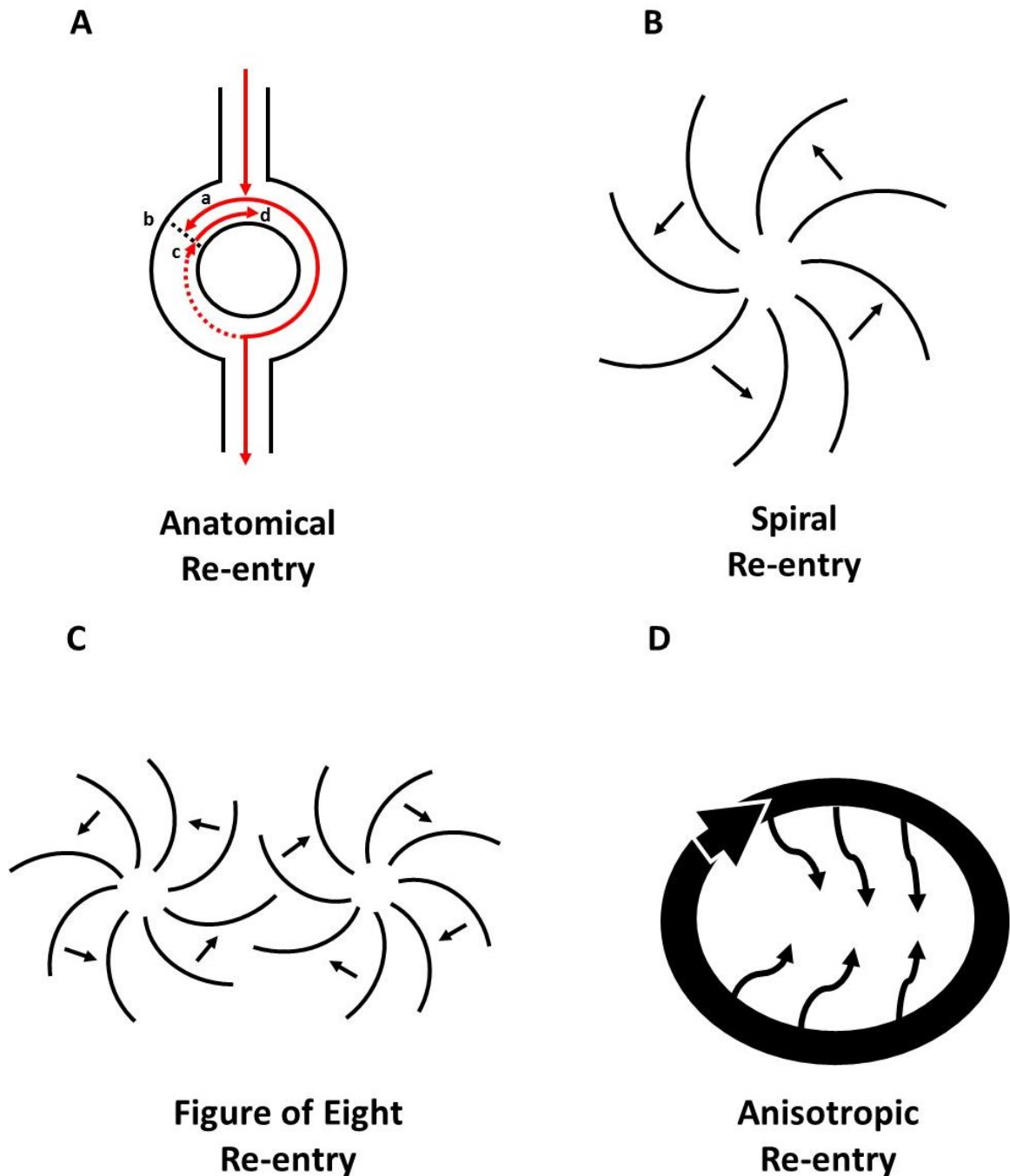


**Figure 1.5.** Examples of re-entry mechanisms.

(A) Anatomical re-entry requires an arriving impulse to meet in-excitable tissue that causes unidirectional block and slow conduction allows re-entry through the other pathway. (B) Spiral wave re-entry activation around an excitable core that is not excited. (C) Figure-of-eight re-entry with two circulating spirals in opposite directions. (D) Anisotropic re-entry from heterogeneity in impulse propagation and smaller, slowly conducting anatomical circuits.

### *Functional Re-Entry*

In functional re-entry, the circuit is not determined by anatomic obstacles, instead it is determined by spatiotemporal heterogeneities of the electrophysiological properties of the myocardium. These include conduction velocity, dispersion of repolarisation and regional areas of block. Fibre orientation can also contribute to functional re-entry. Gap junctions are preferentially distributed on the longitudinal axis of cardiac myocytes, compared to the transverse axis. This means the longitudinal conduction velocity is greater than transverse, resulting in anisotropic conduction in ventricular myocardium.

The major mechanisms of functional re-entry include – Figure 1.5:

1. Spiral (also known as rotor) Wave Re-Entry

Continual activation is anchored around an excitable core that remains in-excited, forming a spiral. Spirals can be independent of each other, migrate around the heart or remain static (Davidenko JM *et al*, 1990; Pertsov AM *et al*, 1993; Issa ZF *et al*, 2009), Figure 1.5B. This pattern of activity has been observed during monomorphic and polymorphic VT, and ventricular fibrillation (VF) (Gray RA *et al*, 1995). Monomorphic VT, the spiral wave is anchored to a fixed point whereas in polymorphic VT the spiral wave travels across the myocardium. During VF, the spiral waves can break up into multiple waves, continuously extinguishing and re-forming.

2. Figure of Eight Re-Entry

Two separate co-existing wavefronts that circulate in opposite directions (clockwise vs. counter-clockwise) around two arcs that can block each other or merge into a central pathway –Figure 1.5C. This type of re-entry arrhythmia is seen during post-infarction VT (El-Sherif N *et al*, 1981; Gaztañaga L *et al*, 2012).

3. Anisotropic Re-Entry

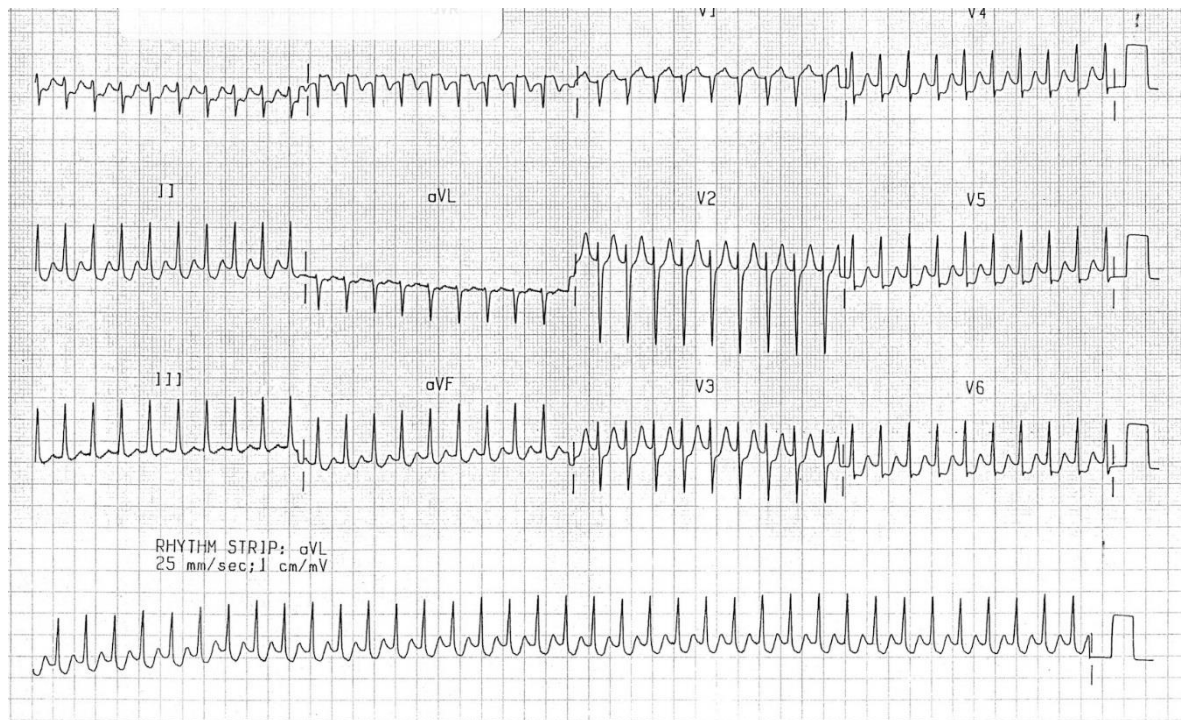
Anisotropy is the variety seen in physical properties along different axis in different substances. Cardiac myocytes are arranged in fibres along their long axis. Anisotropic conduction means that fibre orientation in cardiac tissue can cause heterogeneity in repolarisation and conduction velocities. This can result in slowed

conduction or blocked impulses and allows re-entry in small anatomical circuits, Figure 1.5D. This type of re-entry is seen in VT originating in surviving myocardial tissue following MI (Spach MS *et al*, 1994).

Less typical forms of functional re-entry include reflection and phase 2 re-entry, both of which have been seen experimentally to produce local re-excitation and a PVC. Reflection has been seen in a linear segment of cardiac tissue, where a slow anterograde wave front travels proximally and is followed by a retrograde impulse producing a return PVC (Antzelevitch C, 2001). Phase 2 re-entry has been seen in sheets of myocardial tissue with regional conduction delays and heterogeneous repolarisation, that create areas of longer APD that depolarise in to neighbouring regions and induce local re-excitation and a PVC (Lukas A *et al*, 1996). Reflection and phase 2 are theoretical forms of re-entry and whether these can be elicited in a whole heart to induce sustained arrhythmias is yet to be shown.

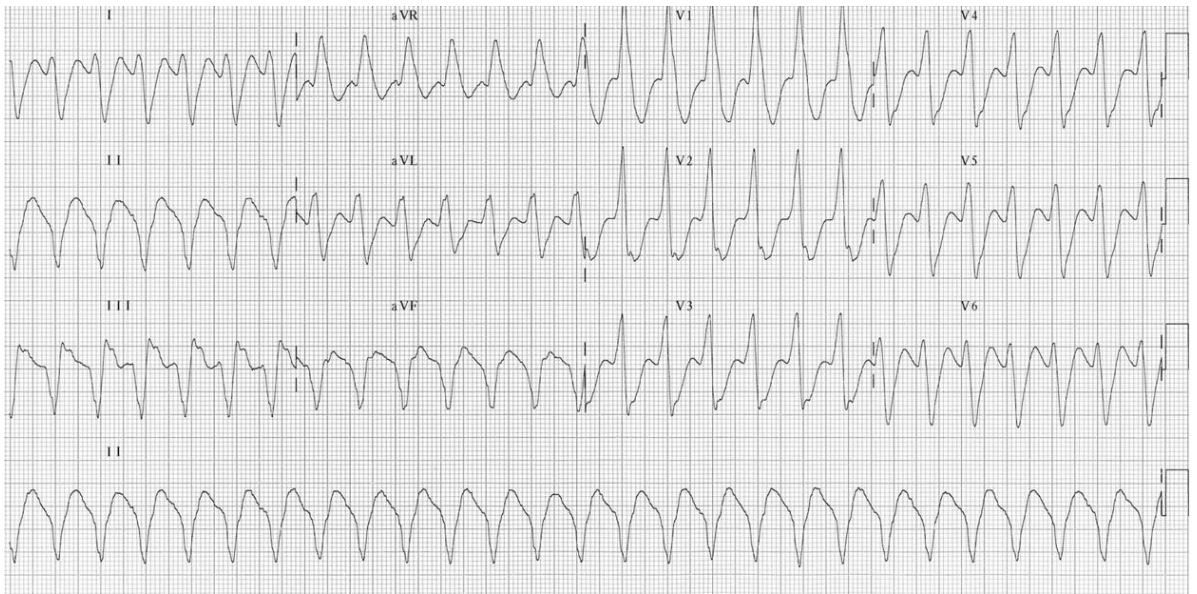
### ***Clinical Examples***

Anatomical re-entry is the underlying cause of AVNRT or AVRT, clinically this causes a regular, narrow complex tachycardia without discernible P waves on a 12-lead ECG. In AVNRT, unless there is underlying bundle branch block, the QRS complexes are narrow. In AVRT, the QRS configuration depends on the direction of the circuit, if it is orthodromic and conducting through the AVN, then the QRS will be narrow. If it is antidromic, then the QRS will be broad. An example of this is shown in Figure 1.6. Functional spiral re-entry can cause sustained monomorphic VT, polymorphic VT and VF. Monomorphic VT appears as a broad complex tachycardia with the same morphology and axis, Figure 1.7. Polymorphic VT is described as a broad complex tachycardia with a characteristic twisting morphology, where the QRS is thought to “twist” around the isoelectric line, Figure 1.8. This is typically initiated by a R-on-T phenomenon, where a PVC occurs on the preceding T-wave. Ventricular fibrillation creates chaotic and irregular deflections of variable amplitude with no identifiable P waves, Figure 1.9.

*Re-Entry*

**Figure 1.6.** Clinical example of a 12-lead ECG showing an orthodromic AVRT.

*Reproduced with permission from Life in the Fast Lane, licensed under a Create Commons Attribution-NonCommercial-ShareAlike 4.0 International Licence (<https://litfl.com/wp-content/uploads/2018/08/Orthodromic-AVRT-1.jpg>).*

*Sustained Monomorphic Ventricular Tachycardia*

**Figure 1.7.** Clinical example of a 12-lead ECG showing sustained monomorphic VT.

VT is determined from broad QRS complexes, abnormal axis with monomorphic morphology, AV dissociation with possible superimposed P waves in lead aVF.

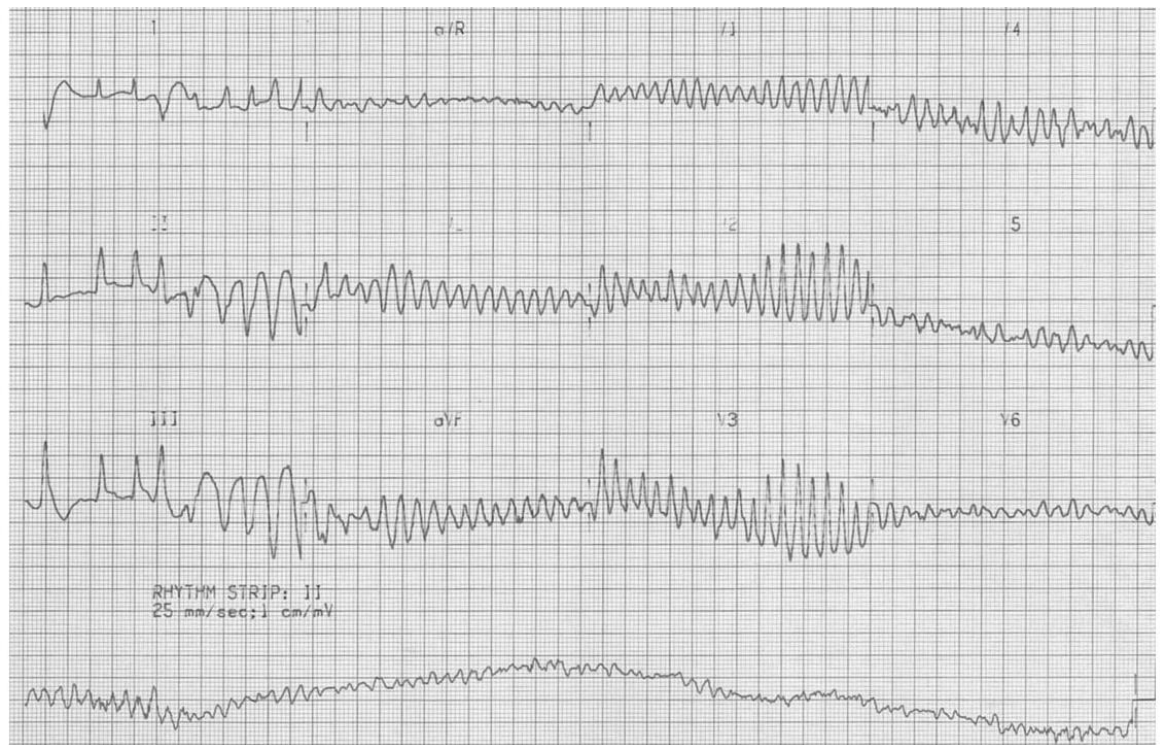
*Reproduced with permission from Life in the Fast Lane, licensed under a Create Commons Attribution-NonCommercial-ShareAlike 4.0 International Licence (<https://litfl.com/wp-content/uploads/2018/08/Monomorphic-ventricular-tachycardia-VT-3.jpg>).*

*Polymorphic Ventricular Tachycardia*

**Figure 1.8.** Clinical example of a 12-lead ECG showing polymorphic VT.

This rhythm starts off as sinus rhythm until beat 9 of the rhythm strip, where a PVC occurs at the end of the preceding T-wave, causing the R-on-T phenomenon and inducing polymorphic VT.

*Reproduced with permission from Life in the Fast Lane, licensed under a Create Commons Attribution-NonCommercial-ShareAlike 4.0 International Licence (<https://litfl.com/wp-content/uploads/2018/08/ECG-hypokalaemia-torsades-2.jpg>).*

*Ventricular Fibrillation*

**Figure 1.9.** Clinical example of a 12-lead ECG showing PVC-dependent induction of PVT and subsequent degeneration to VF.

There is a R-on-T phenomenon at the fourth beat, which degenerates into PVT and then quickly to VF. VF is determined by chaotic and irregular deflections of varying amplitude.

*Reproduced with permission from Life in the Fast Lane, licensed under a Create Commons Attribution-NonCommercial-ShareAlike 4.0 International Licence (<https://litfl.com/wp-content/uploads/2018/08/ECG-Ventricular-fibrillation-VF-original-VF-VT.jpeg>).*



## ***Mechanism of Re-Entry in TdP***

Originally it was hypothesised the mechanism of TdP was two or more foci firing at different frequencies, which created the ‘*typical twisting of the points*’ describing the continual variation in QRS width and axis (Dessertenne F, 1966). Subsequent studies suggested that TdP is caused by a wandering re-entrant wave created under conditions of prolonged APD and APD dispersion (Abildskov JA *et al*, 2000). It has been suggested TdP is initiated by a focal beat from EADs that occur under reduced repolarisation reserve (Asano Y *et al*, 1997; Choi BR *et al*, 2002) but how these foci can propagate to maintain TdP is not clear. There is debate whether a focal mechanism (*e.g.* TA) (Kim TY *et al*, 2015) can initiate TdP or whether meandering re-entry waves are responsible (El-Sherif N *et al*, 1997). More recently, a study using chronic AVN block in dogs used needle electrodes to record electrograms and found every episode of TdP was generated by a focal mechanism (Vandersickel N *et al*, 2017). They suggested both mechanisms are possible and found spontaneously terminating TdP was perpetuated by focal activity, sustained TdP was perpetuated by re-entry and spontaneously terminating TdP had mixed focal activity and re-entry. The same author used computer modelling studies to corroborate this work (Vandersickel N *et al*, 2016). Therapeutic steps to abolish this process involve either abolition of the foci, and so EADs or PVCs themselves; stopping the PVCs interacting with the re-entrant substrate that promotes sustained re-entry or removing the re-entrant substrate if one does exist. To explore this process, what is known about mechanisms of EADs and the LQT substrate must be considered in both cellular and whole heart preparations.

## **Early Afterdepolarisations**

### ***Repolarisation Reserve***

When ionic currents in cardiac myocytes are altered, they possess the ability to compensate by dynamically adjusting alternate currents to minimise APD changes. This is known as repolarisation reserve (Roden DM, 1998; Weiss JN *et al*, 2010). A pre-requisite for cells to experience an EAD, APD prolongation must occur in the setting of reduced repolarisation reserve, where there is either a delay in inactivation of inward Na<sup>+</sup> (Boutijdir *et al*, 1991) or Ca<sup>2+</sup> (January CT *et al*, 1989) currents, or by a reduction in outward K<sup>+</sup> currents (*e.g.* in LQT conditions), or both. Bradycardia causes time-dependent channels like  $I_{Ks}$  to enter a deeply-

closed state, that requires more time for subsequent activation, which is why EADs are typically generated at slow CLs (Silva J *et al*, 2005). Other factors proven to affect repolarisation reserve include adrenergic stimulation (Drouin E *et al*, 1996), hypokalaemia, hypomagnesaemia (Carmeliet EE, 1961), hypocalcaemia (Sano T *et al*, 1972), acidosis (Rozanski GJ *et al*, 1991), hypoxia (Gaur N *et al*, 2009) and many QT<sub>c</sub> prolonging drugs. Ultimately the net outward current required to repolarise the myocyte is compromised and the ability to resist depolarising currents is reduced, and under conditions of APD prolongation there is potential for EAD generation.

### **Source-Sink Mismatch**

Cardiac myocytes are electronically coupled, meaning their cytosolic contents are directly connected with their neighbours through electrical synapses and gap junctions. This allows direct transference of electrical and chemical signals between all coupled cells. The source-sink relationship is the interplay between the “source” (*e.g.* a focal depolarisation) with the surrounding repolarised myocardium known as the “sink”. This is a fundamental difference between isolated myocytes versus the same cell within an intact heart, where neighbouring cells provide an electrotonic sink which will resist any perturbation of  $V_m$  in an isolated cell (Hoyt RH *et al*, 1989; Houser SR, 2000). For a single cell to propagate an abnormal AP, the source density must be large enough to bring the sink to activation threshold. Computer models estimate hundreds of thousands of cells must simultaneously experience an EAD for a single PVC to propagate (Xie Y *et al*, 2010). Stochastic EADs are believed to be random events within cells and whether stochastic events such as these can become spatially synchronised under pathophysiological LQT conditions in the intact heart is unknown. Previous work has shown that spontaneous diastolic  $Ca^{2+}$  release can trigger SR  $Ca^{2+}$  release in adjacent cells, therefore changes in intracellular  $Ca^{2+}$  may explain the synchronising events across a critical volume of tissue (Li Y *et al*, 2012). Overall, if a sufficiently large enough number of cells produce EADs, it produces a depolarising current which is large enough to overcome the source-sink mismatch and provoke a new AP.

## **Cellular Mechanisms of EADs**

Various methods have been used to study the cellular mechanisms involved in the generation of EADs. These include patch clamping (Miura M *et al*, 1995; Studenik CR *et al*, 2001) and monophasic action potential recording (MAPs) (Patterson E *et al*, 1990), each using isolated cells or tissue from various species (*e.g.* rabbit, guinea pig, dog, human *etc*).

At an ionic level, EADs can arise from an imbalance in repolarisation resulting either from disruption of inward or outward currents, or from a combination of the two. To elicit this, experimentation using pharmacological agents to cause single current alterations that impact repolarisation was attempted on  $I_{Na}$ ,  $I_{CaL}$  and  $I_{Kr}$ . EADs were induced from  $I_{Na}$  inactivation using sea anemone ATXII on canine endocardial preparations (Boutjdir M *et al*, 1991);  $I_{Kr}$  blockade using almokalant on Purkinje fibres and ventricular cells of rabbits and cats caused  $QT_c$  prolongation and TdP (Carlsson L *et al*, 1993) and  $Ca^{2+}$  agonist, BAY K 8644 induced EADs in voltage clamped sheep Purkinje fibres that were abolished using a LTCC blocker, nitrendipine (January CT *et al*, 1989). Major emphasis was placed on currents responsible for the EAD upstroke with the potential to create a regenerative inward current, the most evidence for this was found in reactivating  $I_{CaL}$ . Early studies using ferret ventricular muscle found BAY K 8644 potentiated EADs that were abolished using LTCC blockade with nitrendipine, thus identifying  $I_{CaL}$ 's importance (Marban E *et al*, 1986). January CT *et al*, elucidated this further, using BAY K 8644, and concluded EADs are dependent on  $I_{CaL}$  for depolarisation (January CT *et al*, 1989; January CT *et al*, 1990; January CT *et al*, 1991).

The voltage range at which EADs occur, also supports the theory that  $I_{CaL}$  could be responsible. EADs occur during phase 2 or 3 of the AP, this voltage range is typically -40 – 0mV. The major inward currents at this voltage are  $I_{CaL}$  and  $I_{NCX}$ , and major outward currents are the delayed rectifier ( $I_{Ks}$  and  $I_{Kr}$ ). In this period, if  $I_{CaL}$  generates enough depolarisation it can trigger a secondary release of SR  $Ca^{2+}$  changing the  $I_{NCX}$  transporter to inward movement and can induce an EAD (Szabo B *et al*, 1994; Sipido KR *et al*, 1997). However, if  $I_{Ks}$  and  $I_{Kr}$  generate enough outward current then the myocyte will eventually repolarise as normal. During this window, the generation of either inward or outward current is described as moving in a state of dynamic chaos, where conditions can generate EADs and others do not (Qu Z *et al*, 2013).

Other lines of evidence suggest that TA induced by EADs is dependent on intracellular  $\text{Ca}^{2+}$ . Sudden changes in  $\text{Ca}^{2+}$  homeostasis from rapid pacing, rate acceleration during bradycardia or adrenergic stimulation have shown to induce EADs (Damiano BP *et al*, 1984). Any intervention blocking  $I_{\text{NCX}}$  has shown to inhibit EAD generation (Priori SG *et al*, 1990). One study using isoproterenol induced EADs and DADs, found they have a shared mechanism involving cellular  $\text{Ca}^{2+}$  overload and spontaneous SR  $\text{Ca}^{2+}$  release (Volders PG *et al*, 1997). This study also showed raised adrenergic tone increases intracellular  $\text{Ca}^{2+}$  and SR  $\text{Ca}^{2+}$  load, which directly increases the incidence of EADs. Thus, implying SR  $\text{Ca}^{2+}$  has a significant role in the mechanism of EADs.

### ***EADs in Multi-Cellular Preparations / The Intact Heart***

Studies investigating the mechanisms of EADs in whole hearts is necessary given the electrophysiological differences between isolated cells and multi-cellular preparations. It is also crucial when considering key concepts such as source-sink mismatch and repolarisation reserve. The first intact heart preparation elicited both EADs and DADs using caesium (Cs) to block  $\text{K}^+$  channels and cause APD prolongation, where DADs occurred at shorter APDs and EADs during longer (Patterson E *et al*, 1990). This was consistent in future studies, that also demonstrated the simultaneous appearance of both EADs and DADs under similar conditions (Xie JT *et al*, 1992; Xu J *et al*, 1996). This suggests there are similarities in cellular mechanisms to elicit TA. As discussed previously, DADs are known to be caused by spontaneous SR  $\text{Ca}^{2+}$  release under conditions that favour intracellular  $\text{Ca}^{2+}$  loading (Triggered Activity, pp. 37). A model using chronic AV block in anaesthetised dogs elicited EADs, from bradycardia, *d*-sotalol or almokalant and burst pacing (Verduyn SC *et al*, 1995). This model used ECG and MAP analysis to review the effects of ryanodine, it found *d*-sotalol prolonged  $\text{QT}_c$  and ryanodine administration caused  $\text{QT}_c$  shortening. No MAP values were taken during this study. Overall EADs were abolished with ryanodine administration, again suggestive of a SR  $\text{Ca}^{2+}$ -dependent mechanism for the induction of EAD-dependent TdP.

## ***Calcium-Dependent Mechanisms of EADs in Multi-Cellular / Intact Heart***

Cardiac Purkinje fibres from dogs and guinea pigs were used to reproduce LQT conditions using 50%  $K^+$ , Cs to facilitate reduction in  $K^+$  currents and paced at slow pacing cycle lengths (PCLs). Under these conditions, preparations were loaded with  $Ca^{2+}$  and an  $I_{NCX}$  blocker, ouabain which reduced  $I_{NCX}$  and SR  $Ca^{2+}$  release and doing so prevented the induction of EADs (Szabo B *et al*, 1995). A similar study using canine Purkinje fibres and enzymatically dispersed sub-epicardium cardiomyocytes elicited EADs using  $K^+$  channel blockers, clofilium and *d*-sotalol (Patterson E *et al*, 1997). EADs were still prominent after treatment with nifedipine, which implies  $I_{NCX}$  and SR  $Ca^{2+}$  are responsible for triggering EADs and not  $I_{CaL}$ . Anaesthetised dogs with chronic AV block underwent rapid pacing, then administered with  $K^+$  channel blockers, *d*-sotalol or almokalant to induce TdP (Verduyn SC *et al*, 1995). Ryanodine, a selective blocker of SR  $Ca^{2+}$  release was administered that shortened the  $QT_c$  and prevented the induction of EAD-dependent TdP.

These studies have identified key concepts about the mechanisms of EADs. EADs occur under states of APD prolongation and are thought to induce TdP, however APD does not directly dictate the propensity to induce arrhythmia (Connolly SJ, 1999; Ritter JM, 2012). As described in other studies,  $I_{Kr}$  block alone is not sufficient to produce EADs as additional conditions are required to elicit EADs, such as 50% reduction of  $K^+/Mg^{2+}$  in the perfusate and slow PCL, or the introduction of a beta or alpha agonist (*i.e.* isoprenaline or methoxamine). This suggests there are other electrophysiological conditions beyond APD prolongation required for EAD generation, with increasing evidence for a role in the involvement of intracellular  $Ca^{2+}$  or SR  $Ca^{2+}$ .

## ***Models Used to Investigate LQT-Associated Arrhythmias***

To further investigate and understand the arrhythmic mechanisms of EAD-induced arrhythmias, both pharmacological and genetically modified animal models have been used.

### *Pharmacological LQT Models*

Pharmacological LQT models use  $I_{Kr}$  (or hERG) blocking drugs to mimic LQTS2. Historically drugs used to block  $I_{Kr}$  were not selective but rather had mixed ion channel effects. More recently, selective  $I_{Kr}$  blockers have been used, including E-4031 and dofetilide. Several studies using these models have been used to investigate the mechanisms of EAD generation in LQTS2. These are summarised in Table 1.1. Each drug on its own was not enough to generate EADs and required an additional feature to reduce repolarisation reserve, such as 50% reduction in  $K^+/Mg^{2+}$ , beta or alpha-agonist and slow PCL. Choi *et al* performed a dual optical mapping study of intact rabbit hearts using E-4031 (a potent  $I_{Kr}$  blocker) plus slow PCLs and 50%  $K^+/Mg^{2+}$  (Choi BR *et al*, 2002). This showed  $Ca^{2+}$  preceded  $V_m$  where the EAD was elicited and so suggested tissue-level EADs occur in pharmacological LQTS and are  $Ca^{2+}$ -induced. They also identified repolarisation dispersion with apex-base gradients seen in the rabbit epicardium, where APDs at the apex were shorter than the base. Maruyama *et al* used a pharmacological LQT model in cryoablated rabbit hearts to investigate whether EADs occurred on phase 2 or 3 of the cardiac AP, and study the mechanism of EADs (Maruyama M *et al*, 2011). They found phase 2 EADs were  $Ca^{2+}$ -dependent and abolished by a  $Ca^{2+}$  chelator (BAPTA AM), yet phase 3 EADs were not seen to be  $Ca^{2+}$ -dependent. Instead phase 3 EADs were thought to be a tissue-based phenomenon that trigger PVCs/ arrhythmias, at sites of steep AP gradients seen across the ventricular epicardial surface. These gradients were part of the mechanism identified for TA, in that long APD regions caused repetitive TA from single or multiple foci, they also identified a combination of TA and re-entry were occurring in a small subset. This study highlighted the importance of heterogenous repolarisation involvement in LQTS arrhythmogenesis, where the interaction between long and short areas of APD can elicit and maintain TdP. Studies investigating the mechanisms of TdP also found APD gradients to have an important role. Gradients were seen in transgenic LQTS, across the left ventricle (LV) and right ventricle (RV), where VT has been seen to predominantly initiate from the RV due to ventricular APD dispersion (Kim TY *et al*, 2015). There have been reports of higher density

of the outward transient potassium current ( $I_{to}$ ) in the RV compared to LV (Rosati B *et al*, 2003), which may explain this heterogeneity in repolarisation.

### *Transgenic LQT Models*

Genetic manipulation in rodent models is an established method and transgenic mouse models were the first used to study LQTS (London B *et al*, 1998). However, these have failed to translate to the human pathophysiology as there are marked differences in electrophysiological characteristics between the species (*e.g.* species differences of individual channels involved in cardiac repolarisation) and mice LQTS models did not fully reproduce the human phenotype, this makes studying the arrhythmia mechanisms in these models difficult to translate in to humans (Casimiro MC *et al*, 2001; Salama G *et al*, 2007). Transgenic knockout of  $I_{Kr}$  in rabbits proved to be a more reliable physiological model, with easily inducible ventricular arrhythmias (Brunner M *et al*, 2008). These studies have correlated pro-arrhythmic triggers, with the observation that VT/SCD occurs in transgenic animals with both LQTS1 and LQTS2, under stressful situations (Brunner M *et al*, 2008; Odening KE *et al*, 2012), as well as demonstrated the induction of TdP under LQT states originated from the RV and that maintenance of TdP was by multiple shifting foci (Kim TY *et al*, 2015). More recently, transgenic LQTS2 rabbit hearts were used to show that repolarisation gradients and enhanced  $I_{CaL}$  were responsible for both TA and the induction of re-entry (Huang X *et al*, 2016). Transgenic LQTS rabbit hearts were injected with isoproterenol, which caused TA originating from steep APD gradients and sustained VT from re-entrant arrhythmia mechanisms. The use of isoproterenol led to the suggestion that enhanced  $I_{CaL}$  is required to initiate TA.

Transgenic models have their limitations, mainly the effect of gene knockout can have a variety of different impacts on ion channel properties and characteristics. Although these models are designed to create a clean intervention, there is no way to anticipate the widespread effect gene knockout can have on other channels, in either the organ of interest

or beyond. This can impact multiple systems and create other unexpected problems. In most transgenic studies, the non-specific effects are not studied and there are no transgenic control rabbits created with an inert gene. With every transgenic model, the effect it has in one species, does not transfer onto other species. Most transgenic work has been performed on mouse models, since they are less of a challenge to induce transgenic knockout. Fundamentally, mice APs are completely different from human. Their different underlying ion channel profiles and size makes it difficult to elicit a sustained arrhythmia and even if the knockout model does produce a true reflection of the disease, they are still very limited.



LQT Model				Motion artefact	AP recording	Therapy targets tested	Arrhythmia produced	Ref
n =	LQT	Additional features	AVN ablation					
12	E-4031 0.5 $\mu$ M Quinidine 5 $\mu$ M	50% K <sup>+</sup> Burst pacing	High temperature cautery	Background subtraction Motion correction algorithm	di-4 ANEPPS	None	TdP	1
24	D-sotalol 10 $\mu$ M	50% K <sup>+</sup>	Mechanical	n/a	MAP	None	TdP	2
30	Dofetilide 0.7 $\mu$ M E-4031 0.5 $\mu$ M Clofilium 0.3 $\mu$ M D-Sotalol 30 $\mu$ M	Methoxamine 0.03 $\mu$ M Acetylcholine 0.3 $\mu$ M	n/a	n/a	MAP	Nadolol 3 $\mu$ M	TdP	3
37	Erythromycin 300 $\mu$ M Clarithromycin 300 $\mu$ M Azithromycin 300 $\mu$ M	50% K <sup>+</sup>	Mechanical	n/a	MAP	None	TdP	4
28	E-4031 0.5 $\mu$ M	50% K <sup>+</sup> /Mg <sup>2+</sup> Cryoablated endocardium	Pharmacological	DAM Cyto-D	RH237 Rhod-2 AM	None	VT	5
44	E-4031 0.5 $\mu$ M	Isoprenaline 40nM	Mechanical	n/a	di-4 ANEPPS	Propranolol 2.5 $\mu$ M	VT/TdP	6
40	Dofetilide 100nM	SEA0400 (1 $\mu$ mol)	Mechanical	n/a	n/a	Lidocaine 30 $\mu$ M Verapamil 750nM	TdP	7

8	Dofetilide 0.5 $\mu$ M	50% K <sup>+</sup> /Mg <sup>2+</sup>	Electrocautery	Blebbistatin 10 $\mu$ M	Rh237 Rhod-2 AM	Nifedipine 5 $\mu$ M Low external Ca <sup>2+</sup> Thapsigargin 200nM	TdP	8
16	E-4031 0.5 $\mu$ M	50% K <sup>+</sup> /Mg <sup>2+</sup>	Cryo-ablation	Blebbistatin 10 $\mu$ M	RH237 Rhod-2 AM	BAPTA AM (Ca <sup>2+</sup> chelator)	TdP	9
8	Dofetilide 0.5 $\mu$ M	50% K <sup>+</sup> /Mg <sup>2+</sup>	Electrocautery	Blebbistatin 10 $\mu$ M	RH237 Rhod-2 AM	K201 (RyR stabiliser)	VT	10
10	E-4031 0.5 $\mu$ M	50% K <sup>+</sup> /Mg <sup>2+</sup>	Radiofrequency	Blebbistatin 15 $\mu$ M	RH237 Rhod-2 AM	Ryanodine 1 $\mu$ M Thapsigargin 1 $\mu$ M Nifedipine 2 $\mu$ M	TdP	11

**Table 1.2.** Experimental conditions associated with pharmacological rabbit LQT models used to elicit EADs

1. Asano Y *et al*, 1997
2. Eckardt L *et al*, 1998a
3. D'Alonzo AJ *et al*, 1999
4. Milberg P *et al*, 2002
5. Choi BR *et al*, 2002
6. Liu J *et al*, 2005
7. Farkas AS *et al*, 2009
8. Nemeč J *et al*, 2010
9. Maruyama M *et al*, 2011
10. Kim JJ *et al*, 2015
11. Chang PC *et al*, 2015

## ***Dispersion of Ventricular Repolarisation***

The role of dispersion of repolarisation in arrhythmic mechanisms has long been recognised. A study in 1985 observed that the induction of hypothermia and perfusion with regional warm blood, in open-chested canine hearts, created a large area of repolarisation dispersion measured by MAPs, resulting in conduction delay that facilitated the induction of sustained arrhythmia (Kuo CS *et al*, 1985). More recent studies using voltage-clamp in rabbit ventricular myocytes showed higher concentration of  $I_{Kr}/I_{Ks}$  currents at the apex compared with the base and proved regional disparity in APD, which may explain how dispersion of repolarisation can occur (Cheng J *et al*, 1999). Similar findings were found in multi-cellular preparations. Rabbit and cat Purkinje and ventricular cells preparations demonstrated that high rate infusion with  $I_{Kr}$  blockade using almokalant, compared with a low rate infusion, caused  $QT_c$  dispersion and thought to play a role in TdP initiation (Carlsson L *et al*, 1993). This behaviour was also described using canine LV wedge preparations, where repolarisation dispersion was seen to be pro-arrhythmic (Antzelevitch C *et al*, 1996; Shimizu W *et al*, 1997; Yan GX *et al*, 1998; Shimizu W *et al*, 1998). The study of guinea pig APDs using optical mapping studies has found apex-base gradients, with longer APD seen at the base (Efimov IR *et al*, 1994). Apex-base gradients have also been described in an intact rabbit heart model, using pharmacological LQT, that identified these gradients were pro-arrhythmic (Choi BR *et al*, 2002). It has been shown that under LQT conditions baseline heterogeneity of APD is amplified, increasing dispersion of repolarisation and creating a vulnerable window for the induction of re-entry (Antzelevitch C, 2002; Belardinelli L *et al*, 2003).

## ***The Role of $I_{CaL}$ in Arrhythmogenesis in LQTS***

The ability of LTCC blockade to abolish EADs and associated arrhythmias, suggests that  $I_{CaL}$  has a crucial role in the genesis of triggered arrhythmias in LQTS. Therefore, targeting  $I_{CaL}$  as a potential therapeutic target to suppress EADs has been suggested (Madhvani RV *et al*, 2011; Qu Z *et al*, 2012; Qu Z *et al*, 2013). If it were possible to block  $I_{CaL}$  without causing significant effects on  $Ca^{2+}$  cycling or excitation-contraction coupling, then it has been proposed suppression of the  $I_{CaL}$  could potentially be used as a therapeutic target (Huang X *et al*, 2016). The use of  $Ca^{2+}$  channel blockers clinically to treat LQTS has been attempted but only once first-line therapies (*i.e.* beta-blockade) have proved unsuccessful. In one study, a small cohort of LQTS patients ( $n = 6$ ) where beta-blockade failed to prevent TdP, were trialled with 5-10mg verapamil (Jackman WM *et al*, 1990). In all six patients, ECG and MAP recordings were taken and showed verapamil eliminated PVCs and TdP. It was suggested that beta-blockade in combination with  $Ca^{2+}$  channel blockade has a synergistic anti-arrhythmic effect. Other case reports show verapamil has been highly effective at suppressing TdP in patients with anticholinergic-induced arrhythmia (Liao WB *et al*, 1996), congenital LQTS patients with recurrent shocks from their ICD and arrhythmic burden (Kawade M *et al*, 1995; Jacobs A *et al*, 2006; Liu Y *et al*, 2016). There are other clinical reports of verapamil reducing TdP in AV block patients (Cosío FG *et al*, 1991) and incidence of PVCs in congenital LQT when treated in combination with beta-blockade (Shimizu W *et al*, 1994).

Within these studies, there appears to be an anti-arrhythmic effect but in a lot of cases it wasn't clear if this effect resulted because of a specific effect on arrhythmia mechanisms in LQTS or through abolition of the LQT substrate. Patients with congenital LQTS are predisposed to  $QT_c$  prolongation, so it makes sense to attempt to redress the balance. In experimental studies, LTCC blockade has been used as a tool to understand mechanisms of EADs but if  $I_{CaL}$  is reduced enough, then the APD will shorten and the LQT substrate will be lost. This means any anti-arrhythmic effect may be achieved indirectly rather than implicating  $I_{CaL}$  or  $I_{CaL}$ -induced EADs as mechanistic.

## Hypotheses and Aims

This study was designed to investigate the mechanism of PVC induction and the link between EADs and TdP, in an *ex-vivo* pharmacological model of LQT2. The specific hypotheses were:

### **Main Hypotheses**

1. Pharmacological LQT2 would produce EADs, PVCs, bursts and TdP in *ex vivo* rabbit hearts.
2. Synchronisation of  $\text{Ca}^{2+}$ -driven EADs within the intact heart would be responsible for PVC induction.
3. EADs and associated PVCs would be abolished by inhibition of SR  $\text{Ca}^{2+}$  and blockade of  $I_{\text{CaL}}$ .

### **Aims**

In order to test these hypotheses, the following specific experimental aims were set-up:

1. Establish and characterise an experimental *ex vivo* model of LQT2 in the rabbit.
2. Use dual optical mapping of  $V_m$  and  $\text{Ca}^{2+}$  to examine:
  - i) the occurrence of EADs and PVCs.
  - ii) mechanism of EADs and PVCs using inhibition of SR  $\text{Ca}^{2+}$  release and  $I_{\text{CaL}}$ .
  - iii) synchronisation of EADs in coupled tissue and generation of triggered activity.
  - iv) the relationship between EADs, triggered activity and induction of TdP.

## Chapter 2: Methods

## The Experimental Preparation

These studies were performed using Langendorff-perfused rabbit hearts and a pharmacological model of LQT2.

### ***Intact Rabbit Heart***

#### (i) Coupling in the intact heart vs. isolated cells

The electrophysiological characteristics between isolated cardiac myocytes and an intact heart are very different. Intact hearts retain electrotonic coupling, where cell-cell coupling resists a local depolarising current. Overcoming this requires synchronisation across many cells in order to propagate a new AP. It is harder to directly extrapolate the induction and mechanism of focal arrhythmias in isolated cells, and indeed arrhythmias are in fact organ-level events. For these reasons, a whole heart model is preferred.

#### (ii) How translatable are rabbit hearts?

Ideally human tissue would be used to study ventricular arrhythmias, however clinical studies in this area have serious limitations and other than using human explants with end-stage disease, it is difficult to perform whole heart studies in non-diseased human tissue. Historically, and because of their size, pigs and dogs were considered the next best models to study arrhythmogenesis and electrophysiology mechanisms. However, rabbits have since shown important similarities to the human heart, including cellular electrophysiology and propensity to develop sustained re-entrant arrhythmias (Panfilov AV, 2006). When comparing effective heart size, which takes whole heart weight and VF waveform, velocity and frequency patterns into account, the rabbit heart is more comparable to human hearts than dogs or pigs (Panfilov AV, 2006). This means that experimental models in rabbit whole-hearts are useful for studying ventricular arrhythmias.

## ***Langendorff-Perfusion***

Since 1895 the Langendorff preparation has been recognised as a valuable approach for investigating the physiology of the mammalian heart. The aorta is cannulated directly onto a continuous perfusion system, delivering flow to the heart retrograde to the direction of flow *in vivo*. This flow closes the aortic valve, allowing perfusion of the coronary arteries. This highly adaptable set-up can be used to study a variety of mammalian hearts and evidence gathered using this approach has underpinned our understanding of cardiac physiology, contractility, metabolism and coronary perfusion.

## ***Methods***

Licensed heart harvest procedures were carried out by Mr Michael Dunne, Dr Rachel Myles and myself (all PIL holders), in accordance with the UK Animals (Scientific Procedures) Act 1986 and under Project Licence (PPL IE143D87F). Adult male, New Zealand White rabbits (2.5 – 3.5kg) were administered terminal anaesthesia through the marginal ear vein using sodium pentobarbitone (Merial, 200mg/kg) mixed with 1000 IU heparin, before the heart was rapidly removed. This sequence was important to ensure the heart was removed while still beating. Contraction was arrested by immediately immersing the heart in ice cold Tyrode's solution. It was kept submerged to minimise the risk of air embolus from ventricular contraction when the great vessels were open. Hearts were then cannulated, secured by sewing the aorta to the cannula and retrogradely perfused in Langendorff mode. The flow rate was increased (typically to 35-45ml/min) titrated to perfusion pressure (target: 40-60mmHg) to maintain diastolic pressure through the coronary arteries. In these experiments the time from cardiac explant to cannulation was <2 minutes.



## Perfusion System and Physiological Solution

A single-pass perfusion system was custom-built for whole heart Langendorff-perfusion, as shown in Figure 2.1. This included heating components, bubble traps and a peristaltic pump (Gilson Minipuls) to deliver warmed, oxygenated physiological solution to the preparation. The perfusate used was Tyrode's solution at 37°C of the following composition (in mmol/L): NaCl 93, NaHCO<sub>3</sub> 20, NaH<sub>2</sub>PO<sub>4</sub> 1, MgSO<sub>4</sub> 1, KCl 5, C<sub>2</sub>H<sub>3</sub>NaO<sub>2</sub> 20, glucose 25, CaCl<sub>2</sub> 1.9 (pH 7.4 +/- 0.05). Tyrode's was filtered through a 5µM filter (Millipore) before the experiment started and an inline filter of 11µM (Millipore) was placed between the reservoir and perfusion system. The Tyrode's solution was constantly bubbled using a medical gas mixture comprised of 95% oxygen (O<sub>2</sub>) / 5% carbon dioxide (CO<sub>2</sub>) to maintain a target pH of 7.4. Langendorff-perfusion was maintained by titrating the perfusion pump flow rate to a target perfusion pressure. A flow rate of 35-45mL/min was adjusted to maintain a perfusion pressure of 40-60mmHg.

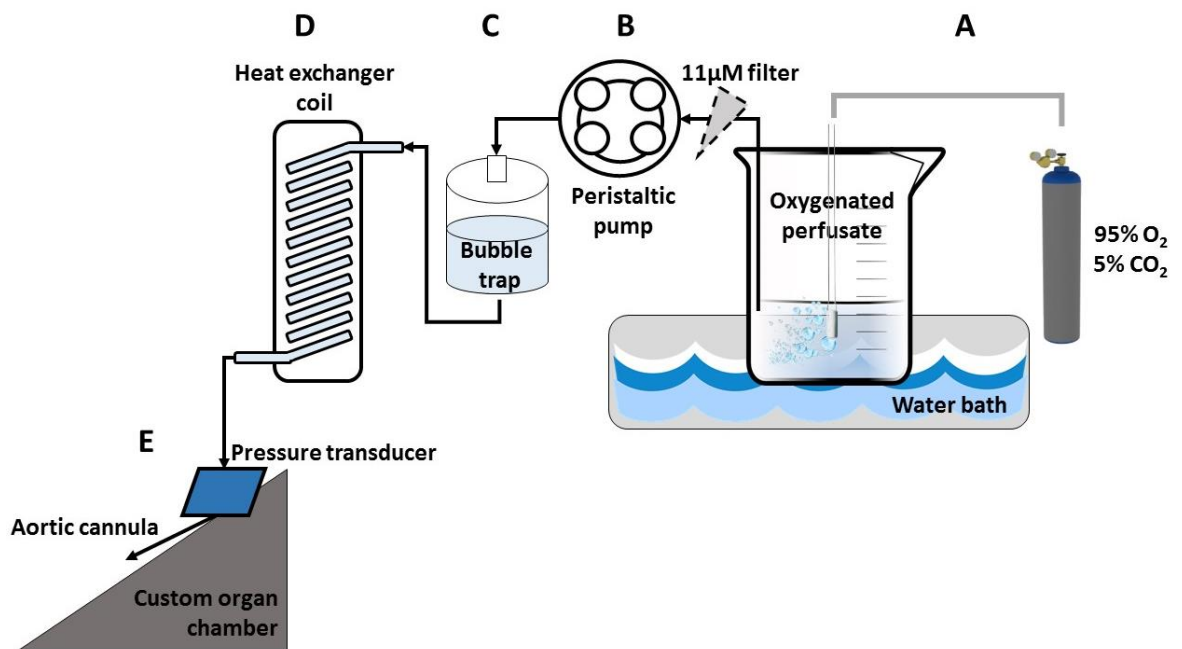


**Figure 2.1.** Diagram of the Langendorff-perfusion system.

Schematic of the perfusion system showing the (A) perfusion reservoir and the oxygenation of the perfusate. (B) peristaltic pump provided adjustable flow rates through the system which contained in series (C) a bubble trap to prevent the passage of air and (D) a heater coil to maintain the temperature. (E) pressure transducer was placed in-line just proximal to the cannula and was used to monitor the perfusion pressure. The temperature of the water bath was regulated and the temperature of the heart was also monitored.

## **Recording ECG Signals**

Two Ag/AgCl disc electrodes were used to record a pseudoECG (pECG) analogous to lead I configuration of a 12-lead ECG. Although the pECG differs from the traditional 12-lead ECG, it is able to give a comparable measure of the electrical activity and capture the major aspects of a true ECG. It is established as an effective tool in optical mapping of the Langendorff-perfused rabbit heart (Lou Q *et al*, 2011b). Disc electrodes were embedded in a custom-built cradle that hearts rested upon during experimentation, Figure 2.2. The disc electrodes were applied to either side of the ventricles and were in direct contact with the heart itself, the Langendorff-perfusion ensured hearts were constantly surrounded in fluid. Signals from these electrodes were amplified by a custom-built isolated amplifier (Medical Electronics, University of Glasgow) and were displayed and recorded using Labchart software. The pacing stimulus and camera shutter position were also recorded along with the pECG and a macro in LabChart (courtesy of Dr Allen Kelly) documented the optical file number with each acquisition. Optical signals and pECG were recorded on the same instrument, direct alignment of pacing stimulation verified both signals were synchronised correctly.

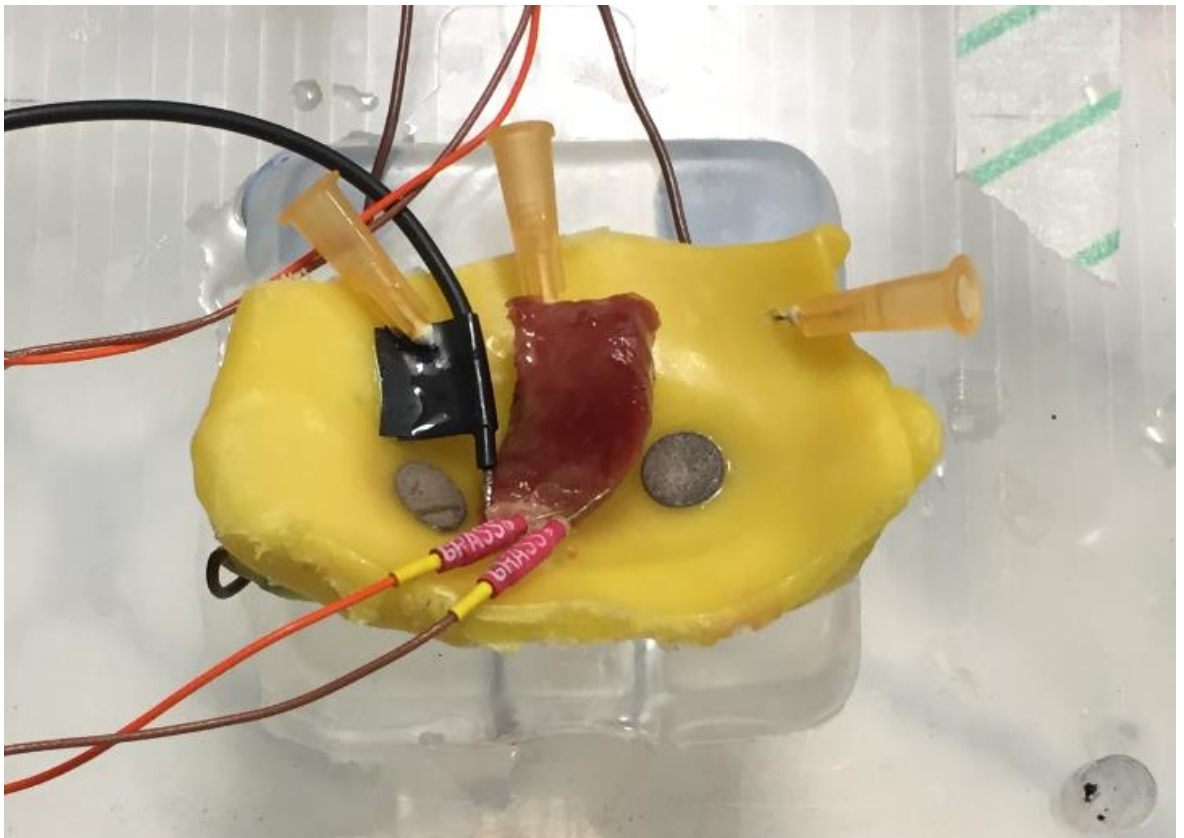
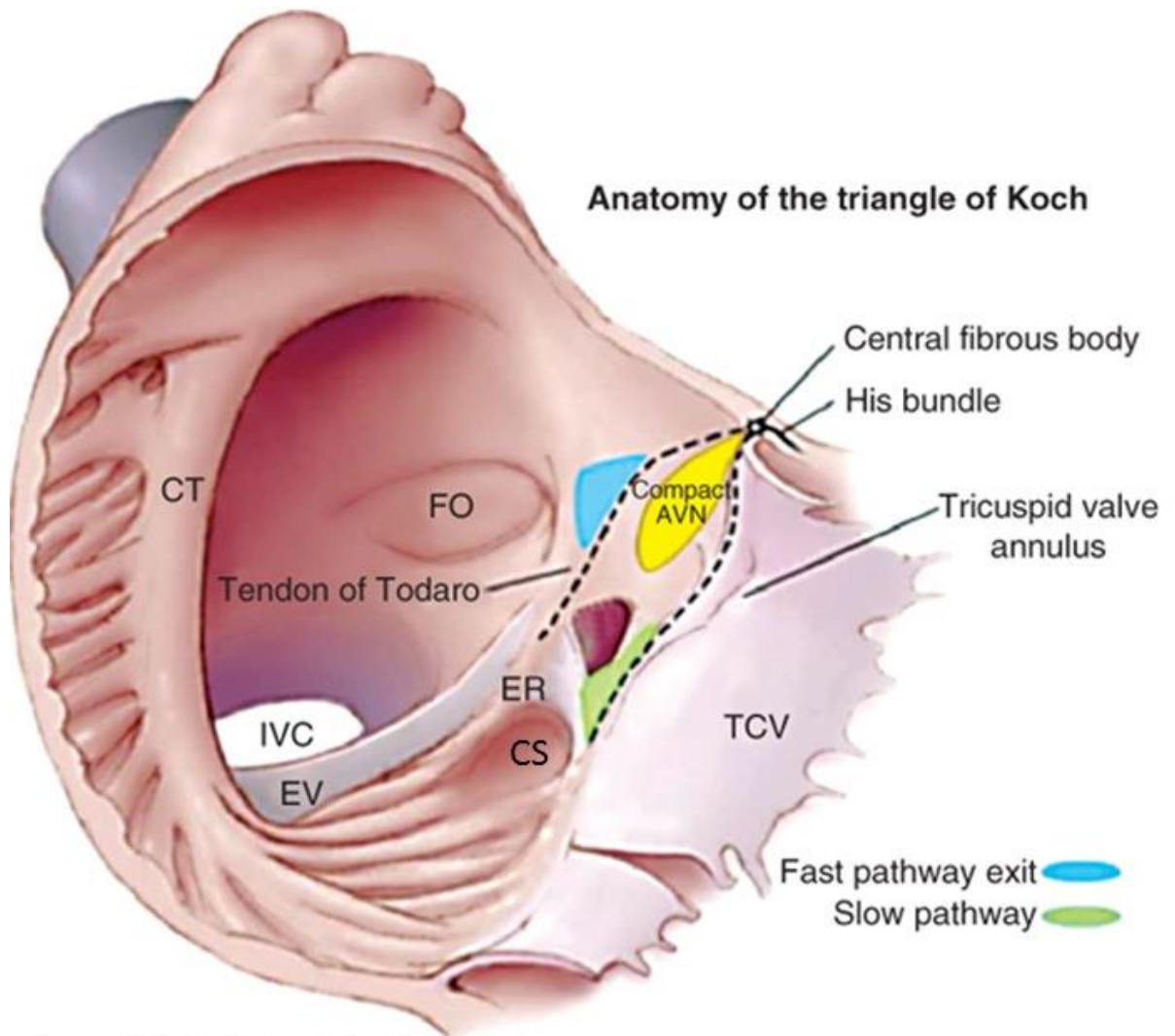


**Figure 2.2.** Example of custom-built ECG cradle with embedded disc electrodes. Picture is taken from wedge section and not representative of the rabbit whole heart set up.

### ***Atrioventricular Node Ablation***

The intrinsic rate of the SAN for a rabbit is 160 – 220bpm, therefore to achieve the slower heart rates required for the model of LQT2, AV nodal conduction was abolished by AV node (ANV) ablation. Multiple methods of AVN ablation have been described in *ex vivo* perfused hearts including electrical, cryotherapy, chemical and mechanical ablation (Boucher M *et al*, 1985). After a series of pilot experiments, chemical ablation was chosen as being the simplest and most effective option. Pharmacological means to reduce heart rate (*i.e.* ivabradine) were considered but given slow PCLs were achieved with AVN ablation alone and the confounding electrophysiological effects of additional drugs was not desirable, this approach was not taken. An atriotomy involving removal of a small area of right atrial free wall revealed the tendon of Todaro, coronary sinus and the tricuspid valve annulus. Together these form the triangle of Koch that are essential landmarks when localising the AVN, Figure 2.3. Mechanical mapping with a 25G needle was performed based on anatomical features and the precise location was determined by transient complete AV block, at which point 0.01 – 0.02mls of 10% formalin was injected. Successful ablation was confirmed by the documentation of persistent AV dissociation with a ventricular escape (rate typically 20-30bpm) on pECG, Figure 2.4. If the AV conduction recovered, the same procedure was repeated up to 3 times.



Source: Valentin Fuster, Robert A. Harrington, Jagat Narula, Zubin J. Eapen: *Hurst's The Heart*, Fourteenth Edition: [www.accessmedicine.com](http://www.accessmedicine.com) Copyright © McGraw-Hill Education. All rights reserved.

**Figure 2.3.** Diagram of the triangle of Koch.

The triangle of Koch was used to identify the position of the AVN. Anatomical landmarks of the triangle included (A) the tendon of Todaro, (B) the coronary sinus (CS) and (C) the Tricuspid valve (TCV) annulus. Other notable landmarks in the right atrium (clockwise from left): Crista terminalis (CT); Foramen ovale (FO); Atrioventricular node (AVN); Eustachian valve (EV); Eustachian ridge (ER)

*Reproduced with permission from McGraw-Hill Education, from Hurst's The Heart, Valentin Fuster, Robert A. Harrington, Jagat Narula, Zubin J. Eapen, Fourteenth Edition: [www.accessmedicine.com](http://www.accessmedicine.com). Copyright © McGraw-Hill Education. All rights reserved. Permission conveyed through Copyright Clearance Center, Inc.*

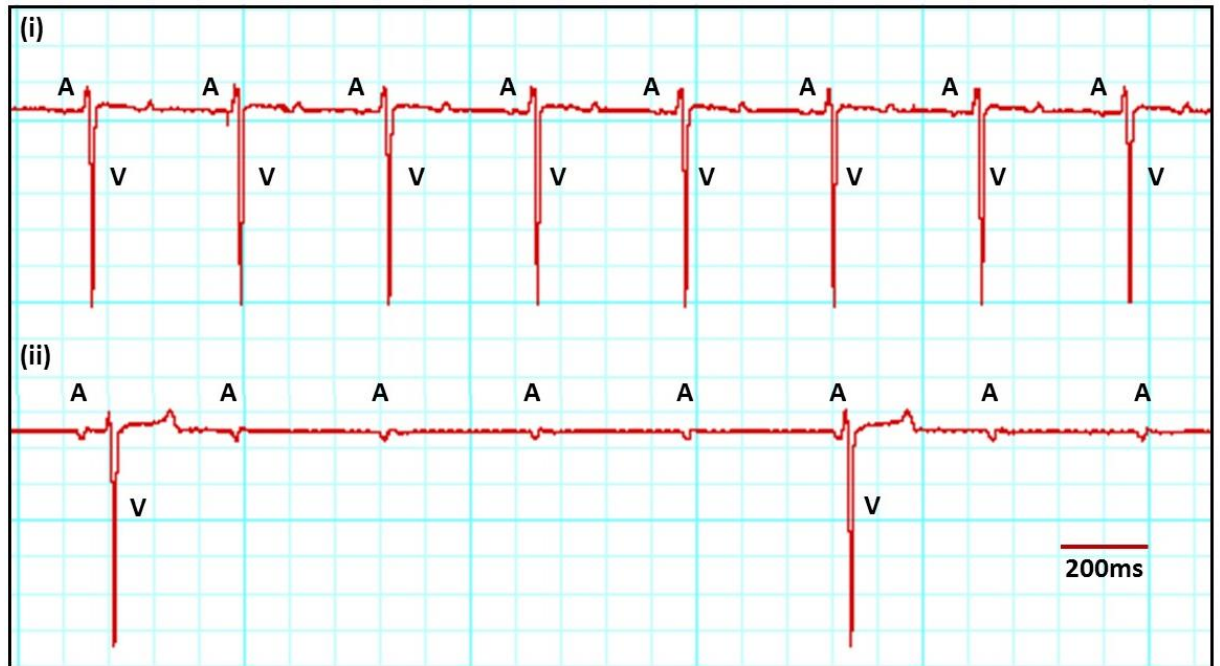


**Figure 2.4.** pECG recording pre and post-AVN ablation.

pECG recording taken (i) pre and (ii) post AVN ablation. (A) denotes atrial activity and (V) ventricular. Following AVN ablation (ii) AV dissociation is seen with a ventricular rate of 20-30bpm.

## ***Pacing Protocols***

Custom made bipolar platinum pacing electrodes were positioned on the apex of the RV epicardium which was stimulated using a 2ms square pulse at twice the diastolic threshold (typical output 2-3V). PCL was varied from 350 – 2000ms during both steady state pacing and S1 – S2 extra-stimulus protocols, during which a 10-beat drive train was used.

## ***Viability of the Preparation***

In the Langendorff-perfused heart, cellular ischaemia can occur from under-perfusion, embolus from air or debris, trauma from instruments used during atriotomy and trauma from needle injection during the AVN ablation. Therefore, the viability of the preparation was continuously monitored and assessed to ensure only healthy preparations were included in the final dataset. A total of 13 out of 62 experiments were excluded from the dataset as they did not meet viability criteria, parameters from the perfusion system and optical measurements were recorded throughout each experiment to discriminate between healthy and unhealthy preparations. The attrition rate is simply down to the learning curve associated with developing the experimental set up and performing a successful AVN ablation, this is discussed in detail in Chapter 3. This included aortic cannulation without air aspiration when transferring the intact heart from cardioplegic solution on to the cannula; absence of air in the perfusing system; initial perfusion pressure of 40-50mmHg; washout of blood from the coronary arteries; absence of ischaemia with good colour and contractility; consistent perfusion pressure of 40-60mmHg throughout the entire experiment; pH maintained between  $7.4 \pm 0.5$  and preparation temperature of  $37 \pm 0.5^{\circ}\text{C}$ . These provided an immediate assessment of viability; however further assessment was performed during data analysis. Measurements of signal-to-noise, rise time and  $\text{APD}_{90}$  were made and compared over time in a subset of hearts ( $n = 13$ ). The most notable marker of ischaemia was the triangulation of the AP, as assessed by  $\text{APD}_{50:90}$  ratio less than 0.75 (these are described in detail in analysis measurements, pp 78). The  $\text{ADP}_{50:90}$  ratio was based on our own observations of normal APs having a consistent  $\text{APD}_{50:90}$  ratio  $>80$ , therefore a cut off of 0.75 was deemed appropriate.

## Optical Mapping

### ***Introduction***

Optical mapping is an imaging methodology used to study cardiac electrophysiology using optical sensors. It works by staining a preparation of interest with a voltage-sensitive dye then using a photodetector to measure changes in fluorescence during depolarisation and repolarisation. Fluorescent dyes are excited with LEDs (excitation light) and emitted light is collected by a series of optics, which also separate the wavelength portion containing the signal of interest and focus it onto the optical sensor. The major benefit of this approach is that multiple simultaneous measurements can be made across the heart. Its use allows comprehensive study of epicardial electrophysiology at the level of the whole organ (Salama G *et al*, 1994), the effects of pacing and defibrillation (Dillon SM, 1991), remodelling in certain disease states (Efimov IR *et al*, 1998; Lou Q *et al*, 2011a), as well as the initiation and maintenance of atrial (Gray RA *et al*; 1997) and ventricular arrhythmias (Gray RA *et al*; 1998). Different parameters can be measured depending on the dyes and optics used and more than one parameter can be mapped simultaneously if the emission spectra are separated. This approach has been employed to combine  $V_m$  and  $Ca^{2+}$  sensitive dyes, to produce simultaneous optical mapping of APs and  $Ca^{2+}$  transients (CaTs) (Choi BR *et al*, 2000). Dual mapping of  $V_m$  and  $Ca^{2+}$  has provided valuable insights into the excitation-contraction coupling and its involvement in arrhythmic mechanisms.

### ***Motion Artefact***

Optical recording is highly sensitive to any form of movement which will distort signals. Elimination of motion can be achieved by mechanical restraint, pharmacological uncoupling or reduction of intracellular  $Ca^{2+}$  ( $Ca^{2+}_i$ ). Each approach comes with adverse effects. In this study, dual optical mapping of  $V_m$  and  $Ca^{2+}$  was used, therefore it was crucial intracellular  $Ca^{2+}$  was maintained. Mechanical restraint is undesirable as it can cause local tissue damage or ischaemia and influence the pattern of APD seen on the epicardial surface. Islands of ischaemia would have the potential to be proarrhythmic. In this study pharmacological uncoupling using blebbistatin was chosen to minimise motion artefact.

Measures taken to ensure exclusion of motion artefact was successful for every experiment included: starting each experiment with a visual inspection for motion and if excessive the heart was given gentle mechanical restraint or further blebbistatin would have been considered. However, additional blebbistatin was never required. During analysis if there were small areas with motion artefact, this was identified by very a short APD, or clearly distorted signals and excluded from analysis.

### ***Blebbistatin***

Blebbistatin inhibits myosin ATPase activity, this prevents cross-bridge cycling and reduces the contraction of skeletal and cardiac muscle. Blebbistatin has been widely used in the study of cardiac electrophysiology and its characteristics are well documented (Kovacs M *et al*, 2004). There have been reports of blebbistatin having potentially pro-arrhythmic effects on cardiac electrophysiology (Brack KE *et al*, 2013). In rabbit myocardium, concentrations of 5-10 $\mu$ M have been shown to eliminate contraction but causes no adverse effects on cellular electrophysiology, including ECG parameters, ventricular refractory periods, activation patterns or AP morphology (Fedorov VV *et al*, 2007). Alternative uncouplers were considered, such as cytochalasin-D and 2,3-butanedione monoxime (BDM) were considered for this study, however these were not selected as were thought to have an adverse effect on APD (Biermann M *et al*, 1998). For this study a concentration of 10 $\mu$ M blebbistatin (Tocris Bioscience, Ellisville) was chosen and was added to the perfusate before mapping commenced. Once LV contractility was terminated, a mitral valvotomy was performed to prevent pressure build up in the LV which can occur once contraction has been reduced. Further attempts to reduce motion artefact involved gentle mechanical restraint from our custom cradle, this ensured the least disturbance or movement to the epicardial surface as possible.

One control experiment recording only perfusion pressure and pECG data, during sinus rhythm, was performed to assess if blebbistatin caused any issues with electrophysiology or if it was proarrhythmic. No arrhythmias were seen and perfusion pressure and pECG parameters were maintained throughout. This single experiment was excluded from the final dataset because there was no optical data taken.



## Voltage/Calcium-Sensitive Dyes

In this study, dual optical mapping was used to record  $V_m$  and  $Ca^{2+}$  signals from the epicardial surface of intact rabbit hearts. The dyes used in this study were RH237 (Molecular Probes Inc, Oregon) and Rhod2AM (Molecular Probes Inc, Oregon). Both are widely used in the study of cardiac electrophysiology and selected because their excitation / emission spectra facilitated dual optical mapping using one imaging system (Choi BR *et al*, 2002; Myles RC *et al*, 2012; Wang L *et al*, 2014). The basic principle of these indicators is based on Stokes shift, where dyes are excited by photons of a given wavelength and then emit light of a different wavelength, Figure 2.5. Voltage-sensitive dyes shift their spectra of fluorescence depending on the  $V_m$ . During depolarisation, voltage changes from -90mV to a more positive 0mV (as described in Chapter 1, pp 32) and doing so shifts the emission spectrum of the dye to the left, Figure 2.5. The wavelength spectrum of emitted light is dependent on  $V_m$  such that optical APs can provide an accurate representation of repolarisation changes seen when compared at a cellular level. Measuring  $Ca^{2+}$  is crucial when monitoring changes in cardiac excitation-contraction coupling. An AP causes an influx of  $Ca^{2+}$  across the sarcolemma ( $I_{CaL}$ ), which triggers the release of intracellular SR  $Ca^{2+}$  stores. Dyes sensitive to cytoplasmic  $Ca^{2+}$  can detect these changes and allow  $Ca^{2+}$  transients to be measured.

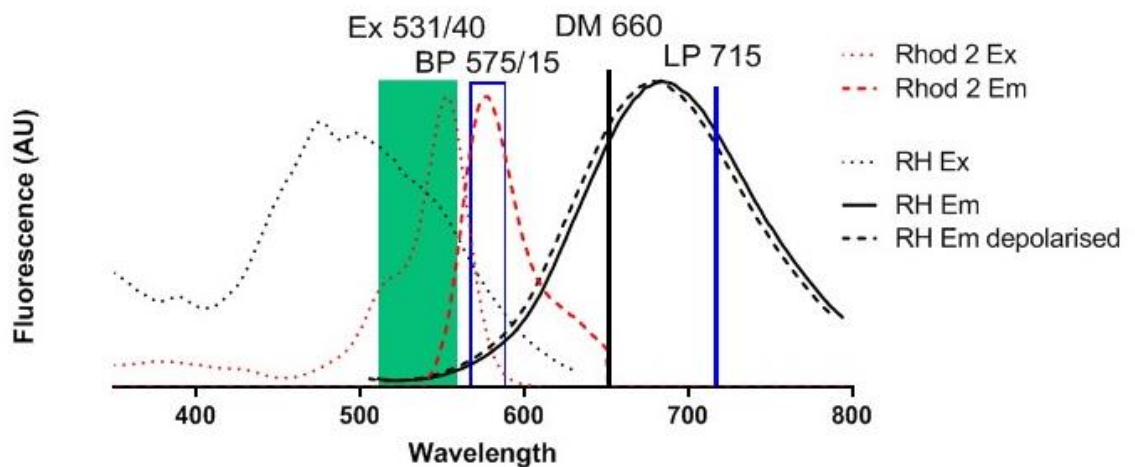


**Figure 2.5.** Spectral properties of RH237 and Rhod2 with optics used in this study.

Diagram showing the spectral properties of the voltage sensitive dye RH237 (black) and  $Ca^{2+}$  sensitive dye Rhod2 (red). Both dyes are excited by the same excitation wavelength (531/40) and elicit differing emission spectra. These are filtered by a dichroic mirror (DM) that separates longer wavelength of RH237 to the shorter Rhod2. This allows dual optical mapping.

### ***Dye Preparation***

Dyes were prepared according to established laboratory protocols. RH237 was made up into 1mg/ml stock solution using DMSO, vials were measured out, then stored at -20°C and protected from the light. On the day, these were thawed out and 100µL bolus was injected into the port proximal to the aortic cannula. Rhod2 was made up on the day, 250µl of 2mg/ml in DMSO, combined with 20% non-ionic detergent pluronic acid (50mg into 250µl of distilled water) was used to increase the aqueous solubility of Rhod2. A mixture of 250µl pluronic acid, 250µl Rhod2 and 500µl perfusate was combined and the entire 1000µl was injected into a port immediately before the bubble trap. For consistency the same dye manufacturer was procured and the same stock was used throughout all experiments. Demonstration that the dyes had been properly prepared were confirmed from good SNR during experiments.

## Optical System and Data Acquisition

A diagram of the optical imaging system is shown in Figure 2.6. Wide-field optical imaging of epicardial  $V_m$  and  $Ca^{2+}_i$  was performed with dual complementary metal oxide semiconductor (CMOS) camera system on a THT microscope (Micam05, SciMedia, Costa Mesa, CA) with a 32 x 32mm (1024mm<sup>2</sup>) field of view resulting in a spatial resolution of 320 $\mu$ m<sup>2</sup>/pixel. All signals were sampled at 1kHz. The anterior epicardial surface, including the RV and LV, was illuminated by LED light sources centred at 530nm (LEX-2G, Sci Media, Ex 531  $\pm$  40nm) that were focused directly on the surface of the preparation. Emitted light was collected using a 0.63x objective lens (Leica, Japan) and split with a dichroic mirror at 660nm (Leica, Japan). The longer wavelength moiety, containing the RH237 signal was long pass filtered at >715nm and focussed onto the first Micam05 sensor for  $V_m$  imaging. The shorter wavelength moiety was bandpass filtered between 575  $\pm$  15nm and focussed onto the second CMOS sensor for  $Ca^{2+}_i$  imaging. Prior to each experiment the focus of both cameras with the dichroic mirror were checked and aligned to minimise malalignment, examples of camera FOV, grid alignment and pixel resolution across the rabbit heart are shown in Figure 2.7.

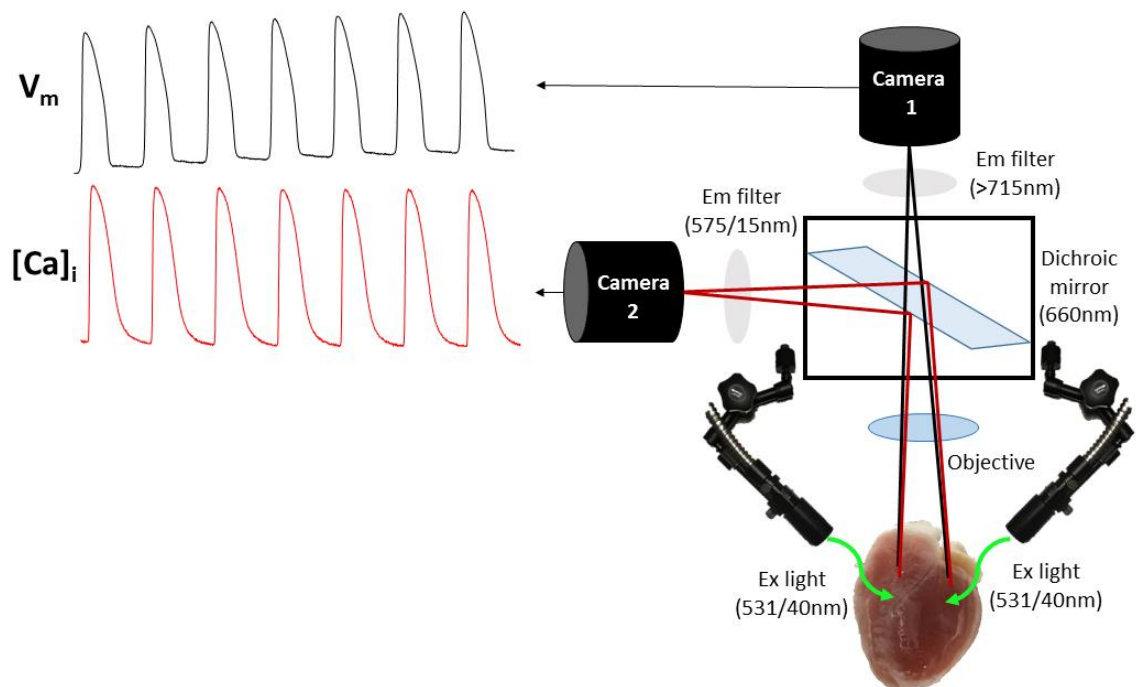


**Figure 2.6.** Diagram of the optical mapping system.

Schematic diagram of the optical mapping system allowing dual optical mapping of  $V_m$  and  $CaTs$ .

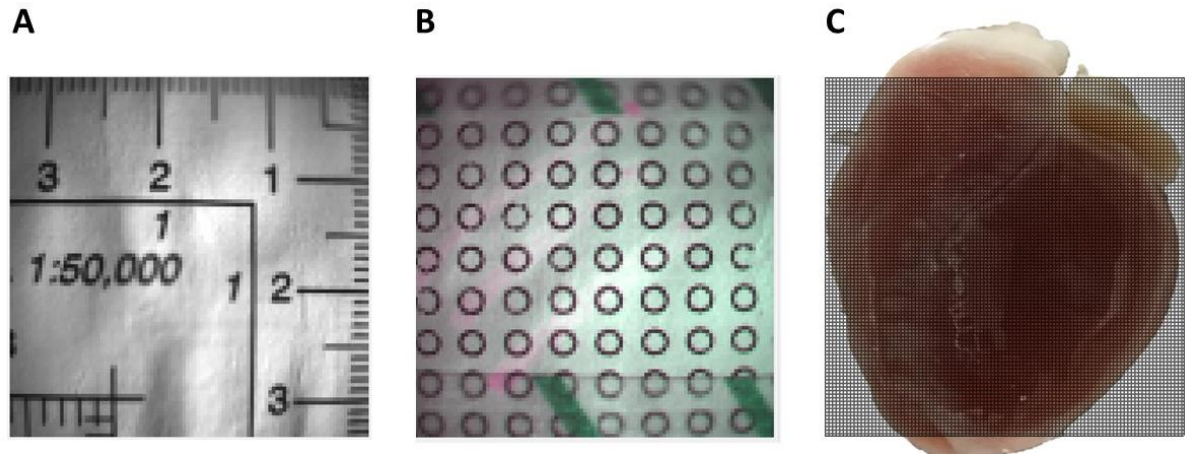


**Figure 2.7.** Examples of camera alignment checks prior to each experiment. (A) Field of view (B) grid alignment with red and green overlap to minimise malalignment and (C) pixel resolution across the rabbit heart.

### ***Limitations of Optical Mapping***

Although a powerful tool, optical mapping does not come without its limitations. These include motion artefact and its suppression (already described), spatial averaging and anatomical limitations. Each optical AP derived from a single pixel, includes a summation of activity taken from a volume of myocytes rather than from a single cell. Although this provides an accurate measure of the AP duration, this spatial averaging increases the optical AP rise time, relative to that recorded by an intracellular microelectrode, Figure 2.8. The differences between the wide-field optical mapping used in the current study and optical recordings with single cell resolution, as detailed in Figure 2.8, highlight that rise time measurements in optical mapping are slower than isolated cell recordings. However, APD recordings during optical mapping are similar to those recorded during 2-photon laser scanning microscopy (2PSLM), therefore represent an accurate measurement. The curvature of an intact heart can also distort signals and so APs derived from a curved or sloping aspect of the heart, may provide inaccurate signals. Optical APs measure change in fluorescence and the actual values of  $V_m$  are not recorded, plus recordings are taken from a 2D surface of a 3D organ. The theoretical depth of penetration for signals recorded in the optical system is approximated at  $400\mu\text{M}$ , with potential signals as deep as 1mm, these references are taken from previous experimental work within the department (Walker NL *et al*, 2007).

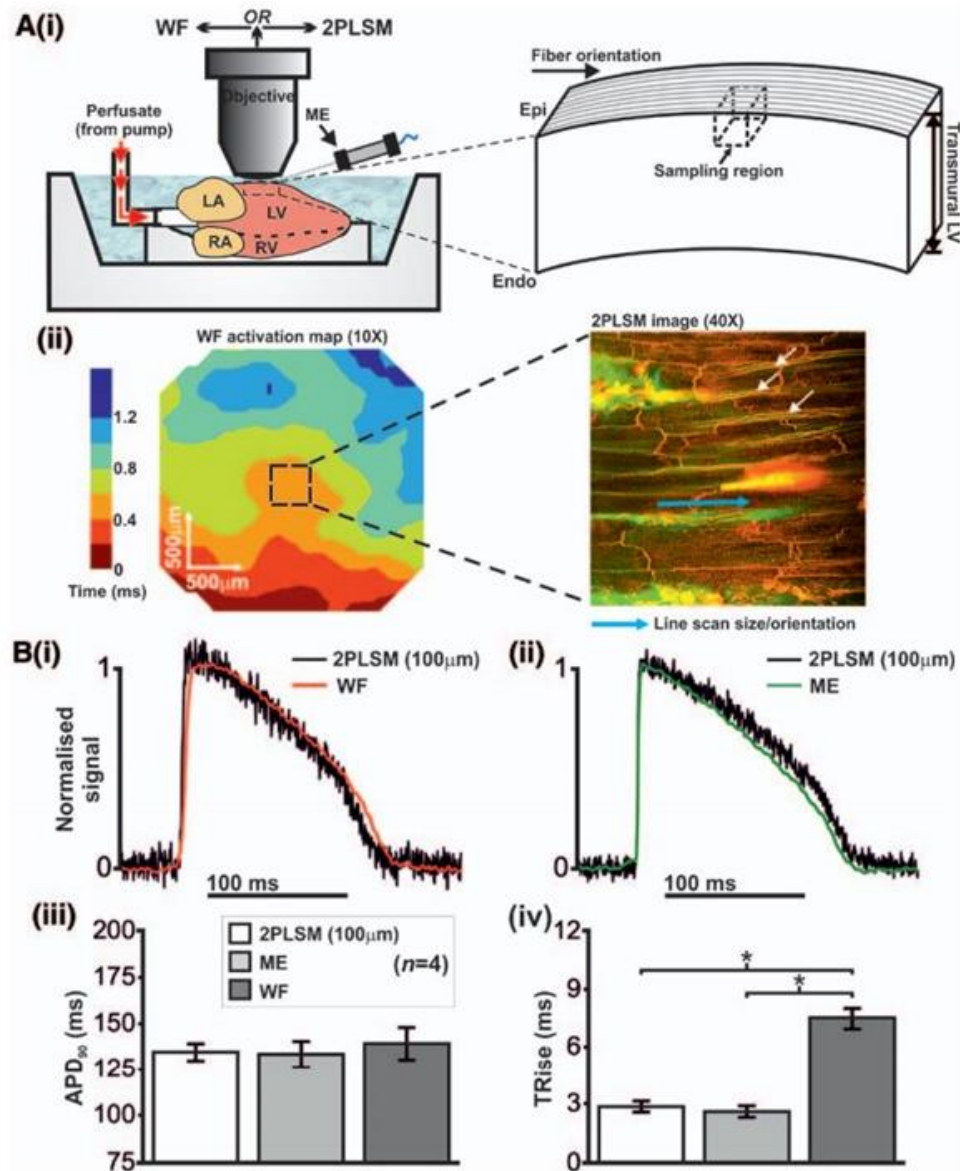


**Figure 2.8.** The effect of spatial averaging on optical AP rise time.

Reproduced from Kelly *et al*, 2013\*. (A) showing the (i) experimental set-up used (left) and diagram of transmural optical sampling region (right). A comparison of (ii) wide-field (WF) activation map (left) and 2PLSM (right) epicardial surface image. Corresponding APs (B) from superimposed (i) WF trace and (ii) microelectrode recordings with (iii) APD<sub>90</sub> and (iv) TRise measurements. This demonstrates the accuracy of AP characteristics, APD<sub>90</sub> in particular, from intact heart wide-field optical recordings.

\* Reproduced with permission from Kelly A *et al*, Subepicardial action potential characteristic are a function of depth and activations sequence in isolated rabbit hearts. *Circulation: Arrhythmia and Electrophysiology*. 2013; 6: 809 – 817. <https://doi.org/10.1161/CIRCEP.113.000334>.

## **Experimental protocols**

Once positioned in the imaging chamber, each experiment started with baseline pacing of the RV epicardium at 350ms PCL. Steady state pacing was performed for at least 30 seconds before any recordings. Optical recordings were taken for 4 seconds during either steady state pacing or intrinsic rhythm. Baseline recordings were taken throughout each parameter change and at the end of each protocol, to assess for changes caused by the experimental conditions as well as highlight any deterioration or compromise of the preparation.

### ***Dynamic Restitution Protocol***

Restitution protocols were performed to understand the change in APD by decreasing the diastolic interval. Dynamic pacing protocols involved pacing at a set rate, starting at PCL of 2000ms then incrementally reducing this in the following order: 1000, 800, 600, 500, 400, 300ms. Any change in pacing rate prompted a 30 second pause before any optical acquisitions were taken. To ascertain the effective refractory period (ERP), the CL was gradually reduced from 300ms in 10ms increments until loss of 1:1 capture was reached (approximately 210-230ms). This was defined as the longest coupling interval that failed to capture the ventricles. In the event of sustained ventricular arrhythmia, a bolus 1ml KCl (1M concentration) was administered into the port proximal to the aortic cannula to provide chemical defibrillation and viability parameters rechecked.

### ***Extra-Stimulus Restitution Protocol***

An extra-stimulus restitution was performed using a drive train of 10 beat (S1 350ms CL) followed by an extra-stimulus (S2). The S1-S2 had progressively shorter intervals in the following order: 2000, 1000, 800, 600, 500, 400, 300ms. From 300ms to 200ms, the S2 was reduced by 10ms until ERP. Each S2 was followed by 30 seconds of S1 350ms until the next cycle.

### ***LQT Pacing Protocol***

Once set up was established and hearts were deemed viable, LQT was induced pharmacologically and data acquisitions were taken at 1000 and 2000ms PCL, for some 3000 – 4000ms. Acquisitions of intrinsic rhythm (>2000ms PCL) were also taken.

## Data Analysis

### *pECG Data*

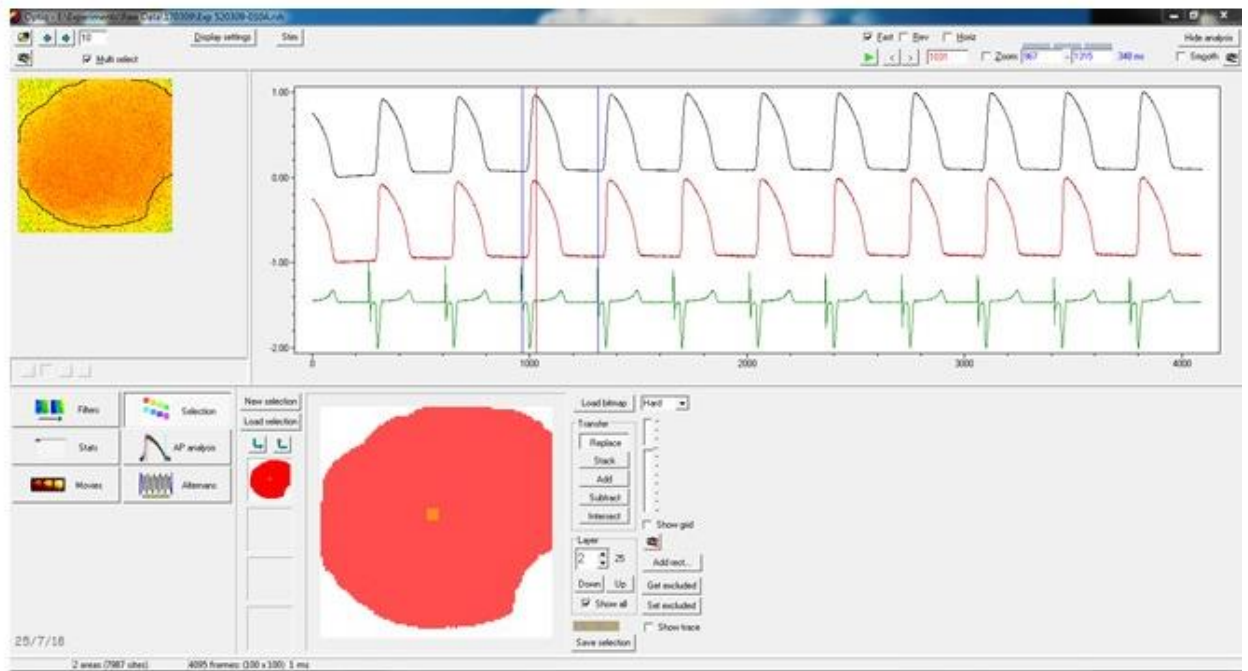
pECG data was recorded on Labchart software throughout each experiment. The software recorded both pECG data, pacing stimulus and shutter opening of the optical camera. This meant all optical recordings were linked with pECG data. All pECG recordings were saved on to the lab computer and external hard drives for back up.

### *Optical Data*

All optical data analysis was performed using custom made software, Optiq, written and provided by Dr Francis Burton, University of Glasgow. All automated analysis was verified visually, and any aberrancy or motion artefact were excluded from data analysis.

Before each experiment, both cameras were tested for focus and alignment. All data acquisitions were saved directly from the CMOS camera onto the lab computer and external hard drives for back up. Each file contained 4s worth of APs for each of the 10,000 pixels in the imaging field of view. The files were imported into Optiq software and were immediately inspected for image quality to exclude those with motion artefact, dye bleaching, saturation, air bubbles or debris appearing on the epicardial surface that would distort images. A corresponding white light image was used to orientate to anatomical features. A single iteration of a Gaussian spatial filter (radius 2 pixels) was applied to all data prior to analysis. Pixels to be analysed were selected by freehand drawing of the area that covered the entire epicardial surface, signal-to-noise ratios (SNRs) for each pixel in this selection were then calculated and any with  $SNR < 20$  were excluded. For consistency, the same area was used throughout the whole experiment. Once the analysis of the selected area was performed, it was possible afterwards to make sub-selections and examine them in more detail. This prevented repeated analysis and minimised error. Once selections were made, two cursors were positioned on either side of the AP or CaT of interest. These cursors corresponded to actual time points taken during the acquisition and were consistently positioned on the pacing stimulus and well after the return to baseline, Figure 2.9.

A



B

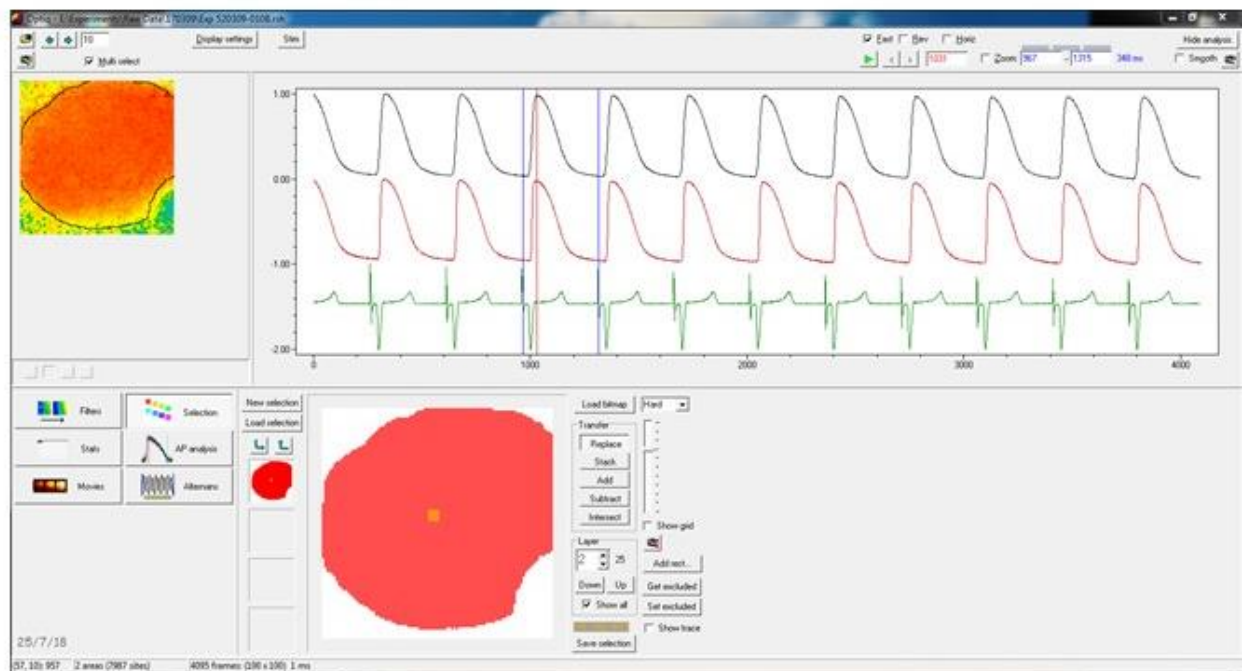


**Figure 2.9.** Snapshots of Optiq analysis of  $V_m$  and CaTs.

Example of Optiq analysis software. (A) APs taken from a whole heart selection (black line) and a 5x5 mm selection (red line). (B) CaTs taken from the same preparation and selections. The green line at the bottom is the corresponding pECG.



## ***Analysis Measurements***

An automated analysis algorithm calculated trace characteristics including, baseline, amplitude, SNR. A standard algorithm was used to identify baseline, peak, activation and repolarisation time of the trace and by using these, AP characteristics could be calculated, Table 2.1 and Figure 2.10.

To better differentiate activation and repolarisation time from the trace, specific filters were used. By the end of each analysis, a total 97 AP parameters for each pixel were calculated. Each parameter had an individual colour scale pixel display which allowed easy identification of misanalysed APs or outliers. Once identified, these were inspected and re-analysed with adjusted parameters or removed from the analysis as appropriate. Occasionally different filter settings or parameter definitions were required for more complex optical data. All data was tabulated in a data matrix and saved as an individual file for that optical AP. This process was repeated for every optical AP or CaT analysed.

CaTs were analysed using the same parameters. Owing to the different morphology and characteristics of CaTs, CaTD<sub>80</sub>, to quantify changes in CaT amplitude, 5x5 selections over areas with the highest SNR were exported in to GraphPad Prism software. These were expressed as arbitrary fluorescence values from Optiq. These were then normalised to the baseline diastolic value (F<sub>0</sub>) and the CaT was quantified as a ratio of the F<sub>0</sub>, the resultant value was denoted as F/F<sub>0</sub> and always more positive than 1. Values were expressed between 1-1.4.

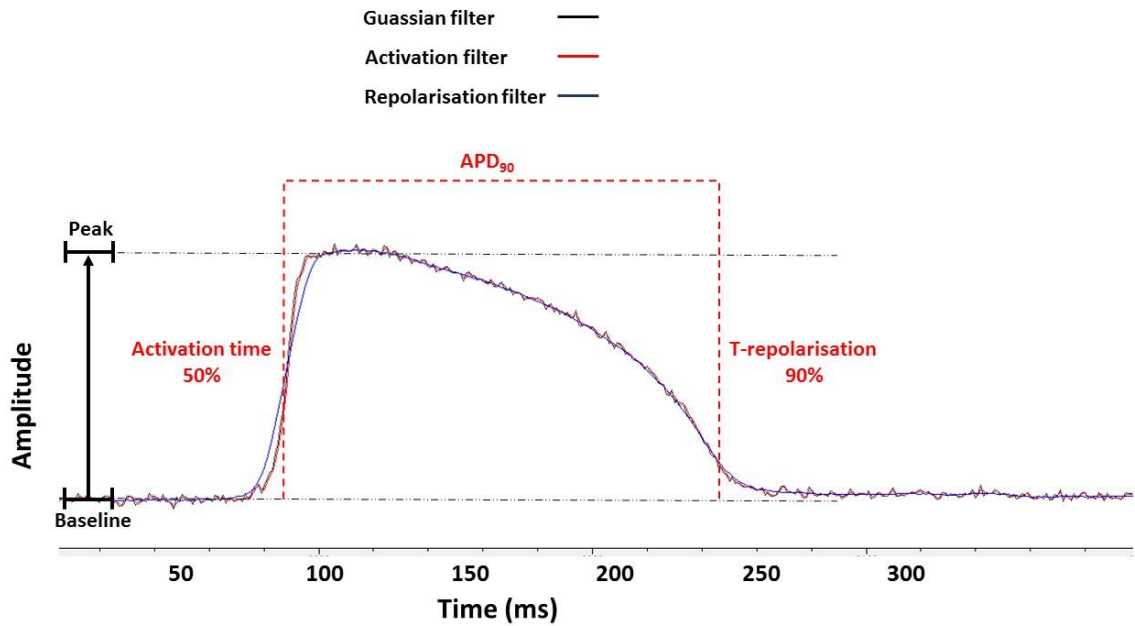


**Figure 2.10.** Gaussian analysis of optical APs.

Activation filter is depicted in red and repolarisation filter in blue.  $APD_{90}$  was calculated using activation time at 50% [Mid-point (50% level) between baseline and peak] minus repolarisation at 90% [time at which trace is 90% peak to baseline], *i.e.*  $APD = RT - AT$ .

Parameter	Calculation
Baseline	Minimum value of median filtered trace
Peak	Maximum value of median filtered trace
SNR	Signal to noise ratio of trace
T-Peak (Peak time)	Time at peak of AP
T-Act M (Midpoint activation time)	Mid-point (50% level) between baseline and peak
T-Act <sub>10</sub>	Time at which trace is 10% from baseline to peak
T-Act <sub>90</sub>	Time at which trace is 90% from baseline to peak
T Rise (Rise time)	Time from 10% - 90% from baseline to peak
T-Repol <sub>50</sub>	Time at which trace is 50% from peak to baseline
T-Repol <sub>90</sub>	Time at which trace is 90% peak to baseline
$APD_{90}$	Interval (difference) between T-Repol <sub>90</sub> minus T-Act M

**Table 2.1.** List of important parameters and their definitions calculated during analysis.

## ***Statistical Analysis***

All data are expressed as mean  $\pm$  standard deviation (SD). All statistical analyses were performed using Graph Pad Prism software. For normally distributed data, comparison of two groups was performed using a Student's t-test (paired where appropriate). Multiple comparisons were performed using a one-way ANOVA or (repeated measures where appropriate), followed by post-testing to allow for multiple comparisons where appropriate. A Fisher's exact test was used for categorical comparisons. A p-value of  $<0.05$  was considered statistically significant.

### *Sample Size Calculation*

Initial power calculations were based on the measured SD of the main parameters. Our power calculations predicted the estimated sample size required (n) at 8-10 animals/group to detect a 10% difference in APD, assuming a standard deviation of half the difference between the two means ( $n = (2 \cdot SD^2 \cdot \text{power index}) / D^2$ ), where power index is equal to 7.9 for 80% power to detect 2-sided significance at  $p < 0.05$ . This would also be sufficient to detect a 10ms difference in APD with the same statistical accuracy. Thapsigargin and nifedipine datasets had smaller sample sizes ( $n = 5-7$  animals) owing to the practical limitations and complexity of experiments. To ensure the optimal statistical power for determining differences between TdP induction, we require a sample size of 12 animals/group. This will allow us to detect a meaningful difference in the proportion of hearts developing TdP (20% vs. 70%) with 80% power to detect 2-sided significance at  $p < 0.05$ .

## **Chapter 3: Set Up of a Pharmacological LQT Model in the Intact Langendorff-Perfused Rabbit Heart**

## Introduction

EAD-triggered APs are thought to be responsible for the induction of TdP in LQTS. EADs are cellular events during which a spontaneous depolarisation occurs during the repolarisation phase of the cardiac AP. In isolated cells, EADs of sufficient magnitude are able to elicit a spontaneous AP. However, this cellular mechanism cannot be directly extrapolated to the intact heart, in which electrotonic coupling between cells opposes any depolarisation arising from a single cell (the “source-sink mismatch”) and so will prevent EAD-triggered APs. Computer modelling studies suggest a single EAD-triggered AP is propagated in the intact heart from spatial synchronisation of EADs across thousands of cells (Xie Y *et al*, 2010). The cellular mechanisms of EADs in the intact heart remain unknown and a conclusive mechanistic link to the induction of TdP has yet to be made (Volders PG *et al*, 2000).

### **Pharmacological LQT Models**

As described in Chapter 1 (pp. 53), experimental LQT models used to investigate the arrhythmic mechanisms include pharmacological and transgenic. Pharmacological LQT involves mimicking LQTS2 by blockade of the  $I_{Kr}$  (hERG) channel, this prolongs the cardiac AP and varying degrees of APD prolongation have been seen. Experiments using this technique requires the use of specific  $I_{Kr}$  blockers, such as E-4031 and dofetilide. Examples of pharmacological LQT models using the Langendorff-perfused intact rabbit heart are summarised in Table 3.1. Other adaptations used to induce LQT states include the *in vivo* complete heart block and hypertrophy model in canines (Vos MA *et al*, 1998). In this study, pacing at slow rates with the addition of *d*-sotalol caused  $QT_c$  prolongation that induced TdP. We believe the PVC and triggering is the final common pathway that occurs through either congenital or acquired LQTS.

Ref	Author	Date	PCL (ms)	$I_{Kr}$ blocker	Additional feature (s)	APD		APD measured
						Baseline	LQT states	
1	Asano Y <i>et al</i>	1997	2000 -3000	E-4031 0.5 $\mu$ M	Quinidine 5 $\mu$ M	212 $\pm$ 8	317 $\pm$ 25	MAP
2	Eckardt L <i>et al</i>	1998	600	D-sotalol 10 $\mu$ M	50% K <sup>+</sup>	164 $\pm$ 15	250 $\pm$ 16	MAP <sub>90</sub>
3	D'Alonzo AJ <i>et al</i>	1999	Intrinsic rhythm	Dofetilide 0.5 $\mu$ M E-4031 0.3 $\mu$ M	Methoxamine + ACh	130 $\pm$ 2 117 $\pm$ 5	231 $\pm$ 15 210 $\pm$ 12	APD <sub>90</sub>
4	Milberg P <i>et al</i>	2002	900	Erythromycin 300 $\mu$ M Clarithromycin 300 $\mu$ M Azithromycin 300 $\mu$ M	50% K <sup>+</sup>	159 $\pm$ 15 175 $\pm$ 16 162 $\pm$ 15	203 $\pm$ 24 227 $\pm$ 39 223 $\pm$ 27	MAP <sub>90</sub>
5	Choi BR <i>et al</i>	2002	1200	E-4031 0.5 $\mu$ M	50% K <sup>+</sup> /Mg <sup>2+</sup>	277 $\pm$ 65	2115 $\pm$ 67	APD <sub>90</sub>
6	Liu T <i>et al</i>	2005	700	E-4031 0.5 $\mu$ M	Isoprenaline 40nM	231 $\pm$ 27	~ 1000	APD <sub>90</sub>
7	Němec J <i>et al</i>	2010	1200	Dofetilide 0.5 $\mu$ M	50% K <sup>+</sup> /Mg <sup>2+</sup>	415 $\pm$ 118	678 $\pm$ 235	APD <sub>90</sub>

Ref	Author	Date	PCL (ms)	$I_{Kr}$ blocker	Additional feature (s)	APD		APD measured
						Baseline	LQT states	
8	Maruyama M <i>et al</i>	2011	1000 – 2000	E-4031 0.5 $\mu$ M	50% $K^+/Mg^{2+}$	217 $\pm$ 23	859 $\pm$ 231	APD <sub>70</sub>
9	Kim JJ <i>et al</i>	2015	500	Dofetilide 0.5 $\mu$ M	50% $K^+/Mg^{2+}$	Not recorded	538 $\pm$ 53	APD <sub>80</sub>
10	Chang PC <i>et al</i>	2015	1000	E-4031 0.5 $\mu$ M	50% $K^+/Mg^{2+}$	298 $\pm$ 30	457 $\pm$ 75	APD <sub>80</sub>

**Table 3.1.** Pharmacological LQT models using Langendorff-perfused rabbit hearts and their corresponding APD values.

### ***Effect of Cycle Length on APD***

Cycle length is a major determinant of APD in cardiac myocytes. The relationship between APD and cycle length is species-dependent, but in mammals such as rabbits with AP shapes similar to humans, the relationship approximates to an exponential function that approaches a maximal APD asymptotically as cycle length is increased (Bass BG, 1975). The mechanistic basis of this non-linear relationship is the relative activation of repolarising currents. A similar relationship is seen when an extra-stimulus protocol is used to determine the restitution characteristics of the tissue, a protocol that establishes the ERP will demonstrate progressively shorter APD values at the shorter S1-S2 intervals, until ERP is reached (Franz MR *et al*, 1988). In the current study, the longest APDs were achieved by pacing the tissue at a rate considerably lower than physiological rates (1000-2000ms, *i.e.* 60-30bpm). At these rates in the rabbit,  $I_{Kr}$  is significantly activated and responds to block with a significant prolongation of APD, a response that is considerably smaller at physiological rates due to the minimal activation of  $I_{Kr}$  (Dorian P *et al*, 2000).

### ***Additional Conditions to Elicit EADs***

As described in Chapter 1, APD prolongation (and so QT<sub>c</sub> prolongation) does not directly dictate the propensity to EADs, or the risk of TdP. Additional electrophysiological conditions are generally required, *e.g.* reduction of perfusate K<sup>+</sup> and Mg<sup>2+</sup>, slower PCL or the use of sympathetic stimulation, such as isoprenaline or methoxamine.



### ***The Involvement of SR Ca<sup>2+</sup> or I<sub>CaL</sub>***

There is now increasing evidence for a role for intracellular Ca<sup>2+</sup> cycling in dictating whether EADs are generated during AP prolongation or indeed are responsible for PVC generation. The role of Ca<sup>2+</sup> in the generation of EADs, takes 2 forms; either re-activation of I<sub>CaL</sub> or spontaneous SR Ca<sup>2+</sup> release that triggers an inward current via the electrogenic I<sub>NCX</sub>. As discussed in Chapter 1 (pp. 50-51), SR Ca<sup>2+</sup> was implicated after studies saw a reduction of SR Ca<sup>2+</sup> release caused abolition of EADs and associated TdP (Szabo B *et al*, 1995; Verduyn SC *et al*, 1995; Patterson E *et al*, 1997). Whereas LTCC blockers have reduced arrhythmia burden in LQTS patients (Jackman WM *et al*, 1990; Liao WB *et al*, 1996), again discussed in Chapter 1 (pp. 59). This was reinforced by computer modelling studies which suggested that I<sub>CaL</sub> was responsible for TA and induction of re-entry (Huang X *et al*, 2016). Dual optical mapping using a pharmacological LQT model in rabbit hearts, showed during an EAD the rise of Ca<sup>2+</sup> preceded the AP and suggested this was spontaneous SR Ca<sup>2+</sup> release that triggered Ca<sup>2+</sup> dependent currents (*e.g.* I<sub>NCX</sub>) (Choi BR *et al*, 2002). But an unequivocal causal link between intracellular Ca<sup>2+</sup> and EAD was not established.

## Aims

The experiments described in this Chapter were designed to establish a pharmacological LQT model and describe the model's electrophysiological characteristics to permit subsequent work examining the generation of EADs and ventricular arrhythmias. The results presented in this Chapter will characterise the APD response to LQTS. The occurrence of EADs and arrhythmias is reported in Chapter 4.

Specific aims were:

1. Design and characterise an experimental *ex vivo* model of LQT2 in the rabbit including:
  - i. Establish and optimise AVN ablation technique to allow the use of long PCL values.
  - ii. Evaluate the preparation's electrophysiological viability over time.
  - iii. Describe electrophysiological characteristics at baseline and under LQT states.

## Methods

In order to characterise an experimental *ex vivo* model of LQT2, optical mapping was used to record optical APs and CaTs from the epicardial surface of Langendorff-perfused intact rabbit hearts. Hearts from 62 male New Zealand White rabbits were used in these experiments, which conform to standards set out in the UK Animals (Scientific Procedures) Act, 1986. Details of how hearts were harvested are already described in Chapter 2 (pp. 63). To allow ventricular pacing at low heart rates (*i.e.* long PCLs) required AVN ablation, this has been described in Chapter 2 (pp. 66).

### ***Experimental Protocols***

Dual optical mapping of Langendorff-perfused rabbit hearts ( $n = 62$ ) was performed as detailed in Chapter 2. A small number of initial experiments without LQT conditions were used to determine electrophysiological recording stability (1 heart) and to test the AVN ablation procedure (1 heart). The restitution protocols were performed in 17 hearts, in which recordings were taken at 350ms PCL and extra-stimulus restitution pacing protocols. Optical AP measurements were also taken during intrinsic rhythm. The effect of  $I_{Kr}$  blockade on optical APs was also examined using dofetilide 0.5 $\mu$ M ( $n = 4$ ) and E-4031 0.5 $\mu$ M ( $n = 13$ ). Previous experiments that were not used for this dataset, used a log scale of dofetilide doses (*e.g.* 20nM, 50nM, 0.2 $\mu$ M, 0.5 $\mu$ M, 2 $\mu$ M) to determine the  $IC_{50}$ . This was felt to be 3nM and a dose of 0.5 $\mu$ M was selected for both dofetilide and E-4031 to have the maximum desired effect, this was consistent with doses used in published work (Choi BR *et al*, 2002). Experimental conditions were incremented to elicit EADs, *i.e.* pacing at slower CLs and a step-wise introduction of LQT conditions, including reduction of 50%  $K^+/Mg^{2+}$  in the perfusate and E-4031 0.5 $\mu$ M ( $n = 10$ ). The experimental protocol is depicted in Figure 3.1.

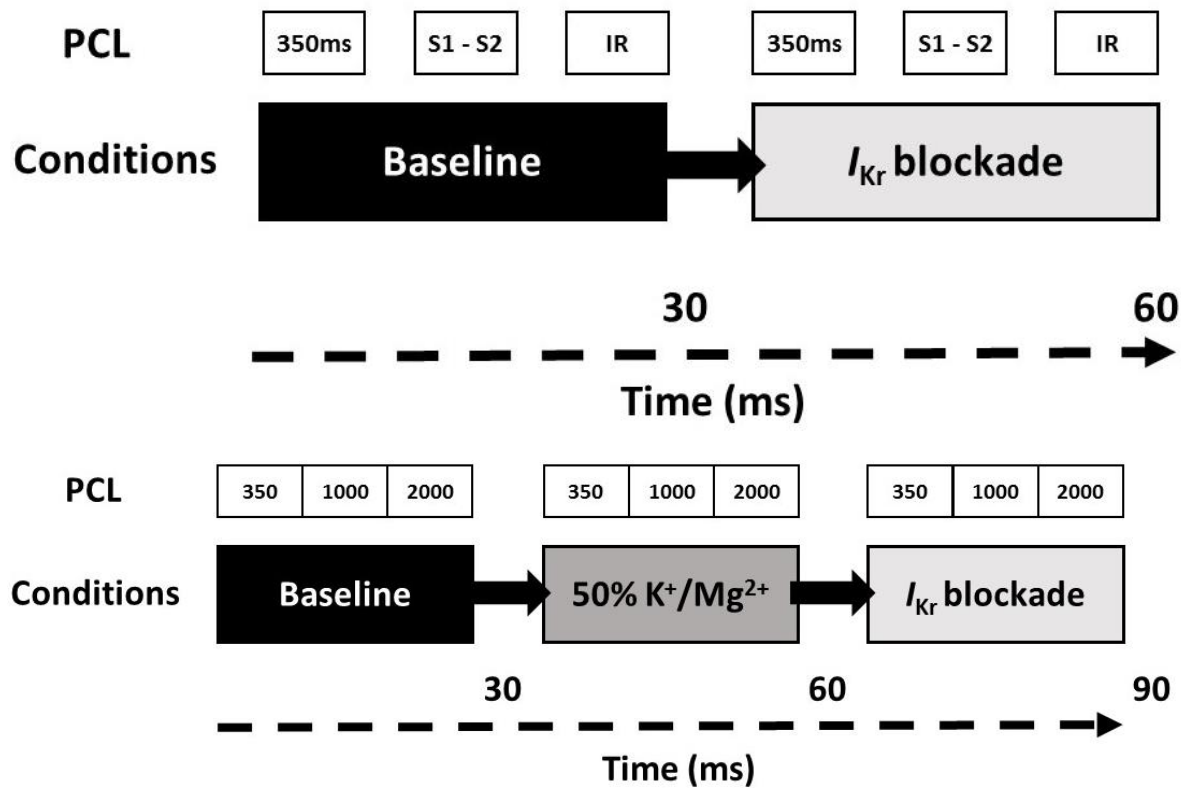


**Figure 3.1** – Summary of experimental protocols.

Experimental protocols used throughout, highlighting order of pacing protocols and changing conditions. IR = intrinsic rhythm. S1-S2 = extra-stimulus restitution.

## Results

### ***Summary of Experimental Numbers***

A detailed account of experimental numbers and outcomes are detailed in Table 3.2. Total hearts used for this study was 62. A total of 13 hearts were excluded as they did not meet the viability criteria as detailed in Chapter 2 (pp. 69). A subset of hearts ( $n = 2$ ) were used to check preparation stability to ensure baseline recordings of physiological and electrophysiological parameters before progressing with LQT protocols and perform an AVN ablation test. This involved troubleshooting the AVN ablation and monitoring for return of intrinsic rhythm under baseline conditions, then incrementally applying blebbistatin, DMSO alone and optical dyes, to identify factors that could be driving the intrinsic rate. Experiments under LQT conditions involved  $I_{Kr}$  blockade with dofetilide ( $n = 13$ ) and E-4031 ( $n = 34$ ). Successful ablation was achieved in 4/13 of the dofetilide hearts, whereas successful ablation was achieved in 31/34 of E-4031 cohort, this was due to the learning curve associated with achieving successful AVN ablation. The E-4031 cohort were used for restitution analysis ( $n = 13$ ) and LQT protocol ( $n = 18$ ).

Study		Total hearts	Successful ablation
LQT conditions	Dofetilide	13	4
	E-4031	34	31
Non-LQT conditions	Test of stability + AVN ablation test	2	-
Excluded	Non-viable	13	-
<b>Total</b>		<b>62</b>	<b>35</b>

**Table 3.2.** Summary of experimental numbers and protocols.

### ***Optimising the AVN Ablation***

Initial development of the AVN ablation involved determining rabbit cardiac anatomy by studying hearts used for other experiments, then observation of experienced operators, before I then practiced and optimised the ablation technique that was used throughout. The methodology of AVN ablation has been described previously in Chapter 2 (pp. 66). Successful AVN ablation was defined as durable AVN ablation that facilitated PCLs >2000ms throughout. In the event of AVN recovery, chemical ablation was repeated three times and mechanical crush was attempted if chemical ablation did not succeed. Throughout the experiments, there was a clear learning curve evident with regards to optimisation of the AVN ablation.

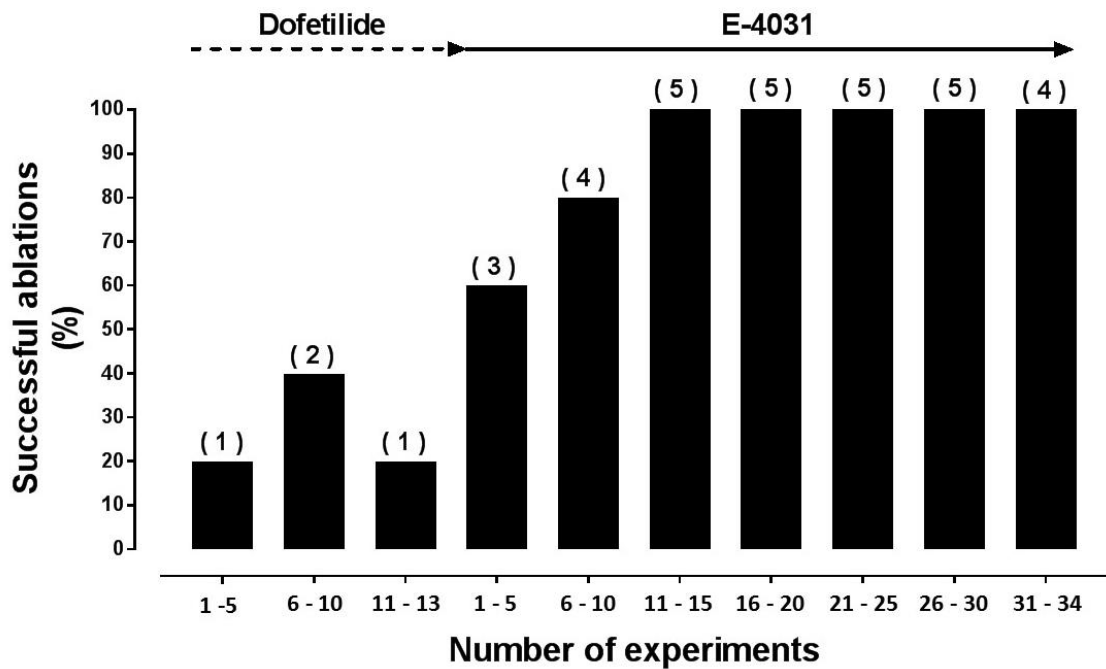


**Figure 3.2.** Number of successful AVN ablations over time.

### ***Preparation Stability***

In all experiments, temperature and pH was checked periodically throughout, as well as electrophysiological assessment of viability (described below, Preparation Viability section). In one experiment, preparation stability was tested by measuring change in APD<sub>90</sub>, APD<sub>50:90</sub>, pH and temperature over time, Figure 3.4. These parameters were recorded at 10-minute intervals under baseline conditions at 350ms PCL. Mean APD<sub>90</sub> at 350ms PCL was  $132 \pm 2.9$ ms and mean APD<sub>50:90</sub> was  $0.802 \pm 0.003$  (SD was too small to plot), both showed no significant variation. Both pH and temperature recordings also showed no significant changes. Overall this demonstrated the preparation had good stability over the time the LQT protocols required.

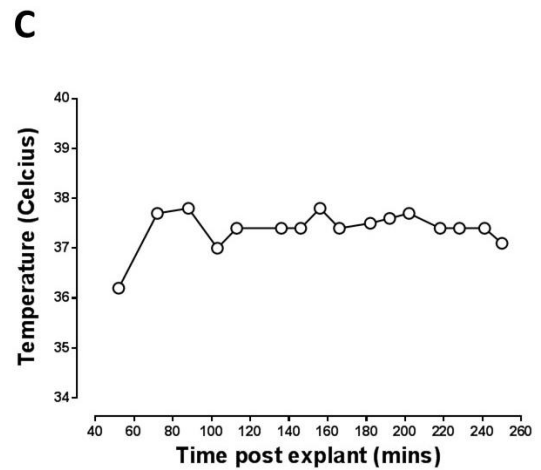
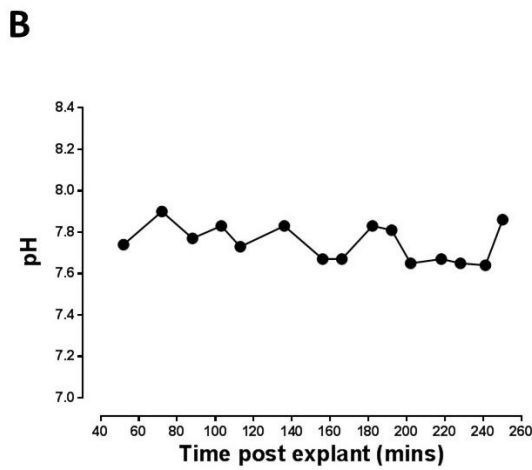
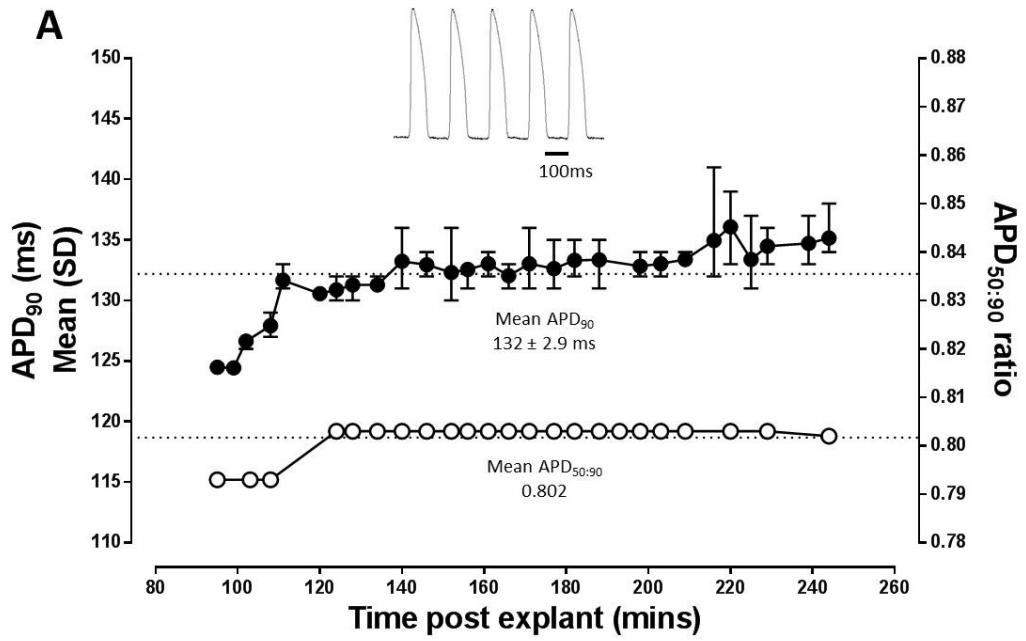


**Figure 3.3.** Baseline APD<sub>90</sub>, pH and temperature over time.

At baseline conditions at 350ms PCL, change in (A) APD<sub>90</sub> and APD<sub>50:90</sub> (B) pH and (C) temperature were recorded and showed no significant change (n = 1).



## Signal-to-Noise Ratio

Epicardial sampling sites and examples of filtered AP and CaT traces at 350ms PCL are shown in Figure 3.4. Typical SNR values, for both RH237 and Rhod2, from one experiment are shown in Figure 3.5. As part of viability assessment, SNR was recorded across multiple experiments ( $n = 13$ ) and was maintained throughout, Figure 3.6. Quality control measures involved removing any SNR value less than 20 during optical analysis, to ensure optimal signals were used for data collection. A number of 20 was determined from visual assessment, as optical signals with a SNR  $<20$  were often poor quality.

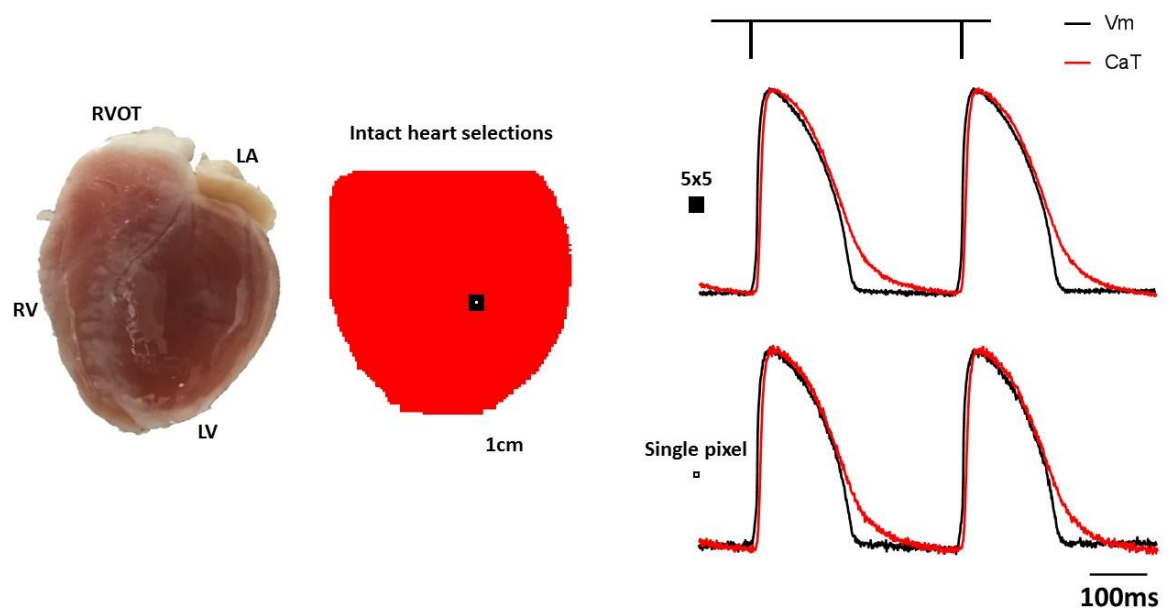


**Figure 3.4.** Epicardial optical APs and corresponding CaTs.

Optical APs and CaTs from single pixel and 5x5 selections taken during baseline conditions at 350ms PCL. Pacing stimulus is depicted by black marker on the top right.

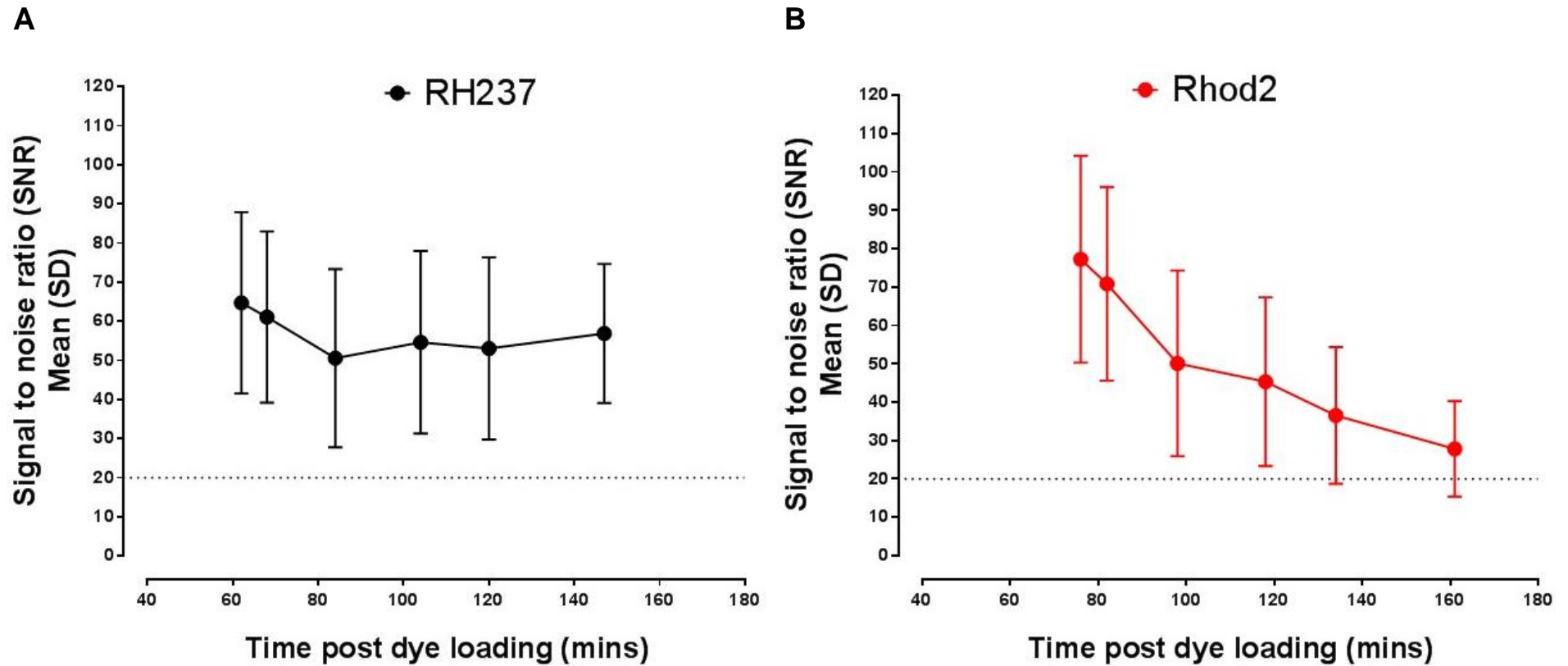


**Figure 3.5.** Change in signal-to-noise over the duration of a single experiment.

Signal to noise for (A) RH237 and (B) Rhod2 over the duration of the experiment ( $n = 1$ ). Time was recorded as time post loading of the dyes. Rhod2 was loaded after RH237. Substandard levels are denoted by a line at a SNR of 20.

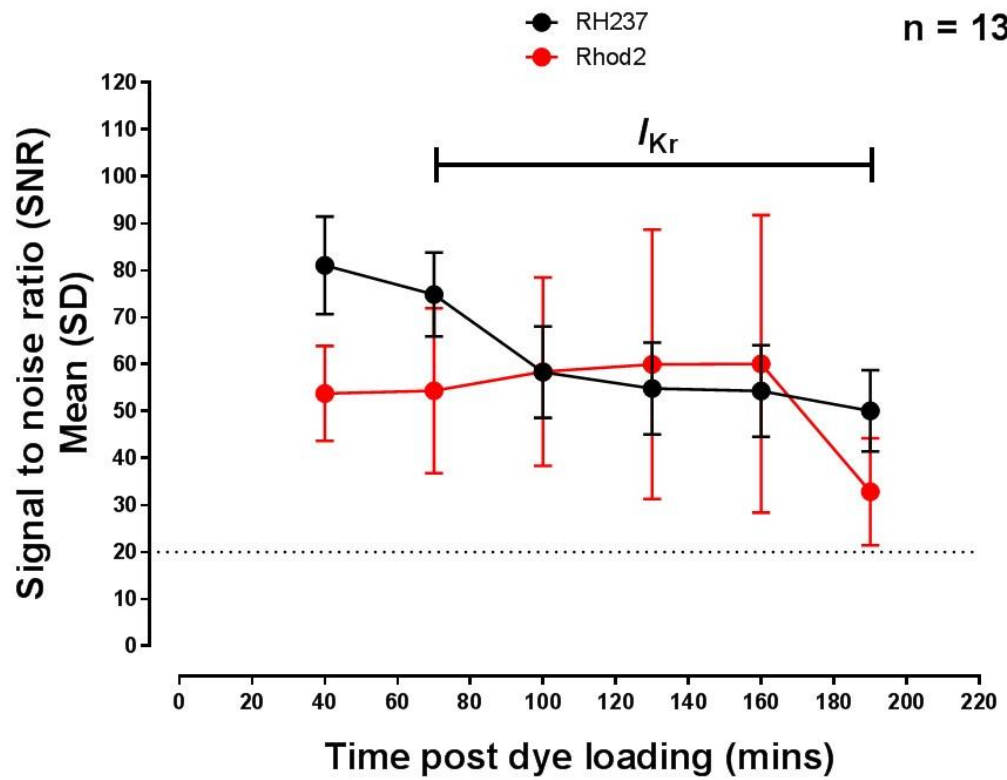


**Figure 3.6.** Change in signal-to-noise over the duration of combined experiments.

Combined SNR values across  $n = 13$ , for RH237 (black) and Rhod2 (red). Threshold for optical analysis (20) is indicated on the graph.

## ***Preparation Viability***

Langendorff preparations are prone to regional or global ischaemia due to block of coronary arteries from air bubbles or particulate matter in the perfusate. Ischaemia causes characteristic changes in AP shape as a result of extracellular and intracellular changes, these include shortening of APD with triangulation of AP shape and reduced rate of initial depolarisation. To identify any compromised preparations, set parameters were recorded and monitored throughout to assess viability. Changes in APD normally associated with ischaemia include change in: APD<sub>90</sub>, APD<sub>50:90</sub>, rise time and range of activation. During ischaemia there were typical changes in AP characteristics that are shown in Figure 3.7. These changes include triangulation of the APD (shorter APD<sub>50:90</sub>), prolonged rise time and increased range of activation over a fixed region (*i.e.* slower conduction velocity). In compromised preparations these changes were seen both at baseline and under  $I_{Kr}$  blockade, Figure 3.8. The total hearts found to have ischaemic-like changes was 13/62 (21%) and these were excluded from the dataset. Hearts found to have ischaemic-like changes typically had a major challenge to the preparation, either from air embolus, mechanical trauma from atriotomy or chemical trauma from AVN ablation. The appearance of the heart in the custom chamber, pECG activity (*i.e.* VT/VF) and  $V_m$  morphology on mapping clearly identified ischaemic-like changes, and so these hearts excluded from the dataset occurred from predictable events. An example of a single experiment viability assessment is shown in Figure 3.9. Average viability assessment from a combined 13/49 hearts is shown in Figure 3.10 (this is not the same 13/62 hearts described above that were found to be ischaemic – those were excluded). Throughout each experiment, incremental doses of  $I_{Kr}$  blockade was introduced that significantly prolonged the APD<sub>90</sub>, whilst other viability parameters had no significant change.

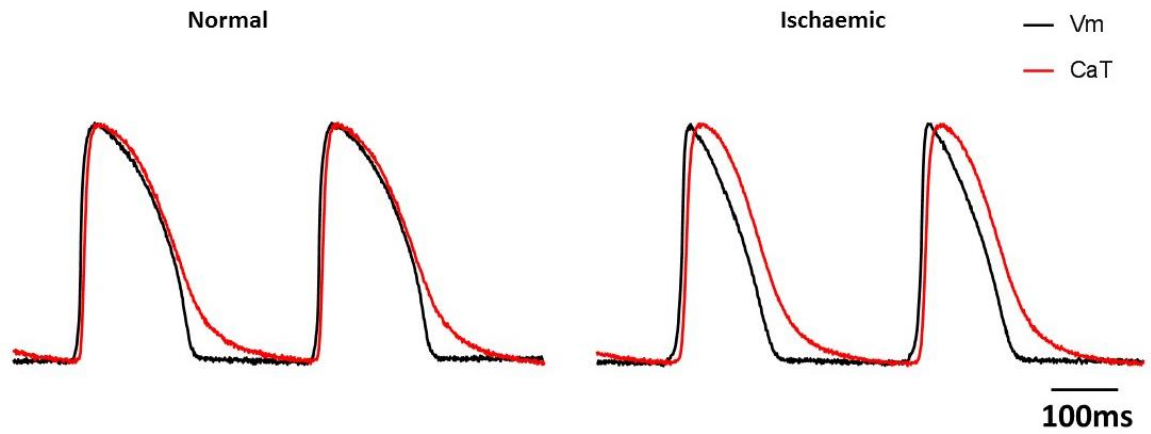


**Figure 3.7.** Normal vs. ischaemic optical APs and CaTs.

Optical APs and CaTs from a 5x5 pixel selection, under baseline conditions at 350ms PCL and corresponding APs/CaTs in the same preparation with ischaemic changes.

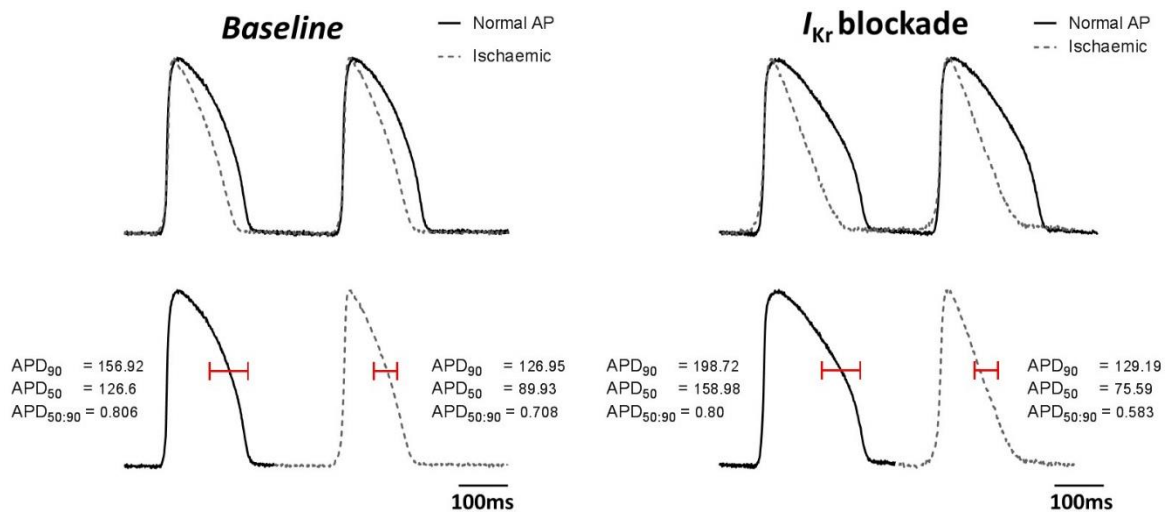


**Figure 3.8.** Normal vs. ischaemic APD changes.

Optical APs from a 5x5 pixel selection, under baseline conditions and *I<sub>Kr</sub>* blockade, at 350ms PCL and corresponding APs in the same preparation with ischaemic changes. Ischaemia causes triangulation of the AP with reduction in APD<sub>50:90</sub>.

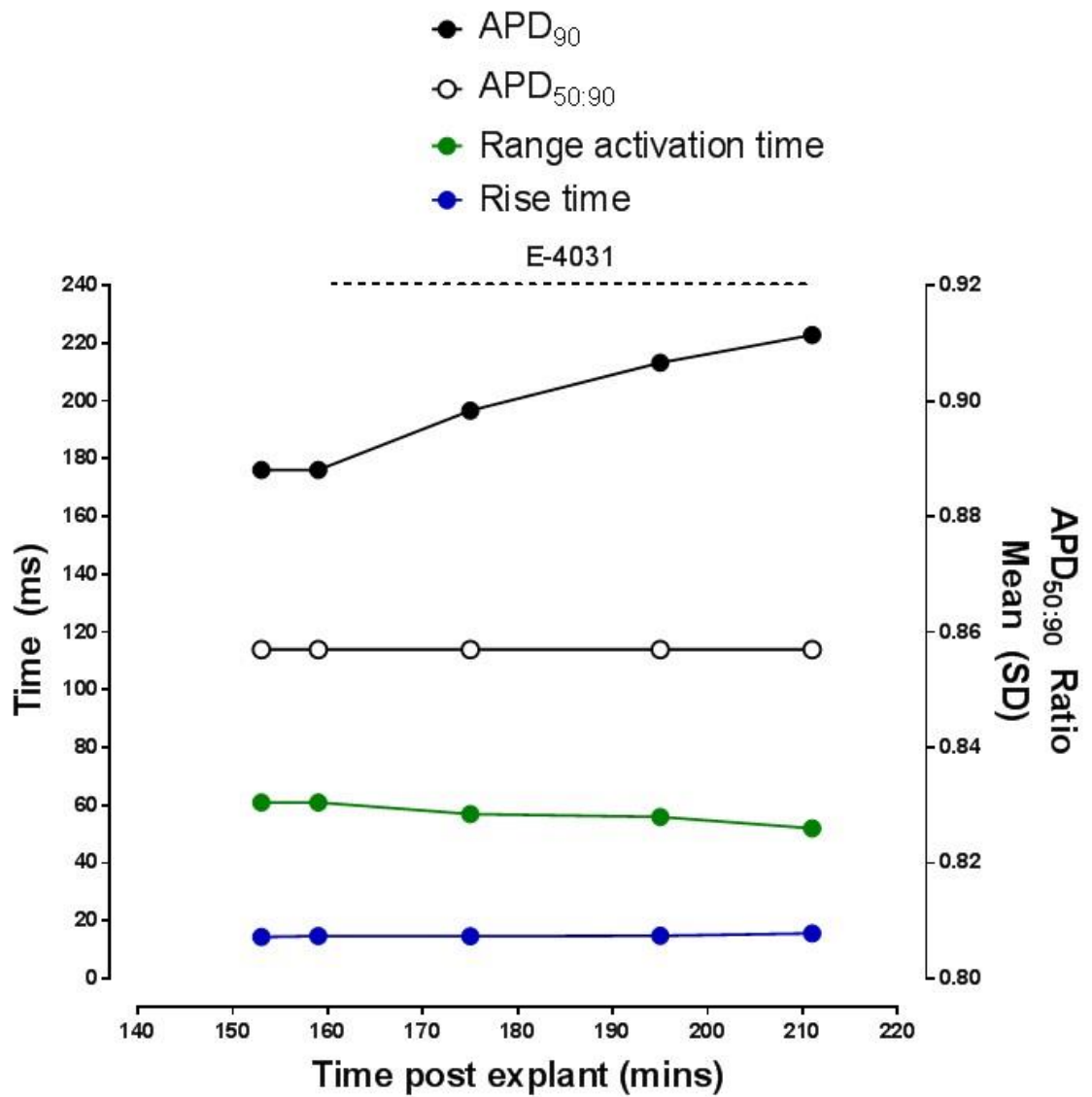


**Figure 3.9.** Viability assessment taken from a single experiment.

Change of APD<sub>90</sub>, APD<sub>50:90</sub>, range of activation and rise time from a single experiment at 350ms PCL. These were taken from a 5x5 pixel selection. Increase in APD<sub>90</sub> is seen from the addition of  $I_{Kr}$  blockade with E-4031 (0.5 $\mu$ M) but other viability parameters show minimal change over the duration of the experiment.

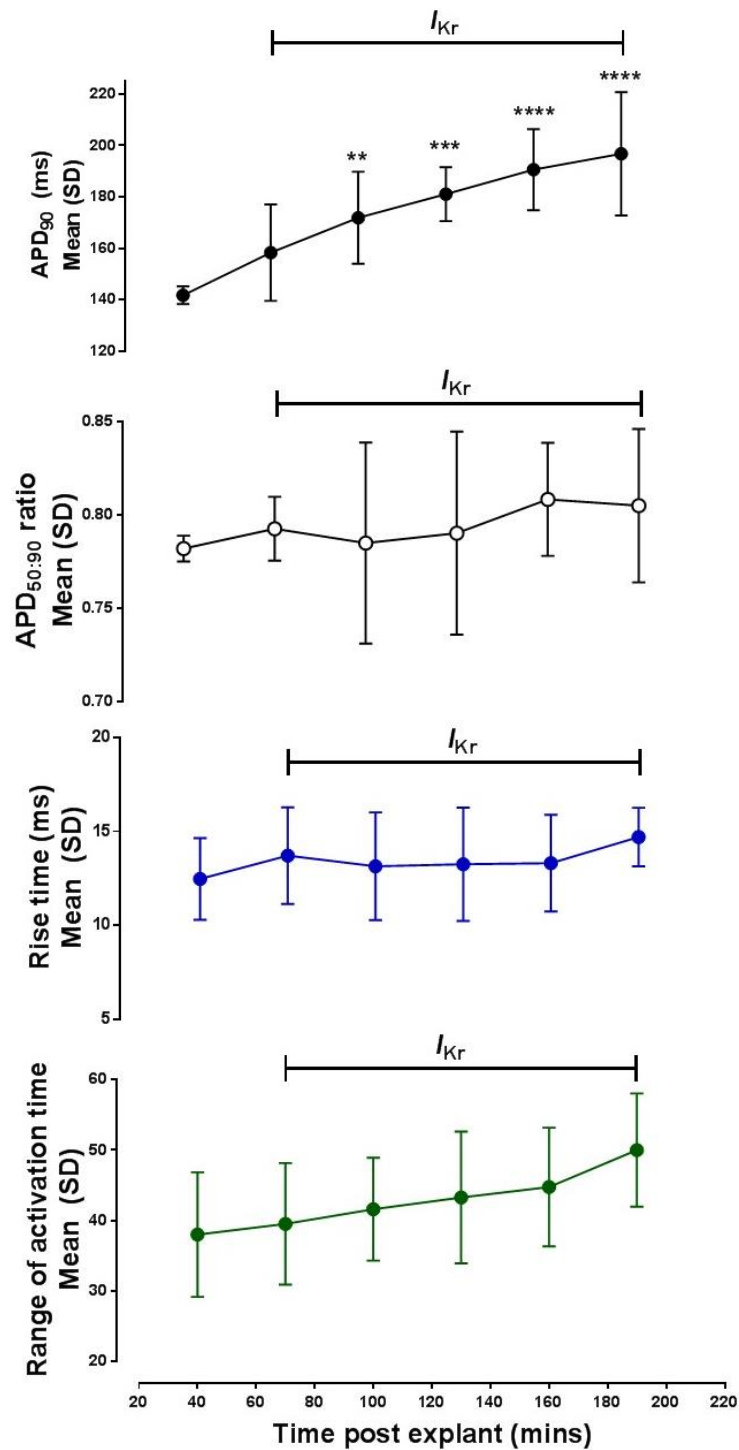


**Figure 3.10.** Viability parameters over time following explant.

Viability recordings were taken throughout each experiment at frequent intervals, using a stimulus rate of 350ms PCL. The introduction of  $I_{Kr}$  blockade in this subset was with E-4031 at incremental concentrations (0.01 $\mu$ M – 0.5 $\mu$ M). Owing to the dynamic timings of experiments, recordings at exact and paired intervals were not possible. Overall recorded viability parameters over time were averaged in 5-12 hearts, one-way ANOVA with Dunnett's multiple comparison test:

\*\*\*\*  $p < 0.0001$ , \*\*\*  $p < 0.001$ , \*\*  $p < 0.01$  vs. baseline. Change in APD<sub>90</sub> showed a significant difference after introduction of  $I_{Kr}$  blockade. Other viability parameters: APD<sub>50:90</sub>, rise time and range of activation had no significant change over time compared to baseline, one-way ANOVA was not significant.

### ***Restitution Analysis***

The data for APD<sub>90</sub> restitution during epicardial stimulation at baseline vs.  $I_{Kr}$  blockade with dofetilide 0.5 $\mu$ M (n=4) and E-4031 0.5 $\mu$ M (n = 12/13) is shown in Figure 3.11. In one of the E-4031 cohort, baseline restitution data was not collected. Mean APD<sub>90</sub> at 1000ms at baseline was 151  $\pm$  16ms vs. 228  $\pm$  18ms with dofetilide ( $p < 0.0001$ ). In the E-4031 cohort (n = 12), mean APD<sub>90</sub> at 1000ms at baseline 149  $\pm$  22ms vs. 191  $\pm$  25ms with E-4031 ( $p < 0.0001$ ).



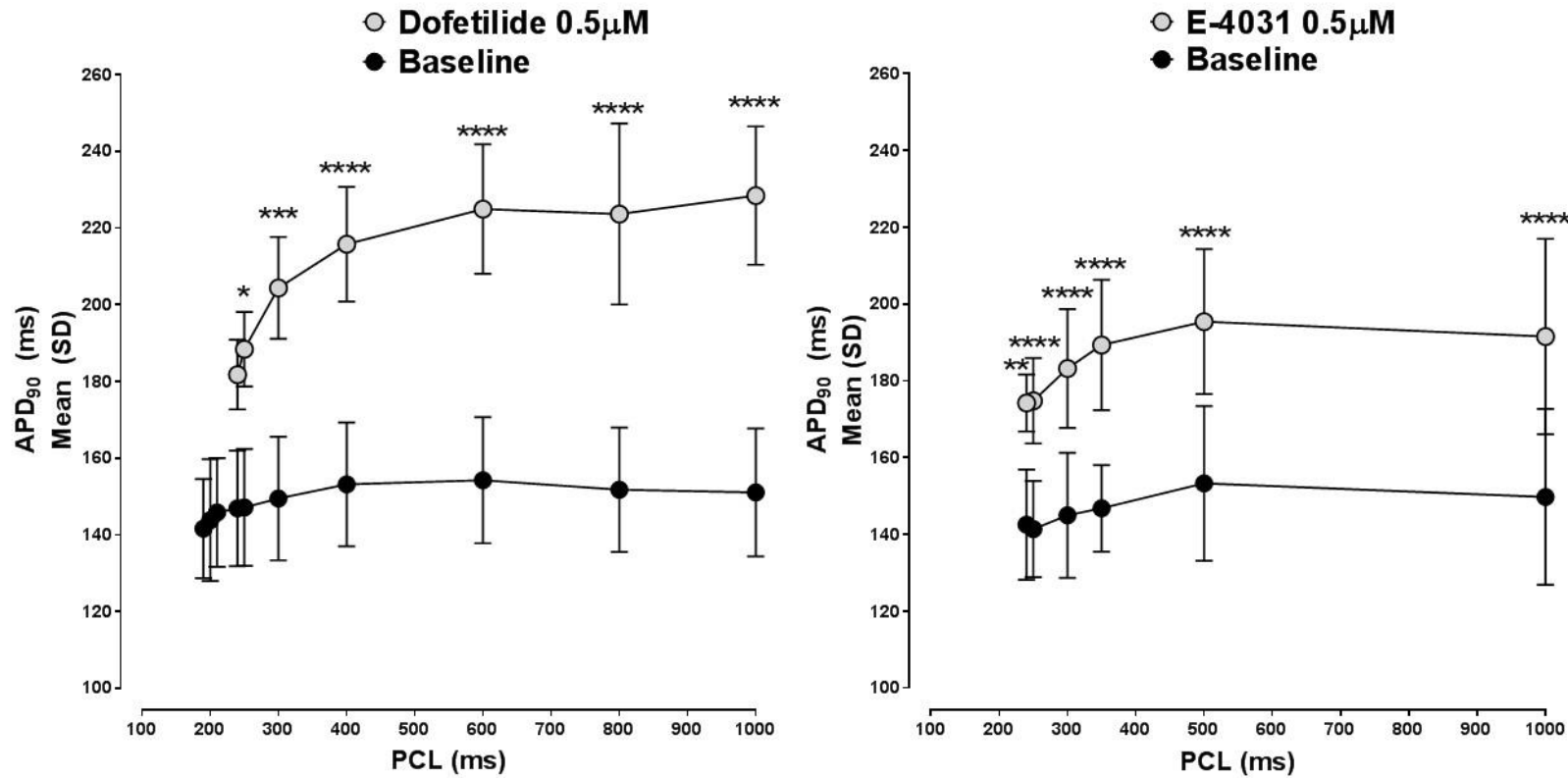


**Figure 3.11.** Effect of  $I_{Kr}$  block on APD restitution.

Extra-stimulus restitution curve for baseline vs. dofetilide 0.5µM (n = 4) and baseline vs. E-4031 0.5µM (n = 12). Two-way ANOVA with Sidak's multiple comparison test: \*\*\*\* p < 0.0001, \*\*\* p < 0.001, \*\* p < 0.01, \* p < 0.05 vs. baseline.

### ***Electrophysiological Characteristics Under LQT States***

EADs and PVCs were not routinely observed in the presence of  $I_{Kr}$  block at PCL of 1000ms, so further APD-prolonging conditions were added incrementally, (PCLs of 2000ms and 50%  $K^+/Mg^{2+}$ ). No PVCs, bursts or ventricular arrhythmias were observed with either dofetilide or E-4031 alone, or 50%  $K^+/Mg^{2+}$  alone. Examples of APs and corresponding pECGs at baseline and during 50%  $K^+/Mg^{2+}$  and then after addition of E-4031 0.5 $\mu$ M at 2000ms PCL are shown in Figure 3.12. Dynamic pacing protocols were performed in a subset of experiments ( $n = 10$ , Figure 3.13). APD<sub>90</sub> values across these incremental conditions, over different CLs, are shown in Table 3.3. Individual mean APD<sub>90</sub> values at 2000ms are shown in Figure 3.14.

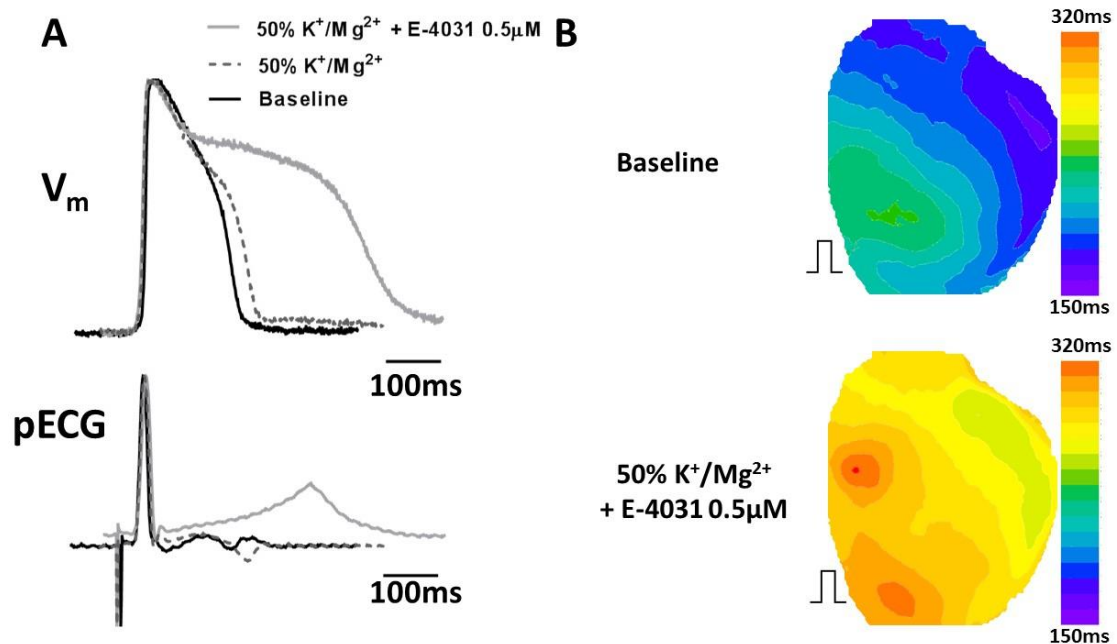


**Figure 3.12.** Examples of APs and corresponding pECGs under LQT conditions.

(A)  $V_m$  and pECG traces from 5x5 pixel selection at baseline, 50%  $K^+/Mg^{2+}$  and E-4031 0.5 $\mu$ M at 2000ms PCL (B) Contour maps of epicardial APD<sub>90</sub> across the whole heart at baseline vs. 50%  $K^+/Mg^{2+}$  + E-4031 0.5 $\mu$ M. The position of the stimulating electrode is indicated by the symbol (┌┐).

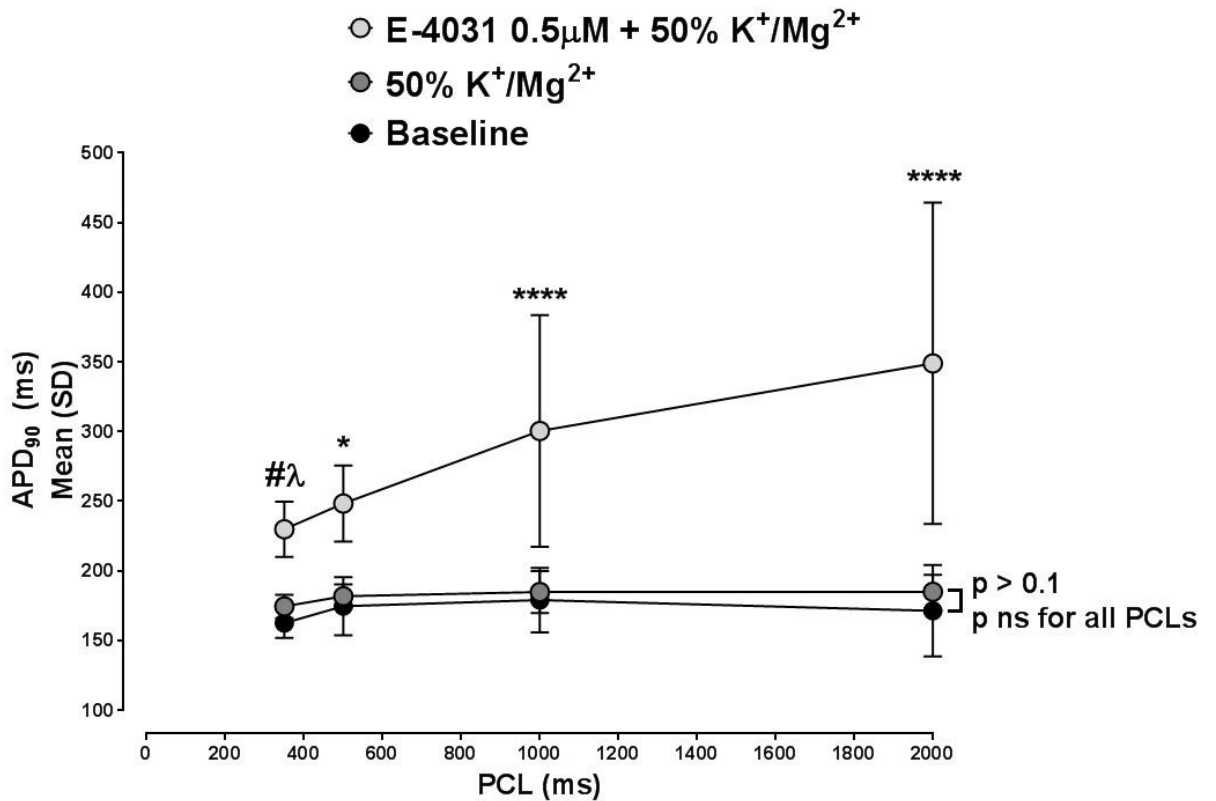


**Figure 3.13.** Change in APD<sub>90</sub> during dynamic restitution protocol.

Change in APD<sub>90</sub> for n = 10, PCLs of 350, 500, 1000 and 2000ms under baseline, 50% K<sup>+</sup>/Mg<sup>2+</sup> and 50% K<sup>+</sup>/Mg<sup>2+</sup> + E-4031 0.5µM. Two-way ANOVA: \*\*\*\* p < 0.0001 vs. baseline and vs. 50% K<sup>+</sup>/Mg<sup>2+</sup>, \* p < 0.05 vs. baseline and vs. 50% K<sup>+</sup>/Mg<sup>2+</sup>, # p < 0.01 vs. baseline, λ p < 0.05 vs. 50% K<sup>+</sup>/Mg<sup>2+</sup>.

PCL (ms)	Mean APD <sub>90</sub> (ms) ± SD			P vs. baseline
	Baseline	50% K <sup>+</sup> /Mg <sup>2+</sup>	50% K <sup>+</sup> /Mg <sup>2+</sup> + E-4031 0.5µM	
2000	171.5 ± 32.8	184.7 ± 12.5	330.0 ± 107.9	< 0.0001
1000	178.9 ± 23.2	184.7 ± 15.1	298.9 ± 84.0	< 0.0001
350	162.3 ± 10.7	174.6 ± 8.5	229.6 ± 19.8	< 0.01

**Table 3.3.** Changes in APD<sub>90</sub> at different cycle lengths and conditions.

Actual APD<sub>90</sub> values for n = 10, over different PCLs of 350, 1000, 2000ms PCL at baseline, 50% K<sup>+</sup>/Mg<sup>2+</sup> and 50% K<sup>+</sup>/Mg<sup>2+</sup> + E-4031 0.5µM. Two-way ANOVA.

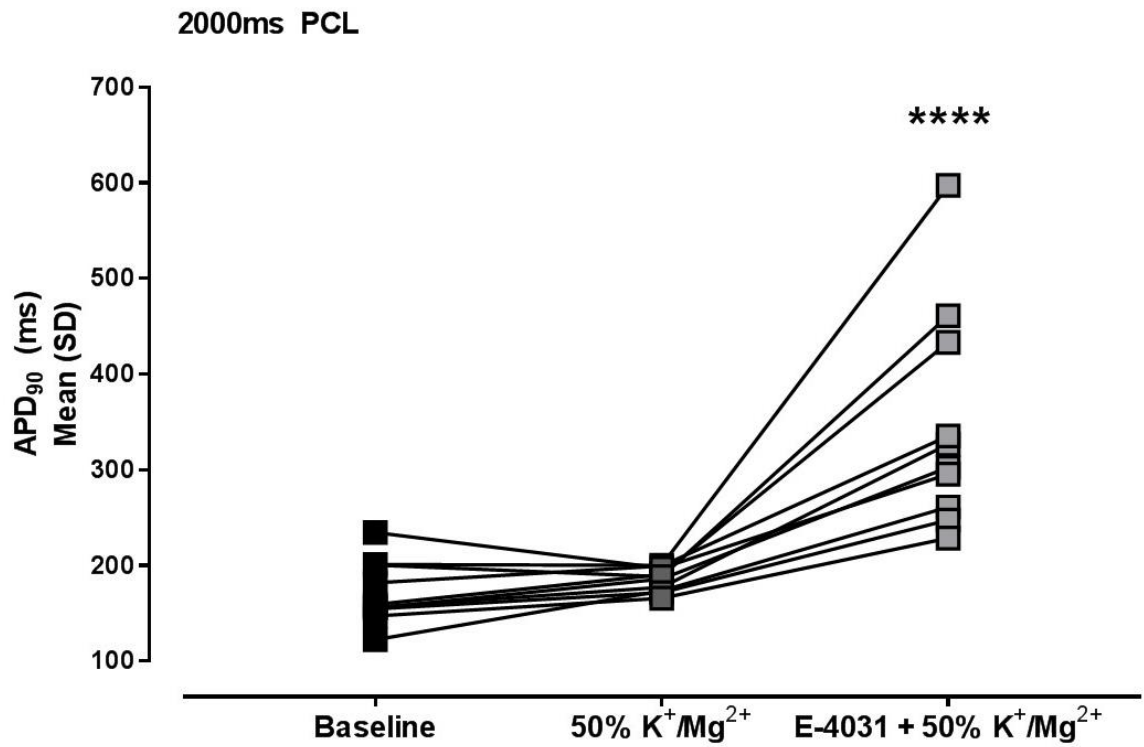


**Figure 3.14.** Change in APD<sub>90</sub> over baseline, 50% K<sup>+</sup>/Mg<sup>2+</sup> and LQT conditions.

Mean epicardial APD<sub>90</sub> at 2000ms PCL at baseline, 50% K<sup>+</sup>/Mg<sup>2+</sup> and LQT conditions for n=10 hearts. Repeated measures one-way ANOVA with Tukey's post-testing: \*\*\*\*\* p < 0.0001 vs. baseline and vs. 50% K<sup>+</sup>/Mg<sup>2+</sup>.

### ***Apex – Base Changes in APD***

In a subset of hearts ( $n = 8-17$ ), apical and basal epicardial APDs were compared across hearts at baseline (350, 500, 1000 and 2000ms PCL, Figure 3.15A) and under LQT conditions (all 2000ms PCL, Figure 3.15B). At baseline in this subset, there was no difference between apical and basal APD<sub>90</sub> at any CL. Similarly, with either 50% K<sup>+</sup>/Mg<sup>2+</sup> alone or E-4031 0.5μM alone, there were no significant differences between apical and basal regions (2000ms only tested). However, when the two conditions were combined (i.e. 50% K<sup>+</sup>/Mg<sup>2+</sup> + E-4031 0.5μM), a significant mean APD difference between apex and base was observed ( $276.8 \pm 58.0\text{ms}$  vs.  $388.4 \pm 205.8\text{ms}$ ,  $p < 0.05$ ).

In a separate subset ( $n = 10$ ), a paired comparison of the difference in APD<sub>90</sub> across apical and basal segments was analysed across 5x5 selections with the highest SNR, at 2000ms PCL at baseline vs. 50% K<sup>+</sup>/Mg<sup>2+</sup> + E-4031 0.5μM. Differences in apex vs. base were significant at baseline but not under LQT conditions (with 50% K<sup>+</sup>/Mg<sup>2+</sup> + E-4031 0.5μM) with the maximum APD prolongation, Figure 3.16. Mean APD<sub>90</sub> at baseline basal segments  $159.4 \pm 24.8\text{ms}$  vs. apical  $170.5 \pm 28.7\text{ms}$  (paired students t-test,  $p < 0.01$ ), and mean APD<sub>90</sub> under LQT conditions in the basal segments was  $313.4 \pm 69.5\text{ms}$  vs.  $384.8 \pm 173\text{ms}$  in the apical region (Wilcoxon matched-pairs signed rank test,  $p = \text{ns}$ ). Note the variability in the apical region, this was felt to be biologically relevant and representative of the widespread APD<sub>90</sub> variability under LQT conditions. There was no technical or experimental reason to exclude any outliers and so all data were included in the analysis.

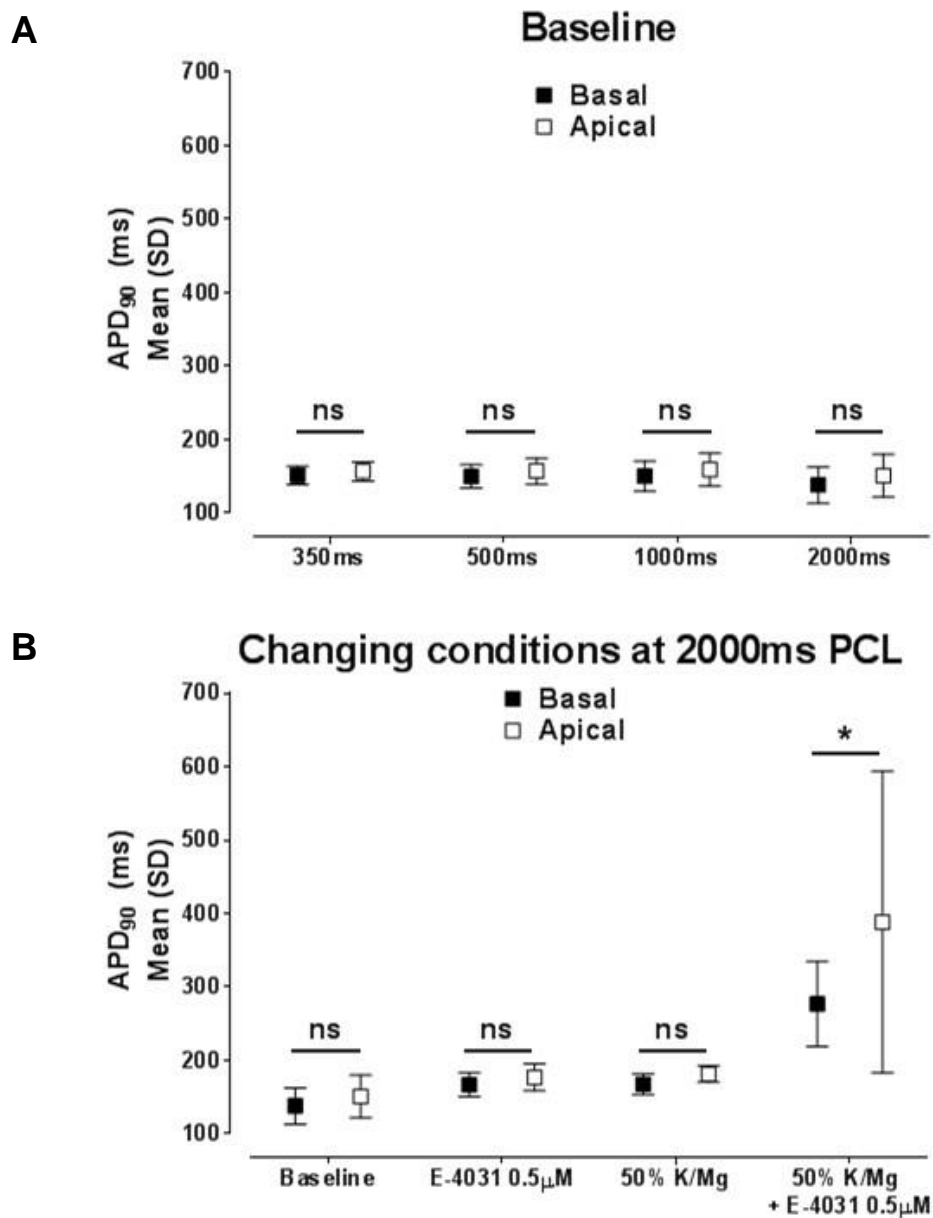


**Figure 3.15.** Comparison of APD<sub>90</sub> between apex and base.

(A). Apex vs. base mean APD<sub>90</sub> under baseline conditions at 350, 500, 1000 and 2000ms PCLs. (B). Apex vs. base mean APD<sub>90</sub> at 2000ms PCL at baseline, E-4031 0.5µM alone, 50% K<sup>+</sup>/Mg<sup>2+</sup> alone and 50% K<sup>+</sup>/Mg<sup>2+</sup> + E-4031 0.5µM. \* p < 0.05 using a two-way ANOVA with Sidak's multiple comparisons. Values taken across 8-17 hearts.

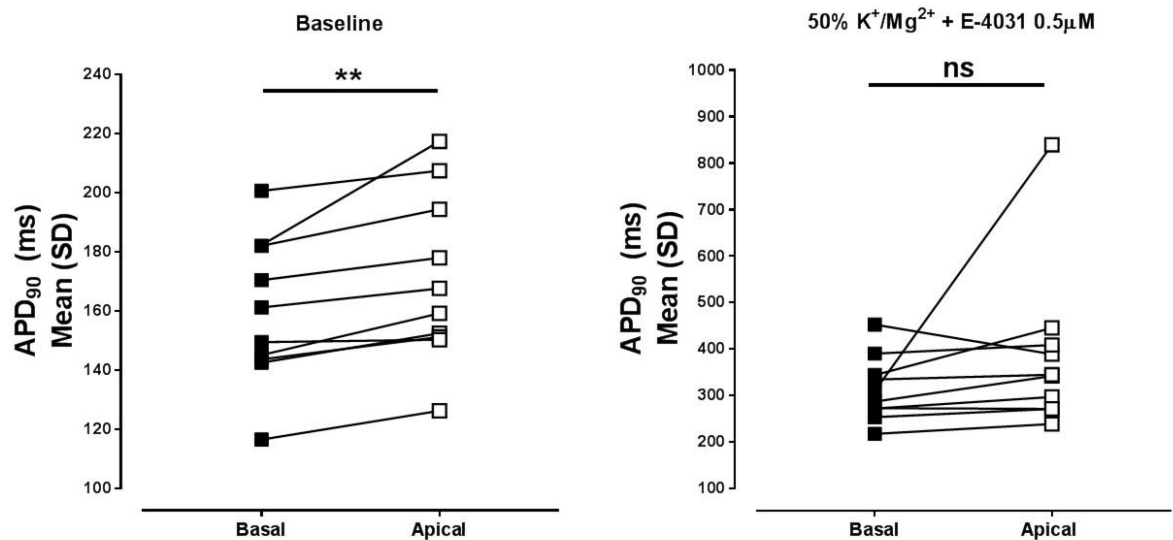


**Figure 3.16.** Comparison of APD<sub>90</sub> between apex and base under LQT conditions.

Mean APD<sub>90</sub> apex vs. base gradients at baseline and 50% K<sup>+</sup>/Mg<sup>2+</sup> + E-4031 0.5µM conditions (n = 10). Note the difference in the Y-axes for the two graphs, LQT conditions are on a much larger scale. Apical vs. basal APD<sub>90</sub> was significantly different under baseline conditions (p < 0.01), paired Students t-test. Under 50% K<sup>+</sup>/Mg<sup>2+</sup> + E-4031 0.5µM, there were no significant apex vs. base difference, Wilcoxon matched-pairs signed rank test (data not normally distributed).

### ***Epicardial Heterogeneity of APD***

To complement this data, the interquartile range (IQR) of APD<sub>90</sub>, was also calculated at baseline vs. 50% K<sup>+</sup>/Mg<sup>2+</sup> + E-4031 0.5μM in the same hearts (n = 10). The IQR was used as a means of assessing within heart variability by measuring the mean APD<sub>90</sub> across the entire epicardial surface. The IQR values were plotted in a scatter plot, Figure 3.17. Mean IQR at baseline was 12 ± 7.67 vs. 50% K<sup>+</sup>/Mg<sup>2+</sup> + E-4031 0.5μM 113 ± 157.2 (Wilcoxon test of IQR, p < 0.01).



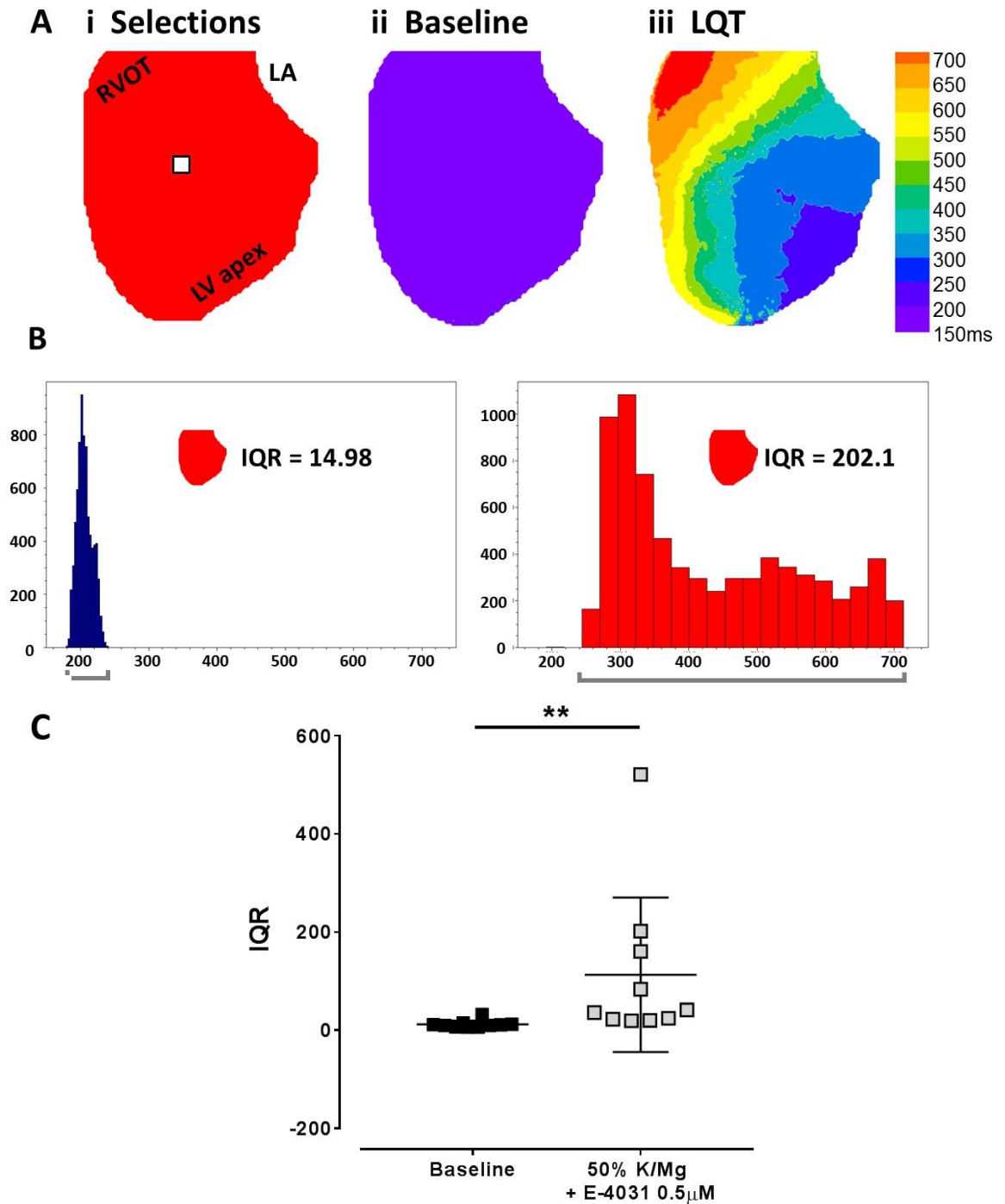


**Figure 3.17.** Variability in APD<sub>90</sub> interquartile range (IQR) under LQT conditions.

(A) Examples of (i) heart orientation with selections used for 5x5 pixels covering mean APD<sub>90</sub> (shown in Figure 3.17) and whole heart selections used for IQR within-heart variability analysis, alongside APD<sub>90</sub> maps for (ii) baseline and (iii) LQT conditions of 50% K<sup>+</sup>/Mg<sup>2+</sup> + E-4031 0.5 $\mu$ M. (B) Histogram of APD<sub>90</sub> distribution at baseline and LQT conditions for corresponding APD<sub>90</sub> maps in (A i-ii), showing skewed APD distribution and higher IQR values under LQT conditions (n = 1). (C) Interquartile range of APD<sub>90</sub> for baseline vs. 50% K<sup>+</sup>/Mg<sup>2+</sup> + E-4031 0.5 $\mu$ M across n = 10 hearts. Baseline IQR shows little variability, however LQT conditions show widespread variability and higher IQR, p < 0.01, Wilcoxon matched-pairs signed rank test.

## Discussion

In this study, a pharmacological *ex vivo* model of LQT2 in an intact rabbit heart, was set-up and characterised.

### ***Optimisation of AVN Ablation Technique***

To permit the use of very long PCLs, the AVN ablation was optimised over a series of experiments. The adopted technique involved chemical ablation, which aimed to induce AV block on the first attempt by injecting the AVN with 0.01mls 10% formalin. This was identified by heart rate response and ECG appearances when applying the needle. Success was considered clear AV dissociation on ECG, allowing PCLs consistently over 2000ms that proved reliable and reproducible and without complication or intrinsic rhythm breakthrough at a faster PCL than required. This typically was achieved on the first attempt but if required, was repeated a maximum of three times, as multiple attempts were associated with chemical damage from formalin. During initial experiments, the AVN ablation was not always successful and saw return of intrinsic rhythm, which precluded data acquisition at slower PCLs. If this occurred, both atria were removed and the AV node was mechanically crushed with forceps. If this was still unsuccessful, the experimental protocol was targeted at baseline or restitution data only as the LQT protocol requiring longer PCLs could not be executed.

### ***Preparation Viability***

Preparation stability and viability were monitored throughout each experiment. These parameters included heart rate, pECG morphology/rate, perfusion pressure, perfusate pH and temperature of: preparation, water bath and perfusate. In one heart, stability parameters were recorded without any intervention or experimental protocol to fully assess this. This proved the set up was stable and suitable for further experimental protocols. Post-experimental analysis checked for viability by quantifying electrophysiological parameters such as APD<sub>90</sub>, rise time, range of activation and SNR. Averaged viability parameters were taken across 13 hearts that show SNR did not drop below 20 throughout. The trends in RH237 and Rhod2, were reflective of their loading protocols and that they bleach at different rates. RH237 was

consistently loaded first and so bleached (*i.e.* loss of the dye from the tissue) earlier and Rhod2 loaded at a later stage, so bleaching occurred at a later timepoint. RH237 is also lipophilic and binds to the membrane directly from extracellular space, whereas Rhod2 is introduced to the intracellular space by perfusing with an AM version of the dye and relies on cleavage of acids by esterases. These two processes did not seem to generate significantly different rates of signal loss. It is unclear whether signals in Rhod2 decreased due to bleaching or loss of the dye from the preparation but data was acquired within the 160-minute time frame before SNR decreased to the point that the analytic accuracy would be compromised, therefore intervention with re-loading or introducing additional pharmacology (*e.g.* probenecid) was not required. Stability and viability parameters were continuously monitored to identify any ischaemic changes as these hearts were excluded from the dataset. This involves measuring APD<sub>90</sub>, APD<sub>50:90</sub>, rise time and range of activation. Examples of  $V_m/Ca^{2+}$  signals in an ischaemic heart were demonstrated, showing the typical changes in  $V_m$  morphology, triangulation of the APD, reduction in APD<sub>50:90</sub> and prolongation of  $V_m/CaT$  delay.

Viability assessment was performed throughout experimental protocols and during these, incremental doses of E-4031 were administered throughout and the effects of  $I_{Kr}$  blockade are seen across 13 hearts. E-4031 caused a significant increase in APD<sub>90</sub> over time, in keeping with  $I_{Kr}$  blockade. Other viability parameters had no significant change over time, proving no negative effects of  $I_{Kr}$  blockade on other important electrophysiological characteristics. It was therefore assumed,  $I_{Kr}$  blockade did not adversely affect the preparation or normal electrophysiological characteristics and any changes seen during experimentation were genuine.

### ***Restitution Analysis Overview***

APD<sub>90</sub> restitution was used to describe the recovery of APD as a function of the diastolic interval, in this study CL was used instead of diastolic interval. This type of analysis was performed in 17 hearts, under baseline conditions and two different types of pharmacological  $I_{Kr}$  blockers. During initial studies, dofetilide 0.5 $\mu$ M was used ( $n = 4$ ) and showed a significant prolongation in APD<sub>90</sub> seen clearly in a restitution curve. The other  $I_{Kr}$  blocker

used was E-4031 0.5 $\mu$ M (n = 13), that also significantly prolonged the APD<sub>90</sub>. This provided a clear understanding of what the average APD for CL, under baseline and  $I_{Kr}$  blockade, and facilitated a reference point when screening for short APs for CL, or indeed longer APs that could be involved with arrhythmogenesis.

### ***Electrophysiological Characteristics Under LQT States Overview***

To induce EADs, additional conditions were required as there were no ventricular arrhythmias with either dofetilide, E-4031 or 50%  $K^+/Mg^{2+}$  alone. This is consistent with other studies, which also required additional conditions to induce TdP, these are listed in Table 3.1 This involved halving the  $K^+/Mg^{2+}$  in the perfusate, additional to  $I_{Kr}$  blockade. The effects of 50%  $K^+/Mg^{2+}$  was minimal, however with the addition of  $I_{Kr}$  blockade, the effect on APD<sub>90</sub> prolongation became more profound.

For a subset of experiments (n = 10), direct comparison of change in APD<sub>90</sub> under incremental LQT conditions was made and plotted on a dynamic restitution curve. This involved dynamic pacing at 350, 500, 1000 and 2000ms PCL under baseline, 50%  $K^+/Mg^{2+}$  alone and 50%  $K^+/Mg^{2+}$  +  $I_{Kr}$  blockade. The difference in APD<sub>90</sub> between baseline and 50%  $K^+/Mg^{2+}$  was not significant, however with the addition of  $I_{Kr}$  blockade with E-4031, APD<sub>90</sub> became significantly prolonged and widely distributed (Two-way ANOVA). A scatter plot highlights the wider distribution and prolongation of APD<sub>90</sub>. The optical APD<sub>90</sub> values reported here are in agreement with those recorded in previous studies, in which the range of epicardial APD<sub>90</sub> at baseline was 200-220ms whilst pacing at 2000ms. Under LQT states however, there is widespread distribution of APD<sub>90</sub> at all CLs, which is keeping with those recorded in this study. Longer PCLs under LQT conditions had variable APD<sub>90</sub> with higher SD values.

### ***Apico-Basal APD Gradients***

The presence of APD gradients across apex and base have been previously described and a recognised physiological phenomenon (Cheng J *et al*, 1999; Choi BR *et al*, 2002). In recognition of this, and its arrhythmic potential, the APD<sub>90</sub> across apical and basal sections were analysed across a subset of experiments (n = 8 – 17). Varying experimental numbers occurred as not all experiments underwent the LQT protocol and so protocols varied. During baseline conditions, over incremental PCLs, there was no obvious difference in apical/basal APD<sub>90</sub> when data was unpaired. When a paired comparison was done on a smaller subset (n = 10) at 2000ms PCL under baseline vs. 50% K<sup>+</sup>/Mg<sup>2+</sup> + E-4031 0.5μM, a significant difference emerged where apical selections were significantly more prolonged than basal.

In this paired subset, differences in apical/basal APD<sub>90</sub> were seen at baseline but not at 50% K<sup>+</sup>/Mg<sup>2+</sup> + E-4031 0.5μM. Under baseline conditions, although there were significant apex-base differences (from paired t -test), the magnitude of difference is fairly small (~10ms). Although a numerically similar difference was present in the larger, unpaired comparison the difference there is not statistically significant. This is likely due to the significant between-heart variability which has a greater impact in the unpaired comparison, rather than representing a biologically discrepant result. Similarly, the apparent discrepancy between the paired and unpaired results under LQTS conditions is likely due to the significant increase in variability seen in APD under LQT conditions. To quantify this increase in within-heart variability, IQR was analysed to calculate the mean APD<sub>90</sub> across the entire epicardial surface and shows within heart variability. Larger IQR values were recorded under 50% K<sup>+</sup>/Mg<sup>2+</sup> + E-4031 0.5μM compared with baseline (Wilcoxon test of IQR, p < 0.01), and suggests differences in APD are more marked under these conditions.

This pattern of delayed repolarisation at the apex compared to the base, has been published before at both baseline and under LQT states. Under baseline conditions, optical mapping of guinea pig ventricles saw longer APDs near the base compared with the apex (Efimov IR *et al*, 1994) and APD gradients with spatial dispersion of repolarisation under steady state pacing (Laurita KR *et al*, 1996). In our model, there were no significant apical/basal differences in APD at baseline. However, under LQT conditions any APD differences became considerably steeper and more marked at the apex. This is consistent with published

work (Choi BR *et al*, 2002), where LQT conditions at long PCLs caused significant APD gradients, with apical sections showing larger variability that created marked dispersion of repolarisation. Differences in ion channel expression between apex and base are thought to be responsible for apical-basal changes seen in APD and these have been implicated in the genesis of the T-wave on ECG (Antzelevitch C, 2004a). Furthermore, it has been observed there is a heterogeneous expression of ion channels across ventricular myocytes, where higher density of  $I_{Kr}/I_{Ks}$  have been found at the apex compared with base (Cheng J *et al*, 1999). Under baseline conditions, APD gradients are negligible or not significant to create an effect, whereas application of  $I_{Kr}$  blockade accentuates the heterogeneity and creates notable repolarisation dispersion and APD gradients. Dispersion of APD under LQT states has been suggested to create a vulnerable substrate to induce re-entry (Antzelevitch C, 2002; Belardinelli L *et al*, 2003). However, the involvement of apical/basal differences in APD and repolarisation heterogeneity in EAD-induced arrhythmias has yet to be seen.

### **Comparison to Other LQT Models**

The major differences between the LQT conditions used in this study compared with other LQT models, include PCL, choice of  $I_{Kr}$  blocker and additional features to induce TdP, listed in Table 3.1. The range of PCL used was between 500 – 3000ms PCL, some studies used intrinsic rhythm. In our study, intrinsic rhythm had variable rates and so we chose to pace at a set PCL for consistency. We used dynamic pacing between 500-2000ms at baseline, 50%  $K^+/Mg^{2+}$  and  $I_{Kr}$  blockade to find the CL that produces the longest APD. In our study, this was found to be 2000ms, hence why we aimed to achieve this CL in all experiments. Choice of  $I_{Kr}$  blockade varies between dofetilide and E-4031 in other studies, indeed we attempted to induce PVCs/TdP with dofetilide but owing to the restraints of successful AVN ablation and shorter PCLs, this was not achieved, and the majority of our data was with E-4031. Additional features required to induce PVCs include 50%  $K^+/Mg^{2+}$ , voltage-gated  $Na^+$  blockade with quinidine and adrenergic agonism with either methoxamine and isoprenaline. In our study, we tried to induce PVCs with the least amount of pharmacological intervention possible, so selected 50%  $K^+/Mg^{2+}$ . Conditions seen with pharmacological  $I_{Kr}$  blockade and 50%  $K^+/Mg^{2+}$  may recapitulate conditions seen in LQTS patients who are pro-arrhythmic during electrolyte disturbances. Results of  $APD_{90}$  at baseline and under LQT, were similar to that found in other pharmacological LQT models. Studies with much longer APD at similar PCLs under LQT states than ours, involved a cryo-

ablation of the preparation (Choi BR *et al* 2002; Maruyama M *et al*, 2011). This affected cell-cell coupling and explains why their APD values were much longer.

## Limitations

The use of pharmacological ablation of the AVN could have caused cellular necrosis or ischaemia in surrounding structures. Every attempt was made to reduce this risk and serial viability assessments allowed any ischaemic preparations to be excluded.

The pharmacological electromechanical uncoupling agent blebbistatin was used in this study to minimise motion artefact during optical recordings and so could have affected AP and  $Ca^{2+}$  parameters. However, the longer values obtained at baseline and under LQT conditions in other LQT studies, who also used 5-15 $\mu$ g blebbistatin, argues against any major effect (Němec J *et al*, 2010; Maruyama M *et al*, 2011; Kim JJ *et al*, 2015; Chang PC *et al*, 2015). The longer APD values recorded by Maruyama *et al* and Němec *et al*, is perhaps explained by the fact they used cryoablated hearts and optically mapped the epicardial surface alone. Blebbistatin has other recognised effects on cardiac physiology, such as reducing LV perfusion pressure by abolition of ventricular contractile force, as well as ventricular electrophysiological effects such as APD prolongation (therefore  $QT_c$  prolongation) and increased threshold for VF (Brack KE *et al*, 2013). All experiments used in this study received blebbistatin and no controls were possible as APD cannot be measured optically in beating hearts, therefore it is impossible to determine the effects on APD without blebbistatin. Ventricular contractile force was not measured in this study and so the effects of this was not determined. Also, although our model had no incidence of VF at baseline conditions, this may be a consequence or a contribution of blebbistatin given it has shown to increase the VF threshold.

## Conclusions

In this study, a pharmacological LQT model was set up and characterised. This model was recapitulated from published experimental models to investigate LQT-induced arrhythmias. Optical APs were recorded from across the epicardial surface of a rabbit ventricle during epicardial pacing at a range of stimulation rates, under baseline and LQT conditions. Results were reproducible and comparable with other studies. To induce LQT,  $I_{Kr}$  blockade was used using E-4031. In keeping with previous work, additional changes were required to lengthen the  $APD_{90}$  and induce EADs, this involved halving the concentration of  $K^+$  and  $Mg^{2+}$  and pacing at 2000ms PCL.



## **Chapter 4: Describing the Mechanism of Triggered Activity**

## Introduction

Prolongation of the  $QT_c$  interval has been implicated in generating the life-threatening ventricular arrhythmia, TdP. Currently, the only preventative therapy for SCD in patients with congenital LQTS is an ICD. These devices are expensive and associated with a variety of complications that have a significant impact on a person's quality of life, particularly in the young (Ezzat VA *et al*, 2015). Ideal preventative treatment would be to prevent arrhythmias, as opposed to reactive treatment when they do occur. Risk stratification of patients with congenital LQTS is imperfect and for many patients their risk of TdP is uncertain. To provide more accurate risk stratification and develop more effective preventative treatment for SCD in patients with congenital LQTS, it is important to fully understand the mechanism of TdP under LQT states as it is currently uncertain, this has been discussed in Chapter 1 (pp. 30).

Various experimental LQT models have been used to investigate the mechanism of EADs and TA to induce TdP. These models range from isolated cells to multi-cellular preparations, including *ex vivo* intact hearts as well as *in vivo* experimentation. Key concepts have been derived from these, for example: it is widely accepted that EADs occur when the normal balance of ionic currents is disrupted to produce an abnormal depolarisation before the AP has completely repolarised (Weiss JN *et al*, 2010). These EADs can occur on phase 2 or 3 of the cardiac AP and are named as such (*e.g.* phase 2 EAD) (Damiano BP *et al*, 1984). To facilitate an EAD, there must be a state of reduced repolarisation reserve from reduced outward current, increased inward current or a combination of both (Qu Z *et al*, 2013). These conditions cause prolongation of the APD from either blockade of the inward  $Na^+$  or  $Ca^{2+}$  currents or reduction in outward  $K^+$ . This can occur from congenital LQTS channel knock out or acquired from drugs and/or electrolyte imbalances. If of a sufficient magnitude EADs can generate a new AP, this form of abnormal impulse generation is called TA, in the intact heart this would manifest as a PVC. EAD activity will also act to prolong APD and thereby potentially lead to heterogeneous repolarisation, and create a pro-arrhythmic substrate. The clinical significance of EADs is their ability to produce a trigger (*i.e.* TA), generating a PVC and inducing TdP.

What is less well characterised experimentally, is the impact of cellular EADs within an intact heart, where cardiomyocytes are electrically coupled to suppress any electrotonic current from surrounding cells (Houser SR *et al*, 2000). Computer modelling has estimated that, for a single PVC to propagate, many thousands of cells must simultaneously have an EAD (Xie Y *et al*, 2010). Whether there is indeed spatial synchronisation of cellular EADs under pathophysiological LQT conditions in the intact heart is unknown. A conclusive mechanistic link between EADs and the induction of TdP is yet to be made.

### **Cellular Mechanisms of EADs**

Isolated cell experiments have established that an EAD can be caused by re-activation of the inward sarcolemmal currents, that is  $I_{Na}$  (Boutjdir M *et al*, 1991) and/or  $I_{CaL}$  (Marban E *et al*, 1986; January CT *et al*, 1990; January CT *et al*, 1991). It is clear however, that the degree of APD prolongation (and so QT prolongation) does not directly dictate the propensity to create EADs, as prolongation of APD alone does not typically induce EADs (Redfern WS *et al*, 2003; Belardinelli L *et al*, 2003; Antzelevitch C, 2004b; Liu T *et al*, 2004). Additional factors to reduce repolarisation reserve are required, these include adrenergic stimulation, female sex, bradycardia, reduced extracellular  $K^+$  and  $Mg^{2+}$  (Drouin E *et al*, 1996; Qu Z *et al*, 2013; Priori SG *et al*, 1990). This suggests other electrophysiological conditions beyond APD prolongation are involved in the generation of EADs.

### **Intracellular $Ca^{2+}$ Modulates EAD Generation During APD Prolongation**

The conditions required to elicit an EAD were also shown to generate DADs, this implied a shared mechanism (Patterson E *et al*, 1990; Volders PG *et al*, 1997). The study of DADs is well known to result from  $Ca^{2+}$  loading of the SR (Schlotthauer K *et al*, 2000; Houser S, 2000). It has been shown that phase 2 EADs result from either spontaneous  $Ca^{2+}$  release from the SR activating  $Ca^{2+}$ -sensitive inward currents (*e.g.* forward mode  $I_{NCX}$ ) or from re-activation of  $I_{CaL}$  and/or  $I_{Na}$  (Volders PG *et al*, 2000; Choi BR *et al*, 2002), or all three. Together, these currents disrupt repolarisation and facilitate the generation of EADs. Studies have attempted to attenuate EADs by using inhibitors of SR  $Ca^{2+}$  reuptake with thapsigargin

(a non-competitive inhibitor of the sarco/endoplasmic reticulum  $\text{Ca}^{2+}$  ATPase), SR  $\text{Ca}^{2+}$  release with ryanodine, or  $I_{\text{CaL}}$  blockade. In a canine chronic AV block model, TdP is induced by administration of *d*-sotalol or almokalant. The addition of ryanodine and  $\text{Ca}^{2+}$  channel antagonist (flunarizine), attenuated EADs and prevented TdP (Verduyn SC *et al*, 1995). More recently, a LQT rabbit model using AV block,  $I_{\text{Kr}}$  blockade with E-4031 and 50% reduction in  $\text{K}^+/\text{Mg}^{2+}$ , showed a secondary rise of intracellular  $\text{Ca}^{2+}$  was associated with EADs and the incidence of TdP (Chang PC *et al*, 2015). Inhibition of SR  $\text{Ca}^{2+}$  reuptake with thapsigargin and  $I_{\text{CaL}}$  blockade with nifedipine, caused a reduction in this secondary intracellular  $\text{Ca}^{2+}$  rise and suppressed EADs. These studies suggest that SR  $\text{Ca}^{2+}$  cycling and  $I_{\text{CaL}}$  are important in the generation of EAD-induced TdP. Carlsson *et al* used a pharmacological LQT model in the rabbit to look at the effect of LTCC blockers on the incidence of TdP, this was studied from the  $\text{QT}_c$  interval on ECG and EADs were not measured (Carlsson L *et al*, 1996). Almokalant was used to create LQT conditions and induce TdP, alongside nisoldipine (a LTCC blocker) and flunarizine which is a low-affinity LTCC blocker which also has actions on intracellular  $\text{Ca}^{2+}$  handling. They found pre-treatment with both, low dose and high dose, nisoldipine and flunarizine reduced the incidence of almokalant-induced TdP but without preventing the development of  $\text{QT}_c$  prolongation. They concluded LTCC is crucial for TdP induction in LQTS but they did not suggest a mechanism for how it achieved this whilst the LQT substrate was preserved.

### ***Generation of EADs in the Intact Heart***

The cellular mechanism of EADs cannot be directly extrapolated to the intact heart, where the source-sink mismatch from electrotonic coupling between cells opposes any depolarisation arising from a single cell, and so would tend to prevent TA. Coronary-perfused left ventricular wedge preparations have been developed to study the transmural electrophysiology in an attempt to address the heterogeneities seen that may affect the electrophysiological substrate that could influence re-entry (Di Diego JM *et al*, 2013). The advent of computational modelling has provided a novel platform to investigate into the whole heart mechanism of EAD-induced TdP with manipulations that are not possible experimentally. Simulations have shown that spatial synchronisation of EADs across hundreds of thousands of cells is required for a single EAD-triggered AP (Xie Y *et al*, 2010). In other modelling studies, an alternative mechanism has been identified where marked heterogeneity in repolarisation facilitates electrotonically-triggered EADs that causes

transmural re-entry within an intact human heart model. In this case the electrotonic flow from regional heterogeneity produces a tissue-level EAD without the requirement for a cellular EAD in a depolarised region (Dutta S *et al*, 2016).

## ***Aims***

The experiments described in this Chapter were designed to describe the occurrence and generation of PVCs and ventricular arrhythmias seen in a pharmacological model of LQT in the intact rabbit heart.

Specific aims were:

1. Quantify occurrence of PVCs and arrhythmias and identify PVCs with the earliest epicardial  $V_m$  activation for mechanistic analysis.
2. Investigate the mechanism of PVC induction by examination of  $V_m$  and  $Ca^{2+}$  dynamics at the origin site.
3. Study the role of SR cycling on the LQT substrate and the occurrence of PVCs and arrhythmias.

## Methods

To investigate the mechanism of PVC induction and the relationship to EADs, the *ex vivo* model of LQT2 and the optical mapping system described in Chapter 2 was used to record optical APs and CaTs from the epicardial surface of Langendorff-perfused intact rabbit hearts. There were 14 hearts with a successful AVN ablation that was used for the LQT protocol. All 14 hearts used in these experiments were from male New Zealand White rabbits, which conform to standards set out in the UK Animals (Scientific Procedures) Act, 1986. Details of the Langendorff-perfusion set up and AVN ablation are detailed in Chapter 2.

### ***Experimental protocols***

Experimental protocols are outlined in Figure 4.1. Dual optical mapping of Langendorff-perfused rabbit hearts ( $n = 14$ ) was performed as detailed in Chapter 2. The characterisation of the LQT model (50%  $K^+/Mg^{2+}$  + E-4031 0.5 $\mu$ M) and APD gradients has been presented for 10 of these hearts in Chapter 3. In the remaining 4 hearts, experiments were performed without recordings at baseline conditions (*i.e.* the experiment started with Tyrode's containing 50%  $K^+/Mg^{2+}$  and E-4031 was added). This allowed more time for the arrhythmia induction protocols and mapping of PVCs. In a subset (5/14) the SERCA blocker thapsigargin (TG) was administered and the results from those protocols are presented here.

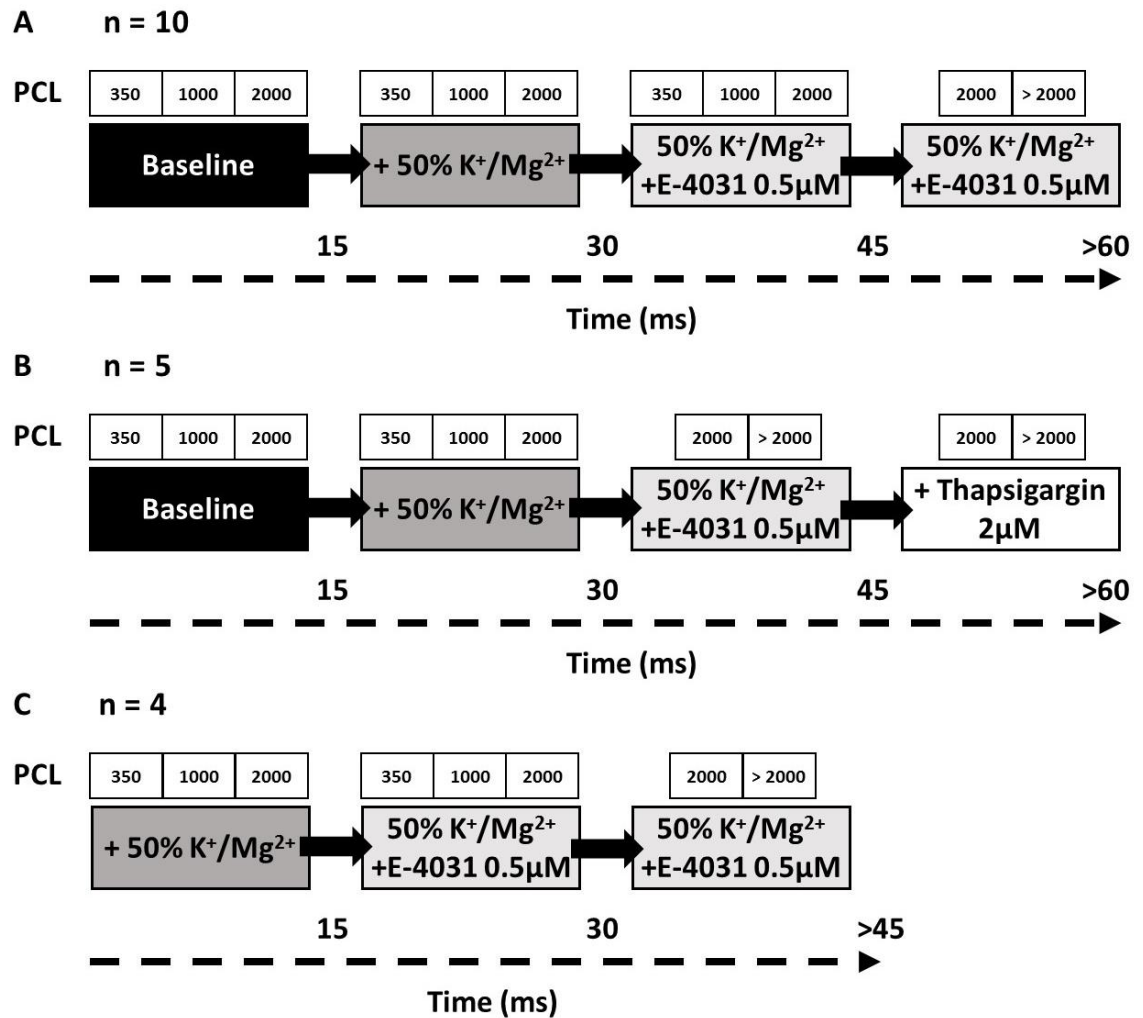


**Figure 4.1** – Diagram of experimental protocol including PCL used throughout and conditions changes over time.

(A) Starting at baseline, adding 50%  $K^+/Mg^{2+}$  then E-4031 0.5 $\mu$ M for 10/14 hearts. (B) Baseline, 50%  $K^+/Mg^{2+}$ , E-4031 0.5 $\mu$ M then TG for 5/14 hearts. (C) Starting 50%  $K^+/Mg^{2+}$  then E-4031 0.5 $\mu$ M for 4/14 hearts.

## ***Quantification of PVC Events***

The occurrence of PVCs on pECG prompted optical mapping acquisition. As per Methods (Chapter 2, pp. 65), pECG signals were digitised and recorded along with the stimulus pulse and the optical signals by the mapping system. Alignment of the pacing stimulus with the pacing artefact on the pECG verified that the recordings were synchronised. For each PVC optically mapped, the earliest epicardial  $V_m$  activation time relative to the QRS was calculated. This involved analysing each optical file acquired during a PVC to identify (Figure 4.2):

1. Earliest activation of QRS during the PVC
2. Earliest epicardial  $V_m$  during the PVC

With these values, the timing of PVC in relation to QRS on the pECG could be calculated which identified PVCs that displayed very early activation on the epicardial surface. These PVCs were considered likely to have been initiated close to the epicardial surface within the mapped region. The initiation of these epicardial PVCs were then selected for further analysis of the PVC induction mechanism.



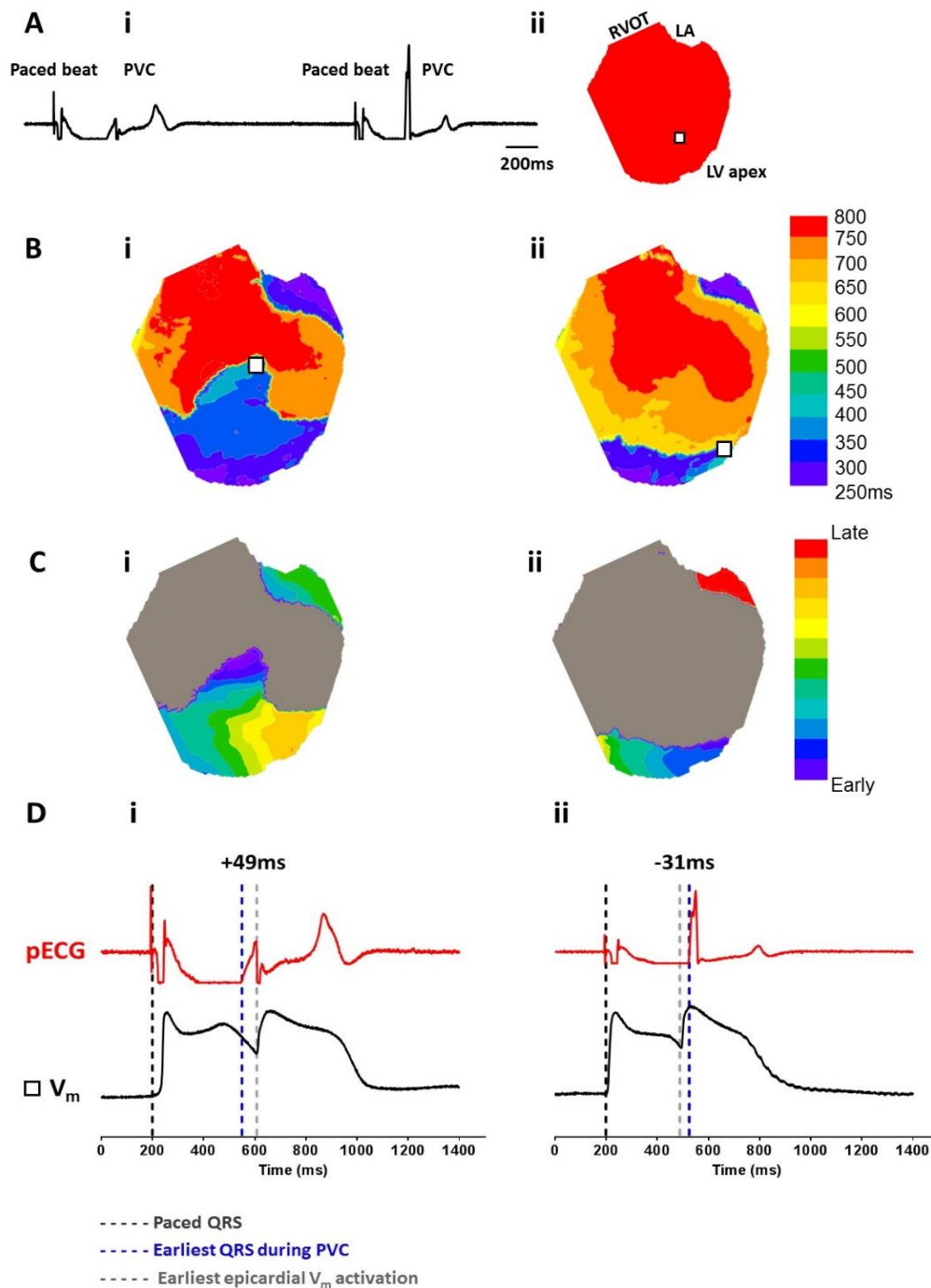


**Figure 4.2.** Identification of epicardial PVCs.

(A) Shows a (i) pECG trace with two optical acquisitions taken from different PVCs in the same heart during 2000ms PCL at 50%  $K^+/Mg^{2+}$  + E-4031 0.5 $\mu$ M, and (ii) whole heart selection with example of 5x5 selection used for highest SNR. (B) APD<sub>90</sub> maps for (i) first complex and (ii) second complex with 5x5 selections used that were focussed at earliest site of activation (white box). (C) Activation maps during PVC, identifying earliest onset of activation during PVC. Grey areas are long AP regions without secondary PVC upstroke. (D) Both (i) and (ii) show paced complex followed by PVC captured on pECG (red) and V<sub>m</sub> trace (black) over time, sampled from a 5x5 selection at the earliest epicardial activation of the PVC (white boxes in B). Dotted lines denote timing of initial paced QRS upstroke (black), earliest QRS during PVC (blue) and earliest V<sub>m</sub> epicardial activation during PVC (grey). The first complex (i) shows the epicardial V<sub>m</sub> activation is later than the pECG (+49ms), whereas the second complex (ii) shows epicardial V<sub>m</sub> activation originating before the pECG (-31ms).

### ***Approaching the Analysis of the Mechanism of Triggered Activity***

Various approaches were used to analyse the relationship between EADs and PVC induction. Firstly, movies of PVC activation were viewed and APD<sub>90</sub> and activation maps were generated from the V<sub>m</sub> traces and reviewed. The next step was to use Lammers' inhomogeneity index (LHI), to delineate areas with the highest repolarisation gradients from the calculated APD values. Lammers *et al* proposed this method to quantify spatial inhomogeneity using atrial cells, this involved taking the mean of the median differences of adjacent sites (Lammers WJ *et al*, 1990). This technique has also been used in ventricular cardiomyocytes (Burton FL *et al*, 2001). An example of this analysis is shown in Figure 4.3. However, the analysis software had to assign an arbitrary cut-off between a paced beat with a prolonged plateau within the long AP island (appearing as a single AP), and areas out-with the long AP island with shorter APD<sub>90</sub> (appearing as two distinct APs on the V<sub>m</sub> traces). Inevitably in this form of analysis, the software had to draw a distinction between long AP areas and short, thereby accentuating gradients of measured APD and explaining the clear demarcation on the Lammers' analysis. Other factors that were considered included the role APD gradients between the apex and base of the epicardial surface, as well as the location of the long AP island seen across hearts (*i.e.* apical or basal on the LV or RV).

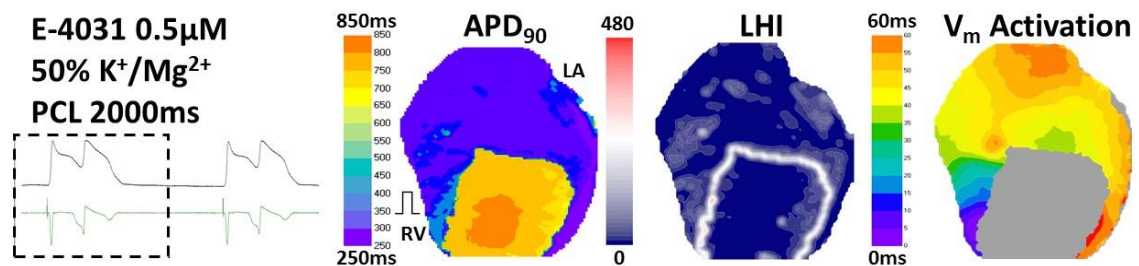


**Figure 4.3.** Quantification of APD gradients using Lammers' inhomogeneity index (LHI).

Example of analysis performed using Lammers' inhomogeneity index (LHI). Analysis of a paced beat at 2000ms PCL under LQT conditions shows a PVC, associated with corresponding APD<sub>90</sub>, activation and LHI maps. The LHI map shows clear delineation between long and short AP regions but does not identify the breakout region seen in the activation map.

### ***Analysis of the Triggered Activity Mechanism***

In order to characterise tissue-level EADs and look for evidence of synchronisation of EADs the plateau voltage, amplitude and  $dF/dt$  of EADs were quantified. This involved calculating the amplitude of the first upstroke taken from the paced beat and expressing the amplitude of any depolarisation during phase 2, as a percentage of the first paced beat. The starting value of the PVC upstroke (expressed as % of normal upstroke) was taken to represent the plateau level of the paced beat, from which EADs and PVCs were generated. The amplitude and  $dF/dt$  of phase 2 depolarisation were also quantified, and in each case presented relative to the normal phase 1 depolarisation of the preceding paced beat. For AP plateau analysis, APs in each pixel were normalised to baseline fluorescence. We assumed the upstroke of a normal AP was an all or nothing phenomenon and could therefore be mapped on to an estimated  $V_m$  range of approximately  $(-90) - 30\text{mV}$ . Using this we could give approximate  $V_m$  ranges at which any events were occurring.

### ***Superimposing $V_m$ Traces to Elucidate the Role of AP Gradients***

To investigate the involvement of EADs and voltage gradients in the induction of PVCs,  $V_m$  traces were examined in detail across the PVC activation. APs and corresponding CaTs were sampled across the border of the long AP island at the point of PVC origin (PVC activation), example of this analysis is shown in Figure 4.4.

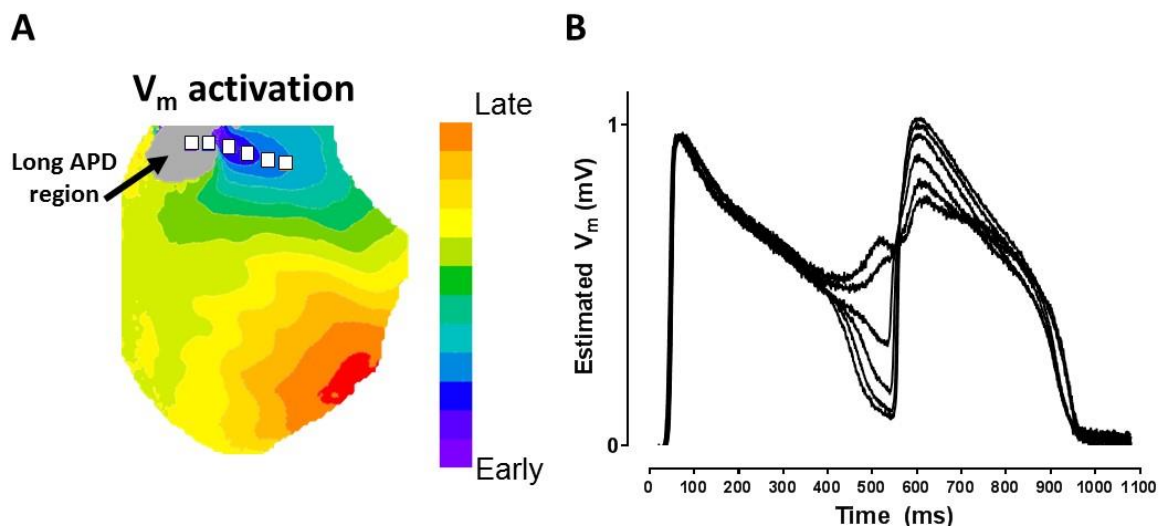


**Figure 4.4.** Example of superimposed  $V_m$  trace analysis taken from PVC activation map.

***Investigation of the Effects of Thapsigargin on Triggered Activity***

The role of SR  $\text{Ca}^{2+}$  cycling in the genesis of EADs was investigated in a subgroup of five hearts using the non-competitive inhibitor of SERCA, TG. The protocol is depicted in Figure 4.1. All five hearts were perfused with 50%  $\text{K}^+/\text{Mg}^{2+}$  + E-4031 0.5 $\mu\text{M}$  at 2000ms PCL and then 2 $\mu\text{M}$  of TG was administered. The dose of TG and timescale was based on concentrations used in previous studies proven to have a significant effect on SR function (Elliot EB *et al*, 2012).

## Results

### Summary of Experiments

A summary of each individual experiment with corresponding mean APD<sub>90</sub> is shown in Table 4.1.

Experiment No.		50% K <sup>+</sup> /Mg <sup>2+</sup> + E-4031 0.5μM @ 2000ms PCL
		Mean APD <sub>90</sub> (ms)
1	✕	228.6 ± 0.62
2	✕	247.4 ± 1.49
3	✕	261.1 ± 1.94
4	✕	284.8 ± 1.01
5	✕	295.6 ± 1.06
6	✕	302.7 ± 2.16
7	✕	306.3 ± 4.02
8	✕	326.9 ± 3.21
9	✕	335.4 ± 2.04
10	✕	428.6 ± 4.14
11	✕	516.4 ± 3.00
12	✕	597.4 ± 5.05
13	✕	602.8 ± 1.80
14	✕	661.8 ± 6.48
<b>Total Mean ± SD</b>		<b>384.7 ± 146.4</b>

**Table 4.1.** Summary of experiments to induce LQT conditions and corresponding APD<sub>90</sub> values.

Total used to induce LQT conditions (n = 14) with corresponding mean APD<sub>90</sub> for each experiment, values taken from 5x5 selections from each heart and are normally distributed (D'Agostino & Pearson normality test). Each coloured cross denotes an individual experiment. Range of APD in keeping with between heart variability seen in Chapter 3.

### ***Occurrence of PVCs and Arrhythmias***

In each experiment, there was rate-dependent APD prolongation seen with LQT conditions. The APD prolonged incrementally from baseline in keeping with the change in conditions, which corresponded with prolongation of the  $QT_c$  on the pECG. The  $QT_c$  interval on pECG was seen to incrementally increase, alongside distinct T-wave changes, until PVCs were seen (see Figure 4.5). PVCs under LQT conditions occurred before the end of the pECG T-wave (*i.e.* R-on-T) and correspondingly interrupted the AP from the previous beat in the  $V_m$  traces. The  $QT_c$  interval across 14 hearts at 2000ms PCL, ranged from 182 – 285ms at baseline (mean  $227.6 \pm 33.9$ ) and 291 – 594ms (mean  $413.2 \pm 110$ ) under 50%  $K^+/Mg^{2+}$  + E-4031  $0.5\mu M$  (paired t-test,  $p < 0.001$ ). Once achieved, the pattern of PVCs would appear to cycle between alternate beats or remain consistently present after each paced beat, Figure 4.5. This occurred during PCLs of 2000ms, in one heart PVCs were seen at 1000ms PCL, and some hearts experienced PVCs during intrinsic rhythm, usually at rates  $<30$ bpm.

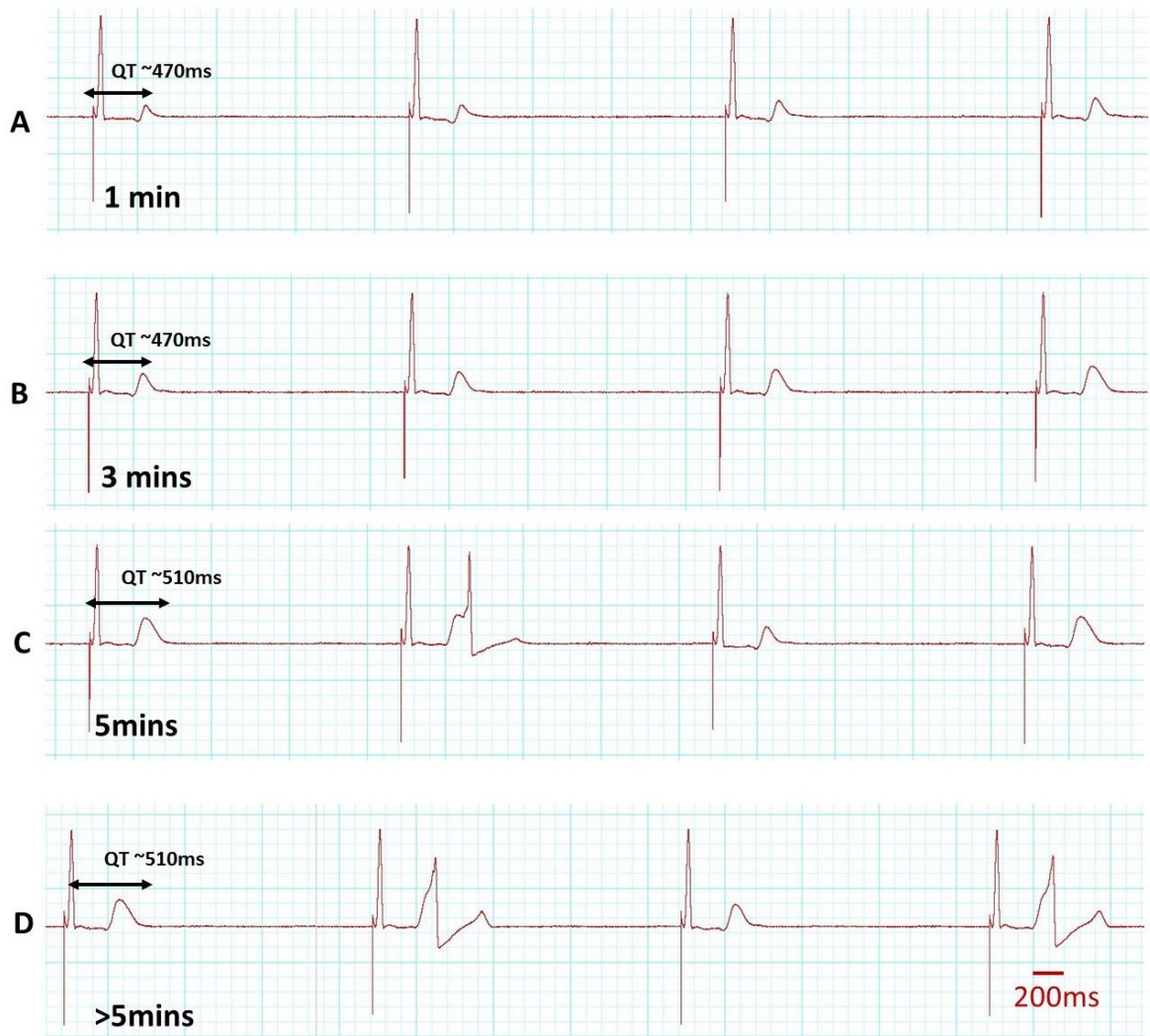


**Figure 4.5.** Changes in  $QT_c$  on pECG under LQT conditions.

(A) pECG taken 1 minute after commencing  $50\% K^+/Mg^{2+} + E-4031 0.5\mu M$  conditions. (B) pECG taken 3 mins after with minor changes in T-wave changes morphology but with no significant change in QT. (C) pECG taken 5 mins after with prolongation of the QT interval and the first PVC seen (beat two). (D) Pattern of activity seen over 5 mins with R-on-T PVCs occurring after alternate paced beats.

There were multiple PVCs, bursts and episodes of TdP induced by PVCs, Figure 4.6. The definition of PVC bursts was any run of PVCs consisting of 2-5 consecutive beats and any over 5 consecutive beats was classified as TdP (Eckardt L *et al*, 1998b). The total incidence of PVCs, bursts and TdP recorded on the pECG per heart is summarised in Table 4.2. Owing to the transient nature of PVC bursts and TdP, optical mapping could not be achieved for every occurrence during experiments. The number of PVC, bursts and TdP that were acquired during optical imaging is summarised in Table 4.3 and Figure 4.7. All 14 hearts demonstrated PVCs under LQT conditions at 2000ms PCL versus 0/14 at baseline ( $p < 0.0001$ ), 13/14 hearts demonstrated bursts under LQT conditions versus 0/14 at baseline ( $p < 0.0001$ ) and 8/14 hearts demonstrated TdP under LQT conditions versus 0/14 at baseline ( $p < 0.0001$ ), each compared using Fisher's exact test. PVCs were mapped in 14/14 of hearts, bursts were mapped in 10/14 and TdP was mapped in 3/14. A total of 236 PVCs was mapped in 14/14 hearts. The mean coupling interval was  $410 \pm 78$ ms. There were 17 PVCs mapped at other CLs (*i.e.* 1000ms PCL or intrinsic rhythm with a diastolic interval  $> 1500$ ms). Of this total, 40 PVCs had  $V_m$  epicardial activation  $> -20$ ms pre-QRS. A summary of epicardial activation for all analysed PVCs and corresponding coupling interval is shown in Figure 4.8. From this analysis, all PVCs demonstrating TA pre and post QRS could be identified, a summary of these is shown in Figure 4.9.



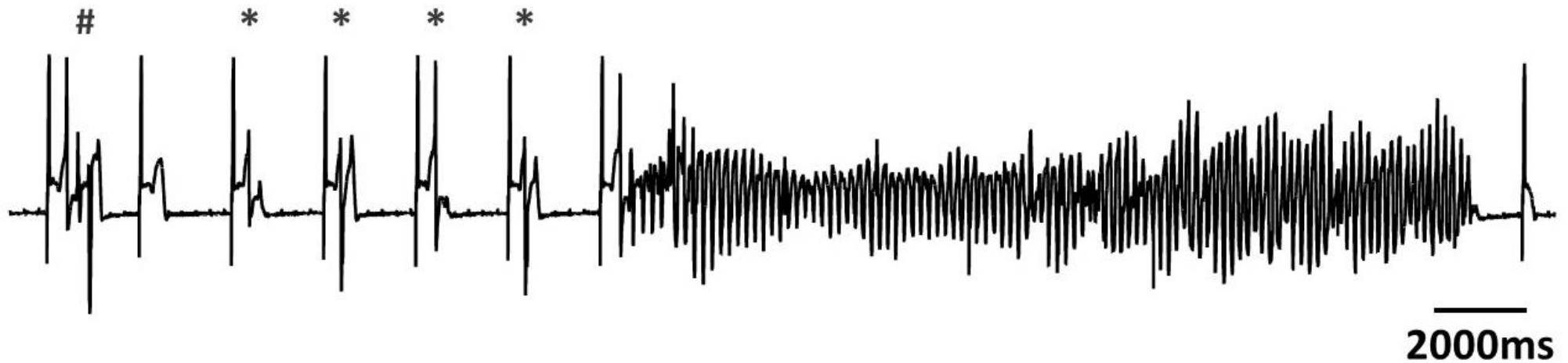








**Figure 4.6.** Example of TdP induction under LQT conditions.

Recorded during 50%  $K^+/Mg^{2+}$  + E-4031 0.5 $\mu$ M, showing AV dissociation and ventricular pacing at 2000ms PCL. The first beat shows a PVC burst (#) that is comprised of 2-5 PVCs, beat 2 has no associated PVC, then PVCs (\*) follow each paced beat before an episode of TdP is initiated on beat seven.

PCL (ms)	PVC			PVC Burst (2 – 5 beats)			TdP (>5 beats)		
	Baseline	50% K <sup>+</sup> /Mg <sup>2+</sup>	50% K <sup>+</sup> /Mg <sup>2+</sup> + E-4031 0.5μM	Baseline	50% K <sup>+</sup> /Mg <sup>2+</sup>	50% K <sup>+</sup> /Mg <sup>2+</sup> + E-4031 0.5μM	Baseline	50% K <sup>+</sup> /Mg <sup>2+</sup>	50% K <sup>+</sup> /Mg <sup>2+</sup> + E-4031 0.5μM
350									
1000									
2000			✖ ✖ ✖ ✖ ✖ ✖ ✖ ✖ ✖ ✖ ✖ ✖ ✖ ✖			✖ ✖ ✖ ✖ ✖ ✖ ✖ ✖ ✖ ✖ ✖ ✖ ✖			✖ ✖ ✖ ✖ ✖ ✖ ✖ ✖
<b>Total hearts (n)</b>	<b>0 / 9</b>	<b>0/14</b>	<b>14/14</b>	<b>0/9</b>	<b>0/14</b>	<b>13/14</b>	<b>0/9</b>	<b>0/14</b>	<b>8/14</b>

**Table 4.2.** pECG analysis of arrhythmic events seen under different conditions.

Incidence of PVCs, bursts of PVCs and TdP at different PCLs in hearts perfused at baseline, 50% K<sup>+</sup>/Mg<sup>2+</sup> and then 50% K<sup>+</sup>/Mg<sup>2+</sup> + E-4031 0.5μM. Note only 9 hearts under baseline conditions as 5/14 hearts had no baseline recordings and commenced at 50% K<sup>+</sup>/Mg<sup>2+</sup>.

	PVC	PVC Burst (2-5 beats)	TdP (>5 beats)
<b>Imaging medium</b>	<b>50% K<sup>+</sup>/Mg<sup>2+</sup> + E-4031 0.5<math>\mu</math>M @ 2000ms PCL</b>		
pECG recording			
Optically mapped			
<b>Total hearts mapped (n)</b>	<b>14/14</b>	<b>10/14</b>	<b>3/14</b>

**Table 4.3.** Arrhythmic events captured on pECG and optical mapping under LQT conditions.

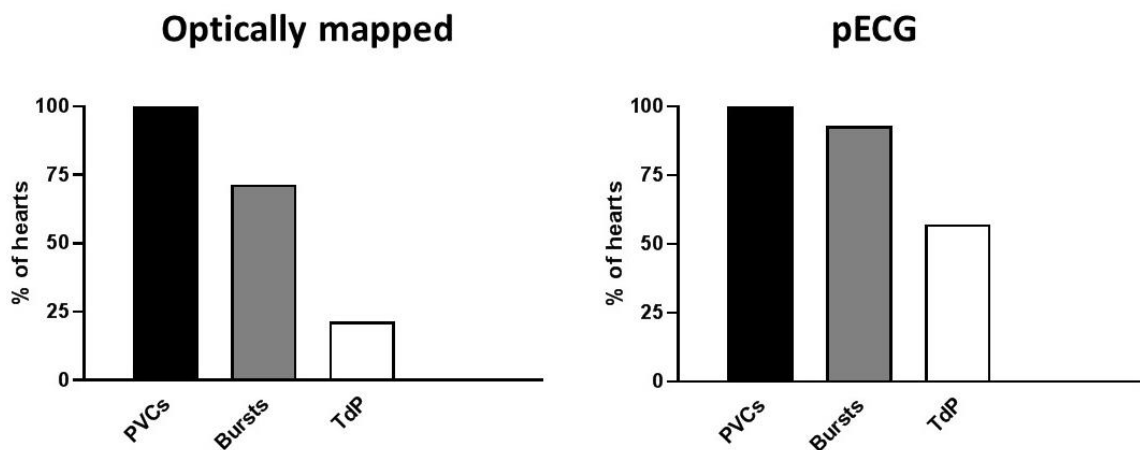


**Figure 4.7.** Quantification of ventricular arrhythmias under LQT conditions.

Percentage of hearts with optically mapped and pECG detected PVCs (black), PVC bursts (2 – 5 beats, grey) and TdP (>5 beats, white) under LQT conditions (n = 14, at 2000ms PCL).

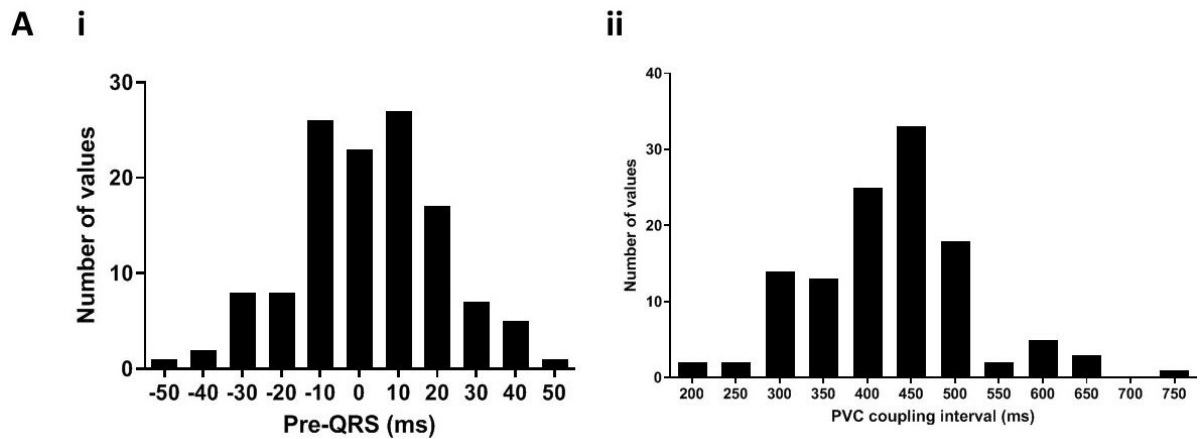


**Figure 4.8.** Characteristics of mapped PVCs.

Histogram of (i) epicardial  $V_m$  activation relative to QRS with all negative values considered pre-QRS. All positive values were considered post-QRS with the PVC onset occurring out with the mapping area and either endocardial or transmural. (ii) Coupling interval for all 236 PVCs in 14 hearts.

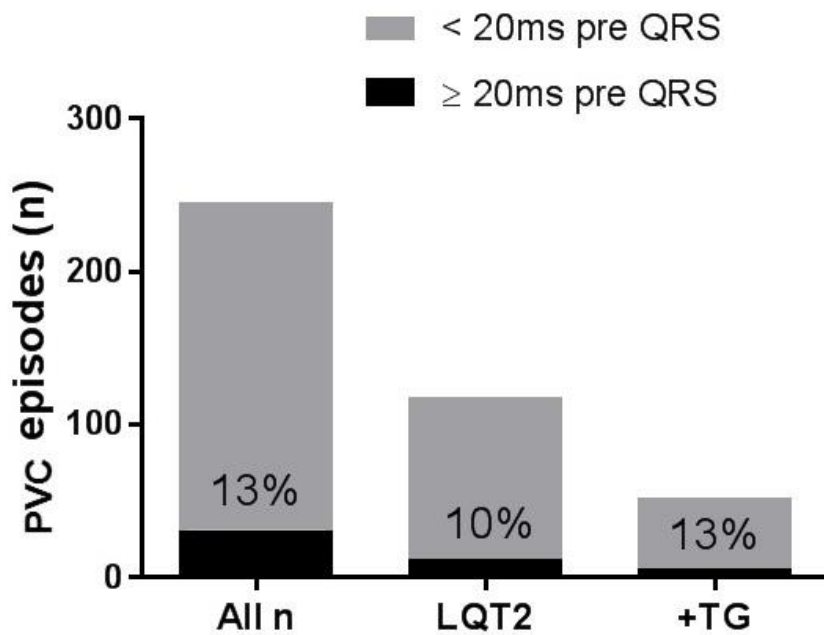


**Figure 4.9.** Summary of earliest epicardial activation in mapped PVC episodes relative to QRS.

Total optically mapped PVCs was 236, these were analysed to identify hearts with earliest  $V_m$  epicardial activation before the QRS on pECG.

## Mechanisms of PVC Induction

To investigate the mechanism of PVC induction, activation and  $APD_{90}$  maps for the paced complex vs. the PVC were compared, an example of this is shown in Figure 4.10. The  $APD_{90}$  map of the paced beat demonstrates an island of long  $APD$ . The PVC is seen to originate from the border of the long  $AP$  island.

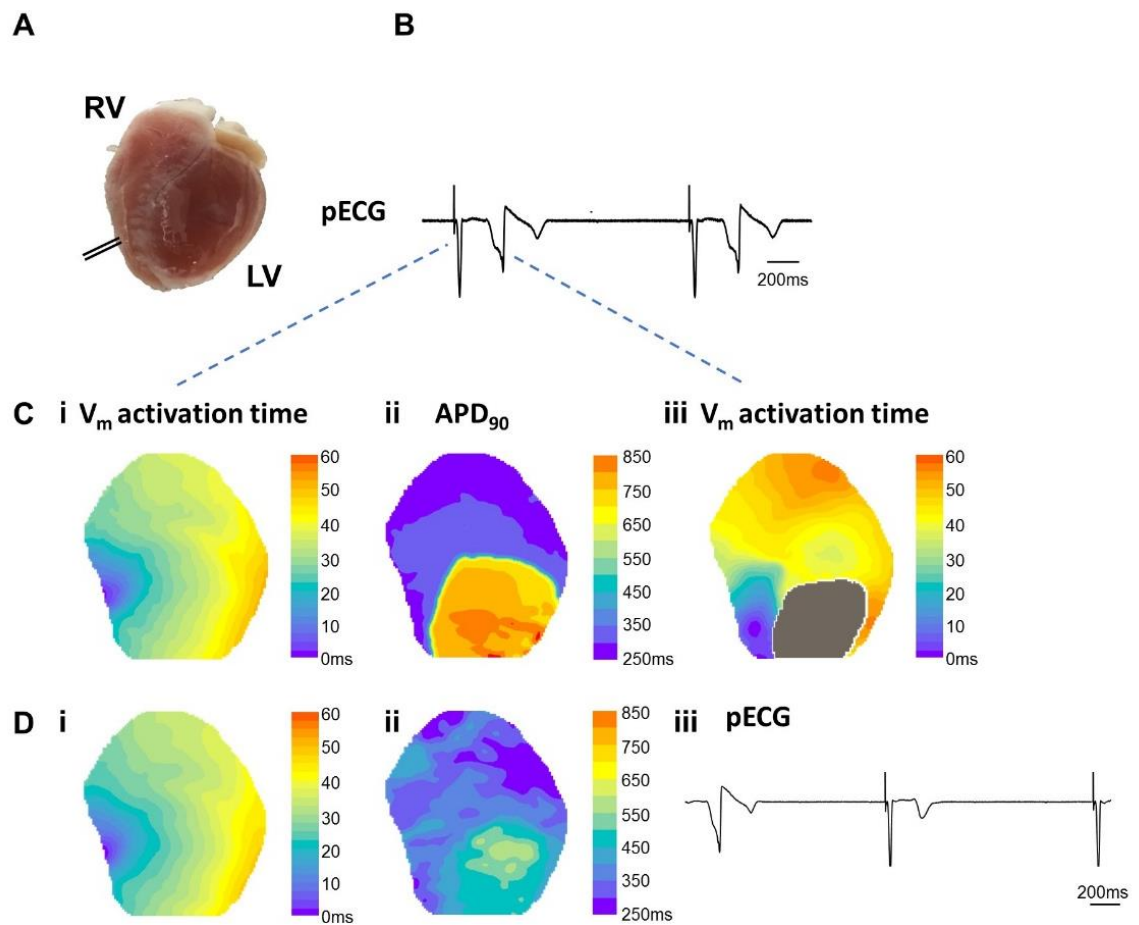


**Figure 4.10.** Analysis of  $V_m$  activation time and  $APD_{90}$  for paced beat and PVC under LQT conditions.

(A) Orientation of the heart preparation. (B) pECG recording showing paced beats with R-on-T PVCs during steady state pacing at 2000ms. (C) (i)  $V_m$  activation map of the first paced beat, (ii) corresponding  $APD_{90}$  for the paced beat and (iii)  $V_m$  activation map for the PVC. (D) Corresponding maps for a paced beat without a PVC (i)  $V_m$  activation map and (ii) map of  $APD_{90}$  and (iii) pECG.

## Early Afterdepolarisations

The  $V_m$  traces were taken from within the long AP island itself, on the border straddling the steep repolarisation gradient and outside the long AP island entirely, Figure 4.11. In order to identify repolarisation time, the analysis algorithm requires a threshold value of trace return to baseline from the peak value. Therefore, although the traces themselves show a more gradual transition between areas which clearly have one AP (i.e. black square) and those which clearly have two (i.e. white square) the analysis software will always represent this as a more abrupt transition. Positive deflections were seen across the plateau of the AP and occurred frequently in long AP island. These were keeping with phase 2 EADs. Phase 3 EADs, were not seen.

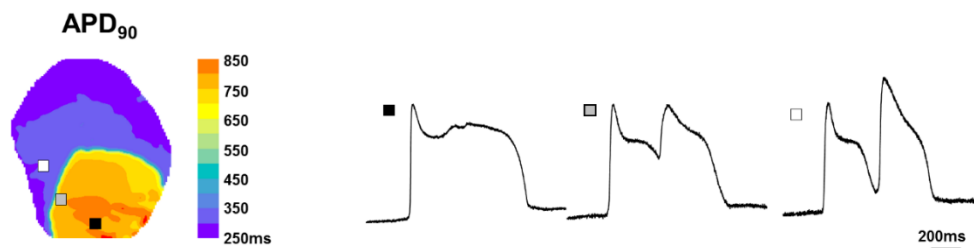


**Figure 4.11.**  $V_m$  traces during R-on-T PVCs.

Map of APD<sub>90</sub> with corresponding 5x5 pixel selections taken from within the long AP island itself (black box), on the border zone covering areas of steep repolarisation gradients (grey box) and out with the long AP zone altogether (white box).

## Plateau Analysis

Plateau analysis determined the relative position of the AP plateau with respect to the peak, and provided an estimation of the voltage range any EADs seen were occurring at, Figure 4.12. Occurrence of EADs were seen across the range 70-80% which corresponded to an estimated  $V_m$  range of  $\sim (-15) - (+10)$  mV.

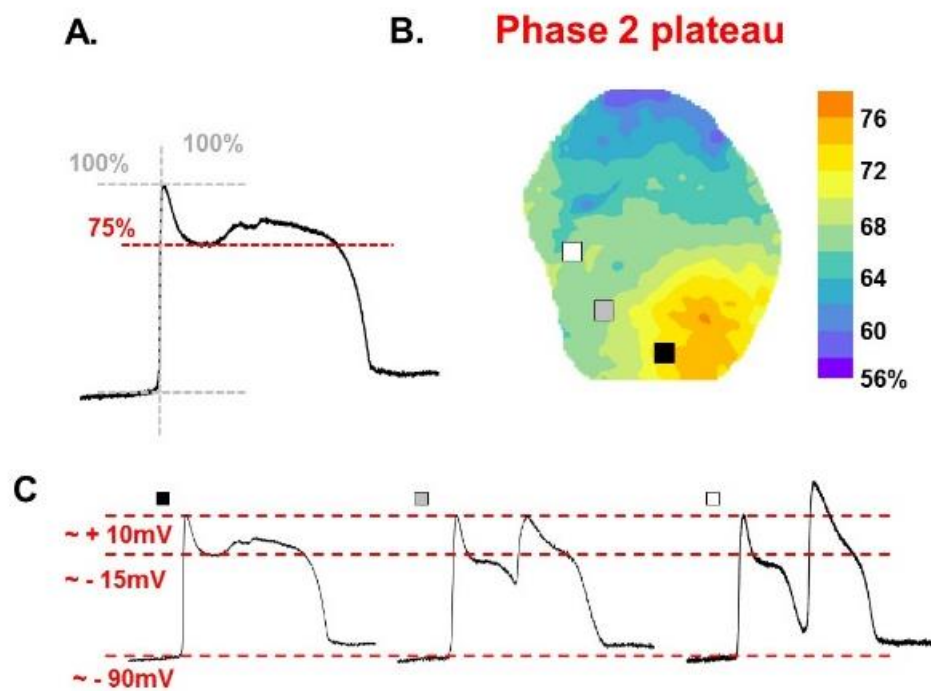


**Figure 4.12.** Plateau analysis of PVC initiation.

(A) AP from with the long APD island (black box) with phase 2 EAD present. (B) Corresponding plateau map and (C) estimated  $V_m$  ranges.

## ***Amplitude Analysis***

The amplitude of any phase 2 depolarisation was quantified in the same way, Figure 4.13. Phase 2 EAD amplitude was defined as the amplitude of any depolarisation that occurred during phase 2 of the AP, measured from the plateau amplitude and expressed as a percentage of the initial upstroke. The amplitude map showed low depolarisations amplitudes across the long APD island with no suggestion of summation towards the centre of the long AP island where source-sink interactions would favour expression of cellular EADs.

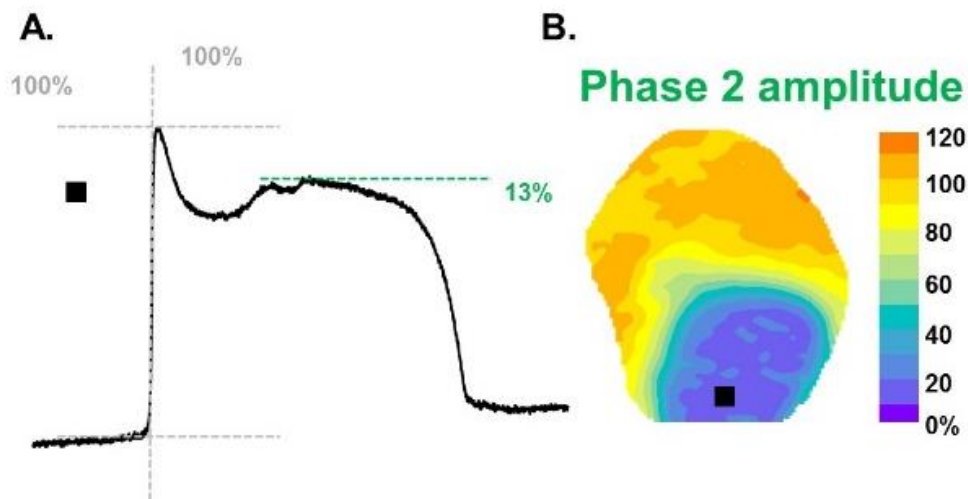


**Figure 4.13.** Amplitude analysis of PVC initiation.

(A) Amplitude analysis performed, green line denotes peak amplitude of phase 2 depolarisation as a percentage of the first upstroke and (B) corresponding amplitude map.



### Analysis of $dF/dt$

To assess the rate of depolarisation during phase 2 and determine whether this was consistent with regenerative current, the rate of depolarisation over time was analysed for EADs observed during phase 2 of the AP, Figure 4.14. In this example, within the long AP island, where EADs were occurring, the  $dF/dt_{\max}$  showed 15% of the initial upstroke and not consistent with regenerative current potential. Areas within the region of PVC origin  $dF/dt_{\max}$  showed 60-80% of the initial upstroke. In comparison, surrounding areas with shorter APs had a  $dF/dt_{\max}$  over 100% and this was more keeping with a propagated AP.

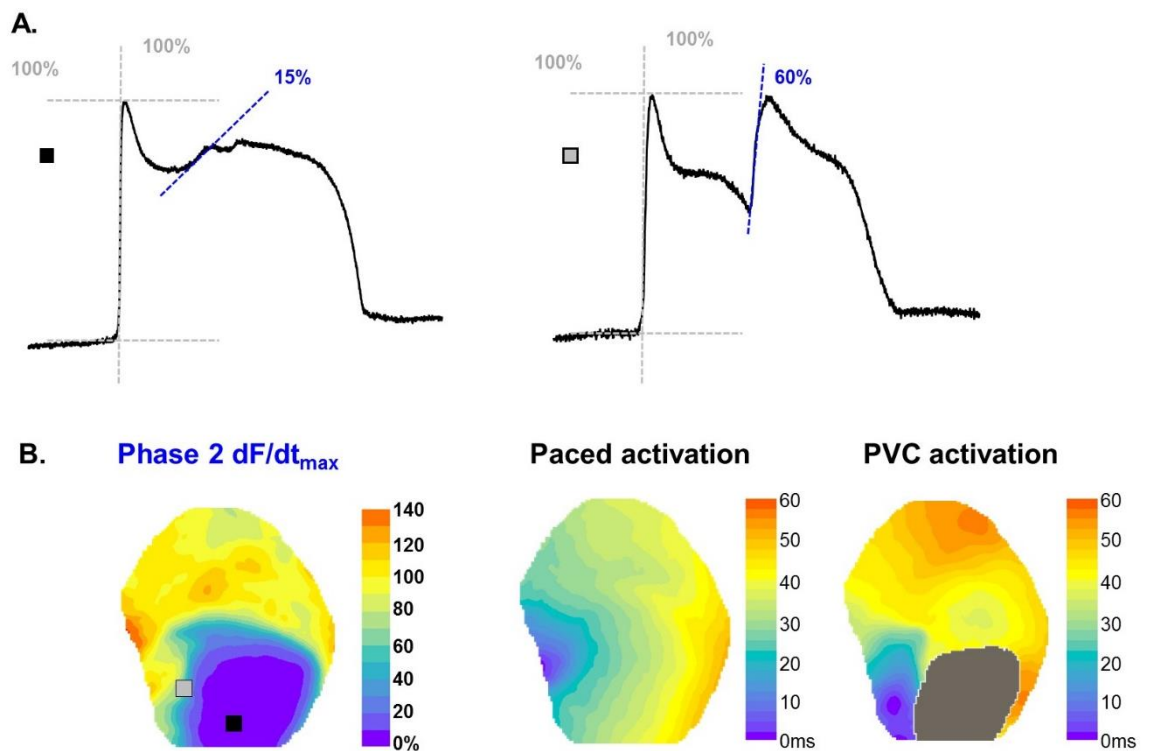


**Figure 4.14.** Analysis of  $dF/dt_{\max}$  of PVC initiation.

(A) Change in  $dF/dt_{\max}$  analysis across 2 sites within the long AP island (black box) and a region in the origin of PVC (grey box), blue line denotes phase 2 depolarisation expressed as a percentage of the first upstroke and (B) corresponding phase 2  $dF/dt_{\max}$  map with paced and PVC activation maps. Activation was defined separately to  $dF/dt_{\max}$ , as 50% level between baseline and peak during upstroke of the AP, as detailed in the methods section (Chapter 2, pp. 80).

## ***Superimposed $V_m$ Traces Highlighting the Role of Voltage Gradients***

To investigate the involvement of voltage gradients in the induction of PVCs,  $V_m - Ca^{2+}$  dynamics were examined in detail. Selections encompassing the long AP island, PVC initiation and propagation are shown in Figure 4.15, alongside accompanying pECG and  $APD_{90}$  and activation maps. PVC initiation occurred -48ms pre-QRS provided reassurance this was epicardial activation and not transmural or endocardial. Figure 4.16 shows the same  $V_m$  traces plotted with estimated  $V_m$  with expanded sections to show the relationship between the peak of the EAD (blue line), peak voltage gradient (red line) and earliest upstroke of the PVC (grey line). Peak EAD activity was defined as the largest phase 2 amplitude seen on the  $V_m$  traces, and peak voltage gradient was defined as the largest difference between traces over 6 contiguous pixels fixed in time, determined from  $V_m$  trace analysis. The earliest activation of the PVC was not seen in the AP island where phase 2 EADs were present. Instead, the earliest breakout occurred in adjacent regions with a large AP gradient (site 3 and denoted by a red star). In the event there were EADs occurring on the border zone between the long AP island and normal AP, this caused a dynamic increase in the AP gradient seen locally. The subsequent beat showed ongoing EAD activity but smaller  $APD$  gradients and no TA was seen (Figure 4.15 Cii and Dii). To quantify this behaviour, the time and distance between the PVC upstroke and (i) the peak of the EAD and (ii) the maximal voltage gradient in beats with and without PVC were reviewed in 13 PVCs taken from 11/14 hearts, Figure 4.17. The peak voltage gradient was more closely associated with the upstroke of the PVC than was the peak EAD, both temporally (Figure 4.17 (Ai),  $7 \pm 5$ ms vs.  $44 \pm 27$ ms,  $p < 0.0001$ ) and spatially (Figure 4.17 (Aii),  $1.0 \pm 0.7$  vs.  $3.6 \pm 0.9$ mm,  $p < 0.0001$ ). Additionally, paced beats associated with PVCs displayed significantly larger voltage gradients than preceding beats which did not support a PVC (Figure 4.17 B,  $53.1 \pm 5.7$  vs.  $23.7 \pm 6.8$  estimated mV/pixel,  $p < 0.0001$ ).

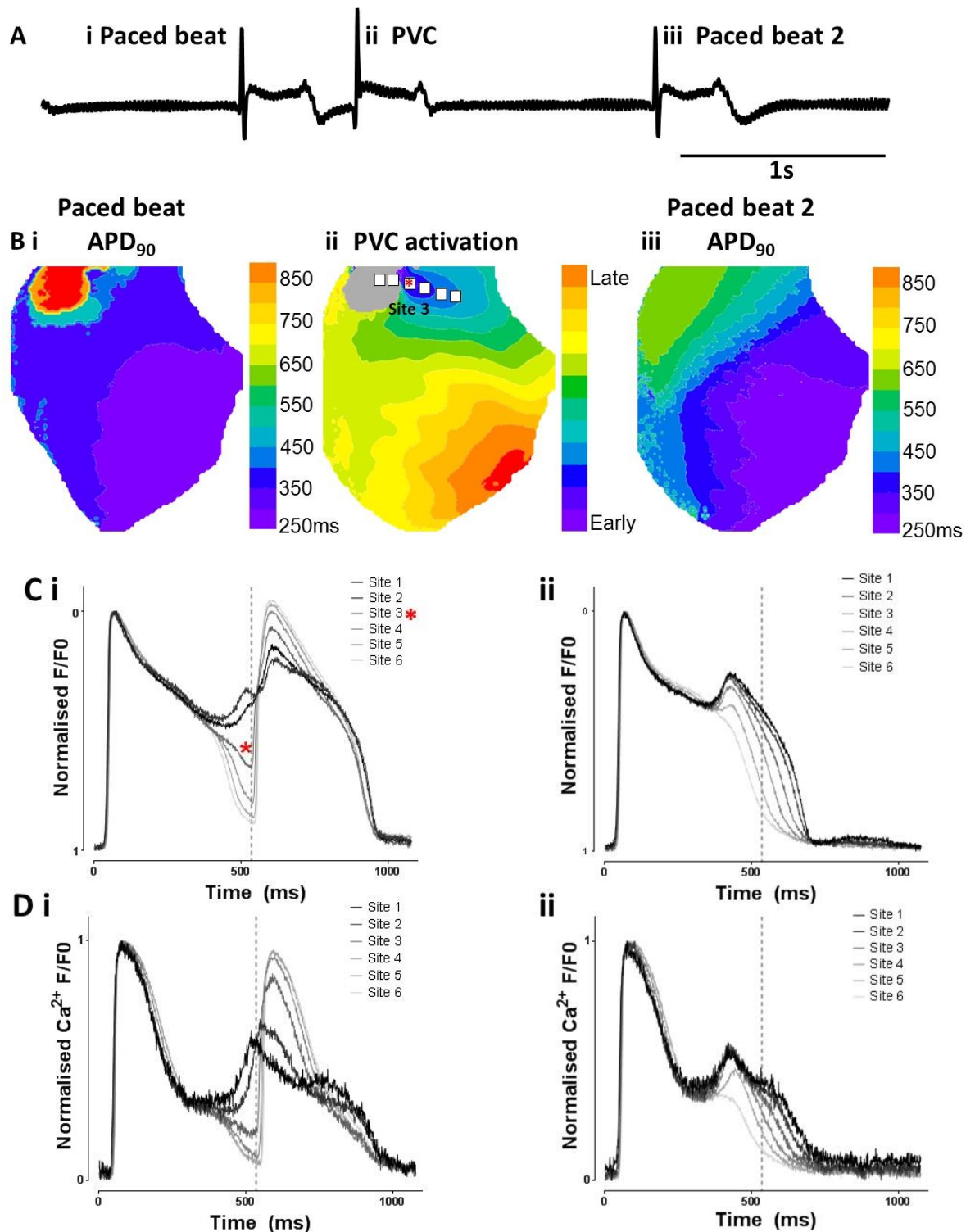


**Figure 4.15.**  $V_m$ - $Ca^{2+}$  dynamics during PVC initiation.

(A) pECG showing a (i) paced beat with (ii) PVC and followed by a (iii) second paced beat with no PVC. Example of PVC initiation with epicardial activation -48ms prior to QRS (B) (i) APD<sub>90</sub> map of the first paced beat showing long AP island in the RVOT region (ii) activation map of the PVC showing earliest breakout and selections used for trace analysis, (iii) APD<sub>90</sub> for second paced beat without PVC. (C)  $V_m$  traces from selections shown in B(ii) for (i) first paced beat with PVC and (ii) second paced beat without PVC. Dotted grey line denotes time of earliest PVC upstroke on  $V_m$  trace. Red star shows peak  $V_m$  gradient and area of earliest breakout (site 3) (D) Corresponding  $Ca^{2+}$  traces for (i) first paced beat with PVC and (ii) second paced beat without PVC.

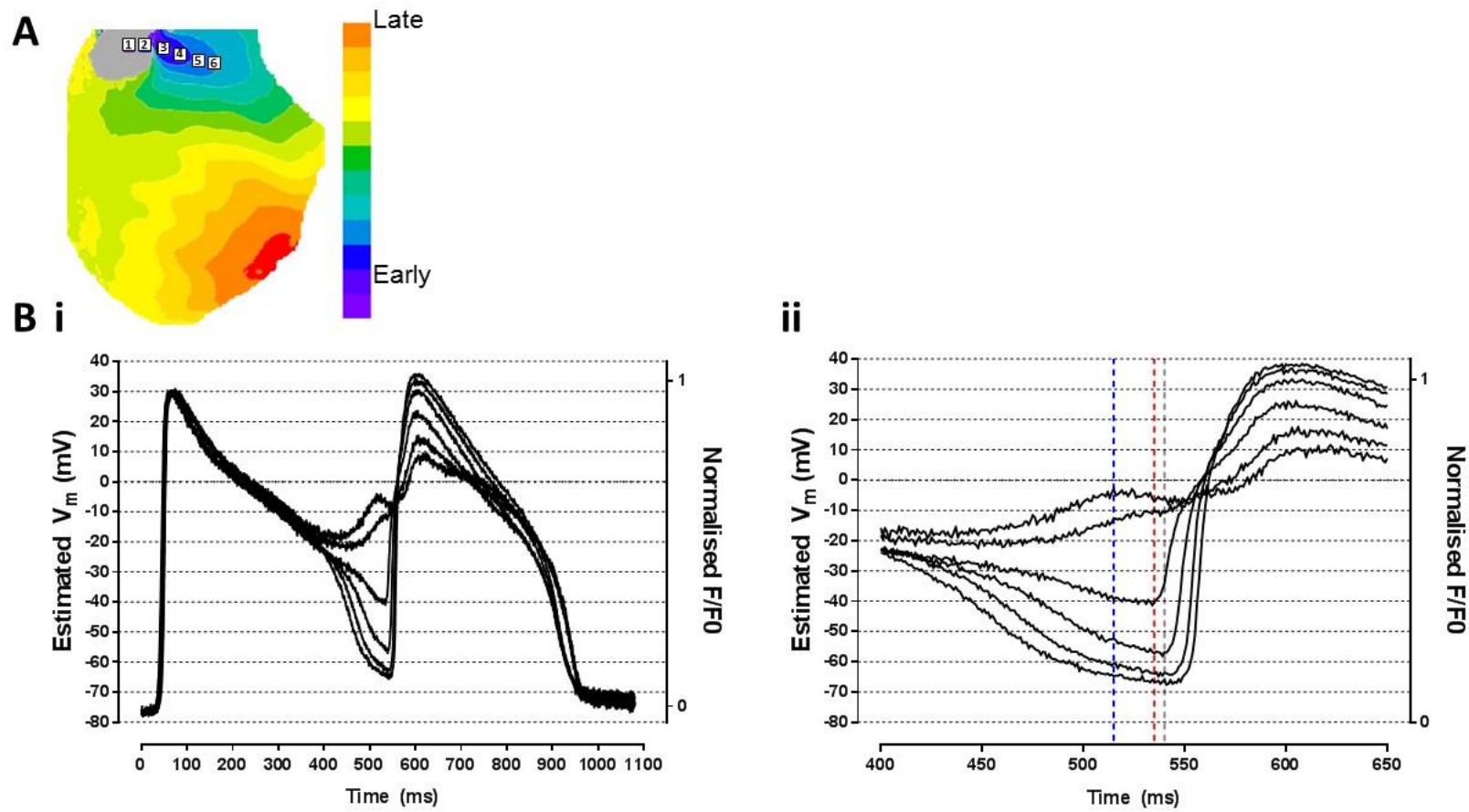


**Figure 4.16.**  $V_m$  trace analysis to determine the role of APD gradients in PVC initiation.

(A) Activation map showing selections used (B) (i)  $V_m$  traces as shown above plotted alongside estimated membrane potential (ii) Expanded  $V_m$  traces showing peak EAD (blue line), peak voltage gradient (red line) and earliest upstroke of the PVC (grey line).

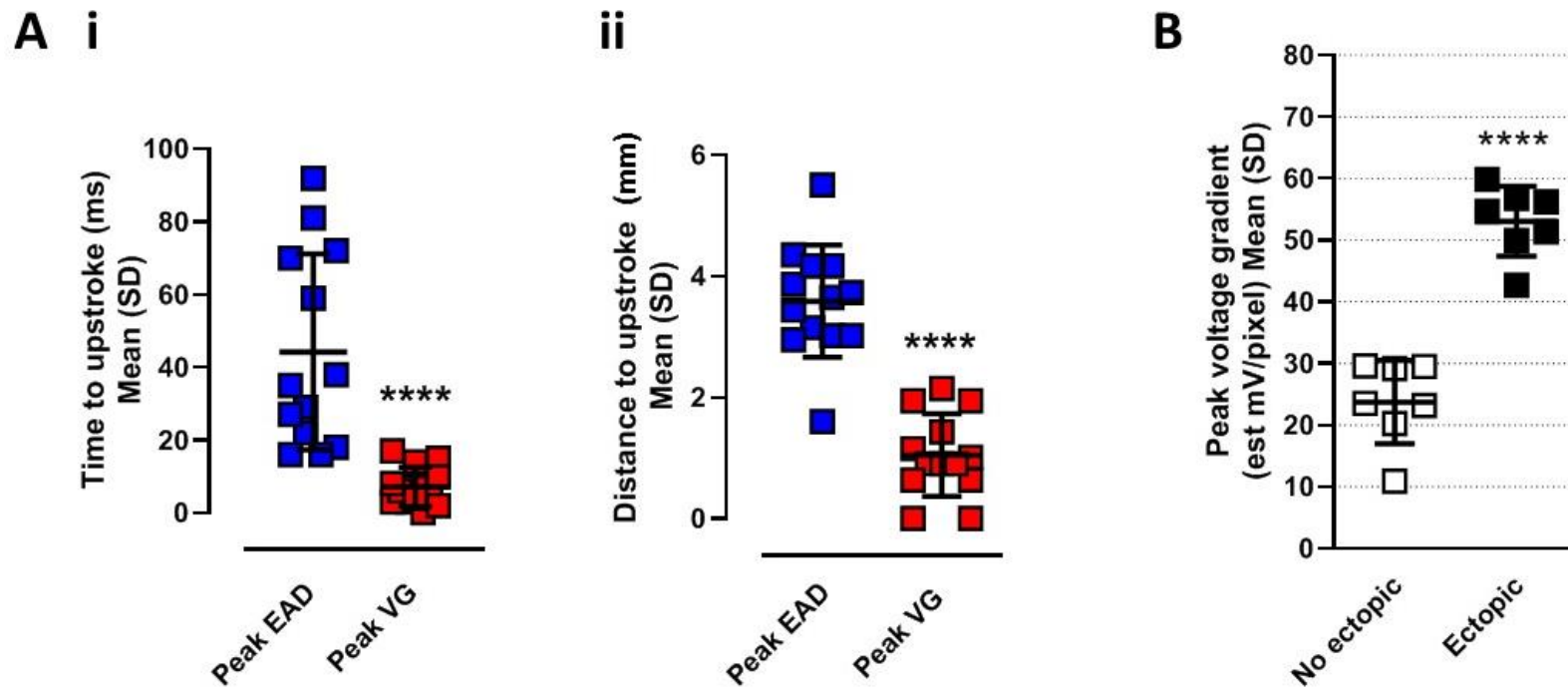


**Figure 4.17.** Relationship between PVC upstroke, EAD and peak voltage gradient.

(A) Mean data from 13 PVCs taken from 11/14 hearts, showing (i) time and (ii) distance to PVC upstroke from the peak EAD (blue) and peak voltage gradient (VG) (red) (B) Mean data over 7 PVCs taken from 5/14 hearts, showing peak voltage gradient in beats with (black symbols) and without (white symbols) taken consecutively during an optical acquisition. Paired Student's t-tests, \*\*\*\*  $p < 0.0001$ .

### ***Intracellular Calcium During PVC Initiation***

Analysis of  $V_m$  and intracellular  $Ca^{2+}$  traces was performed to investigate the role of  $Ca^{2+}$  during PVC initiation. This involved analysis as described above (Figure 4.15) but a detailed examination was performed across only 4 of the 6 sites used (excluding sites 5 and 6), that encompassed the long AP island with EADs (site 1), an intermediate zone (site 2), the breakout zone (site 3) and beyond (site 4), Figure 4.18 and an expanded analysis alongside a  $V_m$ - $Ca^{2+}$  delay map is shown in Figure 4.19. Within the long AP island, EADs were thought to be driven by an increase in intracellular  $Ca^{2+}$ . Site 1 exhibits a rise in  $Ca^{2+}$  before the  $V_m$  depolarisation, with the peak  $Ca^{2+}$  elevation corresponding to the maximal voltage change ( $dF/dt$ ), suggesting  $Ca^{2+}$  is driving this  $V_m$  depolarisation. Within the earliest TA break out zone (site 3),  $V_m$  and  $Ca^{2+}$  rise simultaneously.  $V_m$ - $Ca^{2+}$  delay shows normal EC coupling with positive values in the areas of normal APD confirming that  $V_m$  is rising first, whereas the long AP island shows negative values and similar to the trace analysis shows  $Ca^{2+}$  is rising before  $V_m$  and suggesting this is  $Ca^{2+}$ -led.

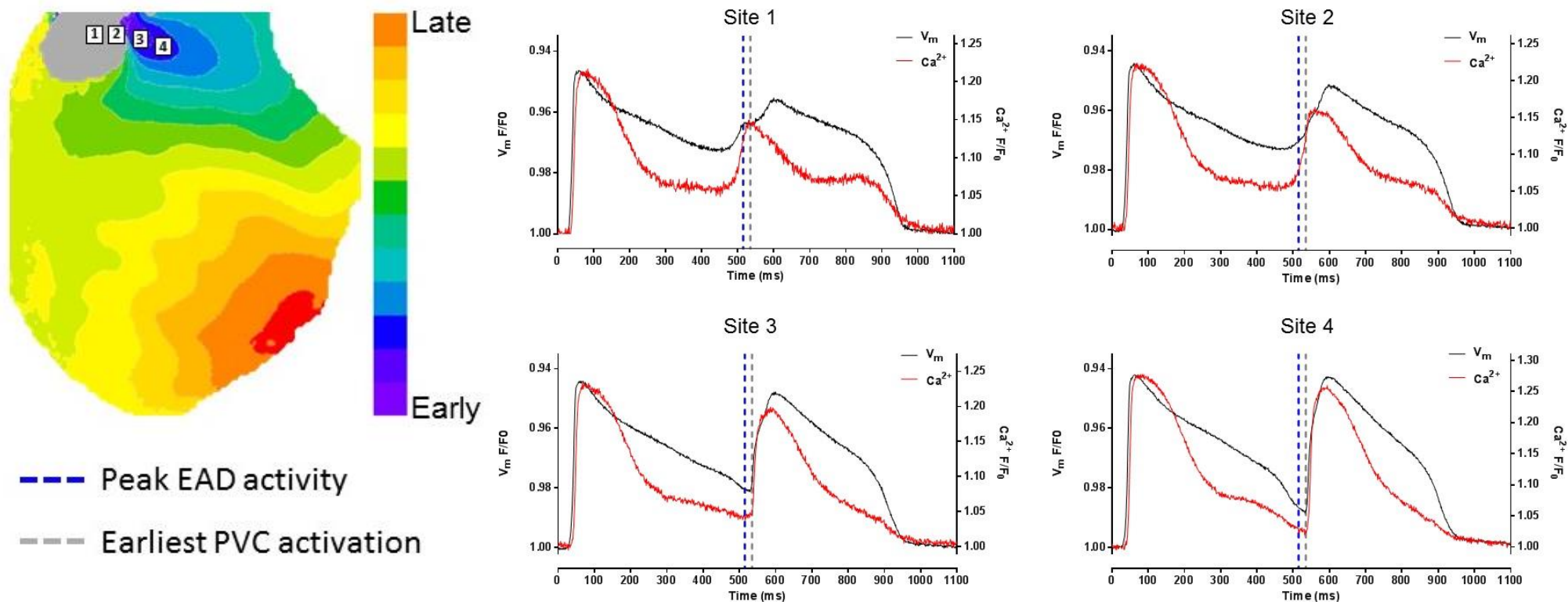


**Figure 4.18.**  $V_m$ - $Ca^{2+}$  dynamics during PVC initiation.

Activation map of PVC taken following a paced beat (same example as Figure 4.15). Long AP island shown as the grey area. Superimposed  $V_m$  (black) and  $Ca^{2+}$  (red) traces from 5x5 pixel selections from within the long AP island, stretching across the breakout zone and sites distal to this. Site 1 lies within the long AP region and demonstrates a  $Ca^{2+}$  driven EAD (peak EAD activity denoted by blue line) followed by a  $V_m$  upstroke that is not associated with a CaT. In site 3, at the earliest activation of the PVC (grey line) there is no EAD and rise of  $V_m$  and  $Ca^{2+}$  during the PVC upstroke is simultaneous. Site 4 is distal to the earliest PVC activation and shows normal EC coupling.



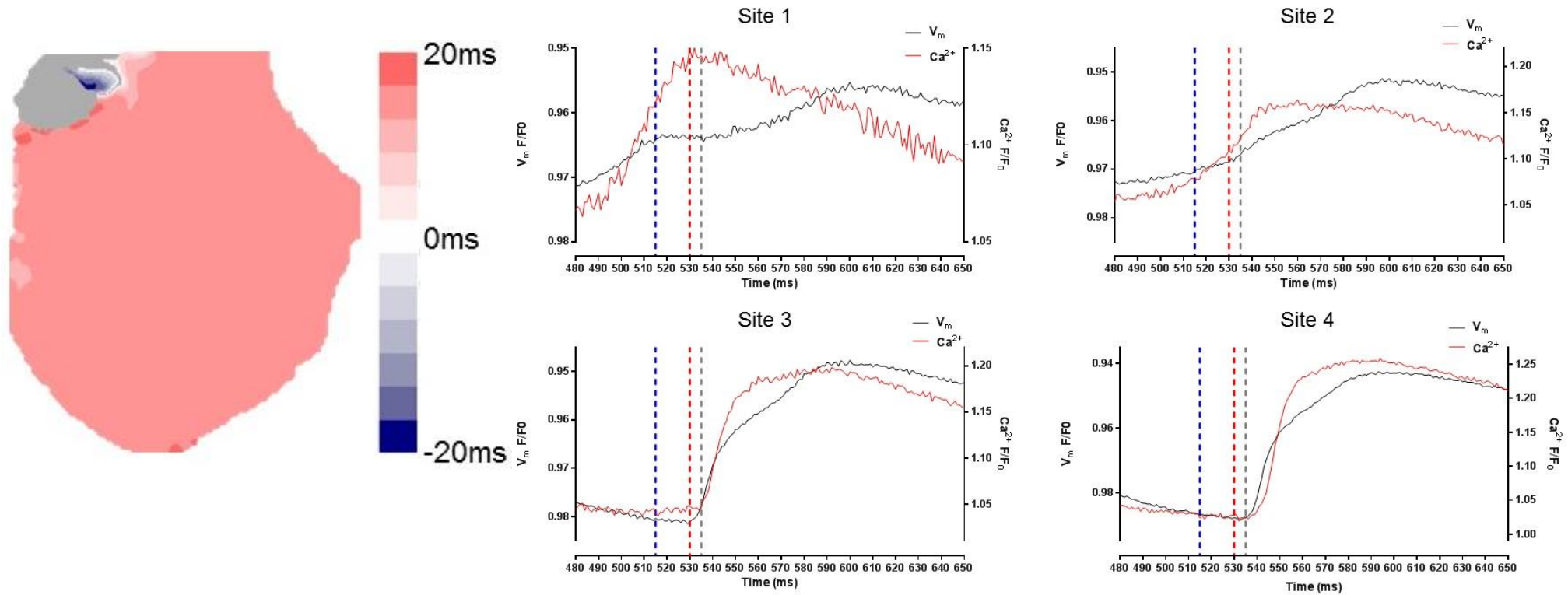


**Figure 4.19.**  $V_m$ - $Ca^{2+}$  dynamics during PVC initiation (2).

$V_m$ - $Ca^{2+}$  delay map taken following a paced beat and during PVC initiation (same example as Fig 4.15) and increased time scale of sites 1-4 shown in Fig. 4.18. Long AP island shown as the grey area. Normal EC coupling seen out with long AP island with positive values and  $V_m$  rising first, long AP region showing negative values and  $Ca^{2+}$  rising first. Site 1 is within the long AP island with EADs present, occurs before peak EAD (blue line). Site 3 is where the peak voltage gradient (red line) and earliest PVC activation (grey line) are seen, here  $V_m$  and  $Ca^{2+}$  are rising simultaneously.

## **The Role of Sarcoplasmic Reticulum Calcium During PVC Induction**

Thapsigargin, a non-competitive inhibitor of SERCA was added in five hearts to ascertain the effects of SERCA blockade on PVC induction. Data from all five hearts regarding establishing the LQT model have been shown already in Chapter 3, and occurrence of PVCs, bursts and TdP have been described above. Inhibition of SERCA activity slows the  $Ca^{2+}_i$  decay rate without affecting the sarcolemmal or  $I_{CaL}$  currents.

### ***Thapsigargin and Intracellular Calcium***

The effects of TG on intracellular  $Ca^{2+}$  duration, are shown in Figure 4.20. To examine the effects of SERCA blockade, the 10-30% decay of the CaT was measured, this is highlighted in Figure 4.21. Mean values of 10-30% decay time for five hearts are shown in Table 4.4 and Figure 4.22. Thapsigargin significantly prolonged 10-30% decay time when compared with baseline at 20 minutes ( $46.60 \pm 3.62$ ,  $p < 0.05$ ) and 30 minutes ( $52.24 \pm 6.97$ ,  $p < 0.001$ ). As described in Chapter 2 (pp. 80), changes in CaT amplitude were measure using F/F<sub>0</sub>. TG did not change CaT amplitude, Figure 4.23.

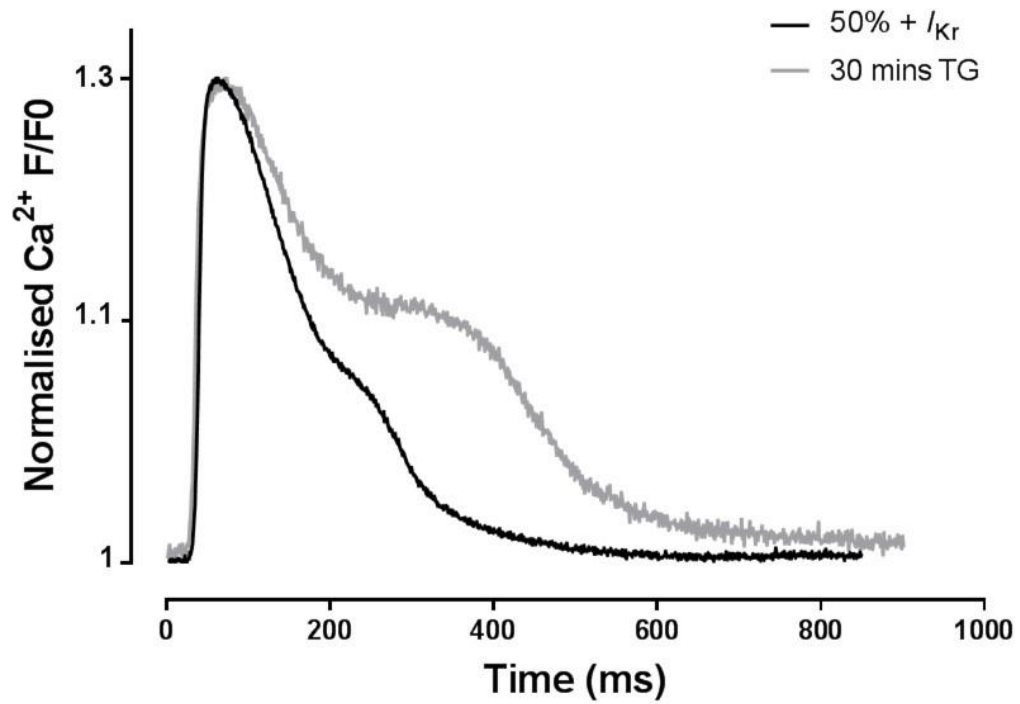


**Figure 4.20.** Effects of TG on intracellular  $\text{Ca}^{2+}$  transients.

Example from a single heart of the change in CaT after TG under LQT conditions.

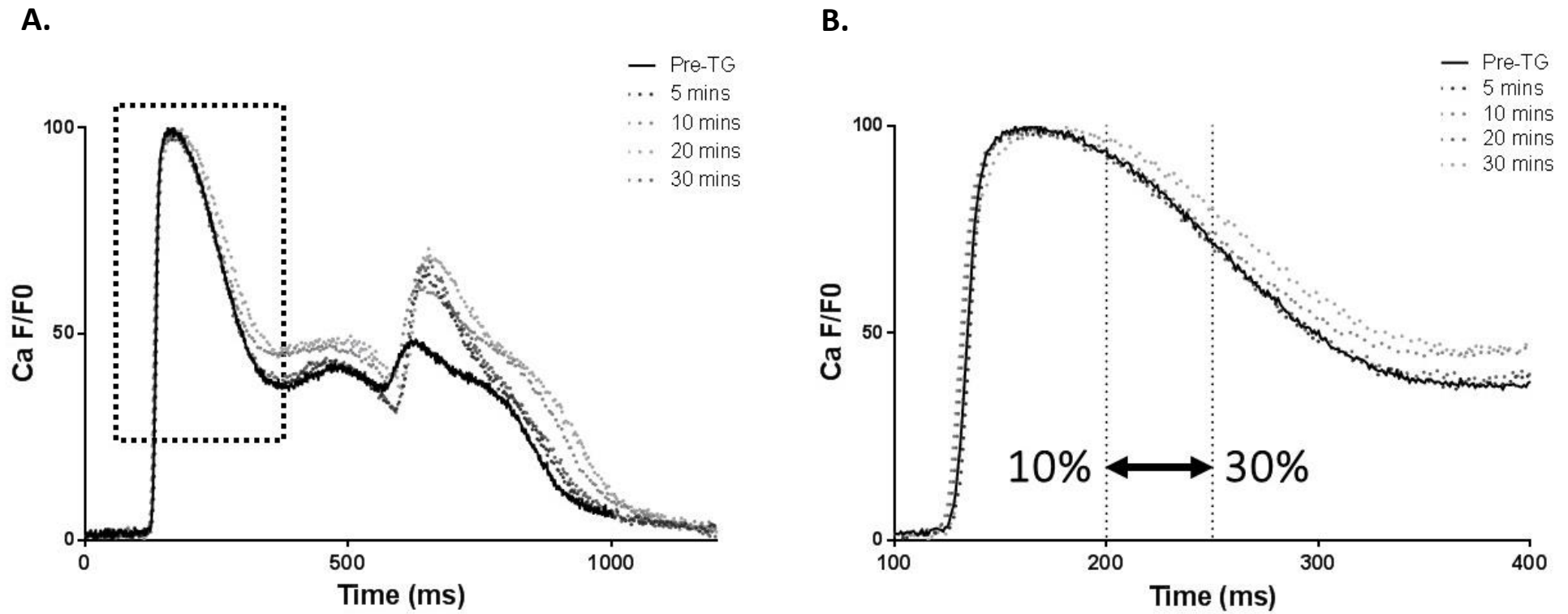


**Figure 4.21.** Effect of TG on CaT decay.

(A) CaTs pre and post -TG 2 $\mu$ M. (B) Expanded time scale from inset in A for same CaTs showing time measurements used to determine 10-30% decay time.

Conditions	Mean 10-30% decay time (ms)	SD	P value vs. LQT
Baseline	38.58	3.00	0.966
LQT	36.76	5.29	-
TG 2 $\mu$ M 10 mins	43.65	1.62	0.151
TG 2 $\mu$ M 20 mins	46.60	3.62	0.018
TG 2 $\mu$ M 30 mins	52.24	6.97	0.0002

**Table 4.4.** Effect of TG on 10-30% decay time.

Mean values of 10-30% decay time post-TG (n = 5) using repeated measures one-way ANOVA with Tukey's multiple comparisons testing.

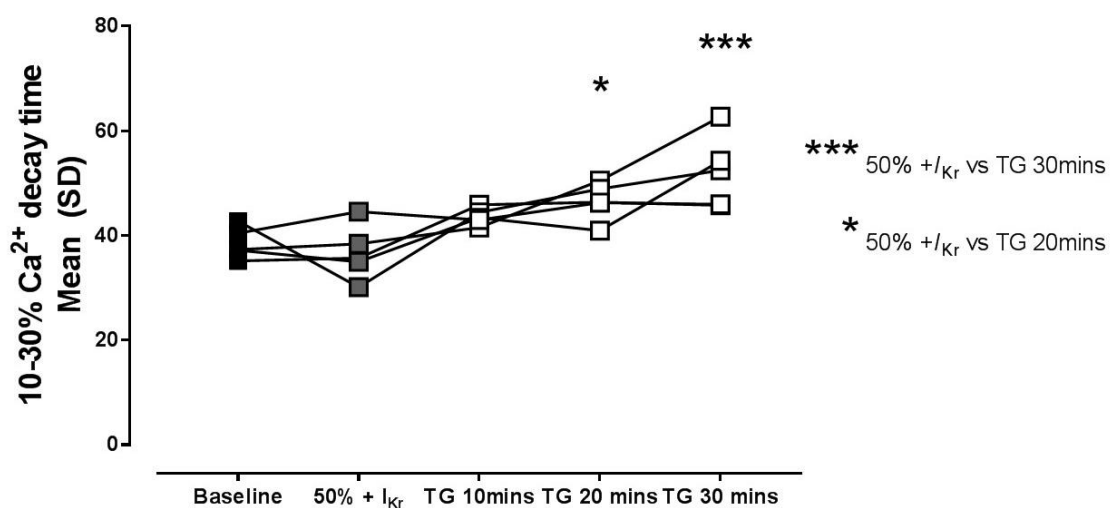


**Figure 4.22.** Effect of TG on Ca<sup>2+</sup> decay time.

Comparison of LQT conditions vs. post-TG 2 $\mu$ M is significantly different at 20 minutes (\* p < 0.05) and 30 minutes (\*\* p < 0.001), repeated measures one-way ANOVA with Tukey's multiple comparisons testing.

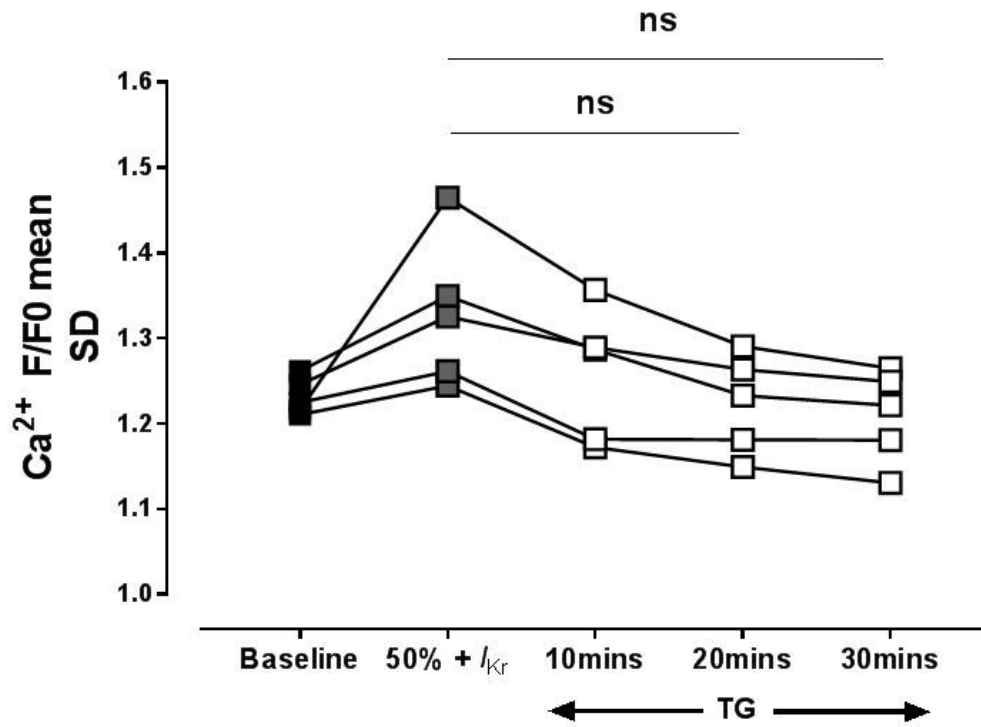


**Figure 4.23.** Mean change in  $\text{Ca}^{2+}$  F/F0 over time pre- and post-TG.

Changes in  $\text{Ca}^{2+}$  F/F0 compared with baseline, LQT and post TG  $2\mu\text{M}$  over 10, 20 and 30 minute interval ( $n = 5$ ). Repeated measures one-way ANOVA with Tukey's multiple comparisons testing.

### ***Thapsigargin and APD<sub>90</sub>***

Thapsigargin significantly prolonged the APD<sub>90</sub> compared with LQT conditions ( $p < 0.01$ ), Figure 4.24. Mean APD<sub>90</sub> values are shown in Table 4.5. An example of APD<sub>90</sub> maps and corresponding  $V_m/Ca^{2+}$  traces for one heart, across baseline, LQT and TG conditions is shown in Figure 4.25. All values shown for TG were taken 30 minutes after TG administration.

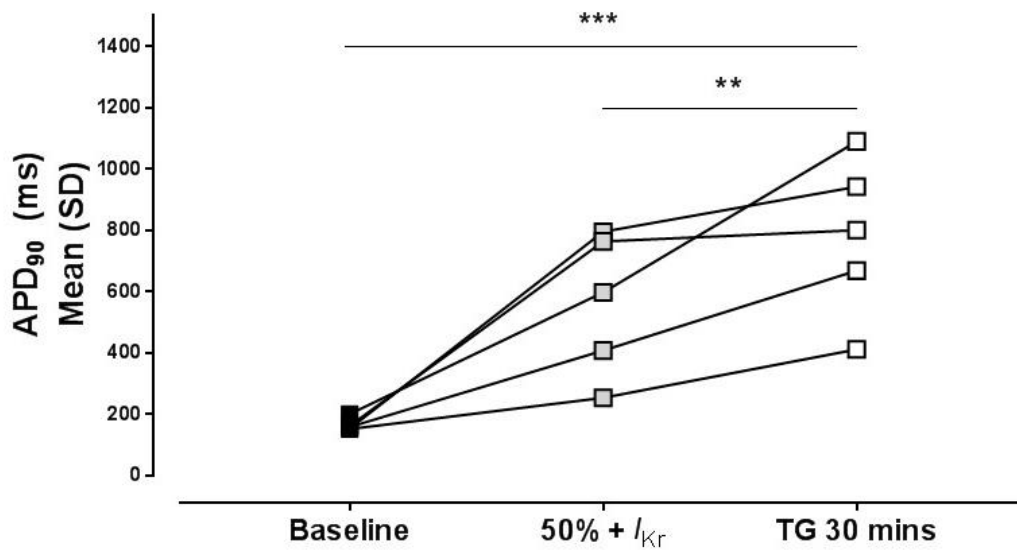


**Figure 4.24.** Effect of TG on APD under LQT conditions.

Mean values of APD<sub>90</sub> at 2000ms PCL at baseline (black), LQT conditions (grey) and + TG 2 $\mu$ M (open squares). Repeated-measures one-way ANOVA with Dunnett's multiple comparisons testing vs. baseline \*\*\*  $p < 0.001$ , \*\*  $p < 0.01$ .

	<b>APD<sub>90</sub> ± SD (ms)</b>	<b>P value vs. baseline</b>
<b>Baseline</b>	165.7 ± 20.28	-
<b>LQT</b>	563.7 ± 231.7	0.0065
<b>LQT + TG 2μM</b>	782.6 ± 260	0.0004

**Table 4.5.** Change in APD<sub>90</sub> with TG.

Values taken from 5x5 pixel selections at 2000ms PCL (n = 5). P values are from a repeated-measures one-way ANOVA with Dunnett's multiple comparisons testing vs. baseline.

### ***Effect of Thapsigargin on Arrhythmias***

PVCs, bursts and TdP occurred in all 5 hearts tested prior to TG administration. After 20 minutes of TG there was no change in arrhythmia incidence (PVCs 5/5, bursts 5/5 and TdP 5/5, all p = NS).



## Discussion

The purpose of this Chapter was to describe the occurrence and generation of PVCs and ventricular arrhythmias seen in a pharmacological model of LQT in the intact rabbit heart. Ventricular arrhythmias in the LQT syndrome are strongly associated with EADs, leading to the suggestion that they are responsible for generating the PVCs which then induce TdP (Cranefield PF, 1977; Roden DM, 1993; Kannankeril PJ *et al*, 2007). Prior studies have shown that EADs result from either spontaneous  $\text{Ca}^{2+}$  release from the SR or from re-activation of  $I_{\text{CaL}}$ . Experimental models of pharmacological LQT, have shown a SR  $\text{Ca}^{2+}$  and LTCC blockade, causes EAD abolition and prevention of PVCs (Verduyn SC *et al*, 1995; Chang PC *et al*, 2015). Computer modelling studies investigating  $I_{\text{CaL}}$  dynamics, showed  $I_{\text{CaL}}$  recovery and reactivation was the mechanism of EAD formation (Zeng J *et al*, 1995), and tissue-scale modelling showed voltage gradients and enhancement of  $I_{\text{CaL}}$  induced EADs and PVCs (Huang X *et al*, 2016). The model used in this study, created reproducible LQT conditions that elicited PVCs, bursts and TdP. These were associated with islands of long APD surrounded by steep voltage gradients, this is consistent with previous data (Maruyama M *et al*, 2011; Chang PC *et al*, 2015). The range of APD seen under these conditions is keeping with the between-heart variability described in Chapter 3, with widespread APD heterogeneity under LQT conditions. The mean APD is keeping with values seen in previous data (Choi BR *et al*, 2002; Maruyama M *et al*, 2011; Change PC *et al*, 2015). We found phase 2 EADs were present within the long APD regions that appeared to be  $\text{Ca}^{2+}$ -driven. However, analysis of the PVC mechanism suggested PVC induction was not directly driven by cellular EADs, instead they were associated with large voltage gradients. Islands with large voltage gradients have also been observed in optical mapping studies of similar LQT models (Choi BR *et al*, 2002; Maruyama M *et al*, 2011). Furthermore, the EADs seen were only involved with PVC initiation when they occurred near the border of a long AP island which amplified the voltage gradients. Our data highlights the importance of steep voltage gradients and their direct involvement in activating the regenerative inward current required to create a PVC.

## ***Mechanism of PVC Induction is Not Directly driven by Cellular EADs***

A common mechanism of PVC induction under LQT conditions was demonstrated. Any PVCs seen were always preceded by a paced beat which exhibited “*islands*” of extreme AP prolongation that were bordered by steep repolarisation gradients. The breakout of PVCs arose from the border between the long and short AP regions. Within areas of long AP islands, phase 2 EADs manifested as positive deflections and occurred frequently throughout the AP plateau. Phase 3 EADs were not seen at any point. Phase 2 EADs were seen at 70% of a full AP upstroke, which would correspond to a voltage around -20mV.

Computer modelling studies, have demonstrated two potential mechanisms for EAD-induced PVCs. The cellular EAD theory states EADs require synchronisation across hundreds of thousands of cardiomyocytes to produce a single triggered PVC (Xie Y *et al*, 2010). An alternative theory for the EAD mechanism, is marked repolarisation heterogeneity causes electrotonically-triggered EADs, to produce transmural re-entry without the requirement of a cellular EAD (Dutta S *et al*, 2016). From the PVCs seen in this study, speculative assessment of EAD amplitude and dF/dt were used to investigate which mechanism was active. Quantitative data was not performed for this analysis as alternative approaches to the same analytic problem were applied. The amplitude analysis required adjusting for differences in fluorescence by calculating the amplitude of phase 2 and expressing this as a percentage of the amplitude of the preceding upstroke. In the case of synchronisation of EADs we expected larger amplitudes within the long AP islands. However, the amplitude map showed relatively low amplitudes across the long AP island with no suggestion of larger amplitudes towards the centre. Calculation of dF/dt was performed to examine the rate of depolarisation occurring in phase 2, as this would help to determine whether regenerative current was playing a role. The  $dF/dt_{max}$  of the phase 2 upstroke was expressed as a percentage of the preceding phase 0 upstroke. These percentage values were used to create a dF/dt map and showed phase 2 depolarisation in the long AP island was sub 15% of initial upstroke. This is not compatible with a regenerative current. If this a cellular EAD-triggered AP, then we would expect to see a fast upstroke, causing TA arising from that focal point. However, in this case nowhere in the long AP island is there a fast upstroke and instead this behaviour is keeping with passive current flow from the persistently depolarised region into the repolarising region just adjacent to it.

### ***PVC Initiation is Associated with Repolarisation Gradients***

Voltage trace analysis was performed to examine voltage gradients and their involvement in generating a PVC in more detail. The PVCs occurred in beats with significantly larger voltage gradients than preceding beats that did not support PVCs. The presence and location of EADs were then examined as it was felt they could contribute to these AP gradients. Our observation was that EADs that appeared to be associated most frequently with PVCs were always associated at the edge of the AP island and in fact, any EADs occurring at the centre of a long AP island were not associated with PVCs. This was in keeping with the suggestion that voltage gradients were important as EADs occurring at the edge of AP islands were contributing towards a dynamic increase in voltage gradients. Overall suggesting steep voltage gradients are responsible for activating the regenerative inward current required to create a PVC, which is amplified by the presence of a local EAD but not exclusively driven by the EAD itself.

### ***EADs are Driven by Intracellular Calcium***

The combination of  $V_m$  and  $Ca^{2+}$  trace analysis was performed to investigate the role of intracellular  $Ca^{2+}$  in EADs and PVCs. Examination of sites exhibiting EADs (site 1 in the analysis), showed the EAD signal was preceded by a rise in  $Ca^{2+}$ , this linkage suggests  $Ca^{2+}$  may be causing a change in the  $V_m$ . The peak directly correlates with the  $V_m$  depolarisation, suggesting EADs are being driven by  $Ca^{2+}$ . If this was  $V_m$  led then we would expect to see the  $V_m$  rise occurring before  $Ca^{2+}$ . It is possible  $Ca^{2+}$  driven EADs are generated either by SR  $Ca^{2+}$  release or by  $I_{CaL}$  as they are occurring within the  $V_m$  range for  $I_{CaL}$  reactivation (Qu Z *et al*, 2013). However, the earliest time of  $V_m$  TA (site 3 in the analysis), showed  $V_m$  and  $Ca^{2+}$  rose simultaneously.  $V_m$ - $Ca^{2+}$  delay maps similarly showed normal EC coupling out with the long AP island with positive values and keeping with  $V_m$  rising first, the long AP island showed negative values and suggestive  $Ca^{2+}$  rose before  $V_m$ . Overall, this suggests intracellular  $Ca^{2+}$  is responsible for driving EADs, which is consistent with previous literature (Volders PG *et al*, 2000, Choi BR *et al*, 2002; Chang PC *et al*, 2015).

## ***Sarcoplasmic Reticulum Calcium Inhibition Does Not Suppress EADs or PVCs***

The purpose of introducing TG into our LQT model was to further understand the role of SR  $\text{Ca}^{2+}$  in the generation of EADs and PVCs, and we sought to ascertain if TG abolished PVCs. Inhibition of SR  $\text{Ca}^{2+}$  reuptake would theoretically prevent SR  $\text{Ca}^{2+}$  driven EADs and thereby abolish PVCs dependent on those EADs. First, we quantified the effect of TG on SERCA by measuring CaT decay. In our subset of 5 hearts, PVC initiation was not affected by TG. The primary effect of TG was on CaT decay, with a significant increase in 10-30%  $\text{Ca}^{2+}$  decay time post-TG. After 30 minutes, where the largest magnitude of  $\text{Ca}^{2+}$  decay was seen, there were still PVCs in all 5 hearts. TG also caused prolongation of  $\text{APD}_{90}$  across all five hearts, which may reflect the changes in the CaT and is keeping with previous work (Elliot EB *et al*, 2012). We did not compare the effects of TG on  $\text{Ca}^{2+}$  decay,  $\text{APD}_{90}$  and PVC induction at baseline conditions (*i.e.* before LQT induction), nor did we test the rate-dependence of TG effects, as this would require further experiments and animal sacrifice and the questions it would answer were not imperative to the overall hypotheses. We had effective controls from baseline and other experiments that were mapped without TG, and these showed no change in  $\text{Ca}^{2+}$  decay or APD over the timescales involved. Furthermore, prior experiments in our group using TG at baseline conditions provided us with control heart data as a reference (Elliot EB *et al*, 2012), which showed TG caused CaT amplitude and cell shortening to reduce to 70% of control.

At present, there is limited published data on the rate dependence of TG and it is difficult to predict what electrophysiological effects the changes in  $\text{Ca}^{2+}$  seen with TG would be expected to have under LQT conditions. Our data was also limited by a drop in SNR at 30 mins of TG, which may have been related to the time taken for the whole protocol. This limited our ability to quantify the electrophysiological changes accurately. Ultimately, we observed no reduction in PVC initiation with TG, suggesting that SR  $\text{Ca}^{2+}$  release is not a critical step in PVC induction but this was not a clean experimental intervention and so it is difficult to draw any mechanistic conclusions from this limited dataset.

## Limitations

The major limitation was the fact only the epicardial surface was optically mapped, which meant any EADs and PVCs occurring within the endocardium, mid-myocardium or sub-endocardium could not be included. This limited the capture, and so study of EADs occurring within these regions. To mitigate this, we identified and studied PVCs that displayed early epicardial activation occurring before the QRS complex on the pECG, in an attempt to only study PVCs that were initiated close to the epicardial surface. Secondly, only a single lead pECG was used which is not capable of identifying any ventricular activation purely orthogonal to that lead. The use of multiple orthogonal ECG leads might have mitigated this limitation. The curvature of the epicardial surface meant signals were distorted or interference from surface artefact, meant potentially valuable optical data was excluded from analysis as it did not have adequate SNR or clear signals.

The study of SR  $\text{Ca}^{2+}$  was complex given the optical dye measured changes in intracellular  $\text{Ca}^{2+}$ , so direct measurements of the effects on SR  $\text{Ca}^{2+}$  could not be monitored. Indeed, the use of 50%  $\text{K}^+/\text{Mg}^{2+}$  + E-4031 0.5 $\mu\text{M}$  + TG 2 $\mu\text{M}$  at 2000ms PCL, created an environment that may be considered physiologically impossible, thus creating results with limited translatable application.

## Conclusion

These data suggest that the mechanism of PVC induction in LQTS is not direct triggering by synchronised cellular EADs but rather that steep voltage gradients are responsible for activating the regenerative inward current required to create a PVC. The voltage gradients are amplified by the presence of a local EAD but not exclusively driven by the EAD itself.

## **Chapter 5: Role of L-Type Calcium Current**

## Introduction

The previous Chapter showed PVC induction was not thought to be driven directly by cellular EADs and instead uniquely linked to steep voltage gradients, where large gradients caused passive electrotonic flow into neighbouring repolarised regions and reactivation of a regenerative current to induce a new PVC. Testing the role of voltage gradients is challenging experimentally, as it is difficult to modulate voltage gradients in an intact model. In order to study this proposed mechanism experimentally, the focus shifted to identifying a current that could produce a PVC upstroke under these circumstances. From the plateau and amplitude analysis in the previous Chapter, the  $V_m$  range PVCs occurred at was between  $\sim 0$  and  $-50$  mV, so  $I_{Na}$  activation is unlikely to occur as the membrane was too depolarised. The next possible channel active within this  $V_m$  range was  $I_{CaL}$ , therefore we hypothesised  $I_{CaL}$  was responsible for the initial triggering of the PVC and so blockade of this channel should abolish PVCs. Within this hypothesis, preservation of the LQT substrate was crucial as it was important to abolish PVCs without concurrent abolition of the LQT substrate. We expected that high doses of  $I_{CaL}$  blockade would remove the LQT substrate by shortening APs and the  $QT_c$  interval, in turn eradicating EADs and  $V_m$  gradients. However, in theory low dose  $I_{CaL}$  blockade that is insufficient enough to affect the LQT substrate, might abolish PVCs in the presence of the LQT substrate.

### ***L-Type Calcium Current***

The L-type  $Ca^{2+}$  current ( $I_{CaL}$ ) has proven to have a significant role in the generation of EADs and under some circumstances it is thought that re-activation of  $I_{CaL}$  is the mechanism of EAD formation (Zeng J *et al*, 1995). The  $I_{CaL}$  current itself possesses regenerative potential, where depolarisation from progressively negative membrane potentials will allow reactivation of increasing proportions of  $I_{CaL}$ , leading to sufficient depolarisation to support an AP (January CT *et al*, 1989; January CT *et al*, 1990). The conductance and state of channel opening of  $I_{CaL}$  is influenced by other factors such as  $K^+$  conductance, voltage range, recovery, membrane depolarisation *etc*, and each factor can vary between APs. Weiss *et al*, proposed during phase 2 of the cardiac AP,  $I_{CaL}$  swings between open and closed and during LQT conditions, the duration of  $I_{CaL}$  opening extends and permits the reactivation of both  $I_{CaL}$  and NCX (Weiss JN *et al*, 2010). Experimentation using voltage-clamped sheep Purkinje fibres studied the mechanism of EADs induced at the AP plateau voltage, and the

use of a  $\text{Ca}^{2+}$  agonist (BAY K 8644), caused  $I_{\text{CaL}}$  recovery from inactivation to reactivation and a new depolarisation to occur (January CT *et al*, 1989). A model using canine Purkinje fibres induced LQT using clofilium or *d,l*-sotalol, found 2 distinct mechanisms for phase 2 and 3 EADs: the use of BAY K 8644 identified phase 2 EADs required reactivation of  $I_{\text{CaL}}$ , whereas phase 3 EADs were induced by the NCX (Patterson E *et al*, 1997). Overall,  $I_{\text{CaL}}$  is thought to have the potential to generate phase 2 EADs by both supporting the upstroke of a triggered AP and sustaining the plateau to prolong APD.

The use of the  $I_{\text{CaL}}$  blocker, nifedipine, in LQT experimental models, is known to abolish phase 2 EADs and suppress arrhythmic activity (Patterson E *et al*, 1997; Chang PC *et al*, 2015). The therapeutic blockade of  $I_{\text{CaL}}$  for LQT patients has been suggested experimentally (Huang X *et al*, 2016) and has been attempted clinically. Case reports of LTCC blockers used as antiarrhythmic therapy in LQTS has been described, *e.g.* one patient with anticholinergic overdose induced arrhythmia was cardioverted and TdP abolished with verapamil (Liao WB *et al*, 1996); congenital LQTS patients with recurrent shocks were given verapamil on top of their beta-blockade which reduced arrhythmic burden (Kawade M *et al*, 1995; Jacobs A *et al*, 2006; Liu Y *et al*, 2016). Limited case series have also been reported *e.g.* verapamil proved to eliminate ventricular ectopy and VT in a study of six patients who were pro-arrhythmic despite beta-blockade (Jackman WM *et al*, 1990). Although there are case reports and clinical studies providing evidence of antiarrhythmic properties of LTCC blockade, studies in this patient cohort are challenging owing to the small numbers of patients enrolled and low event rates. So far, the rationale for this treatment approach has been to shorten the  $\text{QT}_c$  and reverse the LQT phenotype. Doing so would require large doses of LTCC blockers which would succeed in abolishing the substrate but also associated with profound vascular side effects that are recognised with LTCC blockade, *i.e.* vasodilatation. This makes doses required to shorten the  $\text{QT}_c$  highly likely to be intolerable because of hypotension. Furthermore, APD shortening and negative inotropic cardiovascular effects seen with therapeutic LTCC blockade could potentially create proarrhythmic tendencies, however there is no direct evidence for this.  $I_{\text{CaL}}$  blockade for LQT patients is currently not a recognised treatment (Priori SG *et al*, 2013; Priori SG *et al*, 2015).



Within this study so far, the LQT model in an intact rabbit heart has shown reproducible EADs and PVCs. Under LQT conditions, long islands of APD developed that were associated with increased epicardial dispersion of APD (Figure 3.17). Analysis of the PVC mechanism has shown EADs contribute towards triggering but are not directly responsible. Instead, passive electrotonic flow across steep voltage gradients at the border of long AP islands is thought to cause reactivation of  $I_{CaL}$  initiating a PVC. If it were possible to prevent  $I_{CaL}$  reactivation then theoretically this would be possible to abolish PVCs and reduce the arrhythmic risk in LQTS.

## ***Aims***

The experiments described in this Chapter were designed to test the hypothesis that large voltage gradients cause reactivation of  $I_{CaL}$ , thereby aborting repolarisation and producing an  $I_{CaL}$  mediated upstroke which supports a PVC.

Specific aims were:

1. Examine the effects of nifedipine on the induction of PVCs and ventricular arrhythmia in LQT.
2. Determine whether any anti-arrhythmic effect is achieved through effects on the LQT substrate.

## Methods

To investigate the involvement of  $I_{CaL}$  in the initiation of PVCs, the *ex vivo* model of LQT2 using the CMOS-dual optical mapping system described in Chapter 2 was used to record optical APs and CaTs from the epicardial surface of Langendorff-perfused intact rabbit hearts. Hearts from 11 male New Zealand White rabbits were used in these experiments, which conform to standards set out in the UK Animals (Scientific Procedures) Act, 1986.

### **Experimental Protocols**

Experimental protocols are outlined in Figure 5.1. The characterisation of the model has been presented for 4 of these hearts in Chapter 3 and analysis of PVC mechanism in Chapter 4 involved 7 of these hearts. Similar to Chapter 4, a total of 7 hearts the experiments were performed without recordings at baseline conditions (*i.e.* the experiment started with Tyrode's containing 50%  $K^+/Mg^{2+}$  and E-4031 was then added) to allow more time for the drug response protocols.

After initial experiments, testing the effect of 500nM nifedipine (n= 6), 200nM (n=1) and then a concentration-response protocol was performed, quantifying TA occurrence over 10 minutes of 2000ms PCL before drug and then at, 20, 60 and 200nM nifedipine in 4 hearts. In a subset of hearts, confirmatory protocols were attempted where nifedipine was washed out and E-4031 concentration increased. Washout protocol involved switching the perfusate back to 50%  $K^+/Mg^{2+}$  + E-4031 0.5 $\mu$ M for 30 minutes in 3/11 hearts (2/3 nifedipine 200nM; 1/3 nifedipine 500nM) then nifedipine 500nM was re-introduced. In 5/11 the E-4031 concentration was increased from 0.5 to 2 $\mu$ M in 5/11 hearts (2/5 nifedipine 200nM; 3/5 nifedipine 500nM). Protocols are summarised in Table 5.1 and depicted in Figure 5.1.

The concentration of nifedipine used was based on published work (Chang PC *et al*, 2015), a low concentration was selected as it was expected high concentrations (2 $\mu$ M) would shorten the APD, eradicate the LQT substrate and terminate arrhythmias indirectly, therefore an approximate dose close to the  $IC_{50}$  was selected (500nM). However, at this concentration there was an immediate full effect as all PVCs were abolished. Ultimately, we hoped to identify a low dose that was more sensitive than identifying PVC abolition, therefore a lower dose of 200nM was attempted. This concentration also caused total abolition of PVCs. This

led to a concentration-response approach with 10-minute intervals of 20, 60 and then 200nM. Doing so required additional time during experiments, and as previously stated, constant attention was paid to the preparation viability. As discussed in Chapter 3 (pp. 99), experimentation had to occur within a time window where we were confident in the preparation viability. As a result, the protocol had to be redesigned to optimise data collection within this time window. Practically this meant removing baseline recordings. The same principle was applied to nifedipine washout and high dose E-4031 concentration experimental subsets and is also why a washout/high dose E-4031 could not be performed in every experiment.

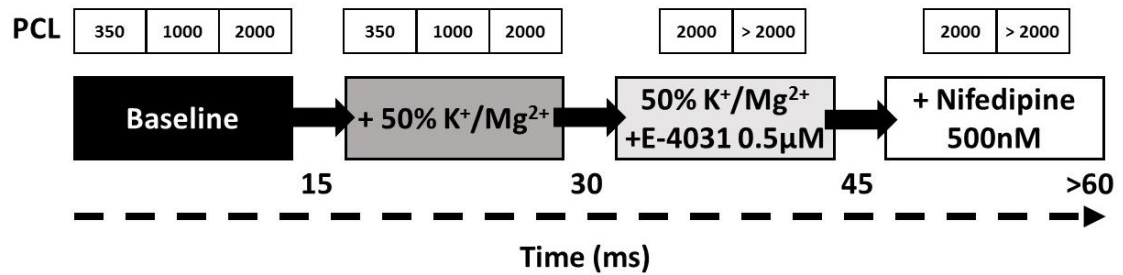
LQT protocol		Nifedipine protocol			Confirmatory Protocol	
		Nifedipine 500nM	Nifedipine 200nM	Nifedipine 20 / 60 / 200 nM	+ E-4031 2 $\mu$ M	Washout
Baseline > 50% K <sup>+</sup> /Mg <sup>2+</sup> > E-4031 0.5 $\mu$ M	4	4	0	0	1	0
50% K <sup>+</sup> /Mg <sup>2+</sup> + E-4031 0.5 $\mu$ M	7	2	1	4	4	3
<b>Total</b>	11	6	1	4	5	3

**Table 5.1.** Summary of experiments used for nifedipine protocol, including change in different conditions and confirmatory subsets.

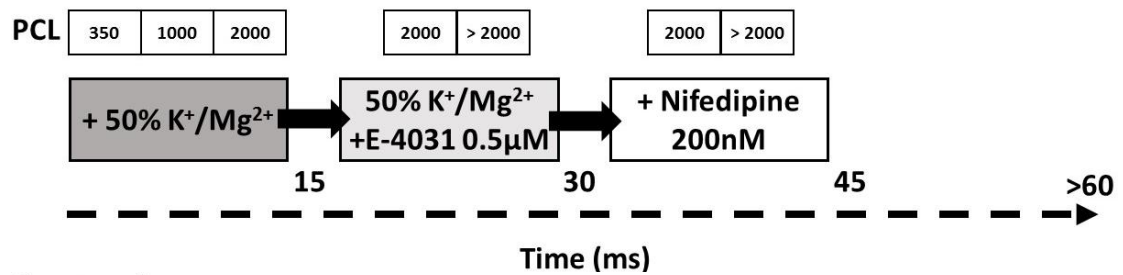
Total hearts used for nifedipine dataset was 11 and different protocols were used. There were 6/11 hearts that received nifedipine 500nM (4 starting at baseline and 2 starting at 50% K<sup>+</sup>/Mg<sup>2+</sup>). The remaining 5/11 hearts received incremental concentrations of nifedipine, one heart received 200nM alone and the remaining 4 received a concentration-response of 20 / 60 / 200nM. Total nifedipine 200nM n = 5 and 500nM n = 6. Further subsets were used that involved an increase in E-4031 2 $\mu$ M (n = 5) and a 30-minute washout of nifedipine (n = 3), these additional protocols were used within the same hearts.

## Nifedipine Protocol

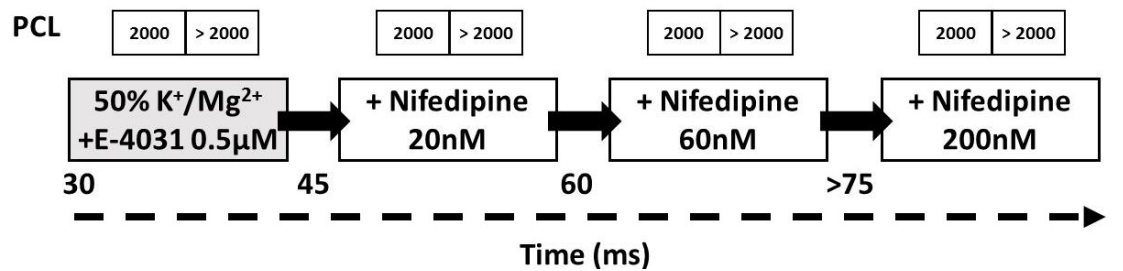
A n = 6



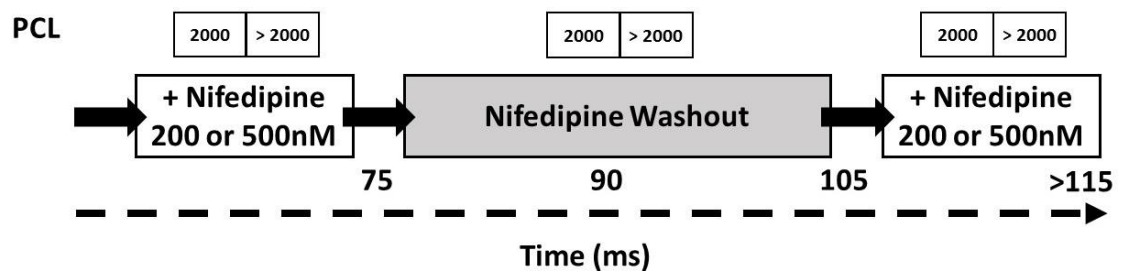
B n = 1



C n = 4



D n = 3



E n = 5

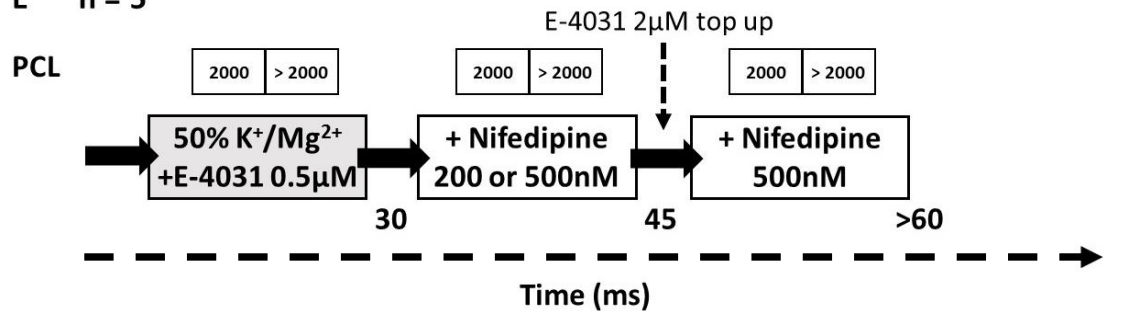


Figure 5.1. Summary of experimental nifedipine and confirmatory protocols.

***Analysis of Calcium Transient Amplitudes***

The effect of nifedipine on CaTs amplitude was calculated for nifedipine 200nM hearts (n=5). Details of this analysis is described in Chapter 2 (pp. 80). In this subset, F/F0 values were expressed as a percentage of the baseline F/F0 value.

## Results

### ***Effect of Nifedipine on Triggered Activity***

The effect of the  $I_{CaL}$  blocker nifedipine on the occurrence of arrhythmias (PVCs, bursts and TdP) was examined in 11 hearts. Pre-nifedipine there was 100% occurrence of PVCs. Nifedipine abolished PVCs in all hearts, after either 500nM (n=6, p<0.001) or 200nM (n=5, p<0.001), shown in Table 5.2 and Figure 5.2. The effects occurred early during nifedipine perfusion, with reduction in PVCs until they were completely abolished over 0 – 4 minutes with nifedipine 200 or 500nM. Nifedipine washout resulted in a return of PVCs in all hearts tested (n=3/3). An increase in E-4031 concentration (from 0.5 $\mu$ M to 2 $\mu$ M) in the presence of nifedipine did not result in a return of PVCs.

A nifedipine concentration-response protocol was performed to quantify arrhythmia occurrence over 10 minutes with nifedipine 20, 60 and 200nM. All 4 hearts had PVCs under LQT conditions. PVCs were abolished in one heart at 60nM and in the other 3 were abolished at 200nM. During the concentration-response, PVCs were counted and saw a progressive reduction with increasing doses of nifedipine, Figure 5.3. There was a mean 62% of beats at baseline, 56% with 20nM nifedipine, 39% with 60nM and 16% with 200nM (p<0.05 vs. baseline).



Conditions All at 2000ms PCL	Hearts (n)	PVCs	PVC Bursts (2-5 beats)	TdP
50% K <sup>+</sup> /Mg <sup>2+</sup> + E-4031 0.5μM	11			
+ Nifedipine 20nM	4		-	-
+ Nifedipine 60nM	4		-	-
+ Nifedipine 200nM	5	-	-	-
+ Nifedipine 500nM	6	-	-	-

**Table 5.2.** Effect of nifedipine on arrhythmias under LQT conditions.

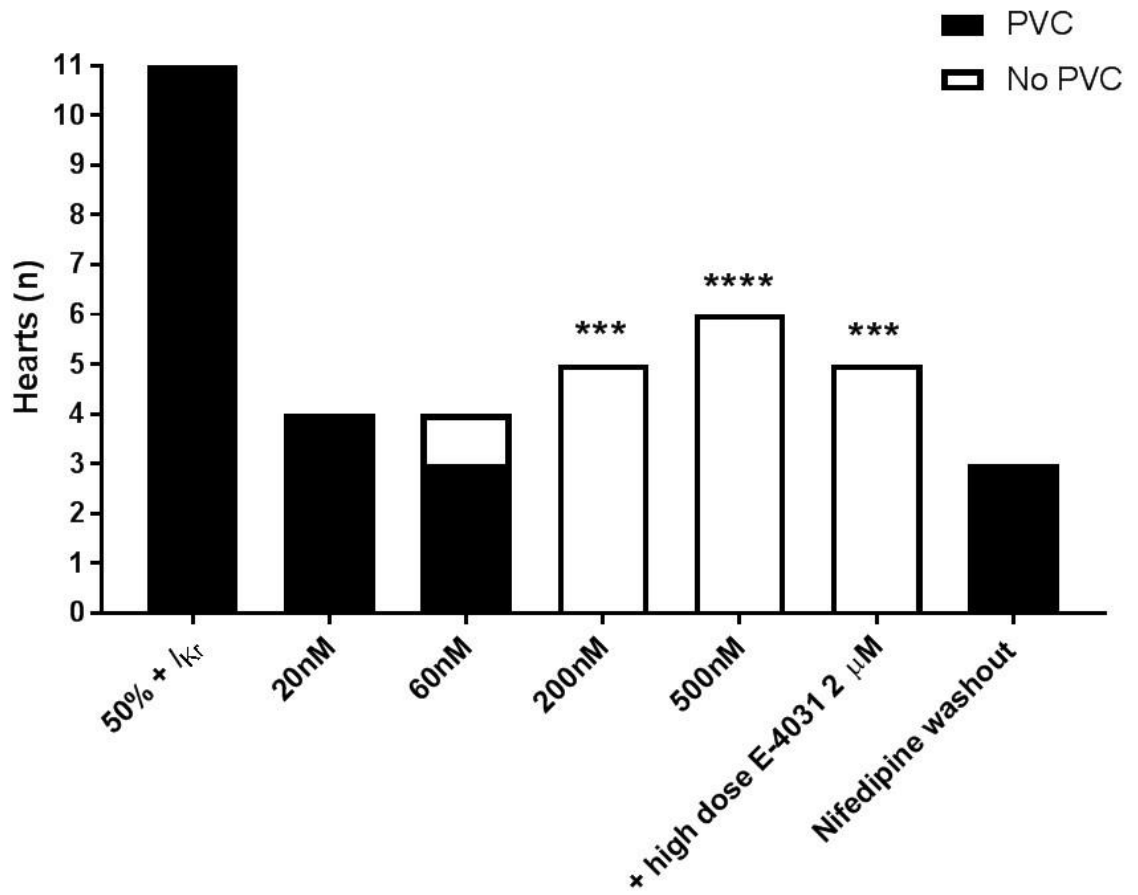


**Figure 5.2.** Effect of nifedipine on the occurrence of PVCs under LQT conditions.

All hearts demonstrated PVCs under LQT conditions. Incremental doses of nifedipine caused a reduction in PVCs with total abolition in all hearts at 200nM. Fisher's exact test, \*\*\*\*  $p < 0.0001$ , \*\*\*  $p < 0.001$ , vs. baseline.

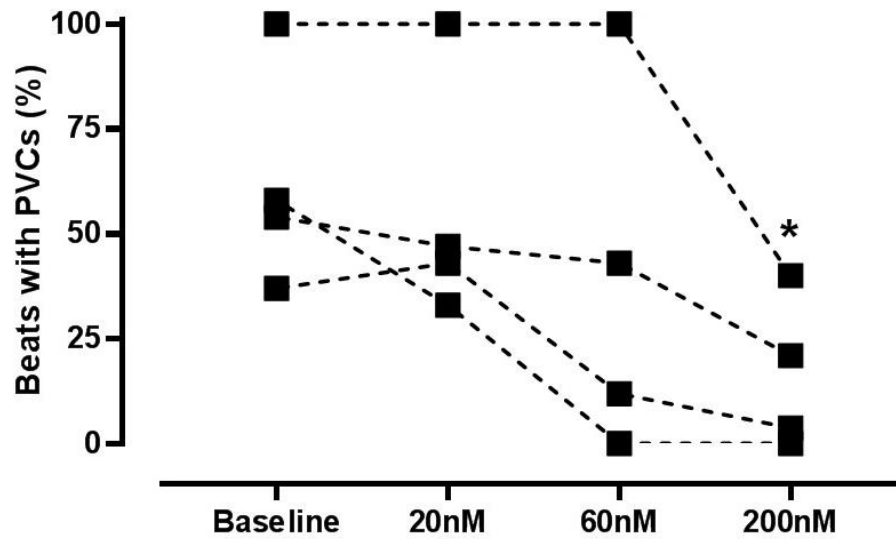


**Figure 5.3.** The effect of nifedipine on the proportion of paced beats with PVCs.

The number of PVCs were counted post-nifedipine and saw a progressive reduction with increasing doses ( $n=4$ ). Mean percentage was 62% at baseline, 56% post-nifedipine 20nM, 39% 60nM and 16% with 200nM. Repeated measures one-way ANOVA with Bonferroni post-testing,  $p<0.05$  vs. baseline.

### ***Effect of Nifedipine on the LQT Substrate***

An example of AP changes during the abolition of PVCs with nifedipine 200nM is shown in Figure 5.4. This shows changes in the QT interval,  $V_m$  traces and fluorescence maps taken pre and post-nifedipine 200nM. Post-nifedipine the  $QT_c$  interval shows very little change. Islands of long APs were seen both pre and post-nifedipine, these are detailed in the fluorescence maps (appearing yellow on the scale). Corresponding single pixel selections of  $V_m$  traces, spanning through these islands and into neighbouring repolarised areas are shown above the fluorescence maps. These demonstrate steep voltage gradients across these regions, with EADs occurring within the long AP islands and both gradients and EADs occurring both pre and post-nifedipine. Progressive changes in  $V_m$  traces between pre-nifedipine, immediately after PVCs were abolished and 15-minutes post-nifedipine are shown in Figure 5.5. This shows a  $V_m$  trace with a PVCs present pre-nifedipine, abolition of PVCs with an EAD present and  $V_m$  appearances 15-minutes post-nifedipine. To quantify the effects on the LQT substrate,  $APD_{90}$  and dispersion of  $APD_{90}$  ( $IP_{95}$  for  $APD_{90}$  values across the whole heart) over the same time points were measured in hearts at 200nM (n=5) and 500nM (n=6), Figure 5.6. These showed no significant change in either metric. Actual values for  $APD_{90}$  are listed in Table 5.3 and dispersion of  $APD_{90}$  are listed in Table 5.4. Overall at the point of PVC abolition, long AP islands with steep voltage gradients and EADs still occurred, confirming the LQT substrate was preserved and the mechanism of abolition of nifedipine was not indirectly through modification of the LQT substrate.

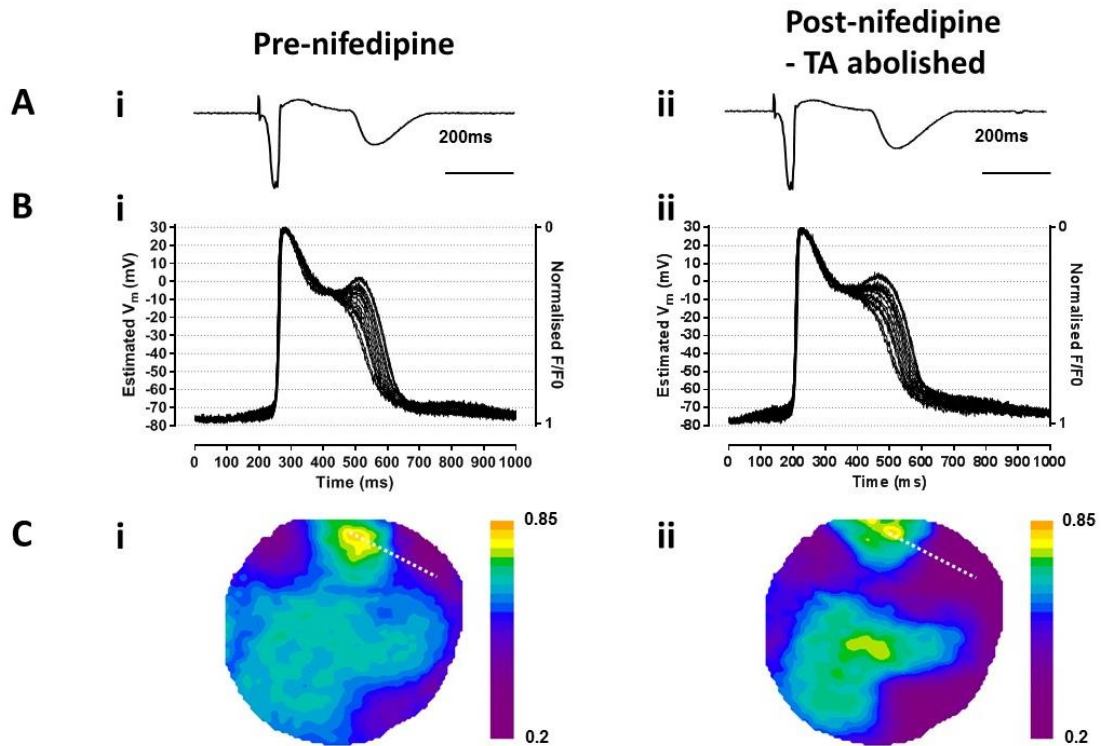


**Figure 5.4.** Effects of nifedipine on EADs and APD gradients.

(A) pECG with QT prolongation (i) before and (ii) after nifedipine 200nM. (B) Contiguous single pixel  $V_m$  traces taken from across the border of the prolonged AP region (white dashed line) in Ci and Cii) both (i) before and (ii) after nifedipine 200nM plotted with estimated  $V_m$  maps. (C) Normalised F maps for voltage with sections used for  $V_m$  traces (dashed white line) showing normalised fluorescence at the peak EAD (i) before and (ii) after nifedipine 200nM.

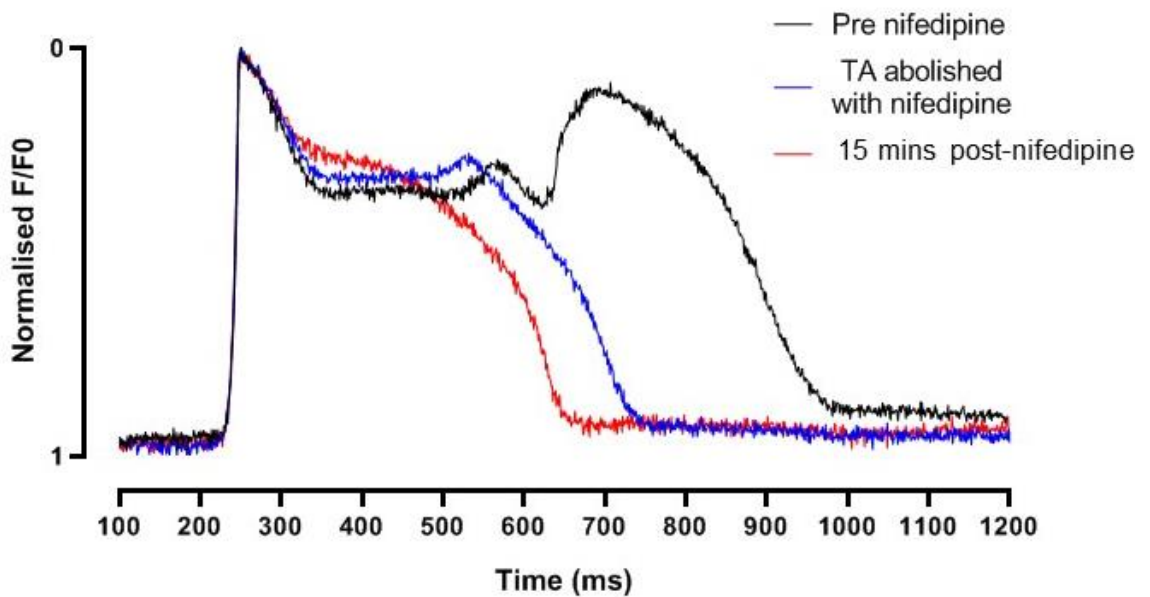


**Figure 5.5.** Progressive changes in APD with nifedipine.

Superimposed  $V_m$  traces pre nifedipine (black line), at the time point of PVC abolition (blue line) at which time AP prolongation and EADs persist and 15 minutes post-nifedipine 200nM (red line) at which time APD shortening corresponds with absence of EADs.

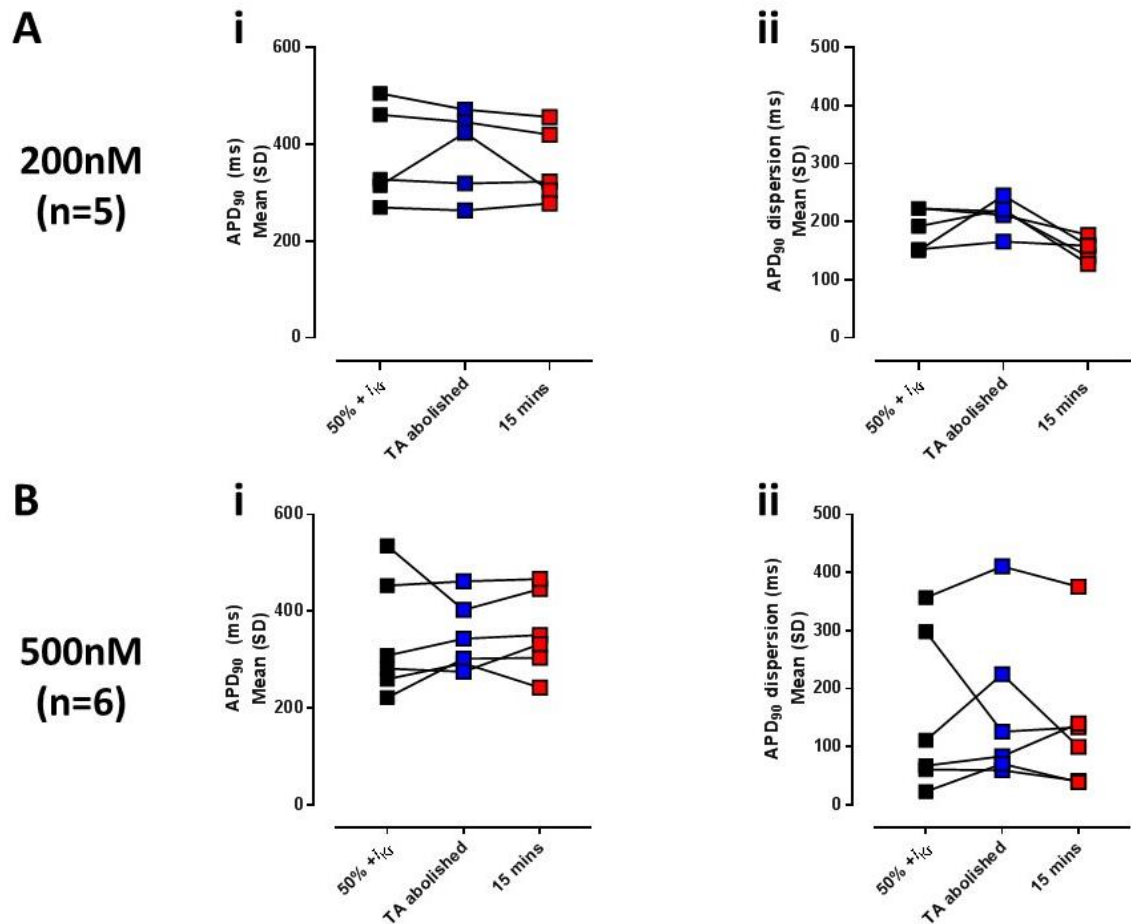


**Figure 5.6.** Effect of nifedipine on APD and APD dispersion under LQT conditions. Change in APD<sub>90</sub> and dispersion of APD<sub>90</sub> before and after nifedipine 200nM (n=5) and 500nM (n=6). Timepoints correspond to those used in Fig 5.4. Both concentrations showed no significant difference in APD<sub>90</sub> or dispersion of APD<sub>90</sub>. (A) Change in (i) APD<sub>90</sub> and (ii) dispersion of APD<sub>90</sub> for 5 hearts at nifedipine 200nM (repeated measures one-way ANOVA, p=NS). (B) Change in (i) APD<sub>90</sub> and (ii) dispersion of APD<sub>90</sub> for 6 hearts at nifedipine 500nM (repeated measures one-way ANOVA, p = NS).

		<b>50% + <math>I_{Kr}</math></b>	<b>TA abolished</b>	<b>15 minutes</b>	<b>P Value 15 mins vs. pre- drug</b>
<b>Mean APD<sub>90</sub> (ms) SD</b>	<b>Nifedipine 200nM (n=5)</b>	375 ± 101	386 ± 89	356 ± 77	0.4015
	<b>Nifedipine 500nM (n=6)</b>	343 ± 123	346 ± 72	357 ± 85	0.9423

**Table 5.3.** APD<sub>90</sub> after abolition of arrhythmia by nifedipine 200nM (n=5) and 500nM (n = 6).

		<b>50% + <math>I_{Kr}</math></b>	<b>TA abolished</b>	<b>15 minutes</b>	<b>P Value 15 mins vs. pre- drug</b>
<b>Dispersion APD<sub>90</sub> (ms) SD</b>	<b>Nifedipine 200nM (n=5)</b>	188 ± 36	212 ± 29	152 ± 19	0.204
	<b>Nifedipine 500nM (n=6)</b>	153 ± 139	163 ± 135	138 ± 124	0.7564

**Table 5.4.** APD<sub>90</sub> dispersion after abolition of arrhythmia by nifedipine 200nM (n=5) and 500nM (n = 6).

### ***Confirmatory Protocols***

Nifedipine washout resulted in a return of PVCs in all hearts tested (n=3/3). In a subset of 5/11 experiments, E-4031 concentration was increased from 0.5 $\mu$ M to 2 $\mu$ M. The results of APD<sub>90</sub> and dispersion of APD<sub>90</sub> from combined 200nM (n=2) and 500nM hearts (n=3) are shown in Figure 5.7. E-4031 2 $\mu$ M caused no significant change in APD<sub>90</sub> or dispersion of APD<sub>90</sub> and return of PVCs was not seen in any heart.



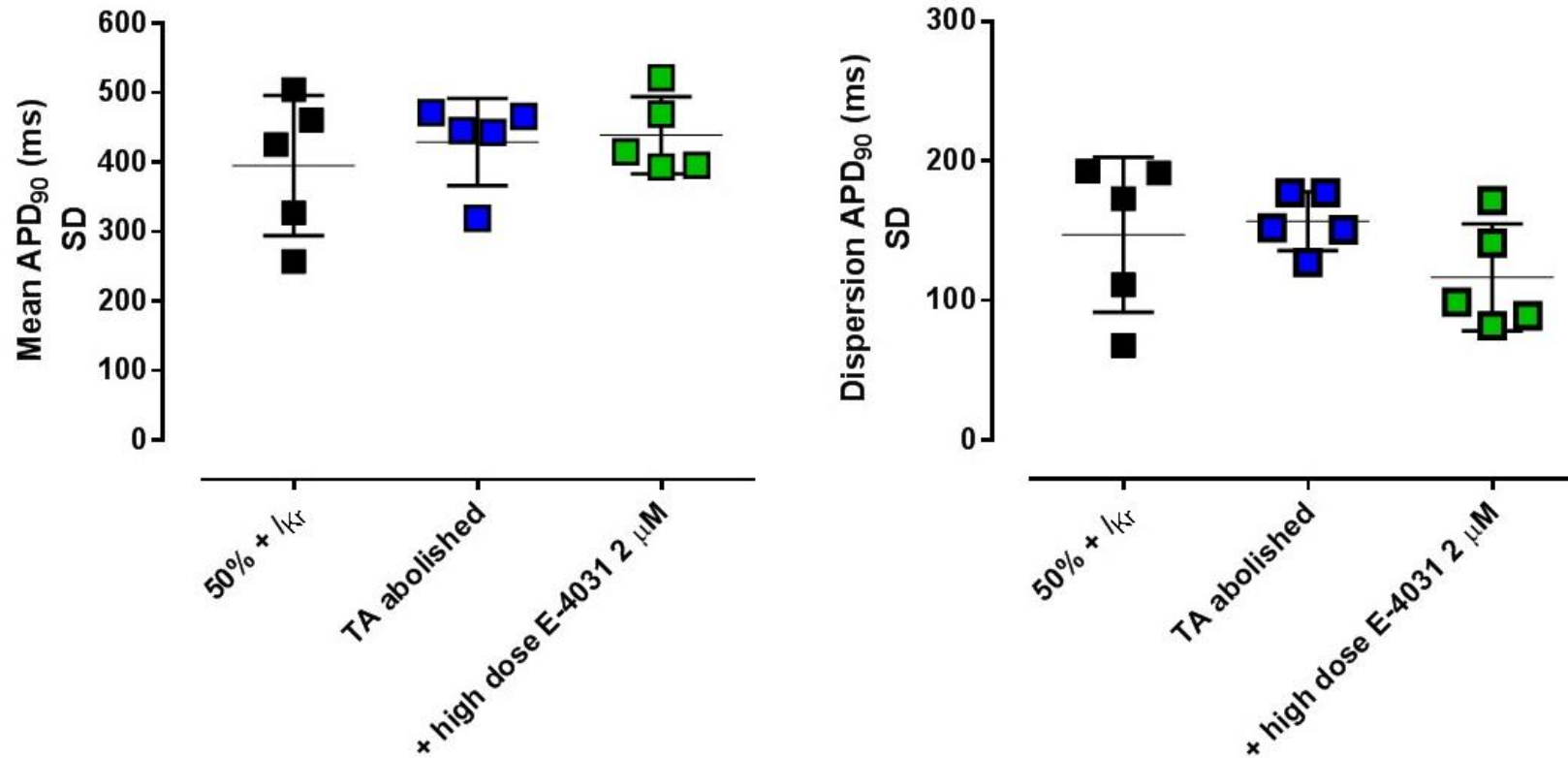


**Figure 5.7.** Effect of high-dose E-4031 on APD<sub>90</sub> and APD<sub>90</sub> dispersion in the presence of nifedipine.

Mean APD<sub>90</sub> and APD<sub>90</sub> dispersion (IP<sub>95</sub>) for (n = 5) was compared between LQT conditions (black), once TA was abolished (blue) and 10 minutes post E-4031 2 μM (green). Timepoints correspond with those in Fig 5.4. There were 2/5 hearts perfused with nifedipine 200nM and 3/5 nifedipine 500nM. There was no significant change in APD<sub>90</sub> or dispersion of APD<sub>90</sub> (repeated measures one-way ANOVA, p = NS).

### ***Effect of Nifedipine on Calcium Transients***

In an attempt to quantify the effects of nifedipine on the  $\text{Ca}^{2+}$  current in these hearts, CaT amplitudes were analysed. Typical trends of normalised  $\text{Ca}^{2+}$   $F/F_0$  would increase over a period of approximately 60 minutes after dye loading with Rhod2, then gradually decrease and so a time control was used. Changes in  $F/F_0$  were calculated (described in Chapter 2, pp. 80) and nifedipine caused a significant reduction in  $F/F_0$  Figure 5.8A. Examples of actual amplitude changes seen are demonstrated in Figure 5.8B.

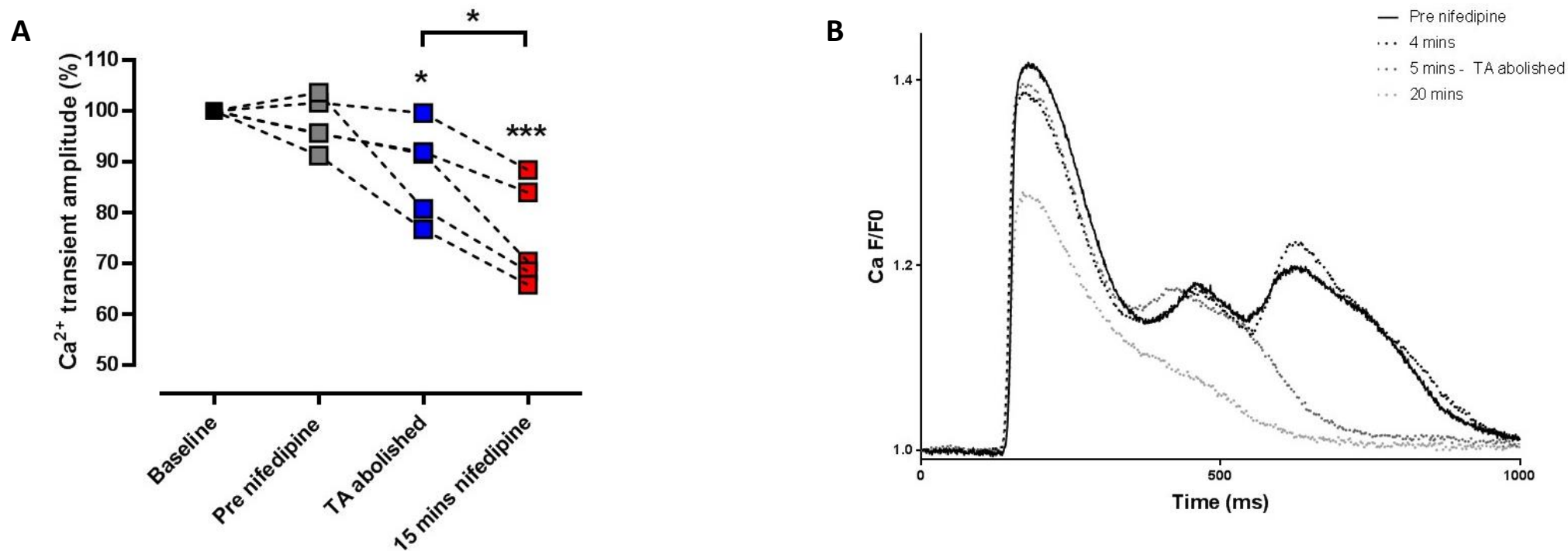


**Figure 5.8.** Effect of nifedipine on CaTs under LQT conditions.

(A) Effect of 200nM nifedipine on CaT amplitude relative to baseline (black), immediately pre-nifedipine and approximately 30 minutes from baseline (grey), abolition of PVCs approximately 30-34 minutes from baseline (0-4mins post nifedipine, blue) and 45 minutes from baseline (15 mins post nifedipine, red), n=5 (repeated measures one-way ANOVA, \*\*\*p<0.001, p<0.05 vs. baseline). Timepoints correspond with those in Figure 5.4. (B) Normalised Ca<sup>2+</sup> traces before and after nifedipine perfusion at 4, 5 and 20-minute intervals in one heart. At 4 minutes there is a drop in peak Ca<sup>2+</sup> F/F<sub>0</sub>, at 5 minutes there is reduction in Ca<sup>2+</sup> F/F<sub>0</sub> with evidence of ongoing EADs and 20 minutes there is loss of diastolic Ca<sup>2+</sup> elevation and significant reduction in F/F<sub>0</sub>.

## Discussion

The purpose of this Chapter was to test the hypothesis that PVCs in LQTS are initiated by large voltage gradients causing reactivation of  $I_{CaL}$  and so that LTCC block would abolish PVCs and ventricular arrhythmias. Low dose nifedipine was chosen, and a concentration-response was performed, as it was thought high dose would dramatically shorten the APD and remove the LQT substrate altogether. In this study there was total abolition of PVCs and arrhythmias in all hearts perfused with 200 or 500nM and this occurred 0 – 4 minutes after perfusion was commenced. The occurrence of PVCs by condition across all hearts was treated as a dichotomous variable. This was because PVCs and associated arrhythmias occurred variably over time even under fixed conditions in a given heart and so it was not meaningful to compare arrhythmia burden between different time periods. Recognising the additional information provided by a comparison of arrhythmia burden, we added time-limited protocols in a subset of hearts and arrhythmia burden for these experiments is presented. PVC abolition is similar to previous data (Chang PC *et al*, 2015) which also showed nifedipine inhibited TdP inducibility under LQT states, however our work differs significantly from their model. Experimentally Chang *et al* used lower  $Mg^{2+}$  concentrations, faster PCLs (1000ms) and induced TdP by pacing, they also used much higher concentrations of nifedipine (2 $\mu$ M), which caused total abolition of the LQT substrate and their major findings were focussed on EAD genesis by inhibition of SR  $Ca^{2+}$  cycling with TG and ryanodine. The combined effects of E-4031, TG, ryanodine and nifedipine, creates much more complex pharmacological conditions compared to our model.

Calculation of  $APD_{90}$  and  $APD_{90}$  dispersion before, immediately after TA was abolished and 15 minutes after nifedipine perfusion showed so no significant change at both 200 and 500nM. Furthermore, within this early onset window where the LQT substrate was preserved whilst PVCs were abolished, EADs were ongoing. In an attempt to further prolong the APD, addition of high dose E-4031 (2 $\mu$ M) was performed in a subset of hearts. This did not cause PVCs and indeed, the LQT substrate was not significantly changed with increased  $I_{Kr}$  blockade. Washout of nifedipine did prove effective, as PVCs were restored (albeit in a small number of hearts) to evidence the effect of nifedipine on  $Ca^{2+}$  the F/F<sub>0</sub> before, immediately once TA was abolished and 15 minutes post-nifedipine perfusion were

examined. This showed a significant reduction in F/F0 post-nifedipine perfusion and confirmed the changes seen were genuine.

This abolition of PVCs in the continued presence of the LQT substrate has not previously been shown and has important implications for our understanding of arrhythmia mechanisms, and also potentially for novel therapeutic approaches. The current theory of LQT associated arrhythmias, is based on the fact that EADs are directly responsible for triggering new APs in isolated cells. EADs are therefore thought to cause PVCs in intact hearts and to be responsible for induction of TdP in patients with LQTS (Volders PG *et al*, 2000; Weiss JN *et al*, 2010). This would require synchronisation of cellular EADs to overcome the source sink mismatch and generate a new AP (Xie Y *et al*, 2010). To explore the electrotonic flow mechanism identified in this study, would require manipulation of the APD gradients in a more comprehensive manner. To achieve this experimentally, without abolishing the LQT substrate or creating non-physiological conditions is challenging. A collaboration project with computer modellers was designed to simulate the conditions found in our model and is detailed in the Appendix. This confirmed EADs were not required for PVC induction, as they were seen to occur in the absence of any prior EAD and PVCs were induced from electrotonic flow between long and short APD regions. Examination of currents mediating PVC induction found this occurred from  $I_{CaL}$  reactivation. A modest (10%) reduction of  $I_{CaL}$  conductance in the model removed PVCs qualitatively recapitulating the effects seen in our experimental model.

## Limitations

The limitations of these experiments mainly included the doses of nifedipine doses used, the use of Rhod2 as a  $Ca^{2+}$  sensitive dye, the effect of mechanical uncoupling and confirmatory protocols with high dose E-4031. Attempts at using an array of nifedipine dosages to quantify a more specific concentration-response of nifedipine's ability to abolish PVCs, proved difficult owing to the time restrictions within experiments to achieve valuable data without ischaemic compromise, dye bleaching or the preparation perishing with time. This meant only a select range of nifedipine concentrations were attempted. Optical mapping

with Rhod2 has the potential limitation that Rhod2 may saturate at peak intracellular  $\text{Ca}^{2+}$  and so Rhod2 signal, under some conditions may not accurately represent CaT amplitude. Although we would not expect to see this effect under our experimental conditions, the data were visually inspected for changes in CaT shape indicating possible saturation and these were not seen. Furthermore, owing to the time restrictions, comparative data looking at  $\text{Ca}^{2+}$  amplitude before and after washout was not included in this study. An increased number of experiments with washout data would have provided more information.

The confirmatory protocol using high dose E-4031  $2\mu\text{M}$  ( $n=5$ ) did not have the desired effect, *i.e.* further  $\text{APD}_{90}$  prolongation to establish whether arrhythmias would recommence. However, the lack of control data made these results difficult to interpret and without this data, it is difficult to draw conclusions. Control experiments comparing E-4031  $0.5\mu\text{M}$  vs.  $2\mu\text{M}$  in the absence of nifedipine, would have clarified if  $2\mu\text{M}$  does actually cause further  $\text{APD}_{90}$  prolongation and/or more severe arrhythmias. It is possible the gradual shortening of APD with nifedipine directly countered the effect of high dose E-4031, and the net effect was no change. Without a control, it makes either of these two outcomes difficult to decipher.

## Conclusion

Nifedipine caused total abolition of PVCs during LQT states but crucially the LQT substrate was preserved, long AP islands,  $V_m$  gradients and EADs were still occurring. This confirms that the abolition of PVCs by nifedipine was not an indirect effect through the modification of the LQT substrate. This suggests a crucial role for  $I_{\text{CaL}}$  in initiating electrotonically-triggered PVCs. This reinforces the theory that voltage gradients are the determining factor in the generation of LQT-associated arrhythmias and not EADs themselves, although these contributed to the voltage gradients seen in this study. These data are suggestive that low dose LTCC blockers could potentially be a novel anti-arrhythmic strategy in LQTS.

## **Chapter 6: Discussion and Conclusions**

## ***Rationale for the Current Study***

LQTS, both inherited and acquired, carries a risk of syncope and SCD by causing a specific form of polymorphic VT, called TdP (Priori SG *et al*, 2001a). This type of arrhythmia only occurs in the context of QT prolongation and frequently degenerates into VF. TdP starts with a PVC occurring before the end of the preceding T-wave to cause the R-on-T phenomenon. Mechanistically, sustained TdP is thought to be PVC-dependent with where either the initial PVC causes re-entry or there is either repetitive TA to induce recurrent PVCs (Maruyama M *et al*, 2011; Vandersickel N *et al*, 2016). Such a fatal arrhythmia can be devastating as typically it presents as sudden cardiac death in the young (Schwartz PJ *et al*, 2009). Therapeutic approaches for managing this condition are suboptimal and currently there is no specific anti-arrhythmic therapy available. Current treatment options include beta-blockade, which reduces the adrenergic drive that acts as a trigger in some patients or an ICD, which prevents SCD but does not prevent the development of TdP. Furthermore, dynamic environmental changes (*e.g.* electrolytes, iatrogenic drug prescribing), gender and genetic heterogeneity of LQT genes creates a management challenge with current risk stratification being suboptimal. As described in Chapter 1 (pp.26), scoring systems have been developed to try and estimate the risk of SCD (Schwartz PJ *et al*, 1993; Priori SG *et al*, 2003). However, these are limited as the relationship between TdP and QT-interval is non-linear, plus there are widespread dynamic, sex and phenotypical variations with incomplete gene penetrance. This means despite scoring systems, there still lies prognostic uncertainty among LQTS patients with no accurate form of risk stratification. The lack of understanding in the arrhythmia mechanisms is what underpins this problem. The clinical rationale for the current study was that a better understanding of the arrhythmia induction mechanisms in LQTS could lead to development of specific anti-arrhythmic approaches and / or improved risk stratification techniques. Theoretically, this new understanding of the importance of voltage gradients in the mechanism of LQTS-associated arrhythmias means that if large voltage gradients could be detected clinically this could potentially be used to identify people at greatest risk. One possibility for this is the developing ECG-imaging technology (ECG-I) which may provide a means to detect voltage gradients clinically in future (Ghanem RN *et al*, 2005).



### ***Cellular Mechanisms of AP Prolongation and EADs***

Studies into the cellular mechanisms of LQT arrhythmias using isolated cardiomyocytes have identified that APD prolongation facilitates EAD generation (Damiano BP *et al*, 1984; Roden DM, 1993; Volders PG *et al*, 2000; Weiss JN *et al*, 2010), this was discussed in Chapter 1 (pp. 50). In isolated cells, EADs are able to produce triggered APs, leading to the suggestion that EADs are responsible for causing PVCs in whole hearts, which may then induce TdP. This has resulted in targeting of APD shortening and abolition of EADs, however this has not led to an effective anti-arrhythmic therapy. Potential reasons for this are the wider cardiovascular effects of the anti-arrhythmics used (*e.g.* verapamil causes severe hypotension secondary to profound peripheral vasodilatation) leading to issues around tolerability and / or pro-arrhythmia at the doses required to shorten APD and abolish EADs (Liu Y *et al*, 2016). Also, EADs can be supported by a series of different ionic mechanisms (Volders PG *et al*, 2000; Weiss JN *et al*, 2010) and so targeting specific EAD mechanisms in the context of QT prolongation may not be effective.

### ***Extrapolating Cellular Mechanisms to the Whole Heart***

Isolated cells used to investigate cellular mechanisms do not share the same electrophysiological characteristics as whole heart preparations because they do not have the same electrotonic coupling. This means arrhythmic mechanisms between cellular and whole heart models may differ. Studies into the behaviour of cellular EADs and the link to PVCs in whole hearts have been done and shown the application of LTCC block causes EAD attenuation and prevention of TdP (Chang PC *et al*, 2015) and tissue-scale computer modelling has suggested voltage gradients and enhancement of  $I_{CaL}$  are responsible for EAD induced PVCs (Huang X *et al*, 2016). Mathematical modelling studies have also been used to estimate the magnitude of synchronisation of EADs required to overcome the source-sink and produce a PVC (Xie Y *et al*, 2010).

### ***Mechanisms of TdP in the Whole Heart***

Repolarisation gradients are thought to play a significant role in the generation of PVCs and possess pro-arrhythmic potential, discussed in Chapter 1 (pp.58). Evidence from various

experimental models including dog and guinea pig Purkinje fibres (El Sherif N *et al*, 1991; Li ZY *et al*, 1992; Carlsson L *et al*, 1993), as well as canine LV wedge (Antzelevitch C *et al*, 1996; Shimizu W *et al*, 1997; Yan GX *et al*, 1998; Shimizu W *et al*, 1998) and intact heart preparations (Kuo CS *et al*, 1985; Maruyama M *et al*, 2011) have identified dispersion of ventricular repolarisation to be pro-arrhythmic. Under LQT conditions, this heterogeneity is amplified (Antzelevitch C, 2002; Belardinelli L *et al*, 2003) with significant differences seen between apex and base prior to TdP induction (Choi BR *et al*, 2002). Dispersion of ventricular repolarisation and associated steep voltage gradients are thought to contribute towards arrhythmia in LQTS, but their exact role was unclear. The main purpose of this study was to build on this knowledge and examine the mechanism of PVC induced TdP in a whole heart model of LQT2, specifically to determine whether the proposed cellular mechanism was active in the whole heart.

## Hypotheses

This study was designed to investigate the mechanism of PVC induction and the link between EADs and TdP, in an *ex-vivo* pharmacological model of LQT2. The specific hypotheses were:

1. Pharmacological LQT2 would produce EADs, PVCs, bursts and TdP in *ex vivo* rabbit hearts.
2. Synchronisation of Ca<sup>2+</sup>-driven EADs within the intact heart would be responsible for PVC induction.
3. EADs and associated PVCs would be abolished by inhibition of SR Ca<sup>2+</sup> and blockade of  $I_{CaL}$ .

## ***Designing and Characterising a LQT2 Model***

A rabbit model of pharmacological LQT was chosen since they share important electrophysiological similarities to human hearts and make an effective surrogate with translatable conclusions for studying ventricular arrhythmias (Panfilov AV, 2006; Brunner *et al*, 2008). Once the model was established, baseline electrophysiological measurements were taken, including APD restitution data, that were reproducible over a series of experiments. This was important to assess the extent of APD prolongation from individual components of the LQT conditions (PCL, 50%  $K^+/Mg^{2+}$  and  $I_{Kr}$  blockade) as we endeavoured to start off with the least extreme model that was clinically relevant. In the first instance this involved  $I_{Kr}$  blockade with dofetilide, which did not yield any EADs or TA, likely due to the fact that normal  $K^+/Mg^{2+}$  were used and AVN ablation was not optimised and so PCLs  $> 1000ms$  were not reliably achieved. A different  $I_{Kr}$  blocker, E-4031, was trialled and additional conditions introduced. Only once all 3  $I_{Kr}$  blockade, 50%  $K^+/Mg^{2+}$  and PCL  $\geq 2000ms$  was achieved were multiple PVCs, bursts and TdP reproducibly observed. Under LQT conditions rate-dependent APD prolongation was seen. Associated increases in APD dispersion were also seen. These values are similar to those observed in similar pharmacological LQT rabbit models (Asano Y *et al*, 1997; Maruyama M *et al*, 2011; Chang PC *et al*, 2015). Although values observed across multiple pharmacological LQT models demonstrate a large variation in APD<sub>80</sub> and APD<sub>90</sub> between studies, with values ranging from 200 – 2115ms at PCLs from 500 – 3000ms.

It is prudent to comment that these experiments were under conditions of extreme bradycardia. Bradycardia and reduced  $K^+$  and  $Mg^{2+}$  are recognised pro-arrhythmic features in clinical LQTS induced arrhythmias, and so these experimental conditions do have some clinical relevance. However, not all arrhythmias in LQTS occur at slow heart rates and it is unclear if the mechanism seen here is important in LQTS patients and it may be that different clinical forms of LQT have different arrhythmia mechanisms.

Once established, 236 PVCs were optically mapped and from these, the earliest epicardial  $V_m$  activation in relation to the earliest upstroke on the PVC from the pECG was calculated. Hearts with epicardial activation  $>20ms$  pre-QRS were considered to have PVCs initiated

close to the epicardial surface and within the mapped region. Within our experimental set-up, only one side of the epicardial surface was seen, yet the pECG detected PVCs arising across the whole heart, including endocardial, transmural and epicardial layers out-with the mapping field of view. There were no differences in either experimental conditions, coupling interval or TdP induction between epicardial and non-epicardial PVCs. Of course, non-epicardial PVCs may differ as there are recognised electrophysiological differences between endocardial myocytes compared with epicardial (*e.g.* longer APD) as seen in rabbit cells (McIntosh MA *et al*, 2000) and wedge preparations (Yan GX *et al*, 2001; Myles RC *et al*, 2010). Endocardial Purkinje fibres may also be involved in triggering PVCs in LQTS and other conditions (Ideker RE *et al*, 2009). Other approaches have been taken to address this, where endocardial cryoablation was performed within a whole heart LQT model, to ensure all EADs and arrhythmia seen were initiated within a depth which was potentially within in the mapped field (Maruyama M *et al*, 2011). The limitations of this meant they studied a sheet of cells, that was effectively uncoupled, with different behaviour to that of a coupled and intact heart. For these reasons, we chose to study conditions with realistic electrotonic coupling.

## **PVC initiation is Directly Associated with Steep Gradients of Repolarisation**

All hearts under LQT conditions demonstrated islands of APD prolongation, and PVCs consistently arose from the border between long and normal APD regions. Islands of long APD have been described in other studies using both pharmacological (Maruyama M *et al*, 2011; Kim TY *et al*, 2015) and transgenic LQT models (Huang X *et al*, 2016). The PVC upstroke was not closely related to the peak of the EAD in either time or space. Only when EADs occurred on the border of a long AP island, did they contribute towards PVC initiation by increasing voltage gradients. Amplitude and  $dF/dt_{\max}$  analysis did not suggest larger amplitudes towards the centre of these long AP islands, and  $dF/dt_{\max}$  was ~5-15% of the initial upstroke. This is not consistent with regenerative current and suggestive the PVC initiation was not through direct triggering by synchronised cellular EADs. Comparison of paced beats with and without a PVC, showed phase 2 EADs occurring in both but those supporting a PVC had larger voltage gradients. Overall these findings suggest that the voltage gradients rather than the EADs themselves are responsible for triggering a PVC.

Similar behaviour has been described in other rabbit models of acquired LQTS. Maruyama *et al* used the same pharmacological LQT model in cryoablated rabbit hearts, and observed both phase 2 and phase 3 EADs within long AP islands (Maruyama M *et al*, 2011). Their qualitative observation was neither phase 2 or 3 EADs occurred near areas of steep voltage gradients. This is congruent with what we observed in our study, except for the fact there were no phase 3 EADs seen at any point. Although both phase 2 and 3 EADs have been described in LQTS, the ionic mechanisms of phase 3 EADs are less clear. Typically phase 3 have not been seen in isolated cells which raises the likelihood they are electrotonic phenomenon only seen in tissue preparations. As detailed above, the major difference in this model is that hearts were cryoablated from the endocardium leaving a 2-3 cell thick layer of epicardium. This represents a semi-uncoupled situation without the same electrotonic influences as the intact myocardium. This may explain why phase 3 EADs were observed in their experiments, as their preparation required much less source to produce an electrotonic effect in AP compared with an intact heart, whereas there was only phase 2 EADs seen in our study.

Kim *et al* (Kim JJ *et al*, 2015) also showed islands of APD prolongation were associated with EADs that contributed towards steep voltage gradients that were responsible for arrhythmia initiation. This study used dofetilide and focussed on spontaneous  $\text{Ca}^{2+}$  release as a factor for EAD induction that was thought to be SR  $\text{Ca}^{2+}$ -mediated given a ryanodine stabiliser eliminated any arrhythmias. However, their intervention using a ryanodine stabiliser caused a marked shortening of APDs and so abolition of the LQT substrate, in contrast to our study where PVCs (and so arrhythmias) were abolished whilst the LQT substrate remained intact. Němec *et al* used dofetilide in a very similar model to ours, found islands of APD prolongation with EADs in the centre with propagation of PVCs occurring at sites with the largest voltage gradients (Němec J *et al*, 2010). Choi *et al* used a pharmacological LQT rabbit model (using 50%  $\text{K}^+/\text{Mg}^{2+}$  and E-4031 0.5 $\mu\text{M}$ ), where both ventricular chambers were cryoablated and contrary to our study, resulted in APDs as long as 2300ms (Choi BR *et al*, 2002). Similarities however, were they elicited enhanced repolarisation gradients across the epicardial surface associated with phase 2 EADs that induced TdP.

Other LQT models using wide field mapping have been performed in transgenic rabbits with  $I_{Kr}$  knockout. These models aim to recapitulate conditions found in congenital LQTS, albeit not completely given the genetic heterogeneity and incomplete penetrance of LQT genes, compounded by additional factors such as environmental (*e.g.* electrolytes, iatrogenic drug prescribing) and gender difference. Huang *et al* used transgenic LQT2 rabbit hearts and found cellular EADs were not required to induce PVCs but were potentiated when they occurred on the border or near regions with large voltage gradients (Huang X *et al*, 2016). They also highlighted the importance of  $I_{CaL}$  and its involvement in PVC induction, as any arrhythmias seen were always initiated with isoproterenol, which causes a two-fold increase in  $I_{CaL}$ . They corroborated their experimental data with computer simulations using 1D and 2D LQT2 rabbit tissue models. In these, they found smaller voltage gradients could still induce PVCs if  $I_{CaL}$  was strong enough to reactivate the regenerative current. However, the effects of  $I_{CaL}$  block were not tested experimentally in their simulations.

Overall, our data and that in the literature, suggest PVC initiation is directly associated with steep voltage gradients seen under LQT states. The involvement of EADs is not their ability to induce PVCs, instead it is their ability to cause a local increase in voltage gradients. This induces a PVC through the electrotonic flow from an area of depolarisation into directly neighbouring, and repolarised, cells. This electrotonic triggering was first suggested by Brugada (Brugada P *et al*, 1985) and Maruyama (Maruyama M *et al*, 2011) demonstrated experimental evidence that PVCs arise through this same mechanism, albeit in cryoablated ventricles with altered electrotonic influences. Our data strongly suggests this mechanism is active in the intact heart under LQT2 conditions and suggests that it can be antagonised using low levels of  $I_{CaL}$  block.

Theoretically, reducing voltage gradients would be a way of dealing with the proposed mechanism of PVC induction, however reducing voltage gradients in tissue is difficult. The gradients are a dynamic phenomenon and without understanding the basis for their formation, it is challenging to propose ways to prevent them. Manipulation of coupling may be a general approach to reducing voltage gradients, but this would be highly likely to be pro-arrhythmic in other ways. Conceptually the main approach is to stop either TdP

initiation or degeneration by either targeting long APD islands, the voltage gradients or  $I_{CaL}$ . Our approach was to target  $I_{CaL}$  as the only experimentally viable approach.

## **PVCs and TdP are Not Abolished by Thapsigargin**

To investigate the role of SR  $Ca^{2+}$  in PVC induction, thapsigargin, a non-competitive inhibitor of SERCA was administered in 5 hearts under LQT conditions. TG caused significant APD prolongation and islands of long AP were present before and after TG. Even after 30 minutes of TG  $2\mu\text{M}$ , there were still EADs observed. There was no change in PVC induction arising from the border and occurring at sites with the largest APD gradient. Nĕmec *et al* saw the opposite observation, in that TG  $200\text{nM}$ , caused total abolition of TdP. The major difference in their study was the administration of TG (albeit lower dose) before  $I_{Kr}$  blockade, which reduced SR  $Ca^{2+}$  loading, shortened the APD and directly altered the LQT substrate. Efforts to assess the effect of TG on SR function was not performed. Other studies assessing the SR  $Ca^{2+}$  effect on TdP using alternatives, such as ryanodine and flunarizine, had similar findings in that blockade of SR  $Ca^{2+}$  release prevented TdP but also reduced  $QT_c$  interval and abolished the LQT substrate (Verduyn SC *et al*, 1995).

## **PVCs and TdP are Abolished by Low-Dose Nifedipine While QT Prolongation and EADs Persist**

We observed total abolition of PVCs, bursts and TdP in all hearts treated with nifedipine with only a slight reduction in amplitude of the CaT ( $\sim 10\%$ ). Crucially, we saw abolition of any arrhythmias without any effect on the LQT substrate. At the point of abolition of arrhythmia, EADs, APD islands and voltage gradients were still present, which suggests nifedipine worked through a different mechanism than modification of the LQT substrate.

Trace analysis of  $V_m$  and intracellular  $Ca^{2+}$  during PVC induction was performed to investigate the initiation events. During EADs occurring within the long AP islands,  $Ca^{2+}$  elevation preceded  $V_m$  elevation suggesting EADs were  $Ca^{2+}$  driven. This is congruent with similar studies (Choi BR *et al*, 2002; Nĕmec J *et al*, 2010; Kim JJ *et al*, 2015). However,

within the earliest PVC breakout zone  $V_m$  and  $Ca^{2+}$  rose simultaneously, which suggests the depolarisation did not occur by normal EC coupling. We suggest that large voltage gradients are responsible for electrotonic current flow which reactivates  $I_{CaL}$  and this current supports the upstroke of the PVC at the relatively depolarised initiation site.

Carlsson *et al* investigated the role of LTCC and the incidence of TdP in a pharmacological LQT model in whole rabbit hearts (Carlsson L *et al*, 1996). In this study EADs were not measured, instead they monitored PVCs and the induction of TdP on the ECG. Pre-treatment with low and high dose LTCC blockade (with nisoldipine) caused a reduction in almokalant-induced TdP in the continued presence of QT prolongation. They conclude LTCC was crucial for TdP induction in LQT but provided no interpretation. Our data provides a mechanistic explanation for how LTCC blockade was able to prevent TdP induction, whilst the LQT substrate was maintained.

## **L-Type Calcium Channel Blockers in LQTS**

The mechanism identified from our study would potentially provide justification for studying the effects of LTCC blockers at low doses in LQTS. These drugs are clinically established, safe, effective and currently prescribed for other cardiac pathologies. In theory, if the mechanism suggested here translated to human LQTS, the use of low dose LTCC blockers would reduce the incidence of life-threatening arrhythmias in patients with either acquired or congenital LQTS. Clinical case reports of the use of the LTCC blocker, verapamil, in patients with LQTS have been published in patients with LQTS. These include: effective treatment of an anticholinergic overdose-induced arrhythmia causing recurrent TdP, which was successfully cardioverted to sinus rhythm with verapamil (Liao WB *et al*, 1996). The  $QT_c$  interval was prolonged (0.48 – 0.6 seconds) before and after verapamil bolus. Congenital LQTS patients experiencing recurrent ICD shocks, were given additional verapamil on top of their beta-blockade, immediately reduced ICD therapies and arrhythmic burden (Kawade M *et al*, 1995; Jacobs A *et al*, 2006; Liu Y *et al*, 2016). Highly effective low dose LTCC was also seen in one of the highlighted case reports (Liu Y *et al*, 2016). Similarly, small case series have reported patients with LQTS had total elimination



of ventricular ectopy and VT with low dose verapamil (5-10mg, normal dosing for adults is 40-120mg, three times daily), in a small study of 6 patients who remained pro-arrhythmic despite beta-blockade (Jackman WM *et al*, 1990); epinephrine-induced PVCs and EADs were abolished when treated in combination with beta-blockade (propranolol) and verapamil (Shimizu W *et al*, 1994) and one study involving patients predisposed to TdP from AV block had complete suppression of TdP and shortening of the QT interval when treated with verapamil (Cosío FG *et al*, 1991).

From these studies, LTCC blockade was used in combination with beta-blockers using doses aimed at shortening the QT interval to cause total abolition of the LQT substrate. At these higher doses, there is a risk of causing adverse cardiovascular effects (*i.e.* hypotension or AV block) or overcorrection of the QT interval could potentially lead to pro-arrhythmia. What our study suggests, is LTCC blockade would be highly effective at preventing the incidence of arrhythmias even when delivered at a low dose without any major effect on the LQT substrate. Clinical doses of nifedipine that would be required to achieve this anti-arrhythmic effect is unclear.

In our study, abolition of PVCs occurred early during nifedipine perfusion whilst using relatively low levels of LTCC block. To quantify this in more detail, we created a concentration-response curve comparing doses achieving PVC abolition with published data of known  $I_{CaL}$  block with nifedipine (Shen JB *et al*, 2000), Figure 6.1. Complete abolition of PVCs occurred at a dose below the  $IC_{50}$  for LTCC block in cardiomyocytes. Comparison of our data, suggests 200nM of nifedipine used in our study caused ~30%  $I_{CaL}$  block. Analysis of the  $Ca^{2+}$  amplitude saw approximately 20% reduction post-nifedipine. This is similar to what the published data would suggest (Shen JB *et al*, 2000), although this assumes the LTCC block in a cell is similar to the reduction seen in  $Ca^{2+}$  amplitude in an intact heart. When considering published work, our data and what was seen in computer modelling (see Appendix), the range of  $I_{CaL}$  block is between 10-30%. This suggests we are dealing with a phenomenon that can be abolished by a relatively small proportion of  $Ca^{2+}$  current block. This mechanism could potentially be translatable to mitigating risk in acquired LQTS. Multiple drugs can cause QT prolongation and indeed, much work is done prior to the

introduction of novel therapies to establish whether they affect hERG channels (Redfern WS *et al*, 2003; Thomas D *et al*, 2006). Studies have shown drugs with multi-channel effects prolong QT but without causing TdP by causing a “balanced” ion channel effect (Kodama I *et al*, 1997; Mirams GR *et al*, 2011). The mechanism observed in our study raises the possibility that this observation is due to coexistence of hERG block with low dose LTCC block in these drugs. The combination could deliver the required drug effect safely, without arrhythmic potential, despite prolongation of the QT<sub>c</sub>. However, comparing the concentration of LTCC block used experimentally compared to that achieved through standard clinical dosing is challenging. Plasma concentration measurements after a fixed dose in healthy subjects are very variable (Traube, M *et al*, 1985; Zodan Marin T *et al*, 2007).

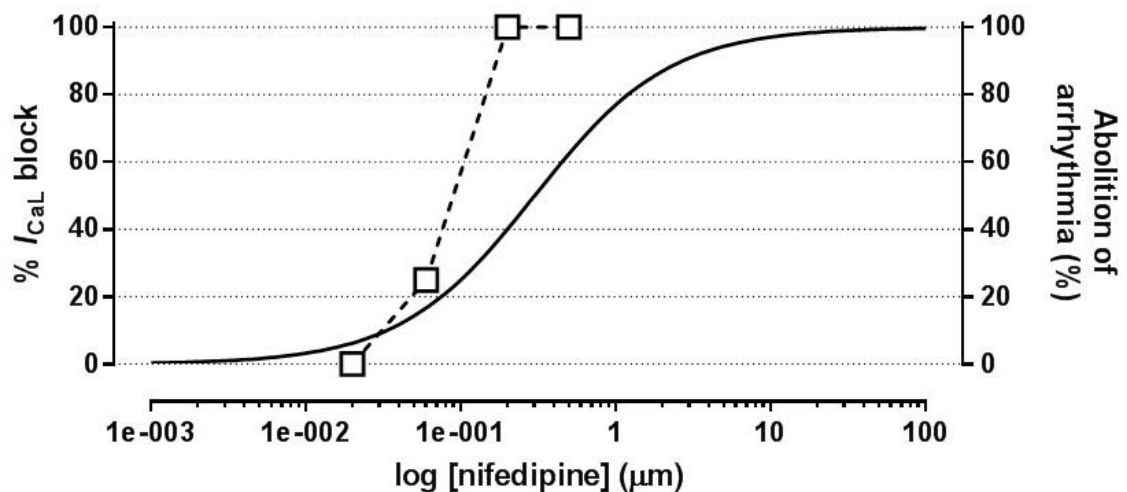


**Figure 6.1.** Dose-response curves for  $I_{CaL}$  block with nifedipine.

Data reproduced from published data on guinea pig cardiomyocytes at -80mV (Shen JB *et al*, 2000) with abolition of TA in experiments in this dataset overlaid (open squares).

## Future Directions

Two main future directions are suggested by this work: first is to consolidate the evidence for the mechanisms suggested by these experiments in order to establish whether steep voltage gradients can trigger PVCs in the absence of EADs. Of course, our data does not provide direct evidence that electrotonic flow is responsible but it is strongly implied by the experimental data. Definitive proof would require a specific intervention that would remove both voltage gradients and electrotonic flow and at present there is no experimental means to do so. Computational modelling could be used to manipulate voltage gradients and the occurrence of EADs independently, which is not possible experimentally. In addition, modelling would allow isolation of the currents responsible for PVC initiation which again is not possible experimentally. These simulations have been performed in collaboration with Dr Martin Bishop (Kings College London) and this work is detailed in the Appendix.

The second is to pursue the potential clinical applicability of these findings. There is a major concern over the potent vascular effects that might be associated with nifedipine use, even at the doses described in our study. Another potential option is to leverage the voltage dependence of other LTCC blockers. The modulated receptor hypothesis states LTCC blockers are modulated by channel state or voltage (Hondeghe LM *et al*, 1984). This state-dependence means that the proportion of channel block differs according to the voltage range or frequency. Nifedipine has little voltage-dependence, whereas diltiazem exhibits block which is both voltage- and frequency-dependent. Voltage-dependent LTCC block would mean relatively greater degrees of LTCC block at more depolarised voltages, potentially providing a route for targeting  $I_{CaL}$  block to the long AP islands and minimising any adverse effects from LTCC block elsewhere in the heart. This suggests diltiazem may be a more effective and potent anti-arrhythmic therapy. Further development of this model would involve *in vivo* experimentation, instead using congenital model (so transgenic LQTS2 rabbits), by theoretically using low dose LTCC blockade (*e.g.* with diltiazem or nifedipine) and assess the effectiveness their anti-arrhythmic potential. Indeed, this study was focussed on arrhythmia mechanisms seen in LQT2, the extent to which this applies to LQT1 and LQT3 is not clear. Ongoing work planned using transgenic animals, in particular LQT1, would address exactly this issue.

Lastly, application of this mechanism into patients with LQTS2, would hypothetically involve a clinical trial of low dose nifedipine in patients with known LQTS2 and ICD *in-situ*. Usage of low dose LTCC blockade should in theory avoid any of the cardiovascular side effects associated and previously seen when treating LQT patients with Ca<sup>2+</sup> channel blockers. Involving patients with an ICD *in-situ* would mean accurate assessment of anti-arrhythmic effects as any arrhythmic burden before and after administration of LTCC could be closely monitored. However, accessing patients meeting this criteria would have to involve large scale databases, such as a European wide study, as numbers of LQTS2 patients with ICDs *in-situ* are limited.

## Conclusions

The main hypothesis of this study was that in LQTS synchronisation of EADs within the intact heart would be responsible for PVCs which would subsequently induce TdP. The experimental data demonstrated two key findings. Firstly, our experimental data suggest the formation of PVCs in the intact heart is not directly mediated by synchronisation of cellular EADs but electrotonically triggered from steep voltage gradients that occur on the border of long AP islands. We observed EADs occurring within long AP islands that did not directly form part of the depolarisation that triggered a PVC, instead they increased local voltage gradients that were closely associated with PVC induction. This crucial distinction implies PVC induction and therefore arrhythmias in LQTS, are tissue-level phenomena which cannot be elucidated from cellular behaviour alone. Secondly, our data suggests a crucial role for  $I_{CaL}$  in generating these electrotonically-triggered PVCs, which were abolished by low doses of LTCC blockade.

This novel mechanism could potentially provide better insights in to the mechanism behind ventricular arrhythmias in LQT patients, and ultimately lead to the development of more effective anti-arrhythmic therapy to reduce the incidence of life-threatening arrhythmias and prevent SCD in the young. This could potentially involve utilising drugs that are already safe, effective and routinely available. Translational studies to explore the potential implications of these data are planned.

## Appendix

## **Introduction**

The dissociation seen between EADs and the PVC upstroke in space, time and voltage range, along with the different  $V_m$ - $Ca^{2+}$  dynamics seen within this dataset, argues against the concept that EADs are directly involved in triggering the inward regenerative current which drives the PVC upstroke. Instead, the steep voltage gradients seen at the border of the APD islands are key. Independent manipulation of voltage gradients is not possible experimentally. Computer modelling was used to overcome this issue and test our hypothesis. A collaboration with computer modellers was developed to model the paradigm with the ability to selectively modulate APD gradients.

## ***Aims***

The aims of this collaborative study were to:

1. Establish whether steep voltage gradients can result in electronic triggering of PVCs in the absence of EADs.
2. Ascertain which current is responsible for electronic capture.

## Methods

Simulations were performed by Dr Martin Bishop, King's College, London. The following methodological description was supplied by Dr Bishop:

A monodomain representation of cardiac electrophysiology was used to simulate a 2-D sheet of cardiac tissue. Cellular ionic dynamics were represented by the general mammalian LuoRudyII cell model (Luo CH *et al*, 1994). To replicate the experimentally-witnessed islands of prolonged APD, the left-half of the tissue was assigned a prolonged APD by modulating the conductance's of the repolarising  $K^+$  channels ( $I_{Kr}$ ,  $I_{Ks}$ ), Figure A. To control the specific repolarisation gradient formed between long APD region (left) and the normal APD region (right), tissue conductivity was globally modulated (Fig.A (B)). Different combinations of prolonged APD and modulated tissue conductivity were used to throughout. The model was paced initially 100 times to reach steady-state. A single S1 beat was then simulated by pacing the entire left-hand edge of the tissue to initiate a planar wave propagating left-to-right. In a sub-set of simulations, an additional S2 was prescribed to represent a pEAD delivered at a controlled specific timing and location, facilitating a direct comparison between different subsequent simulations.  $V_m$ ,  $[Ca]_i$ , fast sodium current ( $I_{Na}$ ) and the L-type calcium current ( $I_{CaL}$ ) were analysed from a series of points located across the center-line separating the long- and normal-APD regions.

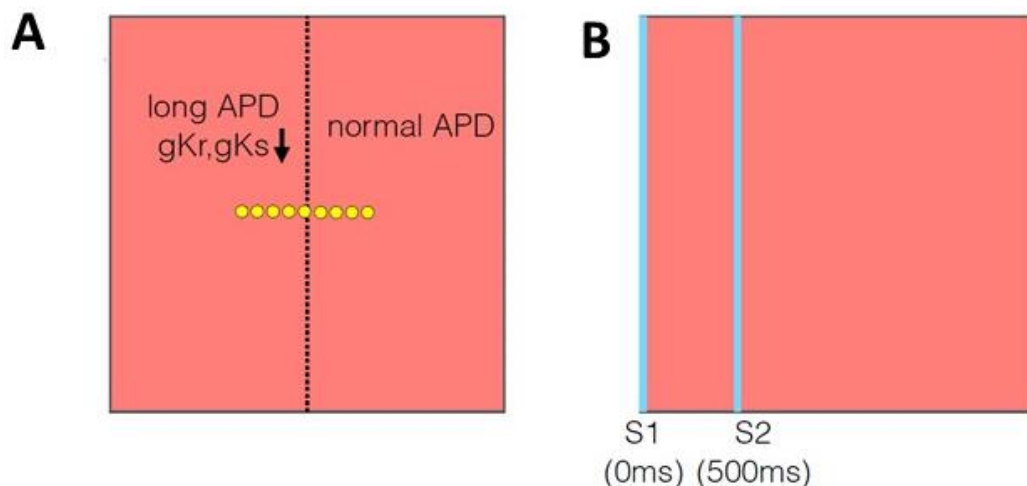


**Figure A.** Schematic representations of model setup.

(A) Schematic showing long and normal APD regions. The recording sites used to analyse ionic currents and membrane potential across the border are indicated by the yellow dots. (B) A single S1 beat was simulated by pacing (blue line) to initiate a planar wave propagating left-to-right. In some of the simulations, an EAD was modelled by an additional stimulus (S2).

## Modelling Results

### ***(i) EADs are Not Required for PVC Capture***

Simulations with 10 and 20% of normal maximal conductance of  $I_{Kr}$  and  $I_{Ks}$  are shown in Figure B. In the case of 10%  $I_{Kr}$  and  $I_{Ks}$  (Figure Bi), high repolarisation gradients developed 400ms after the pacing stimulus, and at 705ms there was spontaneous capture at the border between the long and normal AP regions, which propagated into the normal AP region. This simulated PVC occurred in the absence of any prior EAD and occurred solely through the electrotonic interaction across the high repolarisation gradients. In the case of 20%  $I_{Kr}$  and  $I_{Ks}$  conductance (Figure Bii), the gradients were lower and no PVC capture was seen.  $V_m$ ,  $Ca^{2+}_i$ ,  $I_{CaL}$  and  $I_{Na}$  traces from sites across the border between the long and short AP regions are shown in Figure C(i-iv). A normal AP is seen in the 1mm site, associated with a normal CaT (black traces), but the earliest depolarisation is seen in the -1mm site (brown trace) with no associated CaT. The  $V_m$  trace here is characterised by a slow upstroke arising from a relatively depolarised potential ( $\sim -50mV$ ). There is no  $I_{Na}$  active during this depolarisation, which is generated by  $I_{CaL}$ .



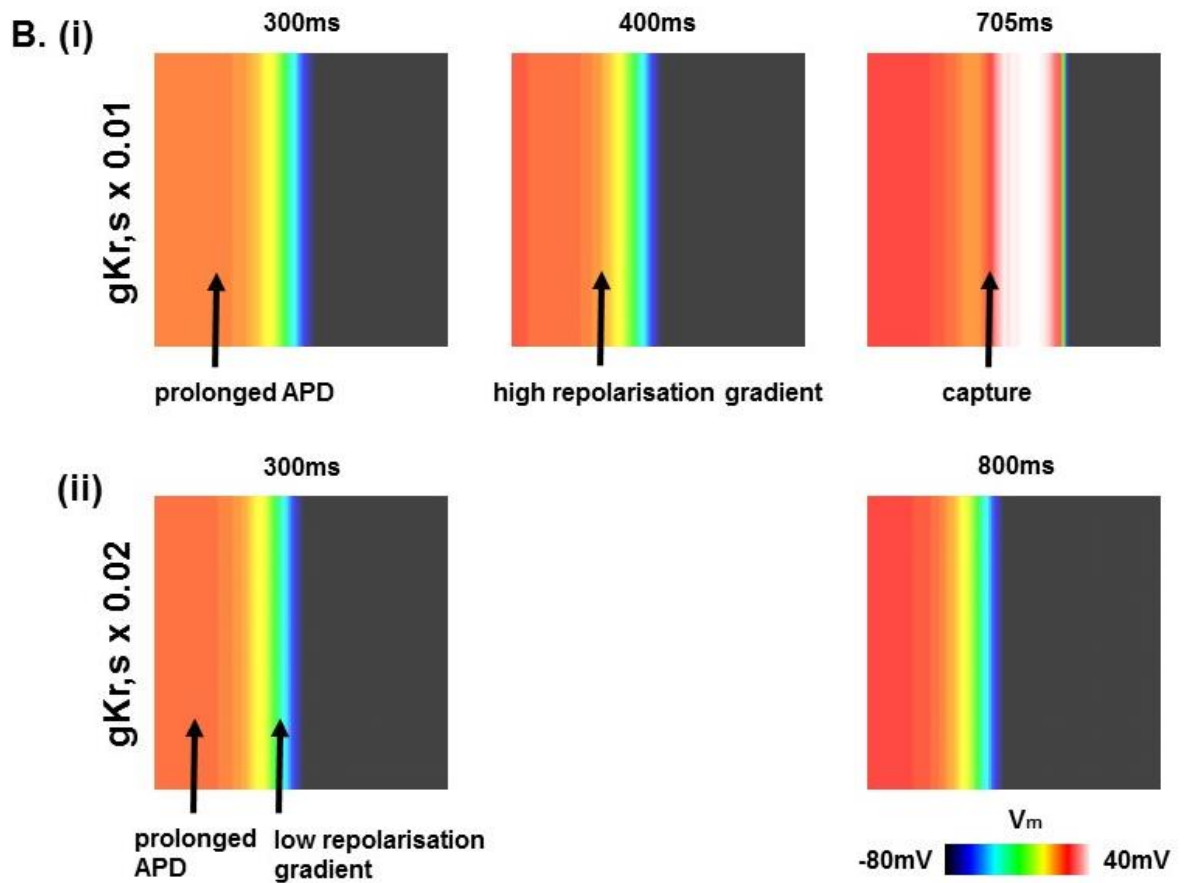


**Figure B.** Computer modelling showing spontaneous capture of tissue from a region of prolonged APD driven by high repolarisation gradient.

Colour maps of spatial  $V_m$  distribution at 300, 400 and 705ms following a paced beat with reduction in  $I_{Kr}$  and  $I_{Ks}$  on the left-hand side of the square to (i) 10% and (ii) 20% of normal values. In the former case, PVC capture occurred at 705ms, driven by a high gradient of repolarisation. The case where repolarisation gradient is lower (ii), no spontaneous capture was seen.

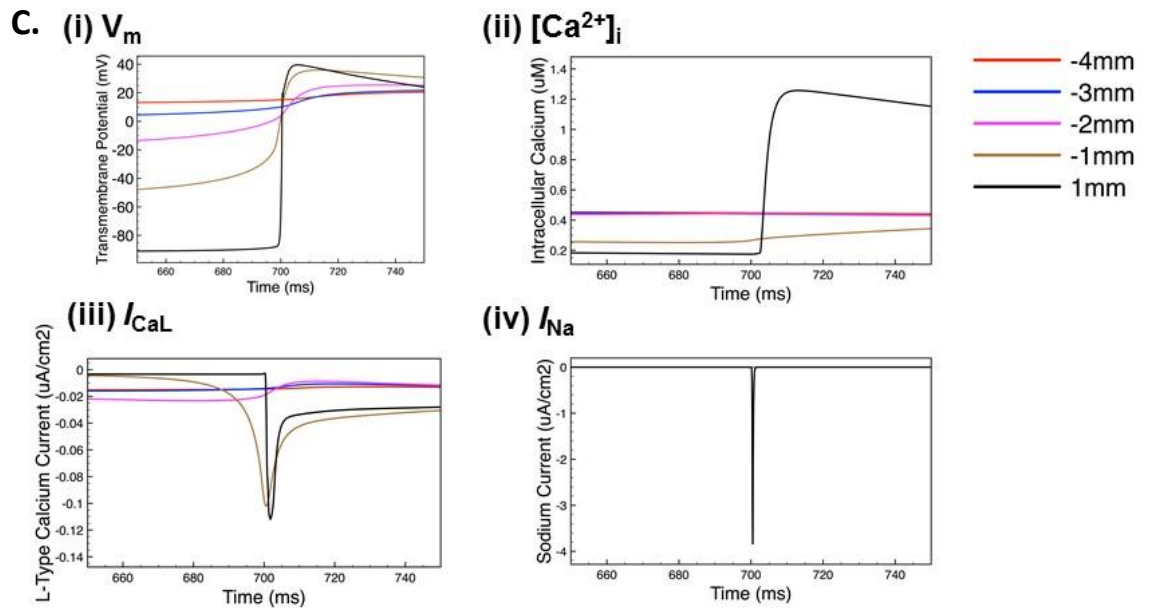


**Figure C.**  $V_m$ ,  $Ca^{2+}_i$ ,  $I_{CaL}$  and  $I_{Na}$  traces from sites across the border between the long and short AP regions.

Graphs to show changes in  $V_m$ ,  $Ca^{2+}_i$ ,  $I_{CaL}$  and  $I_{Na}$  during the spontaneous capture sampled from sites across the border between regions of long and short APD (-4mm to 1mm, L-R), following a paced beat with reduction in  $I_{Kr}$  and  $I_{Ks}$  at 10% - shown in Figure B(i).

***(ii)  $I_{CaL}$  is Required for Mediating PVC Capture***

A pseudo-EAD (pEAD) was modelled by adding a low-amplitude S2 at 500ms, Figure D(i) and corresponding  $V_m$ ,  $Ca^{2+}$ ,  $I_{CaL}$  and  $I_{Na}$  traces, Figure E. This elevated potential was transmitted through the long AP region and caused PVC capture at the border at 530ms. The traces from the simulation suggest that the same mechanism as seen in the absence of the pEAD, except that the capture occurs closer to the long AP region in the simulation which included a pEAD.

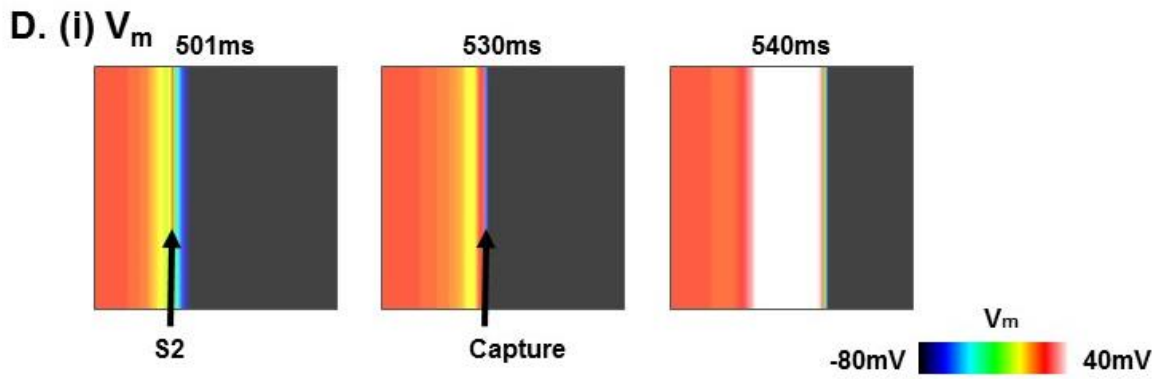


**Figure D.** Effect of pEAD on voltage gradient and PVC capture. Colour maps of spatial  $V_m$  distribution at 501, 530 and 540ms following a paced beat with a pEAD at 530ms and subsequent PVC capture (white region) at 540ms.

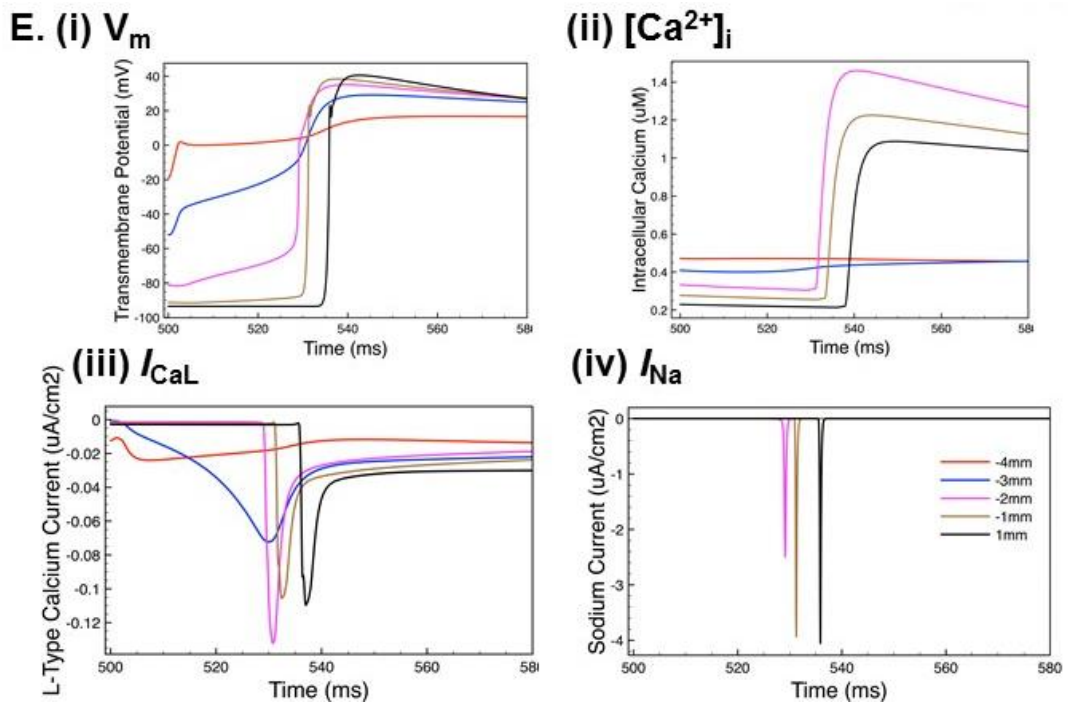


**Figure E.**  $V_m$ ,  $\text{Ca}^{2+}$ ,  $I_{\text{CaL}}$  and  $I_{\text{Na}}$  traces from different sites across the boundary between long and short APD regions from the example in Figure D.

### (iii) PVC Capture is Abolished by Low Levels of $I_{CaL}$ Block

Within the computer modelling framework it was possible to modulate  $I_{CaL}$  by reducing the maximum conductance ( $g_{CaL}$ ), Figure F. Despite reducing  $g_{CaL}$  to 95% of its normal value, the pEAD was still able to cause a successful capture of a PVC. However, reducing  $g_{CaL}$  to 90% of its normal value caused total abolition of PVC capture, Figure F(iii) and Figure F(iv).

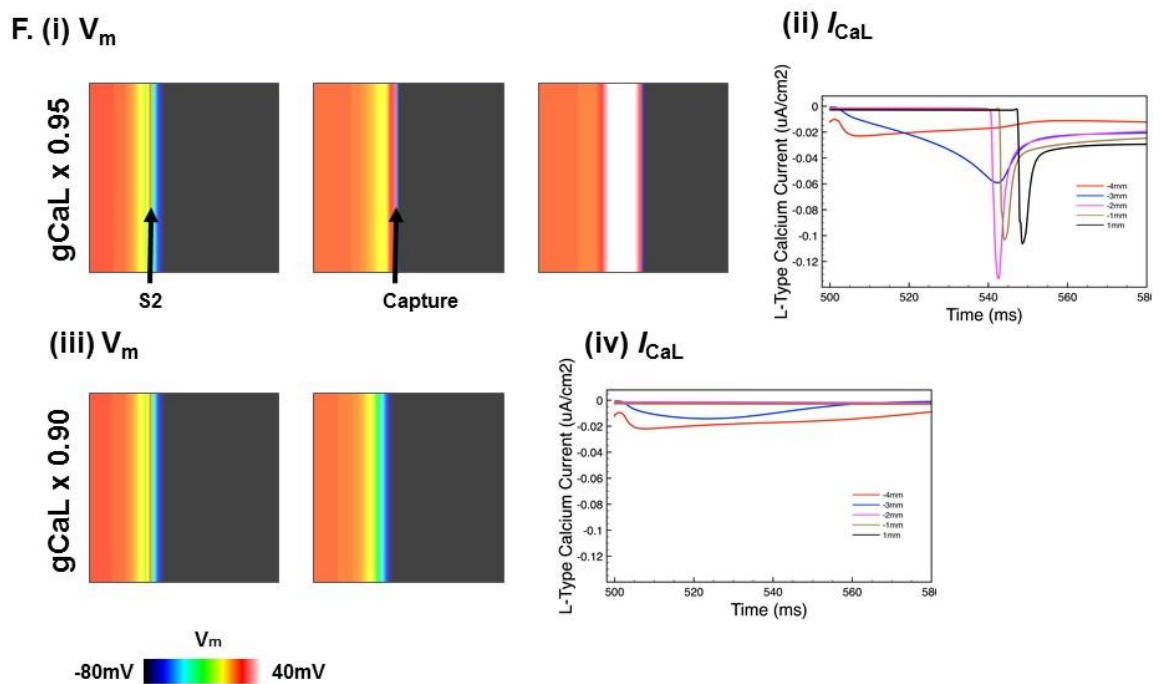


**Figure F.** Effects of  $g_{CaL}$  reduction to 95% and 90% on PVC capture.

(i) Colour maps of spatial distribution of  $V_m$  at 501, 542, 547ms after a paced beat in a model with reduction of  $g_{CaL}$  to 95%, showing spontaneous capture supported by  $I_{CaL}$ . (ii)  $I_{CaL}$  traces over time. Corresponding effects on  $I_{CaL}$  shows the effects of pEAD at -4 and -3mm sites, with  $I_{CaL}$  activation at -2mm. (iii) Colour maps of spatial distribution of  $V_m$  at 501 and 540ms after a paced beat in a model with reduction of  $g_{CaL}$  to 90%, showing abolition of spontaneous capture. (iv)  $I_{CaL}$  traces over time with abolition of PVC capture.

## Discussion

The purpose of this modelling study was to complement the data acquired during the experimental study and to test the hypothesis created from it. In our animal model of pharmacological LQT, long AP islands and the voltage gradients surrounding them were thought to be responsible for inducing PVCs rather than EADs themselves. Indeed, EADs did occur under these conditions but rather than directly triggering PVCs their effect was to increase local voltage gradients in the event they occurred near the boundary of the long AP islands. EADs and steep voltage gradients could not be isolated experimentally and so computer modelling was sought to examine this hypothesis. The use of computer simulations showed PVC capture was possible in the absence of any prior EAD. To complement this, changes in  $V_m$ ,  $Ca^{2+}$ ,  $I_{CaL}$  and  $I_{Na}$  showed that the depolarisation at the capture site was generated by  $I_{CaL}$ .

The effects of  $I_{CaL}$  blockade on PVC capture was tested by modulating  $I_{CaL}$  conductance in the model. Qualitatively this recapitulated the effects of  $I_{CaL}$  blockade in the pharmacological LQT rabbit model seen experimentally. Reduction of  $g_{CaL}$  to 95% of normal values still allowed propagation of the EAD through the long AP region and subsequent PVC capture. When  $g_{CaL}$  was reduced further to 90%, there was complete abolition of PVC capture. Overall, the results of computer modelling collaboration was congruent with the data seen in our model and corroborated our hypothesis that steep voltage gradients are the key step in induction of PVCs in LQTS, through reactivation of  $I_{CaL}$  and that this can be abolished by low dose LTCC block.

## References

- Abildskov, J.A. and Lux, R.L., 2000. Simulated torsade de pointes—the role of conduction defects and mechanism of QRS rotation. *Journal of Electrocardiology*, 33(1), pp.55 - 64.
- Anderson, C.L., Delisle, B.P., Anson, B.D., Kilby, J.A., Will, M.L., Tester, D.J., Gong, Q., Zhou, Z., Ackerman, M.J. and January, C.T., 2006. Most LQT2 mutations reduce Kv11.1 (hERG) current by a class 2 (trafficking-deficient) mechanism. *Circulation*, 113 (3), pp. 365 – 373.
- Antzelevitch, C. and Shimizu, W., 2002. Cellular mechanisms underlying the long QT syndrome. *Current Opinion in Cardiology*, 17 (1), pp. 43 - 51.
- Antzelevitch, C., 2004b. Arrhythmogenic mechanisms of QT prolonging drugs: is QT prolongation really the problem? *Journal of Electrocardiology*, 37, pp. 15 - 24.
- Antzelevitch, C., 2004a. Cellular basis for the repolarization waves of the ECG. *Dynamic Electrocardiography*, pp.289-300.
- Antzelevitch, C., Sun, Z.Q., Zhang, Z.Q. and Yan, G.X., 1996. Cellular and ionic mechanisms underlying erythromycin-induced long QT intervals and torsade de pointes. *Journal of the American College of Cardiology*, 28 (7), pp. 1836 - 1848.
- Antzelevitch, C.H. and Moe, G.K., 1981. Electrotonically mediated delayed conduction and re-entry in relation to "slow responses" in mammalian ventricular conducting tissue. *Circulation Research*, 49 (5), pp. 1129 - 1139.
- Antzelevitch, C.H., 2001. Basic mechanisms of re-entrant arrhythmias. *Current Opinion in Cardiology*, 16 (1), pp. 1 - 7.
- Asano, Y., Davidenko, J.M., Baxter, W.T., Gray, R.A. and Jalife, J. 1997. Optical mapping of drug-induced polymorphic arrhythmias and torsade de pointes in the isolated rabbit heart. *Journal of the American College of Cardiology*, 29 (4), pp. 831 - 842.
- Bass, B.G., 1975. Restitution of the action potential in cat papillary muscle. *American Journal of Physiology-Legacy Content*, 228(6), pp.1717-1724.

- Bazett, H.C. 1920. An analysis of the time-relations of electrocardiograms. *Heart*, 7, pp. 353–370.
- Belardinelli, L., Antzelevitch, C. and Vos, M.A. 2003. Assessing predictors of drug-induced torsade de pointes. *Trends Pharmacological Sciences*, 24, pp. 619 - 625.
- Bennett, P.B., Yazawa, K., Makita, N. and George, A.L. Jr. 1995. Molecular mechanism for an inherited cardiac arrhythmia. *Nature*, 376 (6542), pp. 683 – 685.
- Bers, D.M. 2006. Altered cardiac myocyte Ca regulation in heart failure. *Physiology*, 21 (6), pp. 380 - 387.
- Biermann, M., Rubart, M., Moreno, A., Wu, J., Josiah-Durant, A. and Zipes, D.P. 1998. Differential effects of cytochalasin D and 2, 3 butanedione monoxime on isometric twitch force and transmembrane action potential in isolated ventricular muscle: implications for optical measurements of cardiac repolarizations. *Journal of Cardiovascular Electrophysiology*, 9 (12), pp. 1348 – 1377.
- Boersma, L., Barr, C., Knops, R., Theuns, D., Eckardt, L., Neuzil, P., Scholten, M., Hood, M., Kuschik, J., Jones, P. and Duffy, E., 2017. Implant and midterm outcomes of the subcutaneous implantable cardioverter-defibrillator registry: the EFFORTLESS study. *Journal of the American College of Cardiology*, 70(7), pp.830-841.
- Boucher, M. and Duchene-Marullaz, P. 1985. Methods for producing experimental complete atrioventricular block in dogs. *Journal of Pharmacological Methods*, 13 (2), pp. 95 - 107.
- Boutjdir, M. and El-Sherif, N. 1991. Pharmacological evaluation of early afterdepolarisations induced by sea anemone toxin (ATXII) in dog heart. *Cardiovascular Research*, 25 (10), pp. 815 - 819.
- Brack, K.E., Narang, R., Winter, J. and Ng, G.A. 2013. The mechanical uncoupler blebbistatin is associated with significant electrophysiological effects in the isolated rabbit heart. *Experimental Physiology*, 98 (5), pp. 1009 - 1027.
- Brugada, P. and Wellens, H.J. 1985. Early Afterdepolarizations: Role in Conduction Block, “Prolonged Repolarization-Dependent Reexcitation,” and Tachyarrhythmias in the Human Heart. *Pacing and Clinical Electrophysiology*, 8 (6), pp. 889 - 896.



Brunner, M., Peng, X., Liu, G.X., Ren, X.Q., Ziv, O., Choi, B.R., Mathur, R., Hajjiri, M., Odening, K.E., Steinberg, E. and Folco, E.J. 2008. Mechanisms of cardiac arrhythmias and sudden death in transgenic rabbits with long QT syndrome. *The Journal of Clinical Investigation*, 118 (6), pp. 2246 - 2259.

Burton, F.L. and Cobbe, S.M., 2001. Dispersion of ventricular repolarization and refractory period. *Cardiovascular research*, 50(1), pp.10-23.

Carlsson, L., Abrahamsson, C., Andersson, B., Duker, G. and Schiller-Linhardt, G. 1993. Proarrhythmic effects of the class III agent almokalant: importance of infusion rate, QT dispersion, and early afterdepolarisations. *Cardiovascular Research*, 27 (12), pp. 2186 - 2193.

Carlsson, L., Drews, L. and Duker, G. 1996. Rhythm anomalies related to delayed repolarization in vivo: influence of sarcolemmal Ca<sup>++</sup> entry and intracellular Ca<sup>++</sup> overload. *Journal of Pharmacology and Experimental Therapeutics*, 279 (1), pp. 231 - 239.

Carmeliet, E.E. 1961. Chloride ions and the membrane potential of Purkinje fibres. *The Journal of Physiology*, 156 (2), pp. 375 - 388.

Casimiro, M.C., Knollmann, B.C., Ebert, S.N., Vary, J.C., Greene, A.E., Franz, M.R., Grinberg, A., Huang, S.P. and Pfeifer, K. 2001. Targeted disruption of the *Kcnq1* gene produces a mouse model of Jervell and Lange-Nielsen Syndrome. *Proceedings of the National Academy of Sciences*, 98 (5), pp. 2526 - 2531.

Chang, P.C., Wo, H.T., Lee, H.L., Lin, S.F., Wen, M.S., Chu, Y., Yeh, S.J. and Chou, C.C. 2015. Role of sarcoplasmic reticulum calcium in development of secondary calcium rise and early afterdepolarizations in long QT syndrome rabbit model. *PloS one*, 10 (4).

Cheng, J., Kamiya, K., Liu, W., Tsuji, Y., Toyama, J. and Kodama, I. 1999. Heterogeneous distribution of the two components of delayed rectifier K<sup>+</sup> current: a potential mechanism of the proarrhythmic effects of methanesulfonanilide class III agents. *Cardiovascular Research*, 43 (1), pp. 135 - 147.

- Choi, B.R., Burton, F. and Salama, G. 2002. Cytosolic Ca<sup>2+</sup> triggers early afterdepolarizations and Torsade de Pointes in rabbit hearts with type 2 long QT syndrome. *The Journal of Physiology*, 543 (2), pp. 615 - 631.
- Connolly, S.J. 1999. Evidence-based analysis of amiodarone efficacy and safety. *Circulation*, 100 (19), pp. 2025 – 2034.
- Cosío, F.G., Goicolea, A., Gil, M.L., Kallmeyer, C. and Barroso, J.L. 1991. Suppression of Torsades de Pointes with verapamil in patients with atrio-ventricular block. *European Heart Journal*, 12(5), pp. 635 - 638.
- Cranefield, P.F. 1977. Action potentials, afterpotentials, and arrhythmias. *Circulation Research*, 41 (4), pp. 415 - 423.
- Curran, M.E., Splawski, I., Timothy, K.W., Vincent, G.M., Green, E.D. and Keating, M.T. 1995. A molecular basis for cardiac arrhythmia: HERG mutations cause long QT syndrome. *Cell*, 80 (5), pp. 795 – 803.
- D'Alonzo, A.J., Zhu, J.L. and Darbenzio, R.B. 1999. Effects of class III antiarrhythmic agents in an in vitro rabbit model of spontaneous torsades de pointe. *European Journal of Pharmacology*, 369 (1), pp. 57 - 64.
- Damiano, B.P. and Rosen, M.R. 1984. Effects of pacing on triggered activity induced by early afterdepolarizations. *Circulation*, 69 (5), pp. 1013 - 1025.
- Davey, P.P., 2000. Which lead for QT interval measurements? *Cardiology*, 94(3), pp.159-164.
- Davidenko, J.M., Kent, P.F., Chialvo, D.R., Michaels, D.C. and Jalife, J. 1990. Sustained vortex-like waves in normal isolated ventricular muscle. *Proceedings of the National Academy of Sciences*, 87(22), pp. 8785-8789.
- de Azevedo, I.M., Watanabe, Y. and Dreifus, L.S. 1973. Atrioventricular junctional rhythm: classification and clinical significance. *Chest*, 64 (6), pp. 732 - 740.
- Dessertenne, F., 1966. La tachycardie ventriculaire a deux foyers opposes variables. *Arch Mal Coeur*, 59, pp .263 - 272.

Di Diego, J.M., Sicouri, S., Myles, R.C., Burton, F.L., Smith, G.L. and Antzelevitch, C., 2013. Optical and electrical recordings from isolated coronary-perfused ventricular wedge preparations. *Journal of molecular and cellular cardiology*, 54, pp.53 - 64.

Dillon, S.M. 1991. Optical recordings in the rabbit heart show that defibrillation strength shocks prolong the duration of depolarization and the refractory period. *Circulation Research*, 69 (3), pp. 842 - 856.

Drici, M.D. and Clement, N. 2001. Is gender a risk factor for adverse drug reactions? *Drug Safety*, 24 (8), pp. 575 – 585.

Dorian, P. and Newman, D., 2000. Rate dependence of the effect of antiarrhythmic drugs delaying cardiac repolarization: an overview. *EP Europace*, 2 (4), pp.277 - 285.

Drouin, E., Charpentier, F. and Gauthier, C. 1996.  $\alpha$ 1-Adrenergic stimulation induces early afterdepolarizations in ferret Purkinje fibres. *Journal of Cardiovascular Pharmacology*, 27 (3), pp. 320 - 326.

Duchatelet, S., Crotti, L., Peat, R.A., Denjoy, I., Itoh, H., Berthet, M., Ohno, S., Fressart, V., Monti, M.C., Crocama, C., Pedrazzini, M., Dagradi, F., Vincentini, A., Klug, D., Brink, P.A., Goosen, A., Swan, H., Toivonen, L., Lahtinen, A.M., Kontula, K., Shimizu, W., Horie, M., George, Jr. A.L., Tregouet, D., Guicheney, P. and Schwartz, P.J. 2013. Identification of a KCNQ1 polymorphism acting as a protective modifier against arrhythmic risk in long-QT syndrome. *Circulation: Cardiovascular Genetics*, 6 (4), pp. 354 – 361.

Dutta, S., Mincholé, A., Zacur, E., Quinn, T.A., Taggart, P. and Rodriguez, B. 2016. Early afterdepolarizations promote transmural re-entry in ischemic human ventricles with reduced repolarization reserve. *Progress in Biophysics and Molecular Biology*, 120 (1-3), pp. 236 - 248

Eckardt, L., Haverkamp, W., Borggrefe, M. and Breithardt, G. 1998b. Experimental models of torsade de pointes. *Cardiovascular Research*, 39 (1), pp. 178 - 193.

Eckardt, L., Haverkamp, W., Mertens, H., Johna, R., Clague, J.R., Borggrefe, M. and Breithardt, G. 1998a. Drug-related torsades de pointes in the isolated rabbit heart: comparison of clofilium, d, l-sotalol, and erythromycin. *Journal of Cardiovascular Pharmacology*, 32 (3), pp. 425 - 434.

- Efimov, I.R., Cheng, Y., Van Wagoner, D.R., Mazgalev, T. and Tchou, P.J. 1998. Virtual electrode-induced phase singularity: A basic mechanism of defibrillation failure. *Circulation Research*, 82 (8), pp. 918 - 925.
- Efimov, I.R., Huang, D.T., Rendt, J.M. and Salama, G., 1994. Optical mapping of repolarization and refractoriness from intact hearts. *Circulation*, 90(3), pp.1469-1480.
- Elliott, E.B., Kelly, A., Smith, G.L. and Loughrey, C.M. 2012. Isolated rabbit working heart function during progressive inhibition of myocardial SERCA activity. *Circulation research*, 110 (12), pp. 1618 - 1627.
- El-Sherif, N. 1991. Early afterdepolarizations and arrhythmogenesis. Experimental and clinical aspects. *Archives des maladies du coeur et des vaisseaux*, 84 (2), pp. 227 - 234.
- El-Sherif, N., Chinushi, M., Caref, E.B. and Restivo, M., 1997. Electrophysiological mechanism of the characteristic electrocardiographic morphology of torsade de pointes tachyarrhythmias in the long-QT syndrome: detailed analysis of ventricular tridimensional activation patterns. *Circulation*, 96(12), pp.4392 - 4399.
- El-Sherif, N. and Turitto, G. 2011. Electrolyte disorders and arrhythmogenesis. *Cardiology Journal*, 18 (3), pp. 233 – 245.
- El-Sherif, N., Smith, R.A. and Evans, K. 1981. Canine ventricular arrhythmias in the late myocardial infarction period. 8. Epicardial mapping of re-entrant circuits. *Circulation Research*, 49 (1), pp. 255 - 265.
- Ezzat, V.A., Lee, V., Ahsan, S., Chow, A.W., Segal, O. and Rowland, E. 2015. A systematic review of ICD complications in randomised controlled trials versus registries: is our 'real-world' data an underestimation? *Open Heart*, 2 (1), p.e000198.
- Farkas, A.S., Makra, P., Csík, N., Orosz, S., Shattock, M.J., Fülöp, F., Forster, T., Csanády, M., Papp, J.G., Varró, A. and Farkas, A. 2009. The role of the Na<sup>+</sup>/Ca<sup>2+</sup> exchanger, INa and ICaL in the genesis of dofetilide-induced torsades de pointes in isolated, AV-blocked rabbit hearts. *British Journal of Pharmacology*, 156 (6), pp. 920 - 932.

- Fedorov, V.V., Lozinsky, I.T., Sosunov, E.A., Anyukhovskiy, E.T., Rosen, M.R., Balke, C.W. and Efimov, I.R. 2007. Application of blebbistatin as an excitation-contraction uncoupler for electrophysiologic study of rat and rabbit hearts. *Heart Rhythm*, 4 (5), pp. 619 – 626.
- Franz, M.R., Swerdlow, C.D., Liem, L.B. and Schaefer, J., 1988. Cycle length dependence of human action potential duration in vivo. Effects of single extrastimuli, sudden sustained rate acceleration and deceleration, and different steady-state frequencies. *The Journal of clinical investigation*, 82(3), pp.972-979.
- Fraser, G.R, Froggatt, P. and Murphy, T. 1964. Genetical aspects of the cardio-auditory syndrome of Jervell and Lange-Nielsen (Congenital deafness and electrocardiographic abnormalities). *The American Journal of Human Genetics*, 28, pp. 133 -157.
- Fridericia LS. 1920. The duration of systole in the electrocardiogram of normal subjects and of patients with heart disease. *Acta Medica Scandinavica*, 53, pp. 469–486.
- Fuster, V., Harrington, R.A., Narula, J. and Eapen, Z.J. 2017. *Hurst's The Heart*. Fourteenth Edition. McGraw-Hill Education. 2017. Chapter 78.
- Gaztañaga, L., Marchlinski, F.E. and Betensky, B.P., 2012. Mechanisms of cardiac arrhythmias. *Revista Española de Cardiología (English Edition)*, 65 (2), pp.174 - 185.
- Gaur, N., Rudy, Y. and Hool, L. 2009. Contributions of ion channel currents to ventricular action potential changes and induction of early afterdepolarizations during acute hypoxia. *Circulation Research*, 105 (12), pp. 1196 - 1203.
- Ghanem, R.N., Jia, P., Ramanathan, C., Rya, K., Markowitz, A and Rudy, Y., 2005. Noninvasive electrocardiographic imaging (ECGI): comparison to intraoperative mapping in patients. *Heart Rhythm* 2(4), pp339 – 354.
- Gold, M.R., Aasbo, J.D., El-Chami, M.F., Niebauer, M., Herre, J., Prutkin, J.M., Knight, B.P., Kutalek, S., Hsu, K., Weiss, R. and Bass, E., 2017. Subcutaneous implantable cardioverter-defibrillator Post-Approval Study: clinical characteristics and perioperative results. *Heart Rhythm*, 14(10), pp.1456 - 1463.
- Goyal, A., Spertus, J.A., Gosch, K., Venkitachalam, L., Jones, P.G., Van den Berghe, G. and Kosiborod, M. 2012. Serum potassium levels and mortality in acute myocardial infarction. *Journal of American Medical Association*, 307 (2), pp. 157 – 164.

- Gray, R.A., Ayers, G. and Jalife, J. 1997. Video imaging of atrial defibrillation in the sheep heart. *Circulation*, 95 (4), pp. 1038 - 1047.
- Gray, R.A., Jalife, J., Panfilov, A.V., Baxter, W.T., Cabo, C., Davidenko, J.M., Pertsov, A.M., Hogeweg, P., and Winfree, A.T. 1995. Mechanisms of cardiac fibrillation. *Science*, 270 (5239), pp. 1222 - 1226.
- Gray, R.A., Pertsov, A.M. and Jalife, J. 1998. Spatial and temporal organization during cardiac fibrillation. *Nature*, 392 (6671), pp. 75.
- Guidicessi, J.R. and Ackerman, M.J. 2013. Genotype- and Phenotype- Guided Management of Congenital Long QT Syndrome. *Current Problems in Cardiology*, 38 (10), pp. 417 – 455.
- Helfant, R.H. 1986. Hypokalaemia and arrhythmias. *American Journal of Medicine*, 80 (4A), pp. 13 – 22.
- Hollifield, J.W. 1986. Thiazide treatment of hypertension. Effects of thiazide diuretics on serum potassium, magnesium, and ventricular ectopy. *American Journal of Medicine*, 80 (4A), pp. 8 – 12.
- Hollifield, J.W. 1987. Magnesium depletion, diuretics and arrhythmias. *American Journal of Medicine*, 82 (3A), pp. 30 – 37.
- Hondeghem, L.M. and Katzung, B.G. 1984. Antiarrhythmic agents: the modulated receptor mechanism of action of sodium and calcium channel-blocking drugs. *Annual Review of Pharmacology and Toxicology*, 24(1), pp. 387 - 423.
- Houser, S.R. 2000. When does spontaneous sarcoplasmic reticulum Ca<sup>2+</sup> release cause a triggered arrhythmia? Cellular versus tissue requirements. *Circulation Research*, 87, pp. 725 – 727.
- Hoyt, R.H., Cohen, M.L. and Saffitz, J.E. 1989. Distribution and three-dimensional structure of intercellular junctions in canine myocardium. *Circulation Research*, 64 (3), pp. 563 - 574.

- Huang, X., Kim, T.Y., Koren, G., Choi, B.R. and Qu, Z. 2016. Spontaneous initiation of premature ventricular complexes and arrhythmias in type 2 long QT syndrome. *American Journal of Physiology-Heart and Circulatory Physiology*, 311 (6), pp. 1470-1484.
- Ideker, R.E., Kong, W. and Pogwizd, S., 2009. Purkinje fibers and arrhythmias. *Pacing and clinical electrophysiology: PACE*, 32(3), p.283.
- Issa, Z.F., Miller, J.M. and Zipes, D.P. 2009. Clinical arrhythmology and electrophysiology: A Companion to Braunwald's Heart Disease E-Book: Expert Consult: Online and Print. *Elsevier Health Sciences*.
- Jackman, W.M., Szabo, B., Friday, K.J., Margolis, P.D., Moulton, K., Wang, X., Patterson, E. and Lazzara, R. 1990. Ventricular tachyarrhythmias related to early afterdepolarizations and triggered firing: relationship to QT interval prolongation and potential therapeutic role for calcium channel blocking agents. *Journal of Cardiovascular Electrophysiology*, 1 (2), pp. 170 - 195.
- Jacobs, A., Knight, B.P., McDonald, K.T. and Burke, M.C. 2006. Verapamil decreases ventricular tachyarrhythmias in a patient with Timothy syndrome (LQT8). *Heart Rhythm*, 3(8), pp. 967 - 970.
- Jalife, J., Delmar, M., Anumonwo, J., Berenfeld, O. and Kalifa, J. 2011. Basic mechanisms of cardiac arrhythmias. *Basic Cardiac Electrophysiology for the Clinician*. John Wiley & Sons.
- Janiak, R. and Lewartowski, B., 1996. Early after-depolarisations induced by noradrenaline may be initiated by calcium released from sarcoplasmic reticulum. *Molecular and cellular biochemistry*, 163(1), pp.125-130.
- January, C.T. and Riddle, J.M. 1989. Early afterdepolarizations: mechanism of induction and block. A role for L-type Ca<sup>2+</sup> current. *Circulation Research*, 64 (5), pp. 977 - 990.
- January, C.T. and Shorofsky, S. 1990. Early afterdepolarizations: Newer insights into cellular mechanisms. *Journal of Cardiovascular Electrophysiology*, 1 (2), pp. 161 - 169.

- January, C.T., Chau, V. and Makielski, J.C. 1991. Triggered activity in the heart: cellular mechanisms of early after-depolarizations. *European Heart Journal*. 12 (supplement F), pp. 4-9.
- Jervell, A. and Lange-Nielsen, F. 1957. Congenital deaf-mutism, functional heart disease with prolongation of the Q-T interval and sudden death. *American Heart Journal*, 54 (1), pp. 59-68.
- Kang, J., Wang, L., Chen, X.L., Triggle, D.J. and Rampe, D. 2001. Interactions of a series of fluoroquinolone antibacterial drugs with the human cardiac K<sup>+</sup> channel HERG. *Molecular Pharmacology*, 59 (1), pp. 122 – 126.
- Kannankeril, P.J. and Roden, D.M. 2007. Drug-induced long QT and torsade de pointes: recent advances. *Current opinion in cardiology*, 22 (1), pp. 39 - 43.
- Kawade, M., Ohe, T. and Kamiya, T. 1995. Provocative testing and drug response in a patient with the long QT syndrome. *Heart*, 74(1), pp. 67 - 70.
- Kelly, A., Ghouri, I.A., Kemi, O.J., Bishop, M.J., Bernus, O., Fenton, F.H., Myles, R.C., Burton, F.L. and Smith, G.L. 2013. Subepicardial action potential characteristics are a function of depth and activation sequence in isolated rabbit hearts. *Circulation: Arrhythmia and Electrophysiology*, 6 (4), pp. 809 - 817.
- Kim, J.J., Němec, J., Li, Q. and Salama, G. 2015. Synchronous systolic subcellular Ca<sup>2+</sup>-elevations underlie ventricular arrhythmia in drug-induced long QT type 2. *Circulation: Arrhythmia and Electrophysiology*, 8 (3), pp. 703 - 712.
- Kim, T.Y., Kunitomo, Y., Pfeiffer, Z., Patel, D., Hwang, J., Harrison, K., Patel, B., Jeng, P., Ziv, O., Lu, Y. and Peng, X. 2015. Complex excitation dynamics underlie polymorphic ventricular tachycardia in a transgenic rabbit model of long QT syndrome type 1. *Heart Rhythm*, 12 (1), pp. 220 - 228.
- Kodama, I., Kamiya, K. and Toyama, J. 1997. Cellular electropharmacology of amiodarone. *Cardiovascular Research*, 35 (1), pp. 13 – 29.
- Kovács, M., Tóth, J., Hetényi, C., Málnási-Csizmadia, A. and Sellers, J.R. 2004. Mechanism of blebbistatin inhibition of myosin II. *Journal of Biological Chemistry*, 279 (34), pp. 35557 - 35563.



- Kuo, C.S., Reddy, C.P., Munakata, K. and Surawicz, B. 1985. Mechanism of ventricular arrhythmias caused by increased dispersion of repolarization. *European Heart Journal*, 6 (supplement D), pp. 63-70.
- Lammers, W.J., Schalij, M.J., Kirchhof, C.J. and Allessie, M.A., 1990. Quantification of spatial inhomogeneity in conduction and initiation of reentrant atrial arrhythmias. *American Journal of Physiology-Heart and Circulatory Physiology*, 259(4), pp.H1254-H1263.
- Laurita, K.R., Girouard, S.D. and Rosenbaum, D.S., 1996. Modulation of ventricular repolarization by a premature stimulus: role of epicardial dispersion of repolarization kinetics demonstrated by optical mapping of the intact guinea pig heart. *Circulation Research*, 79(3), pp.493 - 503.
- Lazzara, R. 1989. Amiodarone and torsade de pointes. *Annals of Internal Medicine*, 111 (7), pp. 549 – 551.
- Li, Y., Eisner, D.A. and O'Neill, S.C. 2012. Do calcium waves propagate between cells and synchronize alternating calcium release in rat ventricular myocytes? *The Journal of Physiology*, 590 (24), pp. 6353 - 6361.
- Li, Z.Y., Maldonado, C., Zee-Cheng, C., Hiromasa, S. and Kupersmith, J. 1992. Purkinje fibre-papillary muscle interaction in the genesis of triggered activity in a guinea pig model. *Cardiovascular Research*, 26 (5), pp. 543 - 548.
- Liao, W.B., Bullard, M.J., Kuo, C.T., Hsiao, C.T., Chu, P.H. and Chiang, C.W. 1996. Anticholinergic overdose induced torsade de pointes successfully treated with verapamil. *Japanese Heart Journal*, 37(6), pp. 925 - 931.
- Liu, J. and Laurita, K.R. 2005. The mechanism of pause-induced torsade de pointes in long QT syndrome. *Journal of Cardiovascular Electrophysiology*, 16 (9), pp. 981 - 987.
- Liu, T., Choi, B.R., Drici, M.D. and Salama, G. 2005. Sex modulates the arrhythmogenic substrate in prepubertal rabbit hearts with Long QT 2. *Journal of Cardiovascular Electrophysiology*, 16 (5), pp. 516 - 524.

- Liu, Y., Xue, Y., Wu, S., Duan, J., Lin, L., Wang, L., Zhang, C., Liu, N. and Bai, R. 2016. Effect of verapamil in the treatment of type 2 long QT syndrome is not a dose-dependent pattern: a study from bedside to bench, and back. *European Heart Journal Supplements*, 18(supplement A), pp. A37 - 46.
- London, B., Jeron, A., Zhou, J., Buckett, P., Han, X., Mitchell, G.F. and Koren, G. Long. 1998. QT and ventricular arrhythmias in transgenic mice expressing the N terminus and first transmembrane segment of a voltage-gated potassium channel. *Proceedings of the National Academy of Sciences*, 95 (6), pp. 2926 - 2931.
- Lou, Q., Fedorov, V.V., Glukhov, A.V., Moazami, N., Fast, V.G. and Efimov, I.R. 2011a. Transmural heterogeneity and remodelling of ventricular excitation-contraction coupling in human heart failure. *Circulation*, 123 (17), pp. 1881 - 1890.
- Lou, Q., Li, W and Efimov, I.R., 2011b. Multiparametric optical mapping of the Langendorff-perfused rabbit heart. *JoVE (Journal of Visualized Experiments)*, (55), p.e3160.
- Lukas, A. and Antzelevitch, C. 1996. Phase 2 re-entry as a mechanism of initiation of circus movement re-entry in canine epicardium exposed to simulated ischemia. *Cardiovascular Research*, 32 (3), pp. 593 - 603.
- Luo, C.H and Rudy, Y. 1994. A dynamic model of the cardiac ventricular action potential. I. Simulations of ionic currents and concentration changes. *Circulation Research*, 74 (6), pp. 1071 - 1096.
- Madhvani, R.V., Xie, Y., Pantazis, A., Garfinkel, A., Qu, Z., Weiss, J.N. and Olcese, R. 2011. Shaping a new Ca<sup>2+</sup> conductance to suppress early afterdepolarizations in cardiac myocytes. *The Journal of Physiology*, 589 (24), pp. 6081 - 6092.
- Marban, E., Robinson, S.W. and Wier, W.G. 1986. Mechanisms of arrhythmogenic delayed and early afterdepolarizations in ferret ventricular muscle. *Journal of Clinical Investigation*, 78 (5), pp. 1195 - 1192.
- Marchi, S., Szabo, B. and Lazzara, R., 1991. Adrenergic induction of delayed afterdepolarizations in ventricular myocardial cells:  $\beta$  induction and  $\alpha$  modulation. *Journal of Cardiovascular Electrophysiology*, 2(6), pp.476-491.

- Maruyama, M., Lin, S.F., Xie, Y., Chua, S.K., Joung, B., Han, S., Shinohara, T., Shen M.J., Qu, Z., Weiss, J.N. and Chen, P.S. 2011. Genesis of phase 3 early afterdepolarizations and triggered activity in acquired long-QT syndrome. *Circulation: Arrhythmia and Electrophysiology*, 4 (1), pp. 103 - 111.
- Mason, J.W., Hondeghem, L.M. and Katzung, B.G., 1983. Amiodarone blocks inactivated cardiac sodium channels. *Pflügers Archiv*, 396(1), pp.79 - 81.
- McIntosh, M.A., Cobbe, S.M. and Smith, G.L., 2000. Heterogeneous changes in action potential and intracellular Ca<sup>2+</sup> in left ventricular myocyte sub-types from rabbits with heart failure. *Cardiovascular Research*, 45(2), pp.397-409.
- Milberg, P., Eckardt, L., Bruns, H.J., Biertz, J., Ramtin, S., Reinsch, N., Fleischer, D., Kirchhof, P., Fabritz, L., Breithardt, G. and Haverkamp W. 2002. Divergent proarrhythmic potential of macrolide antibiotics despite similar QT prolongation: fast phase 3 repolarization prevents early afterdepolarizations and torsade de pointes. *Journal of Pharmacology and Experimental Therapeutics*, 303 (1), pp. 218 – 225.
- Mirams, G.R., Cui, Y., Sher, A., Fink, M., Cooper, J., Heath, B.M., McMahon, N.C., Gavaghan, D.J. and Noble, D. 2011. Simulation of multiple ion channel block provides improved early prediction of compounds' clinical torsadogenic risk. *Cardiovascular Research*, 91(1), pp. 53 - 61.
- Miura, M., Ishide, N., Numaguchi, H. and Takishima, T. 1995. Diversity of early afterdepolarizations in guinea pig myocytes: spatial characteristics of intracellular Ca<sup>2+</sup> concentration. *Heart and Vessels*, 10 (5), pp. 266 - 274.
- Moss, A.J., Shimizu, W., Wilde, A.M., Towbin, J.A., Zareba, W., Robinson, J.L., Qi, M., Vincent, G.M., Ackerman, M.J., Kaufman, E.S., Hosman, N., Seth, R., Kamakura, S., Miyamoto, Y., Goldenberg, I., Andrews, M.L. and McNitt, S. 2007. Clinical aspects of type-1 long-QT syndrome by locations, coding type, and biophysical function of mutations involving the KCNQ1 gene. *Circulation*, 115 (9), pp. 2481 – 2489.
- Moss, A.J., Windle, J.R., Hall, W.J., Zareba, W., Robinson, J.L., McNitt, S., Severski, P., Rosero, S., Daubert, J.P., Qi, M., Ciecioraka, M. and Manalan, A.S. 2005. Safety and efficacy of flecainide in subjects with Long QT-3 syndrome (DeltaKPQ mutation): a randomized, double-blind, placebo-controlled clinical trial. *Annals of Non-invasive Electrocardiology*, 10 (4), pp. 59 – 66.

Moss, A.J., Zareba, W., Kaufman, E.S., Gartman, E., Peterson, D.R., Benhorin, J., Towbin, J.A., Keating, M.T., Priori, S.G., Schwartz, P.J. and Vincent, G.M. 2002. Increased risk of arrhythmic events in long-QT syndrome with mutations in the pore region of the human ether-a-go-go-related gene potassium channel. *Circulation*, 105 (7), pp. 794 - 799.

Miura, M., Ishide, N., Numaguchi, H. and Takishima, T., 1995. Diversity of early afterdepolarizations in guinea pig myocytes: spatial characteristics of intracellular Ca<sup>2+</sup> concentration. *Heart and Vessels*, 10(5), pp.266-274.

Myles, R.C., Bernus, O., Burton, F.L., Cobbe, S.M. and Smith, G.L., 2010. Effect of activation sequence on transmural patterns of repolarization and action potential duration in rabbit ventricular myocardium. *American Journal of Physiology-Heart and Circulatory Physiology*, 299(6), pp.H1812-H1822.

Myles, R.C., Wang, L., Kang, C., Bers, D.M. and Ripplinger, C.M., 2012. Local  $\beta$ -adrenergic stimulation overcomes source-sink mismatch to generate focal arrhythmia. *Circulation Research*, 110(11), pp. 1454 - 1464.

Nam, G.B., Burashnikov, A. and Antzelevitch, C. 2005. Cellular mechanisms underlying the development of catecholaminergic ventricular tachycardia. *Circulation*, 111 (21), pp. 2727 - 2733.

Němec, J., Kim, J.J., Gabris, B. and Salama, G. 2010. Calcium oscillations and T-wave lability precede ventricular arrhythmias in acquired long QT type 2. *Heart Rhythm*, 7 (11), pp. 1686 - 1694.

Odening, K.E., Choi, B.R., Liu, G.X., Hartmann, K., Ziv, O., Chaves, L., Schofield, L., Centracchio, J., Zehender, M., Peng, X. and Brunner, M. 2012. Estradiol promotes sudden cardiac death in transgenic long QT type 2 rabbits while progesterone is protective. *Heart Rhythm*, 9 (5), pp. 823 - 832.

Panfilov, A.V. 2006. Is heart size a factor in ventricular fibrillation? Or how close are rabbit and human hearts? *Heart Rhythm*, 3 (7), pp. 862 - 824.

Patterson, E., Scherlag, B.J. and Lazzara, R. 1997. Early Afterdepolarizations Produced by d, 1-Sotalol and Clofilium. *Journal of Cardiovascular Electrophysiology*, 8 (6), pp. 667 - 678.

Patterson, E., Szabo, B., Scherlag, B.J. and Lazzara, R. 1990. Early and delayed afterdepolarizations associated with caesium chloride-induced arrhythmias in the dog. *Journal of Cardiovascular Pharmacology*, 15 (2), pp. 323 - 331.

Pertsov, A.M., Davidenko, J.M., Salomonsz, R., Baxter, W.T. and Jalife, J. 1993. Spiral waves of excitation underlie re-entrant activity in isolated cardiac muscle. *Circulation research*, 72(3), pp. 631 - 650.

Postema, P.G., De Jong, J.S., Van der Bilt, I.A. and Wilde, A.A. 2008. Accurate electrocardiographic assessment of the QT interval: Teach the tangent. *Heart Rhythm*, 5 (7), pp. 1015 -1018.

Priori, S.G. and Corr, P.B. 1990. Mechanisms underlying early and delayed afterdepolarizations induced by catecholamines. *American Journal of Physiology-Heart and Circulatory Physiology*, 258 (6), pp. 1796 - 1805.

Priori, S.G., Bloise, R. and Crotti, L. 2001a. The long QT syndrome. *Europace* 3, pp. 16 – 27.

Priori, S.G., Blomström-Lundqvist, C., Mazzanti, A., Blom, N., Borggrefe, M., Camm, J., Elliott, P.M., Fitzsimons, D., Hatala, R. and Hindricks, G., 2015. 2015 ESC Guidelines for the management of patients with ventricular arrhythmias and the prevention of sudden cardiac death: The Task Force for the Management of Patients with Ventricular Arrhythmias and the Prevention of Sudden Cardiac Death of the European Society of Cardiology (ESC) Endorsed by: Association for European Paediatric and Congenital Cardiology (AEPC). *Ep Europace*, 17(11), pp.1601-1687.

Priori, S.G., Napolitano, C., Schwartz, P.J., Grillo, M., Bloise, R., Ronchetti, E., Moncalvo, C., Tulipani, C., Veia, A., Bottelli, G. and Nastoli, J. 2004. Associated of long QT syndrome loci and cardiac events among patients treated with beta-blockers. *Journal of the American Medical Association*, 292 (11), pp. 1341 – 1344.

Priori, S.G., Napolitano, C., Tiso, N., Memmi, M., Vignati, G., Bloise, R., Sorrentino, V. and Danieli, G.A. 2001b. Mutations in the cardiac ryanodine receptor gene (hRyR2) underlie catecholaminergic polymorphic ventricular tachycardia. *Circulation*, 103 (2), pp. 196 - 200.

- Priori, S.G., Schwartz, P.J., Napolitano, C., Bloise, R., Ronchetti, E., Grillo, M., Vincentini, A., Spazzolini, C., Nastoli, J., Bottelli, G., Folli, R. and Cappelletti, D. 2003. Risk stratification in the Long-QT Syndrome. *New England Journal of Medicine*, 348 (19), pp. 1866 – 1874.
- Priori, S.G., Wilde, A.A., Horie, M., Cho, Y., Behr, E.R., Berul, C., Blom, N., Brugada, J., Chiang, C.E., Huikuri, H., Kannankeril, P., Krahn, A., Leenhardt, A., Moss, A., Schwartz, P.J., Tomaselli, G. and Tracy, C. 2013. HRS/EHRA/APHRS expert consensus statement on the diagnosis and management of patients with inherited primary arrhythmia syndromes: document endorsed by HRS, EHRA, and APHRS in May 2013 and by ACCF, AHA, PACES, and AEPC in June 2013. *Heart Rhythm*, 10 (12), pp. 1932 – 1963.
- Qu, Z. and Chung, D. 2012. Mechanisms and determinants of ultralong action potential duration and slow rate-dependence in cardiac myocytes. *PLoS One*, 7 (8).
- Qu, Z., Xie, L.H., Olcese, R., Karagueuzian, H.S., Chen, P.S., Garfinkel, A. and Weiss, J.N. 2013. Early afterdepolarizations in cardiac myocytes: beyond reduced repolarization reserve. *Cardiovascular Research*, 99 (1), pp. 6 - 15.
- Redfern, W.S., Carlsson, L., Davis, A.S., Lynch, W.G., MacKenzie, I., Palethorpe, S., Siegl, P.K., Strang, I., Sullivan, A.T., Wallis, R. and Camm, A.J. 2003. Relationships between preclinical cardiac electrophysiology, clinical QT interval prolongation and torsade de pointes for a broad range of drugs: evidence for a provisional safety margin in drug development. *Cardiovascular Research*, 58 (1), pp. 32 - 45.
- Ritter, J.M. 2012. Cardiac safety, drug-induced QT prolongation and torsade de pointes (TdP). *British Journal of Clinical Pharmacology*, 73 (3), pp. 331.
- Roden, D.M. 1993. Torsade de pointes. *Clinical Cardiology*, 16 (9), pp. 683 - 686.
- Roden, D.M. 1998. Taking the “idio” out of “idiosyncratic”: predicting torsades de pointes. *Pacing and Clinical Electrophysiology*, 21 (5), pp. 1029 - 1034.
- Rosati, B., Grau, F., Rodriguez, S., Li, H., Nerbonne, J.M. and McKinnon, D. 2003. Concordant expression of KCHIP2 mRNA, protein and transient outward current throughout the canine ventricle. *The Journal of Physiology*, 548 (3), pp. 815 - 822.

- Rosen, M.R. 1985. Cellular electrophysiology of digitalis toxicity. *Journal of the American College of Cardiology*, 5 (5 Supplement 1), pp. 22A - 34A.
- Rozanski, G.J. and Witt, R.C. 1991. Early afterdepolarizations and triggered activity in rabbit cardiac Purkinje fibres recovering from ischemic-like conditions. Role of acidosis. *Circulation*, 83 (4), pp. 1352 - 1360.
- Ruan, Y., Liu, N. and Priori, S.G. 2009. Sodium channel mutations and arrhythmias. *Nature Reviews of Cardiology*, 6 (5), pp. 337 – 348.
- Ruan, Y., Liu, N., Bloise, R., Napolitano, C. and Priori, S.G. 2007. Gating properties of SCN5A mutations and the response to mexiletine in long-QT syndrome type 3 patients. *Circulation*, 116 (10), pp. 1137 – 1144.
- Salama, G. and London, B. 2007. Mouse models of long QT syndrome. *The Journal of Physiology*, 578 (1), pp. 43 - 53.
- Salama, G., Kanai, A. and Efimov, I.R. 1994. Subthreshold stimulation of Purkinje fibres interrupts ventricular tachycardia in intact hearts. Experimental study with voltage-sensitive dyes and imaging techniques. *Circulation Research*, 74 (4), pp. 604 - 619.
- Sanguinetti, M.C., Curran, M.E., Zoue, A., Shen, J., Spector, P.S., Atkinson, D.L. and Keating, M.T. 1996. Coassembly of K(V) LQT1 and minK (IsK) proteins to form cardiac I(Ks) potassium channel. *Nature*, 384 (6604), pp. 80-83.
- Sano, T. and Sawanobori, T. 1972. Abnormal automaticity in canine purkinje fibres focally subjected to low external concentrations of calcium. *Circulation Research*, 31 (2), pp. 158 – 164.
- Schlotthauer, K. and Bers, D.M. 2000. Sarcoplasmic reticulum Ca<sup>2+</sup> release causes myocyte depolarization: underlying mechanism and threshold for triggered action potentials. *Circulation Research*, 87 (9), pp. 774 - 780.
- Schwartz, P.J. 1985. Idiopathic long QT syndrome: progress and questions. *American Heart Journal*, 109 (2), pp. 399 – 411.

Schwartz, P.J., Ackerman, M.J., George, A.L. and Wilde, A.A. 2013. Impact of genetics on the clinical management of channelopathies. *Journal of American College of Cardiology*, 62 (3), pp. 169 – 180.

Schwartz, P.J., Moss, A.J., Vincent, G.M. and Crampton, R.S. 1993. Diagnostic criteria for the long QT syndrome. An update. *Circulation*, 88 (2), pp. 782 – 784.

Schwartz, P.J., Priori, S.G., Cerrone, M., Spazzolini, C., Odero, A., Napolitano, C., Bloise, R., De Ferrari, G.M., Klersy, C., Moss, A.J., Zareba, W., Robinson, J.L., Hall, W.J., Brink, P.A., Toivonen, L., Epstein, A.E., Li, C. and Hu, D. 2004. Left cardiac sympathetic denervation in the management of high-risk patients affected by the long-QT syndrome. *Circulation*, 109 (15), pp. 1826 – 1833.

Schwartz, P.J., Priori, S.G., Spazzolini, C., Moss, A.J., Vincent, G.M., Napolitano, C., Denjoy, I., Guicheney, P., Breithardt, G., Keating, M.T., Towbin, J.A., Beggs, A.H., Brink, P., Wilde, A.A., Toivonen, L., Zareba, W., Robinson, J.L., Timothy, K.W., Corfield, V., Wattanasirichaigoon, D., Corbett, C., Haverkamp, W., Schulze-Bahr, E., Lehmann, M.H., Coumel, P. and Bloise, R. 2001. Genotype-phenotype correlation in the long-QT syndrome: gene specific triggers for life-threatening arrhythmias. *Circulation*, 103 (1), pp. 89 – 95.

Schwartz, P.J., Spazzolini, C., Priori, S.G., Crotti, L., Vincentini, A., Landolina, M., Gasparini, M., Wilde, A.A., Knops, R.E., Denjoy, I. and Toivonen, L. 2010. Who are the long-QT syndrome patients who receive an implantable cardioverter-defibrillator and what happens to them? data from the European Long-QT Syndrome Implantable Cardiovert-Defibrillator (LQTS ICD) Registry. *Circulation*, 122 (13), pp. 1272 – 1282.

Schwartz, P.J., Stramba-Badiale, M., Crotti, L., Pedrazzini, M., Besana, A., Bosi, G., Gabbarini, F., Goulene, K., Insolia, R., Mannarino, S., Mosca, F., Nespoli, L., Rimini, A., Rosati, E., Salice, P. and Spazzolini, C. 2009. Prevalence of the congenital long-qt syndrome. *Circulation*, 120 (18), pp. 1761 -1767.

Seth, R., Moss, A.J., McNitt, S., Zareba, W., Andrews, M.L., Qi, M., Robinson, J.L., Goldenberg, I., Ackerman, M.J., Benhorin, J. and Kaufman, E.S. 2007. Long QT Syndrome and Pregnancy. *Journal of the American College of Cardiology*, 49 (10), pp. 1092 – 1098.



Shen, J.B., Jiang, B. and Pappano, A.J., 2000. Comparison of L-type calcium channel blockade by nifedipine and/or cadmium in guinea pig ventricular myocytes. *Journal of Pharmacology and Experimental Therapeutics*, 294 (2), pp 562-570.

Shimizu, W. and Antzelevitch, C. 1997. Sodium channel block with mexiletine is effective in reducing dispersion of repolarization and preventing torsade de pointes in LQT2 and LQT3 models of the long-QT syndrome. *Circulation*, 96 (6), pp. 2038 - 2047.

Shimizu, W. and Antzelevitch, C. 1998. Cellular basis for the ECG features of the LQT1 form of the long-QT syndrome: effects of  $\beta$ -adrenergic agonists and antagonists and sodium channel blockers on transmural dispersion of repolarization and torsade de pointes. *Circulation*, 98 (21), pp. 2314 - 2322

Shimizu, W., Ohe, T., Kurita, T., Tokuda, T. and Shimomura, K. 1994. Epinephrine-induced ventricular premature complexes due to early afterdepolarizations and effects of verapamil and propranolol in a patient with congenital long QT syndrome. *Journal of Cardiovascular Electrophysiology*, 5 (5), pp. 438 - 444.

Singh, B.N. and Williams, E.V., 1970. The effect of amiodarone, a new anti-anginal drug, on cardiac muscle. *British Journal of Pharmacology*, 39(4), pp.657 - 667.

Silva, J. and Rudy, Y. 2005. Subunit interaction determines  $I_{Ks}$  participation in cardiac repolarization and repolarization reserve. *Circulation*, 112 (10), pp. 1384 – 1391.

Sipido, K.R., Maes, M. and Van de Werf, F. 1997. Low efficiency of  $Ca^{2+}$  entry through the  $Na^{+}-Ca^{2+}$  exchanger as trigger for  $Ca^{2+}$  release from the sarcoplasmic reticulum: a comparison between L-type  $Ca^{2+}$  current and reverse-mode  $Na^{+}-Ca^{2+}$  exchange. *Circulation Research*, 81 (6), pp. 1034 - 1044.

Spach, M.S. and Josephson, M.E. 1994. Initiating re-entry: the role of nonuniform anisotropy in small circuits. *Journal of Cardiovascular Electrophysiology*, 5 (2), pp. 182 - 209.

Splawski, I., Shen, J., Timothy, K.W., Lehmann, M.H., Priori, S.G., Robinson, J.L., Moss, A.J., Schwartz, P.J., Towbin, J.A., Vincent, G.M. and Keating, M.T. 2000. Spectrum of mutations in long-QT syndrome genes. KVLQT1, HERG, SCN5A, KCNE1, and KCNE2. *Circulation*, 102 (10), pp. 1178 – 1185.

- Splawski, I., Timothy, K.W., Vincent, G.M., Atkinson, D.L. and Keating, M.T. 1997. Molecular basis of the long-QT syndrome associated with deafness. *The New England Journal of Medicine*, 336 (22), pp. 1562 – 1567.
- Studenik, C.R., Zhou, Z. and January, C.T. 2001. Differences in action potential and early afterdepolarization properties in LQT2 and LQT3 models of long QT syndrome. *British Journal of Pharmacology*, 132 (1), pp. 85 - 92.
- Suessbrich, H., Schonherr, R., Heinemann, S.H., Attali, B., Lang, F. and Busch, A.E. 1997. The inhibitory effect of the antipsychotic drug haloperidol on HERG potassium channels expressed in *Xenopus* oocytes. *British Journal of Pharmacology*, 120 (5), pp. 968 – 974.
- Suessbrich, H., Waldegger, S., Lang, F. and Busch, A.E. 1996. Blockade of HERG channels expressed in *Xenopus* oocytes by the histamine receptor antagonists terfenadine and astemizole. *FEBS Letters*, 385 (1-2), pp. 77 -80.
- Surawicz, B. 1989. Is hypomagnesemia or magnesium deficiency arrhythmogenic? *Journal of the American College of Cardiology*, 14 (4), pp. 1093 – 1096.
- Surawicz, B., Lepeschkin, E. and Herrlich, H.C. 1961. Low and high magnesium concentrations at various calcium levels: effect on the monophasic action potential, electrocardiogram, and contractility of isolated rabbit hearts. *Circulation research*, 9 (4), pp. 811 – 818.
- Szabo, B., Kovacs, T. and Lazzara R. 1995. Role of calcium loading in early afterdepolarizations generated by Cs<sup>+</sup> in canine and guinea pig Purkinje fibres. *Journal of Cardiovascular Electrophysiology*, 6 (10), pp. 796 - 812.
- Szabo, B., Sweidan, R., Rajagopalan, C.V. and Lazzara, R. 1994. Role of Na<sup>+</sup>: Ca<sup>2+</sup> exchange current in Cs<sup>+</sup>-induced early afterdepolarizations in Purkinje fibres. *Journal of Cardiovascular Electrophysiology*, 5 (11), pp. 933 - 944.
- Teschemacher, A.G., Seward, E.P., Hancox, J.C. and Witchel, H.J. 1999. Inhibition of the current of the heterologously expressed HERG potassium channels by imipramine and amitriptyline. *British Journal of Pharmacology*, 128 (2), pp. 479 – 485.

Tester, D.J., Will, M.L., Haglund, C.M. and Ackerman, M.J. 2005. Compendium of cardiac channel mutations in 541 consecutive unrelated patients referred for long QT syndrome genetic testing. *Heart Rhythm*, 2 (5), pp. 507 – 517.

Thomas, D., Bernd, G., Wendt-Nordahl, G. and Kiehn, J. 2002. The antidepressant drug fluoxetine is an inhibitor of human ether-a-go-go related gene (HERG) potassium channels. *Journal of Pharmacology and Experimental Therapeutics*, 300 (2), pp. 543 – 548.

Thomas, D., Gut, B., Karsai, S., Wimmer, A.B., Wu, K., Wendt-Nordahl, G., Zhang, W., Kathofer, S., Schoels, W., Katus, H.A., Kiehn, J. and Karle, C.A. 2003. Inhibition of cloned HERG potassium channels by the antiestrogen tamoxifen. *Naunyn Schmiedeberg's Archives of Pharmacology*, 368 (1), pp. 41 – 48.

Thomas, D., Hammerling, B.C., Wu, K., Wimmer, A.B., Ficker, E.K., Kirsch, G.E., Kochan, M.C., Wible, B.A., Scholz, E.P., Zitron, E., Kathofer, S., Kreye, V.A., Katus, H.A., Schoels, W., Karle, C.A. and Kiehn J. 2004. Inhibition of cardiac HERG currents by the DNA topoisomerase II inhibitor amsacrine: mode of action. *British Journal of Pharmacology*, 142 (3), pp. 485 – 494.

Thomas, D., Karle, C.A. and Kiehn, J. 2006. The cardiac hERG/IKr potassium channel as pharmacological target: structure, function, regulation, and clinical applications. *Current Pharmaceutical Design*, 12 (18), pp. 2271 - 2283.

Thomas, D., Wu, K., Kathofer, S., Katus, H.A., Schoels, W., Keihn, J. and Karle, C.A. 2003. The antipsychotic drug chlorpromazine inhibits HERG potassium channels. *British Journal of Pharmacology*, 139 (3), pp. 567 – 574.

Traube, M., Hongo, M., McAllister Jr, R.G. and McCallum, R.W., 1985. Correlation of plasma levels of nifedipine and cardiovascular effects after sublingual dosing in normal subjects. *The Journal of Clinical Pharmacology*, 25(2), pp 125 – 129.

Vandersickel, N., de Boer, T.P., Vos, M.A. and Panfilov, A.V., 2016. Perpetuation of torsade de pointes in heterogeneous hearts: competing foci or re-entry? *The Journal of Physiology*, 594(23), pp.6865-6878.

Vandersickel, N., Bossu, A., De Neve, J., Dunnink, A., Meijborg, V.M., van der Heyden, M.A., Beekman, J.D., De Bakker, J.M., Vos, M.A. and Panfilov, A.V., 2017. Short-lasting episodes of torsade de pointes in the chronic atrioventricular block dog model have a focal mechanism, while longer-lasting episodes are maintained by re-entry. *JACC: Clinical Electrophysiology*, 3(13), pp.1565 - 1576.

Verduyn, S.C., Vos, M.A., Gorgels, A.P., van der ZANDE, J.O.L.A.N.D.A., Leunissen, J.D. and Wellens, H.J., 1995. The effect of flunarizine and ryanodine on acquired torsades de pointes arrhythmias in the intact canine heart. *Journal of Cardiovascular Electrophysiology*, 6(3), pp.189-200.

Vincent, G.M., Timothy, K.W., Leppert, M. and Keating, M. 1992. The spectrum of symptoms and QT intervals in carriers of the gene for the long-QT syndrome. *New England Journal of Medicine*, 327 (12), pp. 846 – 852.

Volders, P.G., Kulcsár, A., Vos, M.A., Sipido, K.R., Wellens, H.J., Lazzara, R. and Szabo, B. 1997. Similarities between early and delayed afterdepolarizations induced by isoproterenol in canine ventricular myocytes. *Cardiovascular Research*, 34 (2), pp. 348 - 359.

Volders, P.G., Vos, M.A., Szabo, B., Sipido, K.R., de Groot, S.M., Gorgels, A.P., Wellens, H.J. and Lazzara, R. 2000. Progress in the understanding of cardiac early afterdepolarizations and torsades de pointes: time to revise current concepts. *Cardiovascular Research*, 46 (3), pp. 376 - 392.

Vos, M.A., De Groot, S.H.M., Verduyn, S.C., Van der Zande, J., Leunissen, H.D.M., Cleutjens, J.P.M., Van Bilsen, M., Daemen, M.J.A.P., Schreuder, J.J., Allessie, M.A. and Wellens, H.J.J., 1998. Enhanced susceptibility for acquired torsade de pointes arrhythmias in the dog with chronic, complete AV block is related to cardiac hypertrophy and electrical remodelling. *Circulation*, 98(11), pp.1125-1135.

Walker, N. L., Burton, F.L., Kettlewell, S., Smith, G.L. and Cobbe, S.M., 2007. Mapping of epicardial activation in a rabbit model of chronic myocardial infarction: response to atrial endocardial and epicardial pacing. *Journal of cardiovascular electrophysiology*, 18(8), pp 862 – 868.

Wallis, R.M. 2010. Integrated risk assessment and predictive value to humans of non-clinical repolarizations assays. *British Journal of Pharmacology*, 159 (1), pp. 115 – 121.

- Wang, L., Myles, R.C., De Jesus, N.M., Ohlendorf, A.K., Bers, D.M. and Ripplinger, C.M., 2014. Optical mapping of sarcoplasmic reticulum Ca<sup>2+</sup> in the intact heart: ryanodine receptor refractoriness during alternans and fibrillation. *Circulation Research*, 114(9), pp.1410 - 1421.
- Wang, Q., Shen, J., Splawski, I., Atkinson, D., Li, Z., Robinson, J.L., Moss, A.J., Towbin, J.A. and Keating, M.T. 1995. SCN5A mutations associated with an inherited cardiac arrhythmia, long QT syndrome. *Cell*, 80 (5), pp. 805 – 811.
- Wangemann, P. 2006. Supporting sensory transduction: cochlear fluid homeostasis and the endocochlear potential. *Journal of Physiology*, 576 (1), pp. 11 – 21.
- Ward, O.C. 1964. A new familial cardiac syndrome in children. *Journal of Irish Medical Association*, 54, pp. 103 -106.
- Weiss, J.N., Garfinkel, A., Karagueuzian, H.S., Chen, P.S. and Qu, Z. 2010. Early afterdepolarizations and cardiac arrhythmias. *Heart Rhythm*, 7 (12), pp. 1891 - 1899.
- Wieland, J.M. and Marchlinksi, F.E. 1986. Electrocardiographic Response of Digoxin-Toxic Fascicular Tachycardia to Fab Fragments: Implications for Tachycardia Mechanism. *Pacing and Clinical Electrophysiology*, 9(5), pp. 727 - 738.
- Wilde, A.A., Jongbloed, R.J., Doevendans, P.A., Düren, D.R., Hauer, R.N., van Langen, I.M., van Tintelen, J.P., Smeets, H.J., Meyer, H. and Geelen, J.L., 1999. Auditory stimuli as a trigger for arrhythmic events differentiate HERG-related (LQTS2) patients from KVLQT1-related patients (LQTS1). *Journal of the American College of Cardiology*, 33(2), pp.327-332.
- Xie, J.T. and Li, C.L. 1992. Induction and termination of afterdepolarizations and triggered arrhythmias by drugs in cat heart in vivo. *Methods and Findings in Experimental and Clinical Pharmacology*, 14 (5), pp. 347 - 354.
- Xie, Y., Sato, D., Garfinkel, A., Qu, Z. and Weiss, J.N. 2010. So little source, so much sink: requirements for afterdepolarizations to propagate in tissue. *Biophysical Journal*, 99 (5), pp. 1408 - 1415.
- Xu, J., Zaim, S. and Pelleg, A. 1996. Effects of pinacidil, verapamil, and heart rate on afterdepolarizations in the guinea-pig heart in vivo. *Heart and Vessels*, 11 (6), pp. 289 - 302.

- Yan, G.X. and Antzelevitch, C. 1998. Cellular basis for the normal T wave and the electrocardiographic manifestations of the long-QT syndrome. *Circulation*, 98 (18), pp. 1928 - 1936.
- Yan, G.X., Rials, S.J., Wu, Y., Liu, T., Xu, X., Marinchak, R.A. and Kowey, P.R., 2001. Ventricular hypertrophy amplifies transmural repolarization dispersion and induces early afterdepolarization. *American Journal of Physiology-Heart and Circulatory Physiology*, 281(5), pp.H1968-H1975.
- Zareba, W., 2006. Genotype-specific ECG patterns in long QT syndrome. *Journal of Electrophysiology*, 39(4), pp.S101 - S106.
- Zeng, J. and Rudy, Y. 1995. Early afterdepolarizations in cardiac myocytes: mechanism and rate dependence. *Biophysical Journal*, 68 (3), pp. 949 - 964.
- Zodan Marin, T., Meier, R., Kraehenmann, F., Burkhardt, T. and Zimmermann, R., 2007. Nifedipine serum levels in pregnant women undergoing tocolysis with nifedipine. *Journal of obstetrics and gynaecology*, 27(3), pp260 – 263.